ANALELE
UNIVERSITĂȚII
BUCUREŞTI
CHIMIE
VOLUMUL I
2005

EDITURA UNIVERSITĂȚII DIN BUCUREŞTI
Şos. Panduri nr. 90 Bucureşti
Telefon 410.21.78/122

Mulțumim conducerii Universității din Bucureşti

pentru sprijinul acordat la apariția volumului

omagial dedicat Profesorului

Ioan V. Nicolescu,

Creatorul Şcolii de Cataliză

din Universitatea din Bucureşti

CUPRINS◈ TABLE OF CONTENTS◈SOMMAIRE
VOLUMUL I

PROFESORUL DR. DOCENT IOAN V. NICOLESCU – UN CREATOR DE ŞCOALĂ ŞI ŞTIINŢĂ…….. IX
Catedra de Tehnologie Chimică şi Cataliză

PROFESORUL G.G. LONGINESCU……..... ... XIII
D. Negoiu

TECHNOLOGICAL CHEMISTRY AND CATALYSIS

1. ETHYLENE DIMERIZATION ON NICKEL 4,4'-BIPYRIDINE COMPLEX SUPPORTED ON FAUJASITE TYPE ZEOLITES……. 17
E. Angelescu, Rodica Zăvoianu, O. D. Pavel, Anca Angelescu

2. STUDY OF DEACTIVATION EFFECT OF SO_2 ON SUPPORTED $LaCoO_3$ AND $LaMnO_3$ PEROVSKITES USED AS CATALYSTS FOR TOTAL OXIDATION OF METHANE…….. 25
M. Alifanti, P. Grange, B. Delmon

3. Ru/BEA CATALYSTS FOR SELECTIVE AND STEREO SELECTIVE HYDROGENATION OF PROSTAGLANDIN INTERMEDIATES……... 33
Simona M. Coman

4. PRELIMINARY STUDIES CONCERNING CATALYTIC OXIDATION OF ALKYL MERCAPTANS FROM LIQUID PETROLEUM CUTS IN THE PRESENCE OF Fe(III) CHELATES SUPPORTED ON HYDROTALCITE-LIKE COMPOUNDS…… 41
Anca Cruceanu, Rodica Zăvoianu, Ruxandra Bârjega, Mihaiela Ropot

5. VANADIUM-BASED CATALYSTS FOR PROPANE AMMOXIDATION REACTION……... 49
Mihaela Florea, R. Prada Silvy, P. Grange

6. OXIDATIVE DEHYDROGENATION OF *N*-BUTANE OVER A MgO-SUPPORTED MAGNESIUM VANADATE CATALYST……. 57
I.-C. Marcu, Adriana Urdă, I. Săndulescu

7. [1]HYDROTALCITE-LIKE COMPOUNDS, SOLID-BASE CATALYSTS FOR CYANOETHYLATION REACTION……... 65
O.D. Pavel, Ruxandra Bîrjega, E. Angelescu, S. Popoiu

8. CORRELATION BETWEEN TEXTURAL PARAMETERS AND CATALYTIC ACTIVITY IN OXIDATIVE DEHYDROGENATION OF n-BUTENES OVER Bi-Mo-Fe-O CATALYSTS…… 73
I. Săndulescu, I. V. Nicolescu

9. CONVERSION OF C_6 HYDROCARBONS ON Zn/H(Na,K)L ZEOLITE…….. 81
Adriana Urdă, I. Săndulescu, Mariana Carată

10. THE CATALYTIC SYNTHESIS OF METHYL-ISOBUTYL KETONE FROM ACETONE. THE STUDY OF THE INFLUENCE OF ZINC ADDITION THROUGH IMPREGNATION ON THE BEHAVIOUR OF THE CATALYST Pd/Zn- H-ZSM 5…….. 89
D. Bombos, Mihaela Bombos, Fanica Bacalum, I. Stanciu, Camelia Bala, N. Naum

11. NONIONIC EMULSIFIERS BASED ON STABILIZED POLIOXIETHYLENE-SORBITANS…… 95
D. Bombos, M. Andrei, Maria Mihailescu, Irina Tamas, C. Teodorescu

12. SKELETAL ISOMERISATION ON SULFATED ZIRCONIA MODIFIED BY Ce^{IV} AND Sn^{IV} CATIONS……. 103
Mihaiela Ropot, Ruxandra Barjega, Floreta Constantinescu

ORGANIC CHEMISTRY AND BIOCHEMISTRY

13. PARTICLE-INDUCED X-RAY EMISSION (PIXE): A PRACTICAL APPROACH TO DETERMINE THE MANGANESE ACCUMULATION BY YEAST MITOCHONDRIA…….. 111
Ileana C. Farcasanu, Fumitaka Nishiyama, Tokichi Miyakawa

INORGANIC CHEMISTRY

14. COORDINATION OF Co(II), Ni(II), Cu(II), Zn(II), Cd(II) AND Hg(II) WITH THE NEW SCHIFF-BASE DERIVED FROM 4,5-DIHYDROXIPHTALALDEHIDE AND 2-AMINOTHIAZOLE……. 117
Monica Iliş, Angela Kriza, Veronica Pop, Anca Nicolae

15. TEMPLATE SYNTHESIS AND STRUCTURAL CHARACTERISATION OF FIVE DIFFERENT Co(II) COMPLEXES WITH THE SAME LIGAND…… 123
Angela Kriza, Mariana Loredana Dianu, G. Dianu, N. Stanica

16. COMPLEXES OF Cu(II) AND Mn(II) WITH ACYLATED AMINOACIDS DERIVED FROM GLYCINE AND α-ALANINE…….. 129
Maria Negoiu, T. Rosu, Ioana Saramet, C.A. Matei

17. COMPLEXES WITH AMIDES. PART 3. SYNTHESIS, SPECTROSCOPIC AND THERMAL CHARACTERIZATION OF A CU(II) COMPLEX WITH 2-IODOANILIDE-3-CHLOROBENZO[B]THIOPHENE-2-CARBOXILIC ACID…….. 135
Rodica Olar, Mihaela Badea, Codruta Paraschivescu, Dana Marinescu, I. Baciu

18. CONTROLLED SYNTHESIS III. REACTION OF Sn(IV) and Zr(IV) WITH ISATINS……. 141
Carmen Pârnău, Angela Kriza, Niculae Popa, Silvia Udrea

19. SYNTHÈSE ET CARACTÉRISATION SPECTRALE D'UNE NOUVELLE SÉRIE D'ACÉTYLACÉTONATES MIXTES DU COBALT(II)……..… 147
Ileana Şerban, Mirela Călinescu, A.M. Stadler

20. COMPLEX COMBINATIONS OF Cu(II) WITH MIXED LIGANDS…… 153
T. Rosu, Maria Negoiu, V. Circu

ANALYTICAL CHEMISTRY

21. POLAROGRAPHIC BEHAVIOR OF PALLADIUM ION IN PARTIAL AQUEOUS MEDIUMS……. 161
V. Dumitrescu, N. Dumitrescu, M. Calugareanu

22. DETERMINATION OF VITAMIN C IN DIFFERENT STAGES OF FRUITS GROWING……. 167
N. Rasanu, V. Magearu, Nicoleta Matei, Alina Soceanu

23. ACCUMULATION OF MANGANESE AND IRON IN CITRUS FRUITS…… 173
Alina Soceanu, V. Magearu, Viorica Popescu, Nicoleta Matei

24. ELECTROCHEMICAL DNA BASED BIOSENSOR FOR THE DETECTION OF GENOTOXIC COMPOUNDS IN FISH BILE SAMPLES……. 179
A.M. Tencaliec, G. Bagni, M. Mascini, V. Magearu

25. SULPHOSALICILIC ACID LOADED WOOL NEW CHELATING SORBENT FOR IRON (III) …….. 187
Luminița Vlădescu, Mihaela Costache, Irinel Adriana Badea

PHYSICAL CHEMISTRY

26. EXPERIMENTAL METHODS FOR STUDY HIGH-PRESSURE PHASE BEHAVIOUR. PART I. STATIC METHODS…….. 193
Cristina Bogatu, Rodica Vîlcu, Anca Duță

27. LA STRUCTURE ET LA RÉACTIVITÉ DES NITRILES…….. 205
I. Ciocăzanu, D. Zăvoianu

28. OVERALL ACTIVATION PARAMETERS OF PROPYLENE OXIDATION IN PREMIXED FLAMES…….. 209
Domnina Razus, Codina Movileanu, Venera Branzea**,** D. Oancea

29. A MIXED ELECTRIC DOUBLE LAYER MODEL AT THE SOLID (LIQUID) / ELECTROLYTE INTERFACE……. 215
Gh. Semenescu, C. Cioacă, Gh. Potcovaru

PROFESORUL DR. DOCENT IOAN V. NICOLESCU – UN CREATOR DE ŞCOALĂ ŞI ŞTIINȚĂ

I.V. Nicolescu

profesor

(1911-1988)

Prof. I. V. Nicolescu s-a născut la 3 mai 1911 la Dorohoi. A absolvit Liceul Laurian din Botoşani apoi a urmat cursurile Facultății de Ştiințe – Secția Fizico-Chimice ale Institutului de Chimie Industrială din Universitatea Bucureşti, luându-şi licența în Chimie în 1933. În 1935, sub conducerea ştiințifică a Prof. Ştefan Minovici a susținut doctoratul cu teza "Noi materii colorante mono şi poliazoice", din comisia de examinare făcând parte Profesorii Şt. Minovici, A. Zaharia şi Conf. C. D. Nenițescu.

A devenit membru al corpului didactic al Facultății de Chimie din Universitatea Bucureşti în 1937 funcționând ca asistent şi ulterior şef de lucrări la Catedra de Chimie Organică. A fost colaborator al profesorului Şt. Minovici şi al Prof. Eugen Angelescu.

În 1947 s-a introdus în planul de învățământ al Facultății de Chimie o nouă disciplină - cea de Tehnologie Chimică.

Prof. I. V. Nicolescu a fost avansat profesor primind sarcina de a preda această disciplină de Chimie Aplicată pentru care a organizat şi primul laborator didactic şi de cercetare din învățământul superior românesc.

Până în 1949 grupul de Chimie Tehnologică din cadrul Catedrei de Chimie Organică condus de Prof. I.V. Nicolescu a realizat cercetări privind studiul impurităților şi al vâscozității uleiurilor minerale, separarea izobutenei din gazele de cracare, obținerea alchilatului izobutir-sulfuric din fracția butan-butene şi studiul aromatizării termo-selective a fracțiilor medii de petrol, care s-a materializat în elaborarea procesului SARMIZA pentru obținerea benzinelor

octanice. Procesul, brevetat în România şi Germania, a fost exploatat într-o instalaţie industrială în Brazilia.

Aceste cercetări, unele efectuate în colaborare cu Institutul de Cercetări Petroliere, s-au publicat în reviste internaţionale de mare prestigiu ştiinţific.

Din 1949, Prof. I.V. Nicolescu a condus colectivul de Cataliză din cadrul secţiei de Chimie Generală a Academiei Române. In 1963 se înfiinţează Catedra de Tehnologie Chimică şi Cataliză al cărui şef devine Prof. I. V. Nicolescu.

Prof. I. V. Nicolescu iniţiază, pentru prima dată în România, cercetări sistematice de cataliză eterogenă, realizate în cadrul catedrei şi al colectivului de cercetare al Academiei Române.

Principalele direcţii de cercetare au fost:

- *catalizatori pentru sinteza amoniacului, a reformării benzinelor şi pentru obţinerea simultană a ciclohexanului şi a benzinelor aromatice prin procesul Complex forming;*
- *catalizatori şi procese pentru oxidehidrogenarea butenelor;*
- *preparare de alumine cu proprietăţi prestabilite*
- *catalizatori pentru hidrogenări selective a acetilenei din gazele de piroliză, ale stirenului şi pentru metanarea monoxidului de carbon;*
- *catalizatori organo-metalici pentru polimerizarea stereospecifică a acetilenei şi pentru dimerizări stereoselective de alchene;*
- *catalizatori pentru desulfurarea metanului şi demercaptanizarea benzinelor ;*
- *sinteze Fischer-Tropsch selective, conversia metanolului şi a hidrocarburilor $C_1 - C_4$ de zeoliţi sintetici;*
- *izomerizări şi deshidratări de alcooli pe catalizatori solide acide;*
- *cercetări privind proprietăţile electronice ale catalizatorilor oxizi semiconductori în corelare cu performanţele lor în reacţii de oxidare.*

Aceste cercetări au privit deopotrivă prepararea de catalizatori noi, perfecţionarea unor catalizatori în exploatare şi elaborarea de procese catalitice.

S-a urmărit cu consecvenţă stabilirea de corelaţii între compoziţie, proprietăţile texturale, structurale şi cele catalitice în vederea elaborării de criterii ştiinţifice de selectare şi exploatare optimă a catalizatorilor.

Prof. I. V. Nicolescu s-a implicat permanent în dezvoltarea industriei chimice ca membru în Colegiul de conducere al Ministerului Chimiei şi prin activitatea de consultanţă pentru construcţia Fabricii de Catalizatori de la Rafinăria Vega–Ploieşti sau pentru punerea în operare şi eficientizarea unor unităţi industriale.

Catedra condusă cu competenţă de Prof. I. V. Nicolescu s-a constituit ca un centru de pregătire, perfecţionare şi specializare pentru mulţi cercetători din ţară şi străinătate.

Încă din 1954 Prof. I. V. Nicolescu a introdus pentru prima dată în ţară un curs de Cataliză în Chimia Organică.

Sub conducerea sa s-au elaborat 32 teze de doctorat în domeniul Catalizei Eterogene.

Prof. I. V. Nicolescu a fost un creator de ştiinţă, un întemeietor de şcoală, un mare profesor, un om bun şi generos.

A ştiut să formeze şi să consolideze echipa de cercetare arătând colaboratorilor şi studenţilor înţelegere, îngăduinţă, prietenie, dar şi exigenţă.

Înzestrat cu o imensă putere de muncă, a fost un spirit pătrunzător, analitic şi sintetic. Raţionamentele sale bazate pe o vastă cultură chimică şi pe un simţ practic deosebit erau de o logică perfectă, ţinteau esenţialul, idea inovatoare, corectitudinea şi rigoarea ştiinţifică.

Din vasta sa experienţă a oferit cu generozitate celor ce i-au fost aproape. A împărţit în jurul sau binele, sfatul bun, vorba caldă, prietenia şi o nesfârşită dragoste de viaţă.

Colaboratorilor săi le-a modelat pregătirea cu discreţie, eleganţă şi pricepere. I-a făcut să înţeleagă că succesul necesită muncă, stăruinţă şi încredere în propriile forţe.

A părăsit această lume într-o zi frumoasă de iarnă a anului 1988 rămânând o amintire luminoasă între marii oameni ai neamului care prin activitatea lor au lăsat urme adânci in cultura şi ştiinţa românească.

Pentru modul în care a slujit o viaţă şcoala şi ştiinţa chimică aducem astăzi omagiul nostru de respect, preţuire şi gratitudine memoriei prof. I.V. Nicolescu.

CATEDRA DE TEHNOLOGIE
CHIMICĂ ŞI CATALIZĂ

P.S. Catedra mulţumeşte d-nei Prof. Dr. Docent Rodica Vîlcu pentru amabilitatea de a ne oferi prilejul ca prin intermediul "Analelor Universităţii din Bucureşti" să aducem omagiul nostru marelui OM care a fost Prof. I. V. Nicolescu.

PROFESORUL G.G. LONGINESCU

"Numai prin ştiinţă şi credinţă
România mare va deveni şi România tare"

G.G. Longinescu

G.G. Longinescu
profesor
(1869-1939)

S-a născut la Focşani în anul 1869. A fost profesor secundar la Liceul "Sf. Sava". Longinescu a funcţionat, un timp, ca asistent la cursul de chimie neorganică, ţinut de doctorul Istrati între anii 1902-1906, calitate în care începe să predea un curs de chimie generală. Felul în care se achita de sarcinile sale didactice îi aduce promovarea în anul 1906 în funcţia de profesor agregat de chimie neorganică la Universitatea bucureşteană. A lucrat în laboratorul lui Emil Fischer sub îndrumarea cunoscutului savant german W. Traube. Teza sa de doctorat intitulată "Despre acizii aminici din seria alifatică" s-a bucurat de o serioasă apreciere a forurilor ştiinţifice.

G.G. Longinescu a lăsat şi o serioasă contribuţie proprie pe frontul didactic prin cărţile pe care le-a scris, cursuri şi manuale. "Cursul metodic de chimie şi mineralogie" scris iniţial de el în colaborare cu Istrati, reeditat şi adus la zi, prin neobosita sa grijă, de-a lungul multor ediţii, a fost unul dintre manualele de căpătâi în didactica chimică românească din şcolile secundare. De asemenea, "Cursul de chimie neorganică" predat studenţilor din anul întâi al Facultăţii de Ştiinţe din Bucureşti, s-a bucurat de o unanimă şi largă apreciere. A scris în anul 1929 o excepţională carte de "Analiză calitativă" – Editura Copuzeanu 1929, după care s-au instruit generaţii de studenţi. A reeditat-o prof. dr. doc. George Emil Baiulescu în anul 2000 după un exemplar pus la dispoziţie de autorul acestor rânduri. Este şi astăzi, o carte bună, ceea ce este incredibil ca o carte ştiinţifică să fie bună după o sută de ani. "Cursul metodic de chimie şi mineralogie" a fost tradus în limba franceză şi a fost reeditat în 17 ediţii. Cine a mai realizat astfel de performanţe? A mai scris un "Curs de chimie analitică (1914-1919).

Împreună cu Gheorghe Ţiţeica a înfiinţat revista "Natura" (1905). Preocupările sale de răspândire a culturii ştiinţifice în masele largi au determinat rodnica sa colaborare la această revistă, mai mult de 25 de ani.

G.G. Longinescu a scris articole despre Petru Poni, Istrati şi Teclu, precum şi multe articole de popularizare a ştiinţei, într-un stil bogat, clar şi vibrant.

Generaţii de studenţi au fost pregătiţi pentru a conduce şcolile statului, în laboratoare şi în industrie.

În laboratorul de chimie anorganică au lucrat peste 2.000 de studenţi dintre care, cel puţin 12 au fost profesori universitari, mai multe sute au fost profesori de liceu, foarte mulţi au fost ingineri în fabrici, chimişti în laboratoarele Ministerului Apărării Naţionale şi ale Ministerului Finanţelor sau cele particulare.

G.G. Longinescu a publicat 9 lucrări privind temperatura de fierbere a lichidelor organice, a polimerizării corpurilor organice şi anorganice, asupra stabilităţii corpurilor şi asupra constantelor lor fizice.

Gheorghe G. Longinescu a stabilit în anul 1901 "Relaţia asociaţiilor moleculare", care pune în legătură temperaturile de fierbere, densităţile şi numărul moleculelor ce alcătuiesc două corpuri considerate. În anul 1903 dă o nouă expresie acestei relaţii, care permite să se calculeze precis numărul atomilor unei molecule de lichid organic şi gradul de asociere al lichidelor pure, se determină constanta care îi poartă numele şi s-a elaborat o nouă formulă a legii lui Avogadro.

G.G. Longinescu a publicat 17 lucrări, majoritatea în domeniul chimiei analitice în colaborare cu Dr. Gabriela Chaborschi, Dr. G.P. Teodorescu, I.N. Longinescu, C.N. Theodosiu, Eufrosina Petrescu, Margareta N. Bădescu, Th.I. Pirtea. Lucrările respective se referă la recunoaşterea acidului clorhidric în prezenţa altor acizi halogenaţi, la recunoaşterea calciului în prezenţa bariului, la separarea metalelor din grupa a III-a, la experienţe de curs, la dozarea halogenilor. Longinescu a perfecţionat şi metodele de analiză gravimetrică în chimie, ajungând la concluzii care după cunoscutul savant francez A. Boutaric reprezintă "unul dintre cele mai mari progrese realizate în acest domeniu de o sută de ani".

Prof. dr. G.G. Longinescu a făcut doi doctori în chimie, pe Theodor Pirtea şi Gabriela Chaborschi.

G.G. Longinescu a fost un înflăcărat Patriot, un mare iubitor de Neam şi de Limbă românească.

Prof. dr. G.G. Longinescu a fost membru corespondent al Academiei Române.

A ajuns până la noi o excepţională experienţă de curs, printr-un şef de lucrări al său, excepţional şi el, C.N. Theodosiu, care îi pregătea experienţele. Se prezenta clorul. Gazul respectiv se prindea într-un cilindru. Longinescu scria pe o foaie de hârtie: "Duşmanii poporului". O introducea în cilindrul cu clor şi duşmanii poporului nu rezistau în clor, scrisul dispărea. Apoi scotea din buzunar ziarul "Românul" şi introducea titlul său în clor. Titlul ziarului nu dispărea. Longinescu exclama: "Românul nici în clor nu piere".

La deschiderea anului şcolar, Longinescu aducea cărţile, o balanţă şi greutăţi. Punea cărţile într-un platan şi căuta să echilibreze balanţa cu greutăţi. Nu-i ajungeau greutăţile. Longinescu exclama: "Chimia este o ştiinţă grea, nu-i ca fieşte ce ştiinţă"!

G.G. Longinescu nu a colaborat cu Ştefan Minovici la construcţia Institutului de Chimie din Splaiul Independenţei nr. 89. El era de părere ca mai întâi să utilăm laboratoarele şi apoi să construim un nou local. Laboratorul său din curtea Facultăţii de Chimie ni-l prezintă pe prof. Longinescu, Theodor Pirtea şi Gabriela Chaborschi în mijlocul studenţilor, toţi în halate albe. Am văzut scris pe o carte a lui Longinescu, de mâna lui, expresia: "Nu mi-a ajutat Dumnezeu să construiesc Facultatea de Chimie fără politică". Ceea ce prof. Ştefan Minovici a făcut cu multă dăruire, a căzut la cutremurul din anul 1977, datorită încărcării clădirii la etajul III cu mese de beton de către Catedra de Chimie Analitică. Inginerii constructori ai Universităţii au fost absenţi. Ei nu au intervenit când aceşti chimişti nu ştiau ce fac.

G.G. Longinescu a murit după o viaţă de muncă încordată şi chinuitoare luptându-se cu lipsurile laboratoarelor sale neînzestrate, dar mai cu seamă cu lipsa celui mai necesar simţ al omului, al cărturarului şi mai ales al chimistului: vederea.

S-a retras la pensie pe ziua de 1 octombrie 1938 cu aureola de mare savant şi ilustru profesor, pe care a meritat-o pe deplin.

S-a stins în seara Vinerii Mari în vârstă de 70 de ani.

Pe mormântul acestui mare Patriot stă scris: "Care nu a luat din drepturile nimănui şi din drepturile lui a dat la alţii".

Prof. dr. doc. Dumitru Negoiu

ETHYLENE DIMERIZATION ON NICKEL 4,4'-BIPYRIDINE COMPLEX SUPPORTED ON FAUJASITE TYPE ZEOLITES

E. Angelescu[*], Rodica Zăvoianu[*], O.D. Pavel[*], Anca Angelescu[**]

abstract: This paper presents the activity and selectivity of a catalyst based on Ni(4,4'-bipyridine)Cl_2 complex co-activated with $AlCl(C_2H_5)_2$ and supported on faujasite-type zeolite Y utilised in the dimerization of ethylene at 298K in continuous flow of reactant. Chemo- and stereo-selectivity effects expressed as selectivity for dimers and oligomers, and respectively, the concentration of 1-C_4H_8 in C_4H_8 fraction and the molar ratios 2-trans-C_4H_8/2-cis-C_4H_8 are discussed. The results are correlated with the steric and diffusion hindrances induced by the microporous structure of the porous solid matrix.

keywords: ethylene dimerization, Ni(4,4'-bipyridine)Cl_2-$AlCl(C_2H_5)_2$, Y zeolite supported complex catalysts

Introduction

Heterogeneized complexes on zeolite supports are known to be catalysts [1-5] or electrocatalysts [6-8] with high activity and selectivity. Metal chelate complexes, such as Fe, Cu, Co, Ni – phtalocyanines and metal-Salen encapsulated in the supercage structure of synthetic faujasite type zeolites X or Y, have been extensively studied as "ship-in-a-bottle" zeolite based catalysts and they were tested in hydrogenation, regio- and enantio-selective oxidation of olefins and as catalysts for fine chemical synthesis [1-5].

Nickel complexes with phosphine and acetylacetonate ligands co-activated with aluminium alkyls solved in hydrocarbons [9-14] or supported on SiO_2, Al_2O_3, SiO_2-Al_2O_3 carriers [15-17] were mainly utilised for reactions involving chain growth such as dimerization and oligomerization. The role of the co-activator is to generate Ni(I) or Ni(0) complex species with active bonds Ni-H or Ni-C which favour the insertion of the monomer previously activated by its coordination on Ni reduced sites [9-17]. In homogeneous catalysis, the oligomerization of olefins on Ni-complex catalysts has been already industrially applied in DIMERSOL (IFP) [18-21], and SHOP (Shell) processes [22]. However, these homogeneous processes present some disadvantages concerning the separation and the recovery of the catalyst from the reaction products.

[*] University of Bucharest, Faculty of Chemistry, Dept. of Chemical Technology and Catalysis, Bd. Regina Elisabeta, Nº 4-12, Bucharest 3, 000318, Romania
[**] Economical Studies Academy, ASE-Bucharest

Analele Universităţii din Bucureşti – Chimie, Anul XIV (serie nouă), vol. I-II, pg. 17-24

Recently, coordination polymers formed by open supramolecular coordination networks from molecular blocks of Me(4,4'-bipyridine)X_2 (Me=Fe, Co, Ni, Cu; X=Cl, NO_3, ClO_4, N_3, O_2CCF_3) were reported as being crystalline materials with controlled pore size, shape and functions and high thermal stability. Their bidimensional structure contains transition metal centres octahedral coordinated by four bridging chlorine and two bipyridine ligands in trans positions [23-25].

In a recent work we reported that Ni(4,4'-bipyridine)Cl_2 complex supported on Y zeolite and co-activated with $AlCl(C_2H_5)_2$ presented good activity in selective ethylene dimerization to n-butylenes when operated at 298K in static regime under an initial pressure of ethylene equal to 12 atm [26]. In this case after 5 hours reaction time the conversion of ethylene reached 50% while the selectivity to n-butylenes was higher than 90%. Since the discontinuous processes are less advantageous in industrial appliances, the present work was directed towards the study of the catalytic performances of these catalysts operated under continuous flow of reactant.

Experimental

$NiCl_2 \bullet 6H_2O$ p.a. (Merck), 4,4'-bipyridine p.a. (LOBA FEINCHEMIE), $AlCl(C_2H_5)_2$ 98% (Merck-Suchardt) and zeolite Y (Si/Al = 2.31) (synthesised by the Institute of Research for Petroleum Refining and Petrochemistry (INCERP) – Ploieşti – Romania) were the raw materials utilised for the preparation of the complex catalysts. Before the preparation of the supported complex catalyst, the support was calcined at 460^{o}C during 4 hours.

The pure complex Ni(4,4'-bipyridine)Cl_2 (K) and the supported complex catalyst K/Y were prepared according to the methods described in detail in our previous work [26]. Briefly, the precipitation of the pure complex is performed by drop wise addition of a methanolic solution of 4,4'-bipyridine to an aqueous solution of $NiCl_2$ under stirring. K/Y was prepared by adding the support powder in the $NiCl_2$ solution at the beginning of the preparation and further addition of the methanolic solution of 4,4'-bipyridine. The content of Ni in the resulting solid was 3.5 wt.%. The obtained solid was washed with distilled water, methanol and acetone to remove the weakly hold amounts of un-reacted $NiCl_2$ and 4,4'-bipyridine from the surface of the support. Coactivation was realised in situ using the appropriate amounts of $AlCl(C_2H_5)_2$ in order to yield a molar ratio Al/Ni=5/1 in the catalyst.

The catalysts were characterized by elemental analysis, XRD, Diffuse Reflectance UV-VIS (DR-UV-VIS), and FTIR spectroscopy.

Elemental analysis was performed on Carlo Erba equipment. The XRD analysis was performed with a Philips equipment using Cu Kα radiation. All measurements were made in a 2θ range of 5-80^o at the operating power of 40kV/40mA. The refinement of the diffraction patterns was performed using JADE (Windows) software.

The DR-UV-VIS spectra were recorded at room temperature with a JASCO V570 spectrometer in the range 250-850 nm. The spectrometer is equipped for reflectance studies

with an integration sphere coated with MgO taken as a reference. Infrared spectra in the region 400-4000 cm^{-1} were recorded on a BioRad FTS 135 spectrometer.

Samples were prepared using the technique with KBr discs. Resolutions of 8 cm^{-1} and 16 scans were used.

The tests performed in continuous flow of reactant were realised at 298 K under atmospheric pressure in a glass microreactor with a fixed bed of catalyst. The contact time varied in the range 1 – 8 s. Analysis of the reaction products was performed at 15 minutes intervals until steady state was reached. Ethylene (99% purity) produced at PETROBRAZI – Ploieşti Romania was used as reactant. The reaction products were analysed with a Thermoquest chromatograph equipped with FID detector and a capillary column Al_2O_3-PLOT (30 m length).

Results and Discussion

The elemental analysis of the synthesized complex Ni(4,4'-bipyridine)Cl_2 gave the following results: 41.3 wt.% C, 3.15 wt. % H, 8.96 wt.% N and 20.42 wt. % Ni. The slight discrepancy between these values and the values calculated considering the chemical formula (e.g. 42 wt.% C, 2.8 wt. % H, 9.8 wt.% N and 20.55 wt. % Ni) is likely caused by the presence of water molecules in the crystal lattice. In agreement with the published data [25], the results of the XRD analysis of the neat complex show that the complex has an orthorhombic symmetry, belonging to space group C_{mmm} (Nº 65) (a = 11.974; b=11.335; c=3.584).

The electronic spectrum of the complex (fig. 1) presents the most intense bands due to Ni cation in octahedral coordination at 298 nm (charge transfer from ligand to metal), 409 nm and 713 nm (d-d spin allowed transitions) and the other bands corresponding to π-π^* transitions characteristic to the ligand [27,28]. The same bands are also noticed in the spectra of the supported complex catalyst. Their intensity is lower due to the low concentration of complex in the catalyst.

The FTIR spectra are presented in fig. 2. The main bands of the parent zeolite corresponding to Si-O vibrations (1000 and 1100 cm^{-1}), Al-O (700 and 780 cm^{-1}), D6R and D4R (570, 440 and 460 cm^{-1}) are not significantly modified following the deposition of the complex indicating that the structure of the zeolite is not destroyed [29]. Several new bands appear in the regions where the neat complex presents its highest intensity bands, e.g. 637 cm^{-1}, 809 cm^{-1}, 1420 cm^{-1}, 1609 cm^{-1} and 2366 cm^{-1}. Their intensity is not too pronounced since the amount of the complex on the support is rather small (19.2 wt. %). The bands of the complex at 494 cm^{-1} and those in the region 1000-1223 cm^{-1} are overlapped by the bands corresponding to the support at 440-570 cm^{-1} and 1000-1100 cm^{-1}, respectively. Due to this overlapping, in the spectrum of K/Y, the bands at 484 cm^{-1} and respectively 1028 cm^{-1} are broader and more intense than those of the parent zeolite. The most significant difference between the spectrum of Y zeolite and K/Y is noticed in the region where the vibrations corresponding to the hydroxyl groups appear. Thus, K/Y spectrum presents a

very low intensity of these bands, which are also shifted to higher wavenumbers, e.g. 3555 cm^{-1} and 3627 cm^{-1} compared to 3140 cm^{-1} and respectively 3446 cm^{-1} in the spectrum of the parent zeolite.

This could be an effect of the screening of the hydroxyl groups by the complex supported on the zeolite surface.

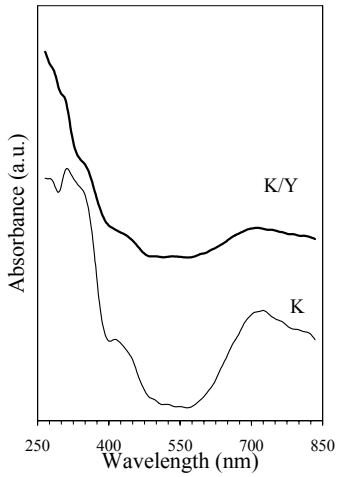

Fig. 1. *DR-UV VIS spectra of K, and K/Y*

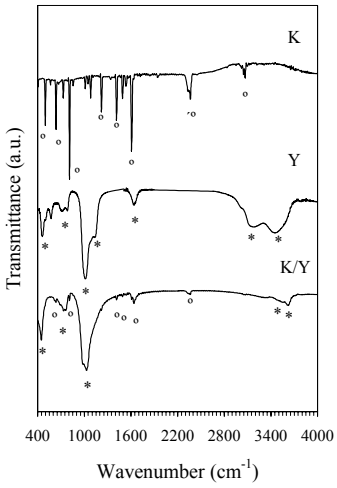

Fig. 2. *FTIR spectra of 4,4'-bipyridine, K, Y, and K/Y (most intense bands: complex - # ; Y zeolite - *)*

The results of the catalytic tests for ethylene dimerization at 298K and continuous flow of reactant using K and K/Y catalysts co-activated with $AlCl(C_2H_5)_2$ are presented in figs. 3-6. The data presented in Fig. 3 show that for both catalysts ethylene conversion increases with the contact time and the supported complex is always more active than the unsupported complex catalyst, probably due to the higher dispersion of the active sites in K/Y. There is a significant increase of conversion up to a contact time of 5 s. Once rising above this value of the contact time the conversions does not increase significantly, the values being around 15% for the unsupported complex and respectively 30% for K/Y.

Fig. 4 shows that both catalysts are more selective for dimerization than for oligomerization since the selectivity for n-butylenes is higher than 80%. The increase of the contact time leads to a decrease of the selectivity to n-butylenes accompanied by an increase of the selectivity to oligomers. This fact suggests that the production of oligomers is a slower process, which requires in a first stage the obtaining of n-butylenes [10-20, 26]. Probably, the lower selectivity to oligomers obtained for K/Y could be related to the diffusion hindrances that appear subsequently to the encapsulation of the complex in the porous carrier.

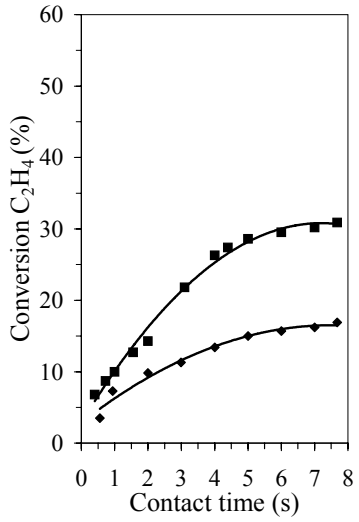

Fig. 3. *Variation of ethylene conversion as a function of the contact time on K -♦-, and K/Y -■- catalysts co-activated with $AlCl(C_2H_5)_2$ (Al:Ni=5:1)*

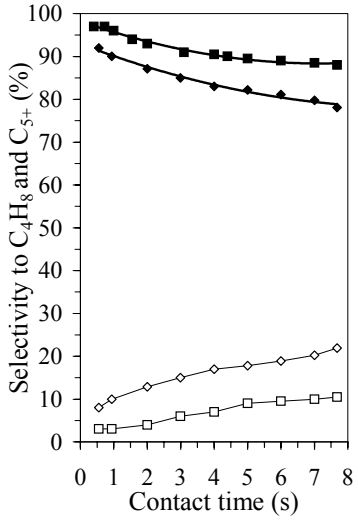

Fig. 4. *Variation of the selectivities to n-C_4H_8 (♦, ■) and C_5 (◊, □)$_+$ as a function of the contact time K (diamond symbols) and K/Y (square symbols)*

As it may be seen from Fig. 5, the prevailing isomer present in n-butylenes fraction is 1-butylene which represents more than 78%, value much higher than the one corresponds to thermodynamic equilibrium, e.g. 2.5% [10-13].

The decrease of the concentration of 1-C_4H_8 with the contact time indicates that 2-C_4H_8 is formed by subsequent isomerization of 1-C_4H_8 [15-20]. This behaviour is more significant for K than for K/Y (e.g. almost 10% for K and only 5% for K/Y). However K/Y is less selective for 1-C_4H_8 than the neat complex suggesting that in this case there is likely a slight contribution of the residual acid sites of the support. The data from Fig. 6 show that the increase of the contact time above 2 s does not influence the ratio between *trans* and *cis* isomers of 2-C_4H_8. For both catalysts the formation of *cis* isomer is increased since the value of the ratio *trans*-2-C_4H_8/*cis*-2-C_4H_8 is less than half of the value corresponding to thermodynamic equilibrium (e.g. 3.22).

A comparison between the results obtained with K and K/Y catalysts when operated in continuous flow of reactant and in static regime is presented in Table 1.

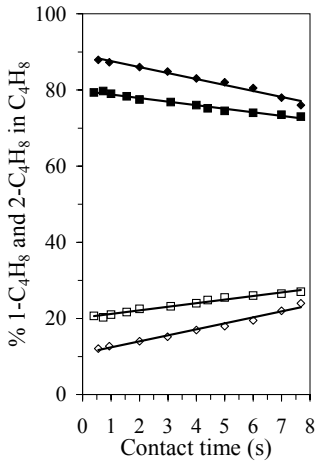

Fig. 5. *Variation of the concentrations of 1-C_4H_8 (♦, ■) and 2-C_4H_8 (◊, □) in n-C_4H_8 fraction+ as a function of the contact time K (diamonds) and K/Y (squares)*

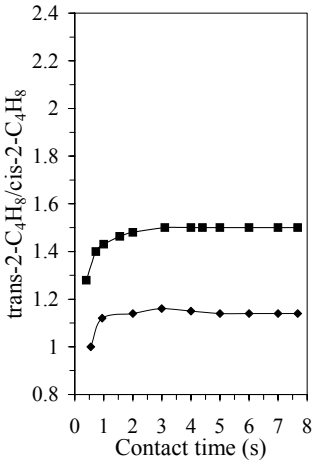

Fig. 6. *Variation of the ratio trans-2-C_4H_8/cis-2-C_4H_8 as a function of the contact time on K -♦-, and K/Y -■- catalysts*

*The intrinsic activity was calculated taking into account the bulk Ni amount in the catalyst sample. The concentration of complex in supported catalysts was 19.2 wt.%. For all the tests 0.2 g catalyst were used.

Table 1. Comparison of the results obtained at ethylene dimerization on complex catalysts K and K/Y co-activated with $AlCl(C_2H_5)_2$; Molar ratio Al/Ni = 5/1, T = 298 K

Operating conditions	Continuous flow, p = 1atm., 0.2 grams of catalyst, contact time 5 s, steady state conditions		Static regime, $p_{C_2H_4}$ = 12 atm., 5 h reaction time, 0.2 grams catalyst	
Catalyst	K	K/Y	K	K/Y
Intrinsic activity * $\left[\frac{\text{moles of } C_2H_4 \text{ transformed}}{\text{moles of Ni} \bullet h}\right]$	3.2	8.0	4.1	29.5
Selectivity to C_4H_8 (%)	82.2	89.5	91.6	93.4
% 1-C_4H_8 in n-C_4H_8 fraction	82.0	74.5	71.6	38.7
$\left[\frac{trans\text{-}2\text{-}C_4H_8}{cis\text{-}2\text{-}C_4H_8}\right]$	1.1	1.5	1.33	1.3
Selectivity to oligomers C_{5+} (%)	17.8	10.5	8.4	6.6

Equilibrium composition at 298 K: %1-C_4H_8 in n-C_4H_8 fraction = 2.5%; Trans-2-C_4H_8/Cis-2-C_4H_8= 3.22

The data presented in table 1 show that both the intrinsic activity and the selectivity for dimerization are higher for the supported catalyst than for the neat complex. This fact may be related to the more uniform dispersion of Ni complex active sites on the support. Both the intrinsic activities and the selectivity for dimerization are enhanced in the tests performed in static regime. The higher activity for oligomerization in tests carried out in continuous flow of reactant may be a consequence of a more facile desorption of the reaction products under these operating conditions. The lower selectivity for 1-C_4H_8 in tests carried out under static regime may be a consequence of an increased isomerization to 2-C_4H_8 at long contact time. However, the ratio between *trans* and *cis* isomers of 2-C_4H_8 is not influenced significantly by the operating conditions.

Aiming to study the leaching possibility under continuous flow of ethylene at atmospheric pressure, catalytic tests using 20 cm^3 of catalyst at a contact time 1.5 s were performed during 4 hours. In the colourless oligomer fraction collected after this reaction time only traces of Al not exceeding 13 ppm and no traces of Ni could be detected. Therefore it may be concluded that during the catalytic tests the complex Ni(4,4'-bipyridine)Cl_2 was not washed out by the reagent flow.

Conclusion

Ni(4,4'-bipyridine)Cl_2 complex co-activated with $AlCl(C_2H_5)_2$ and dispersed on Y zeolite is an active and selective catalyst for ethylene dimerization to n-butylenes under normal conditions of temperature and pressure. The higher activity compared to that of the neat complex might be a consequence of a more uniform dispersion of Ni active sites.

When this catalyst is operated under dynamic regime, at low contact time, high concentrations of 1-butylene may be produced as a consequence of the steric hindrances imposed to the molecular traffic by the supported complex.

REFERENCES

1. DeVos, D.E., Thibault-Starzyk, F., Knops-Gerrits, P.P., Parton, R.F., Jacobs, P.A. (1994) *Macromol. Symp.* **80** 157-65.
2. Schulz-Ekloff, G., Ernst, S. (1999) in ***Preparation of Solid Catalysts (****G. Ertl, H. Knözinger, J. Weitkamp Eds.)*, Wiley VCH Verlang Gmbh, D-69469 Weinheim, Germany, "Zeolite-Entrapped Metal-Complexes" p. 405-30.
3. Keim, W., Drießen-Hölscher, D. (1999) in ***Preparation of Solid Catalysts (****G. Ertl, H. Knözinger, J. Weitkamp Eds.)*, Wiley VCH Verlang Gmbh, D-69469 Weinheim, Germany, "Heterogeneization of Complexes", p. 355-82.
4. DeVos, D.E., Knops-Gerrits, P.P., Parton, R.F., Weckhuysen, B.M., Jacobs, P.A., Schoonheydt, R.A. (1995) *J. Inclusion Phenomena and Molecular Recognition in Chemistry* **21**, 185-98.
5. Knops-Gerrits, P.P., Verbeckmoes, A., Schoonheydt, R., Ishikawa, M., Jacobs, P.A. (1998), *Microporous and Mesoporous Materials* **21** 475-84.
6. Bedioui, F., Roue, L., Devynck, J., Balkus Jr., K.J., (1994) *Stud. Surf. Sci. Catal.* **84** 917-28.
7. Balkus Jr., K.I., Hargis, C.D., Kowalak, S. (1995) ACS Symp. Ser. **499** 347-54.
8. Balkus Jr., K.I., Gabrielov, A.S. (1995) *J. Inclusion Phenomena and Molecular Recognition in Chemistry* **21** 159-68.
9. Carlini, C., Isola, M., Liuzzo, V., Raspalli Galletti, A.M., Sbrana, G. (2002) *Appl. Catal. A. General* **231** 307-16.
10. Angelescu, E., Angelescu, A., Nicolescu, I.V. (1979) *Rev. Chimie – Bucureşti* **30(**6) 533-36.
11. Angelescu, E., Angelescu, A., Nicolescu, I.V. (1981) *Rev. Chimie – Bucureşti* **32**(6) 559-62.
12. Angelescu, E., Angelescu, A., Nicolescu, I.V. (1981) *Rev. Chimie – Bucureşti* **32**(7) 633-38.
13. Angelescu, E., Angelescu, A., Nicolescu, I.V. (1982) *Rev. Chimie – Bucureşti*, **33**(2) 137-40.

14. Hartley, F.R. (1987) in **Supported Metal Complexes** – Royal Military College of Science Shirivenham, Wiltshire, SN6 8LA England, p. 252-262.

15. Zăvoianu, R., Angelescu, E., Nenu, C., Năstase, N. (1999) *Rev. Roum. Chimie, Roumanian Academy* **44**(11-12) 1101-6.

16. Carpentier, J., Lamonier, J.F., Siffert, S., Zhilinskaya, E.A., Abaukaais, A. (2002) *Appl. Catal. A. General*, **234** 91-8.

17. Bonneviot, L., Olivier, D., Che, M. (1983) *J. Mol. Catal*. **21** 415-20.

18. Chauvin, Y., Gaillard, J., Leonard, J., Bounifay, P., Andrews, K.W. (1982) *Hydroc. Proc*. **61** 110-4.

19. Commereuc, D., Chauvin, Y., Gaillard, J., Leonard, J., Andrews, K.W. (1984) *Hydroc. Proc*. **63** 118-20.

20. Convers, A., Commereuc, Torek, D. B. (1994) *Rev. de l'Institut Français de Pétrole* **49** 437-40.

21. (1991) **KirkOthmer Encyclopedia of Chemical Technology**, Fourth Edition, John Wiley & Sons, vol. 1., p. 908.

22. Moulijn, J.A., van Leeuwen, P.W.N.M., van Santen, R.A. (1993) „**An Integrated Approach to Homogeneous, Heterogeneous and Industrial Catalysis"**, Catalysis vol. 79, Elsevier Science, p. 45-48.

23. Lawandi, M.A., Huang, X., Wang R.-J, Li, J, Lu, J. Y., Yuen, T., Lin, C.L. (1999) *Inorg. Chem*. **38** 5410-4.

24. Zhang, Y.S., Enright, G.D., Breeze, S.R., Wang, S. (1999) *New J. Chem.* **23** 625-30.

25. Shen, H.Y., Bu, W.M., Gao, E.Q., Liao, D.Z., Jiang, Z.H., Yan, S.P., Wang, G..L. (2000) *Inorg. Chem* **39** 396-42.

26. Angelescu, E., Che, M., Andruh, M., Zăvoianu, R., Costentin, G., Mirică, C., Pavel, O.D. (2004) *J. Mol. Catal. A:Chemical* **219** 13-19.

27. Balaban, A.T., Banciu, M., Pogany I. (1983) **Aplicații ale Metodelor Fizice în Chimia Organică**, Ed. Stiințifică și Enciclopedică, București, 105-130.

28. Lever A.B.P. (1984) **Inorganic Electronic Spectroscopy**, Pergamon Press, N.Y., 135.

29. Flanigen, E.M., Khatami, H., and Szymanski, H.A., (1971), *in Molecular Sieves Zeolites I, eds. Flanigen E.M. and Sand L. B., ACS Monograph* **101**, *A.m..Chem. Soc., Washington, DC,* 201-210

STUDY OF DEACTIVATION EFFECT OF SO_2 ON SUPPORTED $LaCoO_3$ AND $LaMnO_3$ PEROVSKITES USED AS CATALYSTS FOR TOTAL OXIDATION OF METHANE

M. Alifanti[*], P. Grange[**], B. Delmon[**]

Supported $LaCoO_3$ and $LaMnO_3$ perovskites were prepared by different synthesis procedures. Chosen carrier was $Ce_{0.8}Zr_{0.2}O_2$ solid solution. All catalysts were thoroughly characterized by S_{BET}, XRD and XPS. Catalytic activity with time-on-stream was evaluated for complete oxidation of methane in the presence of 20ppm of SO_2. The most robust catalysts were those prepared starting from citrate precursors that had increased resistance to deactivation with respect to the corresponding unsupported peroskite. Some factors responsible for perovskite deactivation in the presence of SO_2 are presented.

Introduction

Perovskites are largely used as total oxidation catalysts. This class of mixed oxides is less expensive and thermally more stable than noble metals when used for environmental purposes. However, the major limitation arises from their lower surface area thus another approach appears to be tempting, namely the deposition of the perovskites on adequate thermally stable oxides.

Gallagher et al. [1, 2] and Johnson et al. [3, 4] reported for the first time their attempts for supporting perovskites on cordierite monoliths. However, the perovskite components (mainly Co-based perovskites) usually react with the commonly used supports (alumina, silica) yielding stable compounds such as spinels, which are catalytically inactive [16-18]. For such cases a solution is the pre-coating of Al-containing support with La_2O_3 proved to be effective in preventing Co migration into the bulk of the carrier oxide [5-8].

An interesting study of Fujii et al. [9] showed that Co-based perovskites are loaded on different carrier oxides the reaction rate for propane oxidation depend in a large extent to the nature of the support. The most active catalysts were those supported on ceria and zirconia. With respect to the deposition method of perovskite on adequate supports,

[*] University of Bucharest, Faculty of Chemistry, Department of Chemical Technology and Catalysis, B-dul Regina Elisabeta, 4-12, 030016, Bucharest, fax: +40 21 3159249, email: m_alifanti@pcnet.ro
[**] Université Catholique de Louvain, Unité de Catalyse et Chimie des Matériaux Divisés, Croix du Sud 2, Boite 17, 1348 Louvain-la-Neuve, Belgium, fax : +32 10 473649

Analele Universităţii din Bucureşti – Chimie, Anul XIV (serie nouă), vol. I-II, pg. 25-32

decomposition of the citrate precursors offers the possibility to obtain small particle-size perovskite-type oxides at relatively low temperatures, such as 600-700°C [10-12].

The metal loading of supported oxide catalysts is typically much higher (one or two orders of magnitude) than for noble metals due to their generally low inherent activity per exposed atom of catalysts [13-15]. An advantage for some applications, however, is that the higher overall loading of metal oxide catalyst makes them more tolerant to catalyst poisons. In the case of supported noble metal catalysts some compounds, even at low concentration, may quickly deactivate the apparently limited number of oxidation sites present [16].

In the present study were prepared $LaCoO_3$ and $LaMnO_3$ perovskites supported on $Ce_{0.8}Zr_{0.2}O_2$ (Table 1) and their robustness was evaluated in the reaction of total oxidation of methane. Several preparation methods were employed in order to see how the physico-chemical properties and the resistance to SO_2 depend on the synthesis route.

Experimental

a) Preparation of the support

The used carrier for perovskite loading was $Ce_{0.8}Zr_{0.2}O_2$. $Ce_{0.8}Zr_{0.2}O_2$ solid solution was prepared by the "citrate" method [17] and was calcined at 700°C. The calcined material was pressed at 5t/cm² into binderless wafers, crushed and sieved to 40-100μm particle size before perovskite deposition.

b) Preparation of supported perovskites

$La(NO_3)_3 \cdot 6H_2O$ (Aldrich), $Ce(NO_3)_3 \cdot 6H_2O$ (Fluka), $Co(NO_3)_2 \cdot 6H_2O$ (Aldrich), $Mn(NO_3)_2 \cdot 4H_2O$ (Merck) and citric acid monohydrate (Merck) were used as starting materials. Aqueous solutions with cation ratio La:M of 1:1 and La:Ce:M of 0.8:0.2:1 (M=Co, Mn) were prepared. Wet impregnation was realized following two routes:

i) by contacting the $Ce_{0.8}Zr_{0.2}O_2$ support with a solution containing the corresponding nitrates (ratio solution/solid = 10/1) in order to obtain perovskite loadings of 2, 5, 10, 15, 20 and 30%wt. The corresponding samples will be denoted as NIT-catalysts.

ii) by contacting the $Ce_{0.8}Zr_{0.2}O_2$ support with a solution of nitrates and citric acid. The amount of salts was calculated as to correspond to 2, 5, 10, 15, 20 and 30%wt perovskite on the surface of the support. The corresponding samples will be denoted as CIT-catalysts.

The obtained slurries were stirred for 5h and the water was slowly evaporated at room temperature in a revolving flask. The drying process was completed by heating the powder in a vacuum oven set at 60°C under a pressure of 200kPa for 16h.

Four samples with the nominal compositions 10%wt $LaMO_3/Ce_{0.8}Zr_{0.2}O_2$ and 20%wt $LaMO_3/Ce_{0.8}Zr_{0.2}O_2$ (M=Co, Mn) were prepared by the citrate method [17], namely mixing the corresponding nitrates with citric acid. It should be mentioned that in this case the notation $LaMO_3$ does not represent the perovskite structure but the composition. The corresponding samples will be denoted as CITRATE-catalysts.

All the samples were calcined for 5h at 700°C in air.

Two samples were prepared by mechanical mixing of appropriate amounts (10 wt% and 20 wt%, respectively) of $LaCoO_3$ previously prepared by the citrate method [17] with $Ce_{0.8}Zr_{0.2}O_2$. These oxides were calcined at 700°C before mixing. The corresponding samples will be denoted as MM-catalysts.

c) Catalyst characterization

BET specific surface areas (SSA) were determined by nitrogen adsorption on a Micromeritics ASAP 2000 instrument. Prior to each analysis the catalyst powder was degassed 2 h at 150°C under a pressure of 0.1 Pa.

XRD patterns were recorded on a Kristalloflex Siemens D5000 diffractometer using the Cu-$K\alpha$ radiation at λ=1.5418 Å. Data acquisition was realized in the 2θ range 2-65° with a scan step size of 0.03°.

XPS spectra were recorded at room temperature and under a pressure of 10^{-7} Pa on a SSX-100 Model 206 Surface Science Instrument spectrometer with monochromatized Al-$K\alpha$ radiation (hν=1486.6eV). Charge correction was made considering that the C1s signal of contaminating carbon (C-C or C-H bonds) was centered at 284.8 eV.

d) Catalytic activity evaluation

Deactivation studies were performed measuring the methane conversion (1% methane in air, 0.1 g of catalyst loaded in a U-shape quartz microreactor operating in a down-flow mode at atmospheric pressure, total flow: 75 ml/min) in isothermal conditions at 600°C in the presence of 20ppmV of SO_2. Prior to each evaluation, the catalyst was activated 2 h at 650°C under flow of air and then cooled to 600°C. The outlet and inlet gas compositions were followed using an on-line Delsi 2000 gas-chromatograph, equipped with a Carbosphere packed column and a thermal conductivity detector (TCD). Helium was used as a carrier gas at a flow of 25 ml/min and the analysis was conducted isothermally at 150°C. The intensity of deactivation can be represented by Relative Loss of Activity (RLA) defined as

$$RLA = \frac{X(0) - X(15)}{X(0)}$$

where X(15) is the fractional conversion of methane after 15 hours on-stream in the presence of sulfur-dioxide and X(0) represents the initial conversion. According to the definition, the lower the value of RLA the more resistant is the catalyst.

Results and discussion

Table 1 comprises the results of textural and structural characterization of the considered catalysts. Both CIT- and NIT-samples have a lower specific surface area than $Ce_{0.8}Zr_{0.2}O_2$ support (40m²/g). The surface area decreases in parallel with the active phase loading, independent to the nature of the precursor. This shows that the materials deposited on the

support block some pores for loadings larger than 2%wt. The NIT-samples present SSA systematically lower than the CIT-corresponding materials whatever the loading. XRD patterns showed either for CIT- or NIT-samples no other phases than the cubic $Ce_{0.8}Zr_{0.2}O_2$ if the loading was less than 15%wt (Table 1). Perovskite phase formation at the surface of $Ce_{0.8}Zr_{0.2}O_2$ is evidenced by XRD starting with 15%wt $LaCoO_3$.

For the NIT-sample (Table 1), apart from perovskite lines, only traces of Co_3O_4 were observed. La_2O_3 signals, indicating an incomplete perovskite formation is XRD silent showing that La^{3+} is soluble in ceria. In the case of supported $LaMnO_3$, only the perovskite peaks were observed.

The patterns of supported $La_{0.8}Ce_{0.2}MO_3$ (M=Co, Mn) were similar to the corresponding $LaMO_3$ [18]. No new lines that might be ascribed to the formation of new phases by means of a solid state reaction between La, Co or Mn with the support have been detected. In conclusion, XRD patterns showed that a pure perovskite was obtained only for impregnation with citrates, namely for CIT-catalysts.

Table 1. Specific surface area (m^2/g) and phase composition of the investigated catalysts as a function of the synthesis route. Values in the parenthesis stand for bulk perovskite surface area

Catalyst	Loading (%wt)	Synthesis route			Crystallographic phases[a]		
		CIT	NIT	CITRATE	CIT	NIT	CITRATE
$LaCoO_3$ (11.3)	2	38.0	36.2	-	CZ	CZ	-
	5	30.2	27.7	-	CZ	CZ	-
	10	28.4	23.4	20.5	CZ	CZ	CZ
	15	28.2	21.7	-	CZ+P	CZ+P+Co	-
	20	25.3	19.8	18.5	CZ+P	CZ+P+Co	CZ+Co
	30	24.6	18.2	-	CZ+P	CZ+P+Co	-
$LaMnO_3$ (16.5)	5	33.2	27.2	-	CZ	CZ	-
	10	29.2	22.7	38.5	CZ	CZ	CZ
	15	27.4	19.7	-	CZ+P	CZ+P	-
	20	25.6	17.6	36.3	CZ+P	CZ+P	CZ
	30	24.2	17.8	-	CZ+P	CZ+P	-
$La_{0.8}Ce_{0.2}CoO_3$ (14.2)	10	27.3	24.4	-	CZ	CZ	-
	20	21.7	19.5	-	CZ+P	CZ+P+Co	-
$La_{0.8}Ce_{0.2}MnO_3$ (32.6)	10	32.2	21.1	-	CZ	CZ	-
	20	27.8	19.8	-	CZ+P	CZ+P	-

[a]P = perovskite phase; CZ = ceria-zirconia phase; Co – Co_3O_4 phase

Table 2 Binding energies (eV) for supported $LaCoO_3$

Loading	La 3d5		Co 2p3		Ce 3d5		Zr 3d5	
(%wt)	CIT	NIT	CIT	NIT	CIT	NIT	CIT	NIT
0	-	-	-	-	882.3	-	182.1	-
10	834.1	834.2	779.7	779.9	882.1	882.3	182.0	182.0
20	834.2	834.4	779.7	779.5	882.2	882.3	182.1	182.0
30	833.9	834.1	779.4	779.6	882.4	882.2	182.0	182.1
100	834.0	-	779.9	-	-	-	-	-

Table 3 Binding energies (eV) for supported $LaMnO_3$

Loading	La 3d5		Mn 2p3		Ce 3d5		Zr 3d5	
(%wt)	CIT	NIT	CIT	NIT	CIT	NIT	CIT	NIT
0	-	-	-	-	882.3	-	182.1	-
5	834.1	834.1	641.3	641.2	882.2	882.1	182.1	182.0
10	834.2	834.1	641.3	641.3	882.4	882.2	182.0	181.9
100	834.3	-	641.6	-	-	-	-	-

Tables 2 and 3 show some data obtained by XPS for selected catalysts. Binding energies showed that all elements are in their fully oxidized form. No significant shift of the binding energies of the elements occurred as compared to the bulk perovskites (Tables 2 and 3). Even if $LaCoO_3$ is deposited at the surface of $Ce_{0.8}Zr_{0.2}O_2$ the structure of oxygen signal remained unchanged, presenting the two characteristic peaks associated to lattice and adsorbed oxygen species (not shown).

The percent conversion of methane was used as a measure of catalytic activity.

Table 4 gives the values of Relative Loss of Activity (RLA) after 15h of isothermal combustion of methane at 600°C in the presence of 20ppm of SO_2. From the data presented, no clear-cut correlation could be seen between the loading or the nature of the phase deposited on $Ce_{0.8}Zr_{0.2}O_2$ and the resistance to SO_2. However, some observations may be made:

i) CIT-catalysts were generally more resistant than the corresponding NIT-samples;

ii) The RLA was around 0.4 for 20%wt and 30%wt loading while for loadings of 15%wt and below, the RLA was between 0.7 and 0.9. It appears that the samples with high perovskite loading had a better resistance to poisoning;

iii) mechanical mixtures and CITRATE-catalysts were the most poisoned. This is consistent with the high deactivation levels observed for bulk $LaCoO_3$, $LaMnO_3$, Co_3O_4, Mn_2O_3 [19] and $Ce_{0.8}Zr_{0.2}O_2$.

Table 4. Relative Loss of Activity (RLA) due to poisoning by SO_2

Catalyst	Loading, %wt	Relative loss of activity			
		CIT	NIT	CITRATE	MM
$LaCoO_3$	5	0.72	0.83	-	-
	10	0.75	0.41	0.75	-
	15	0.61	0.70	-	-
	20	0.38	0.61	0.87	-
	30	0.18	0.41	-	-
$LaMnO_3$	5	0.72	0.78	-	-
	10	0.66	0.71	0.82	0.79
	15	0.46	0.62	-	-
	20	0.41	0.89	0.96	0.82
	30	0.43	0.56	-	-
$La_{0.8}Ce_{0.2}CoO_3$	10	0.72	0.81	-	0.76
	20	0.34	0.88	-	0.55
$La_{0.8}Ce_{0.2}MnO_3$	10	0.52	-	-	-
	20	0.42	0.89	-	-
$Ce_{0.8}Zr_{0.2}O_2$	-	-	-	0.93	-

The tested catalysts were investigated by XRD, S_{BET} and XPS.

XRD indicated a loss of crystallinity after 15h of methane combustion in the presence of 20ppmV SO_2 at 600°C (Fig. 1). At the same time, the perovskite phase signals disappeared in parallel with Co_3O_4 formation. For Mn-containing catalysts the loss of crystallinity is accompanied by a disappearance of the perovskite signals without any new XRD detectable phase formation. These modifications are clearly caused by the SO_2 presence in the feed mixture. However, no reflection of a S-containing phase could be seen.

The used catalysts had systematically lower surface areas by about 10-20% than the fresh materials. This proved that the structural changes observed by XRD also modified the textural properties of our catalysts.

XPS measurements performed on the samples tested in the presence of SO_2 showed that the binding energy of the constitutive elements of the catalysts remained unchanged except for the case of La. The signal of $La3d_{5/2}$ had a shift from 834eV in the fresh samples (Tables 2 and 3) to 834.8-836eV (Fig. 2). The sulfur present at the surface was exclusively in the S^{6+} state (BE~169eV). According to these observations it appears that mainly lanthanum is affected, leading to superficial sulfate formation [19]. $La_2(SO_4)_3$ formation brings about the collapse of the perovskite structure by La extraction as sulfate.

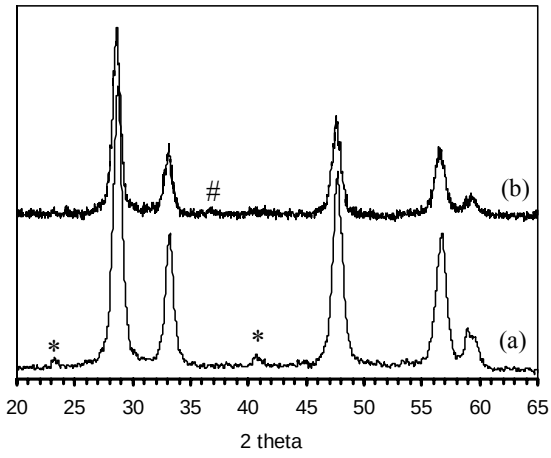

Fig. 1. *XRD patterns for CIT-20%wt $LaCoO_3$: (a) fresh sample and (b) tested in the presence of 20ppmV SO_2 at 600°C for 15h; (*) perovskite phase, (#) Co_3O_4*

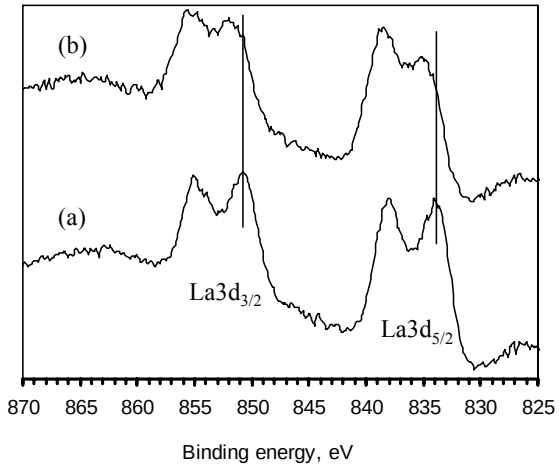

Fig. 2. *XPS signal for La3d level from a supported $LaMnO_3$ sample; (a) fresh catalyst and (b) tested 15h at 600°C for methane combustion (1%vol in air)in the presence of 20ppmV SO_2*

CIT-catalysts were more resistant to deactivation than the corresponding NIT-samples. This could be due to a much uniform coating of the support and, more probably, to a more homogeneous surface composition obtained by citrate decomposition [11, 18, 20]. Indeed, Co_3O_4 phase observed in XRD for fresh NIT-catalysts is the result of incomplete perovskite phase formation. For NIT-$LaMnO_3$, the parallel information provided by XRD, on which only the perovskite-phase signal is observed, and XPS, which showed surface composition different to the one of bulk $LaMnO_3$, suggest the incomplete perovskite formation and the presence of very dispersed Mn_2O_3 [18]. At the same time, it was shown that bulk Co_3O_4 and Mn_2O_3 are very active but easily poisoned by SO_2 [19]. Thus, the initial high activity that might be induced by Co or Mn oxide presence at the surface is rapidly lost.

Conclusions

A uniform dispersion of the $LaCoO_3$ and $LaMnO_3$ perovskites on $Ce_{0.8}Zr_{0.2}O_2$ support can be realized by *in situ* perovskite formation via the corresponding citrates decomposition. This facilitates the apparition of a homogeneous perovskite phase at lower temperatures than the decomposition of La, Co or Mn nitrates.

By deposition of $LaCoO_3$ and $LaMnO_3$ on $Ce_{0.8}Zr_{0.2}O_2$ the deactivation rate in the presence of SO_2 is retarded when compared to bulk perovskite. The perovskite – CeO_2 phase cooperation that was suggested in previous papers [11, 21] for explaining the abnormal resistance of $La_{1-x}Ce_xMO_3$ (x>0)(M=Co, Mn) seems to occur in the same way.

Acknowledgements

We thank the Commission of the European Union for the financial support of this research under the contract ENV4-CT97-0599.

REFERENCES

1. Gallagher, P.K., Johnson Jr., D.W., Schrey, F. (1974) *Mater. Res. Bull.* **9**, 1345

2. Gallagher, P.K., Johnson Jr., D.W., Vogel, E.M. (1977) *J. Am. Ceram. Soc.* **60**, 28

3. Johnson Jr., D.W., Gallagher, P.K., Schrey, F., Rhodes, W.W. (1976) *Am. Ceram. Soc. Bull.* **55**, 520

4. Johnson Jr., D.W., Gallagher, P.K., Schnettler, F.J., Vogel, E.M. (1977) *Am. Ceram. Soc. Bull.* **56**, 785

5. Mizuno, N., Fujii, H., Misono, M. (1986) *Chem Lett.* 1333

6. Burch, R., Harris, P.J.F., Pipe, C. (2001) *Appl. Catal. A: General* **210**, 63

7. Nudel, J.N., Umansky, B.S., Lombardo, E.A. (1987) *Appl. Catal.* **31**, 275

8. de Collongue, B., Garbowski, E., Primet, M. (1991) *J. Chem. Soc. Faraday Trans.* **87**, 2493

9. Fujii, H., Mizuno, N., Misono, M. (1987) *Chem Lett.* 2147

10. Ferri, D., Forni, L. (1998) *Appl. Catal. B : Environmental* **16**, 119

11. Kirchnerova, J., Alifanti, M., Delmon, B. (2002) *Appl. Catal. A: General* **231**, 65

12. Geus, J.W., van Giezen, J.C. (1999) *Catal. Today* **47**, 169

13. Klvana, D., Kirchnerova, J., Chaouki, J., Delval, J., Yaïci, W. (1999) *Catal. Today* **47**, 115

14. Klvana, D., Delval, J., Kirchnerova, J., Chaouki, J., (1997) *Appl. Catal. A: General* **165**, 171

15. Zhang, H.M., Teraoka, Y., Yamazoe, N. (1988) *Appl. Catal.* **41**, 137

16. Spivey, J.J., Butt, J.B. (1992) *Catal. Today* **11**, 465

17. Alifanti, M., Baps, B., Blangenois, N., Naud, J., Grange, P., Delmon, B. (2003) *Chem. Mater.* **15**, 395

18. Alifanti, M., Blangenois, N., Florea, M., Delmon, B. *Appl. Catal. A: General* (in press)

19. Alifanti, M., Auer, R., Kirchnerova, J., Thyrion, F., Grange, P., Delmon, B. (2003) *Applied Catal. B: Environmental* **41**, 71

20. Zhang, H.M., Teraoka, Y., Yamazoe, N. (1987) *Chem. Lett.* 665

21. Forni, L., Oliva, C., Vatti, F.P., Kandala, M.A., Ezerets, A.M., Vishniakov, A.V. (1996) *Appl. Catal. B: Environmental* **7**, 269

RU/BEA CATALYSTS FOR SELECTIVE AND STEREO SELECTIVE HYDROGENATION OF PROSTAGLANDIN INTERMEDIATES

Simona M. Coman*

Ru-BEA catalysts with 5.0wt% Ru were prepared following an "ionic exchange" procedure. These catalysts were investigated using pyridine (Py), 2,6-di-tert-butyl-pyridine (DTBPy), CO-FT-IR spectroscopy and H_2-chemisorption and were tested in the diastereoselective hydrogenation of a prostaglandin intermediate enone. The relation between the activity, the chemoselectivity to allylic alcohol, the diastereoselectivity, and the metal particle size and the acidity of the support was investigated. The effect of the hydrogen pressure, the substrate/Ru ratio and the reaction time was also studied. It was found that by modification of these properties and of the reaction parameters it is possible to "tune" the activity and selectivity of the catalyst in the investigated hydrogenation reaction.

Introduction

The selective hydrogenation of α,β-unsaturated compounds to produce allylic alcohols has recently attracted much attention because of its importance in the fine chemicals and pharmaceutical industries [1-3]. Studies done up to now in heterogeneous catalysis showed that this reaction may be influenced by modifying the surface properties [4], the presence of the promoters [5], with changes in the metal particle size and morphology [6] or with changes in the nature of the support. Some other authors suggested that the improvement of the chemoselectivity to allylic alcohol was related to the presence of Lewis acidity [7].

BEA zeolite currently received much attention as a potential catalyst in many reactions [8]. In addition to its Brönsted acidic properties, BEA zeolite displays Lewis acidity as well. This Lewis acidity is generated by the extra-framework aluminum species (as is known for USY samples [9]), and also by the framework aluminum atoms in a non-tetrahedral environment. On the other side the replacing of the H or Na compensating cations in zeolites with K cations leads to an increases of the selectivity to unsaturated alcohol [3, 10-11].

In the present paper ruthenium was supported on H-BEA and ion-exchanged K-BEA zeolite supports and were studied in the liquid-phase, batch hydrogenation of a prostaglandin intermediate ($PGF_{2\alpha}$). Earlier work of our group [12] showed that the

* University of Bucharest, Faculty of Chemistry, Department of Chemical Technology and Catalysis, Bdul Regina Elisabeta 4-12, Bucharest 030018, Romania

Analele Universităţii din Bucureşti – Chimie, Anul XIV (serie nouă), vol. I-II, pg. 33-40

microporous structure of zeolites imposed molecular constraints on the mobility of the organic, bulk substrate within pores containing metal clusters and favored the so-called "exo-selectivity" in the hydrogenation of large enones. Therefore, the reaction occurred selectively and diastereoselectively on the metal clusters mainly exposed on the external surface of the zeolites.

Zeolite supports induce the possibility of metal-support interactions in addition to shape selectivity or geometric hindrances. H-BEA and K-exchanged H-BEA were chosen in the present study to investigate the effect of the type of neutralizing cation on the selectivity. Cation effects in Ru/Y zeolites have been observed in CO hydrogenation reactions [13]; where increased basicity of the cation resulted in a decrease in the capacity for C=C hydrogenation of primary olefinic products.

Experimental

HBEA zeolite (PQ, SiO_2/Al_2O_3=21.6; S_{sp}=739 m^2/g) was used as received and was modified to produce KBEA support. In this modification, the HBEA was exhaustively ion-exchanged with potassium from an aqueous solution of KCl (0.1 M and 1g solid / 100 ml solution) at room temperature, for 24 h, under stirring. After separation by filtration the solid was washed, dried at 333 K, for 4 h, and calcined at 723 K, for another 4 h, in air flow (1 K/min). Chemical analysis revealed that 92% of the H was exchanged for K in this procedure.

Ru-loaded zeolite catalysts were prepared by the impregnation of the HBEA and KBEA supports with $[Ru(NH_3)_6]Cl_3$ ($3x10^{-2}$ M) as follow: (a) impregnation at room temperature (HBEA or KBEA supports), for 36 h, and then at 353 K, for another 12 h. After that, the catalyst was dried at 333 K for 4 h, and reduced at 623 K, for 4 h, in H_2 flow (1K/min). The obtained catalyst was named Ru-H and Ru-K; (b) part of the Ru-H catalyst was promoted with potassium in a second impregnation step from an aqueous solution of KCl (0.1 M KCl, 1 g solid / 100 ml solution) to give a molar ratio of K^+:Ru = 20:1. After separation, the catalyst precursor was washed and dried at 333 K, for 4 h, and reduced at 623 K, for another 4 h, in hydrogen flow (1K/min). The catalyst was named RuH-K. After reduction, all catalysts contain 5.0 %wt.Ru.

For the catalysts characterization, the FT-IR measurements were recorded at 4000 to 400 cm^{-1} region at room temperature on a Magna-IR system 550 FT-IR (Nicolet) spectrometer using a MCT-B liquid nitrogen cooled detector, and equipped with a heatable cell (up to 773 K) with NaCl windows connected to a vacuum system and a gas manifold. Samples in the form of self-supporting pellets (around 5 mg/cm^2) were placed into a carousel sample holder for up to 6 pellets. Usually 200 scans were recorded at a resolution of 2 cm^{-1} for a single spectrum. IR spectra were normalized to the weight of 10 mg/cm^2. Prior to adsorption of the base the samples were dehydrated by evacuation at 673 K, overnight. The molecule of base like Py was adsorbed at room temperature for 30 min on dehydrated samples, while DTBPy molecule was adsorbed at 423 K. Desorption was carried out by evacuation (vacuum better than 10^{-4} Torr) for 30 min, at each temperature step up to 673 K. The adsorption of CO was carried out in two steps, at 35 Torr and 95 Torr, respectively, at room temperature, for 30 min, followed by evacuation to 10^{-5} Torr. Desorption experiments

were performed by heating the adsorbed samples at different temperatures (373, 423, 473, 523 and 623 K) under vacuum. Except the experiments with CO, the maximal desorption temperature was of 673 K. In the case of CO, the maximal desorption temperature was 643 K when the CO is completely eliminated.

H_2-chemisorption measurements were carried out using a Micromeritics ASAP 2010C apparatus. The reduced samples were evacuated, first at 393 K and then at 723 K. Soon after, a hydrogen flow was passed initially at 308 K for 15 min and then temperature was increased at 723 K at a heating rate of 10 K/min and maintained for 2 h. After reduction, the samples were purged with a helium flow at 690 K for 2 h and then at 308 K for another 30 min. The amounts of chemisorbed hydrogen were measured at 308 K by the desorption method after equilibration for 45 min in 300 Torr of adsorbate. The total hydrogen uptake was determined by extrapolating the linear portion of the adsorption isotherm to zero pressure. Reversible H_2 sorption was measured by out gassing at 5 x 10^{-5} Torr at the adsorption temperature and running a second isotherm. The difference between the total and reversible uptakes was ascribed to irreversible hydrogen. The particle sizes were determined assuming a H : Ru stoichiometry of 1.

The liquid-phase hydrogenation reactions of the prostaglandin intermediate were carried out in a well-stirred batch autoclave under 2-6 atm of hydrogen at room temperature using 25-50 mg of catalyst (1,25 – 2,5 mg of Ru) and 15-50 mg of prostaglandin intermediate (substrate/Ru molar ratio = 2-30). Methanol (7 ml) was used as a solvent.

Results and discussion

FT-IR measurements shows that following the described preparation procedure Ru did not occupied any cationic position in the zeolite framework. No band in the spectral region 800 – 1000 cm^{-1} was detected indicating any perturbation of the zeolite framework by these cations. The deposition of ruthenium by ion exchange implies that some Ru ions should act as charge compensating ions that is not the case here. As we previously shown [14] hydrolysis of ruthenium cations is also very probable. The reduction of these cations with hydrogen may result in a generation of protons, whereas reduction of oxo-ions, such as $[Ru\text{-}O]^+$, will lead to the formation of water molecule and a proton. Py adsorption reveals the presence of strong Lewis acid sites, as characterized by the ν_{8a} band at 1620 cm^{-1} and of Brönsted acid sites, as characterized by the ν_{8a} band at 1638 cm^{-1}. A simple comparison of the intensity of the ν_{19b} bands at 1445 and 1545 cm^{-1}, characteristic to Lewis and Brönsted acid sites, suggests that in all catalysts Lewis sites are dominant. However, both the Lewis and Brönsted sites are enough strong to be determined even after the samples were out gassed at 623 K. In the case of Ru-K and RuH-K samples the intensity of the band characteristic to Lewis acid sites is even higher. This is a consequence of the fact that an important amount of Brönsted acid sites disappear as a result of the ion-exchange process with potassium chloride.

DTBPy-FT-IR spectra shows bands at 3370, 1616, and 1530 cm^{-1} which can be assigned to $DTBPyH^+$ ion and which can, in principal, be used to survey Brönsted acid sites [15]. The intensity of these bands strongly decreased in the case of Ru-K and RuH-K samples. Even so, in all catalysts, irrespective of the support nature, an easy penetration of DTBPy into the

BEA pore network and a complete disappearance of the OH acidic band at 3610 cm^{-1} was observed which suggested a large accessibility and the formation of large bidimensional patches.

CO-FT-IR spectra of the reduced samples shown for all samples four bands at 2110, 2102, 2095 and 2088 cm^{-1}. The intensity of the band centered at 2088 cm^{-1} slowly increased in the case of Ru-H and RuH-K samples. According to literature [16], the CO vibrational bands at 2163 and 2110 cm^{-1} correspond to CO bonded to an irreducible Ru^{n+} in strong interaction with the support; the one at 2088 cm^{-1} is due to the Ru carbonyl, and the bands at 2102 and 2095 cm^{-1} to the multiple adsorption of CO on reduced Ru particles. The position of the CO bands in these spectra may account to the size of the supported species. For alumina-supported rutenium catalysts, Dalla Betta [17] indicated that the band at 2028 cm^{-1} might be attributed to particles of 90 Å while smaller bands near 2140, 2080 and 2040 cm^{-1} corresponded to particles of 60 Å. The same behaviour was observed by other authors [16, 18]. The first band may correspond to highly dispersed Ru, the second to clusterized Ru, which by adsorption of CO yields a carbonyl cluster, and the third to Ru metal particles with a diameter equally or greater than 1.0 nm.

In correlation with CO adsorption results, the hydrogen chemisorption on Ru-H and Ru-K gave metal particle sizes of 1.3 and 1.8 nm respectively, based on the irreversible hydrogen chemisorption and on the assumption of a five-sided cube for particle morphology.

The deposition of Ru on the zeolite surface could occur in several ways both on Al sites and framework silanols, following an ion-exchange and grafting mechanism [14]. Py-FT-IR analysis indicated the consumption of the zeolite Brönsted sites but in this process occurred Ru did not occupied any cationic position in the zeolite framework. CO-FT-IR analysis indicated that irrespective of the support nature, at least four species could be formed. Anyway, it seems that the main species are the irreducible Ru^{n+} species.
The possible paths of prostaglandin intermediate hydrogenation are given in Scheme 1.

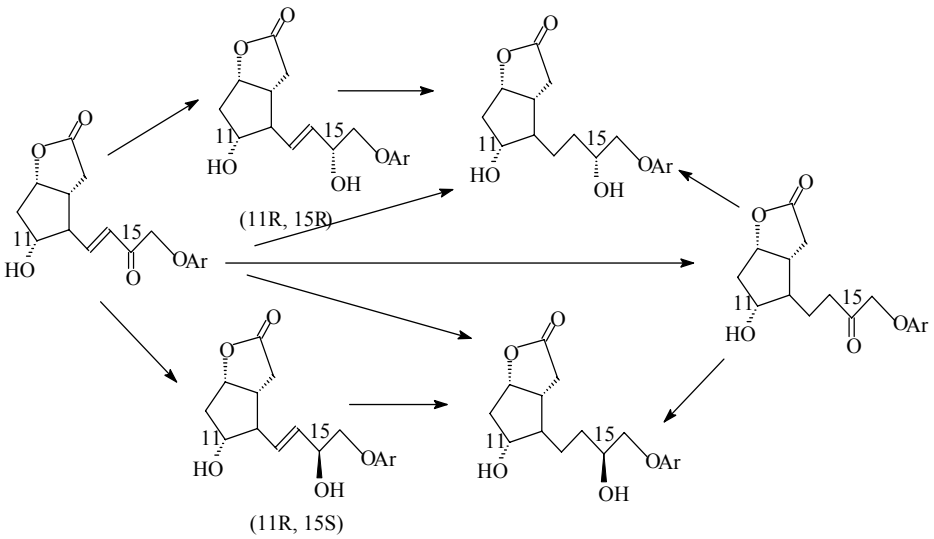

Scheme 1. Possible pathways in the hydrogenation of prostaglandin intermediate

Catalytic results obtained in the presence of Ru-H, Ru-K and RuH-K samples are listed in Table 1:

Table 1. Influence of the acido-base properties upon the catalytic performances (6 atm of hydrogen, substrate/Ru ratio = 7; reaction time 15 min).

Catalyst	Ru-K	Ru-H	RuH-K
Conversion, %	77.98	93.94	81.22
Selectivity to allylic alcohol, %	11.04	0.31	0.95
D.e. (configuration), %	80 (R)	racemic	10.50 (S)

As is shown in Table 1, a high acidity of the support favors the hydrogenation of C=C double bond. On Ru-K catalyst, the selectivity to allylic alcohol increases, in agreement with the literature reports [3, 10-11]. The acid strength of the protons in BEA zeolite decreases if protons are changed with potassium. This decrease in acidity results in greater electron density on the small metal particles onto the zeolite support. An increases in charge density of the metal may cause a suppression in the C=C hydrogenation rate by enhancing the delocalization of electrons in the adsorbed conjugated substrate. Selectivity to allylic alcohol would thus be enhanced.

Other suggestions have been made to describe the apparent electronic effects of alkali species on adsorption and reaction on metal catalysts. Therefore, the higher selectivity to allylic alcohol may be due to the combination of an increases in the C=O hydrogenation rate due to direct C=O-K interactions and a decreases in the C=C hydrogenation rate due to suppression of C=C-Ru interaction because of increased electron density of the metal particles.

The diastereoselection is also influenced by the acidic-base properties of the catalyst. Therefore, for a more basic catalyst (Ru-K sample) the formation of the *epi-configuration* of allylic alcohol (80%) is favored whereas for an acidic one (Ru-H sample) the allylic alcohol obtained is in *racemic form* (Table 1). The addition of alkali promoter to Ru-H catalyst (the RuH-K sample) result in a significant change in the diastereoselection from the *epi-configuration* to the *natural* one. The selectivity in allylic alcohol is not much increased in this case.

It is very well known that under homogeneous conditions, the stereoselectivity may be predicted and controlled considering the Cram rules [19] and the properties of the ligands exhibit a crucial contribution in such processes. To generate and control the diastereoselectivity is more complicated in heterogeneous catalysis conditions. The catalysts used in these reactions generally involve supported metal species with relatively low dispersions. Such catalysts are obtained by deposition of a relatively high amount of metal, usually higher than 5 wt.%, which determines a quite large reduction in metal surface area [20]. In addition, many of the molecules subjected to diastereoselective reactions are quite large. Very recently we have shown that when using mesoporous molecular sieves as support, the porous structure can also exhibit an influence on the stereoselective reactions [21]. Therefore, experiments carried out using MCM materials showed that the pore diameter is large enough to be penetrated by molecules as large as prostaglandin intermediates and could, furthermore, allow better stereoselectivities in hydrogenation reactions. But on almost all porous catalysts the reactions occur on the external surface, the pores being inaccessible for these molecules [22]. This is also the case of employing BEA zeolite as carrier for ruthenium species. Therefore, the hydrogenation

reaction takes place in fact on the active sites located on the external surface of the support. In this case we can not talk about a possible sterically hindered due to of the support pores.

The variation of the conversion, the chemoselectivity to allylic alcohol and the d.e. to epi-configuration, as a function of the hydrogen pressure, on Ru-K catalyst, is shown in Figure 1. The conversion increases with the hydrogen pressure whereas the chemoselectivity to allylic alcohol and the d.e. in epi-configuration decreases with the same parameter.

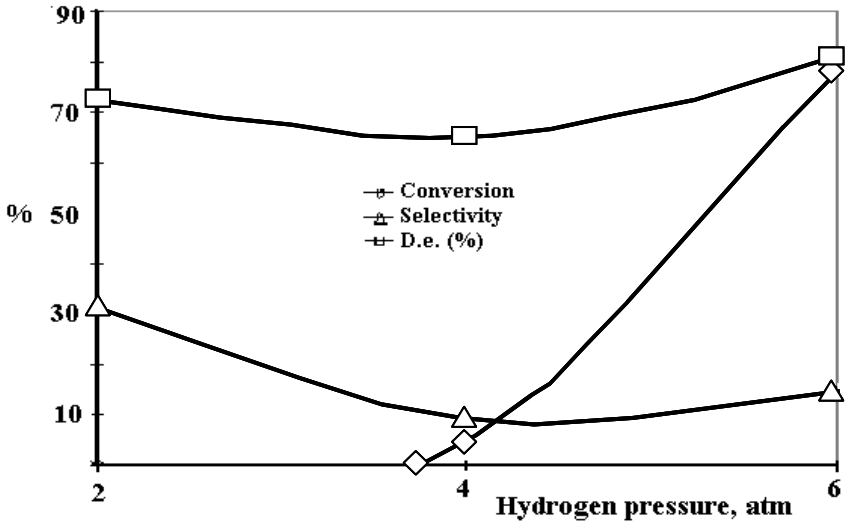

Fig. 1. *The variation of the conversion, the chemoselectivity to allylic alcohol and the diastereoselectivity as a function of the hydrogen pressure (RT, 25 mg Ru-K catalyst, substrate/Ru=7, 15 min)*

A high hydrogen pressure will ensure not only a high amount of hydrogen present in the gas phase but also will increases the gas/liquid transport and the solubility of the gas in the liquid phase. These factors increase the availability of the hydrogen to the catalyst. For 2 bars of hydrogen, the selectivity to allylic alcohol may reach almost 31% with a d.e. in epi-configuration higher than 70%, but the conversion is only few percent. An increase of hydrogen pressure will leads to an advanced hydrogenation of the allylic alcohol to saturated alcohol decreasing in this way the chemoselectivity to allylic alcohol.

The catalytic activity, the chemoselectivity to allylic alcohol and the diastereoselectivity to epi-configuration was also influenced by the substrate/Ru ratio. For a substrate/Ru ratio higher than 12, the d.e. to this configuration started to decrease (till almost 20%). The fact that the d.e. decreased parallel with the chemoselectivity to allylic alcohol may be an indication that the epi-configuration of allylic alcohol was faster transformed in saturated alcohol than the natural one. The best chemoselectivities to allylic alcohol and d.e. to epi-configuration were obtained at low hydrogen pressure (2 atm) and at low substrate/Ru ratio (Ent/Ru=7) but in these conditions the conversion was very low. Varying the quantity of the catalyst in the reaction medium is also a way of modifying the hydrogen availability to the catalyst. A larger quantity of catalyst represents, in fact, a

larger liquid/solid interfacial area. A given concentration of dissolved hydrogen is spread over this area so the concentration per unit area is smaller. Therefore, an increases of the catalyst amount (substrate/Ru=2) will have the same effect as the hydrogen pressure.

The variation of the conversion, the selectivity to allilyc alohol and the d.e. as a function of the reaction time shown that the chemoselectivity to allylic alcohol has a maximum at 84.6% with a d.e. of 94.3% to epi-configuration, for a conversion of 34.8%, after 270 min (Figure 2).

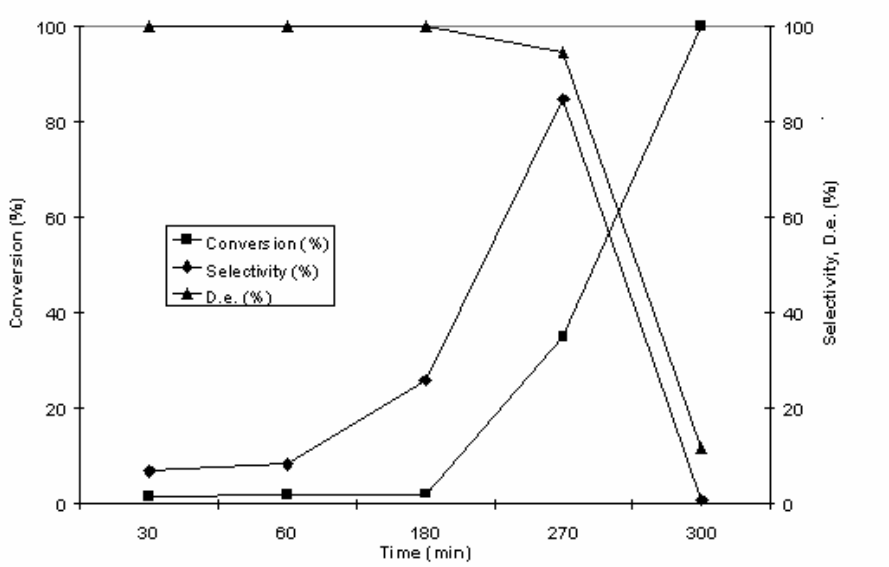

Fig. 2. *The variation of the conversion, the chemoselectivity to allylic alcohol and the d.e., on 5%Ru/K-BEA catalyst (50 mg catalyst, 2 atm, substrate/Ru=2)*

Conclusion

The deposition of Ru on the zeolite surface could occur in several ways both on Al sites and framework silanols, following an ion-exchange and grafting mechanism. Therefore, the process implies that some Ru ions should act as charge compensating ions. The FT-IR analysis of the catalysts showed that the acidity is especially due to the ruthenium species deposed on the support surface. Remaining Brönsted acidity makes an important contribution in controlling the catalysts activity. Replacing of the H^+ compensating cations in the BEA zeolite with K^+ cations and an optimisation of the parameters of the reaction can lead to very good results. For instance, on Ru-K catalyst, for a conversion of 34.8%, the chemoselectivity to allylic alcohol may reach 84.6% with a d.e. to epi-configuration of 94.3%. The addition of alkali promoter (K^+) to the Ru-H catalyst result in a significant change in the diastereoselection from epi to natural-configuration but the chemoselectivity to allylic alcohol is not much improved in this case. These results can be explaned if we take into account the effect of the alkali cations and of the ruthenium particle size.

Therefore, to be an active and selective catalyst there is an ideal combination between the nature of the ruthenium particles (as chemical nature and particles size) and the catalyst acidity. These results show that the catalyst can be "tuned" to give enhanced activities and chemoselectivities to allylic alcohol..

REFERENCE TITLE

1. Vannice, M. A., and Sen, B., (1989) *J. Catal*., **115**, 65
2. Nitta, Y., Ueno, K., and Imanaka, T., (1989) *Appl. Catal*., **56**, 9
3. Blackmond, D., Oukaci, R., Blanc, B., and Gallezot, P., (1991) *J. Catal*., **131**, 401
4. Gallezot, P., and Richard, D., (1998) *Catal. Rev. – Sci. Eng*., **40**, 81
5. Richard, D., Ockelford, J., Giroir-Fendler, A., and Gallezot, P., (1989) *Catal. Lett*., **3**, 53
6. Giroir-Fendler, A., Richard, D., and Gallezot, P., (1990) *Catal. Lett*., **5**, 175
7. Halpern, J., Okamoto, T. and Zakhariev, A. (1977) *J. Mol. Catal*., **3**, 65
8. Jansen, J. C., Creyghton, E. J., Njo, S. L., van Koningsveld, H., and van Bekkum, H., (1997) *Catal. Today*, 205
9. Sanz, J., Fornes, V., and Corma, A., (1988) *J. Chem. Soc. Faraday Trans*., **84**, 3113
10. Creyghton, E. J., and Downing, R. S., (1998) *J. Mol. Catal*., **134**, 47
11. Waghray, A., Wang, J., Oukaci, R., and Blackmond, D. G., (1992) *J. Phys. Chem*., **96**, 5954
12. Coman, S., Pârvulescu, V. I., conference to "STEREOCAT 2002 –Stereoselective Transition Metal-Catalysed Reactions", Dublin, Ireland, September 12-15 2002, P. Guiry (Ed.), Abstract book, p.C6
13. Cavalcanti, F. A. P., Blackmond, D. G., Oukaci, R., Sayari, A., Erdem-Senatalar, A., and Wender, I., (1988) *J. Catal*., **113**, 1
14. Parvulescu V. I., Coman S., Palade P., Teodorescu C. M., Filoti, G., Molina, R., Poncelet, G.,Wagner, F. E., (1999) *Appl. Surf. Sci*., **141**, 164
15. Corma A., Fornes V., Forni L., Marquez F., Martinez-Triguero J., Moscotti D., (1998) *J. Catal.*, **179**, 451
16. Solymosi, F., Rasko, J., (1989) *J. Catal*., **115**, 107
17. Dalla Betta, R. A., (1975) *J. Phys. Chem*., **79**, 2519
18. Martins, R. L., Baldanza, M. A. S., Schmal, M., (2001) *J. Phys. Chem. B*, **105**, 10303
19. Mengel A., Reiser O., (1999) *Chem. Rev*., **99**, 1191
20. De Vos D. E., De bruyn M., Parvulescu V. I., Cocu F. G., Jacobs P. A., Chiral Catalyst Immobilization and Recycling, Wiley-VCH, D. E. De Vos, I. F. J. Vankelecom, P. A. Jacobs (Eds.) 2000
21. Coman S., Florea M., Cocu F., Parvulescu V. I., Jacobs P. A., Danumah C., Kaliaguine S., (1999) *Chem. Commun*., 2175
22. Cocu F., Coman S., Tanase C., Macovei D., Parvulescu V. I., (1997) *Stud. Surf. Sci. Catal*., **108**, 207

PRELIMINARY STUDIES CONCERNING CATALYTIC OXIDATION OF ALKYL MERCAPTANS FROM LIQUID PETROLEUM CUTS IN THE PRESENCE OF FE(III) CHELATES SUPPORTED ON HYDROTALCITE-LIKE COMPOUNDS

Anca Cruceanu*, Rodica Zavoianu, Ruxandra Bârjega, Mihaiela Ropot

abstract: The aim of this work is to prepare a bifunctional solid catalyst to convert unwanted mercaptans from the petroleum cuts into disulfides, avoiding the consumption of a non-easily regenerated caustic solution. Catalysts containing Fe(III)EDTA-citrate chelate supported on Mg-Al hydrotalcite were prepared by impregnation method. Their activity for mercaptans oxidation was tested and compared to that of the neat support and the one exhibited by the pure iron chelate in alkaline solution. In the presence of the hydrotalcites-supported catalysts, conversions of methyl-mercaptan to disulfide higher than 85% were obtained even if the initial concentration of mercaptan was relatively high.

keywords: Mg–Al hydrotalcite, Mercaptan oxidation, iron chelates

Introduction

Mercaptans present in crude oil and petroleum cuts are toxic and corrosive impurities distributed among petroleum products. Therefore, it is necessary to remove them, either by extraction or by their subsequent transforming to inoffensive alkyl disulfides. In the petroleum industry, such processes are usually called "sweetening". The most widely used process of sweetening is Merox developed by UOP [1-3]. This process is based on the ability of a metal chelate, i.e. sulfonated cobalt phthalocyanine (CoPcS), to catalyze the oxidation of mercaptans to alkyl disulfides under caustic condition by molecular oxygen or by air. The overall reaction of the process is:

$$2\mathbf{RSH} + 1/2\mathbf{O}_2 \xrightarrow[\mathbf{OH}^-]{\text{Merox Catalyst}} \mathbf{RSSR} + \mathbf{H}_2\mathbf{O}$$

* University of Bucharest, Faculty of Chemistry, Department of Chemical Technology and Catalysis, Bd. Regina Elisabeta, Nº 4-12, Bucharest 3, 70346, Romania

Analele Universităţii din Bucureşti – Chimie, Anul XIV (serie nouă), vol. I-II, pg. 41-48

The reaction consists of two major steps: first, mercaptan is transformed to mercaptide anion by a base (sodium hydroxide or ammonia); second, mercaptide is oxidized to dialkylsulfide via the formation of a ternary complex involving CoPcS, mercaptide anion and molecular oxygen. The ligand, RS^- binds to CoPcS more strongly than RSH, so the first step, in which RSH is converted to RS^- by a base, is of primary importance to sweetening**.** Besides this process, which is currently utilized in refineries, there are literature data [4-10] claiming the possibility of mercaptans oxidation with oxygen at pH=8,5-10 and ambiental temperature and pressure in the presence of transitional metal (Fe, Co, Cr, or V) chelates solutions. The global process, which is similar to Merox, consists in aerobic oxidation of alkyl-mercaptans to alkyl-disulfides using as catalysts chelates of transitional metals in their high oxidation state. The reducing of the transitional metal ion by RS^- takes place simultaneously with the oxidation of the reduced species by the oxygen.

A fundamental problem of the above mentioned procedures is associated with the use of caustic solutions which cannot be converted to a valuable product. Even worse, their discharge enhances the costs of the environmental protection. Overcoming this situation requires minimizing or eliminating the use of caustic solutions wherever possible. Solid bases emerge as an ideal alternative to the aqueous bases to overcome this problem. Aqueous alkali can be completely replaced in the mercaptan oxidation reaction by incorporating solid basic materials into the catalyst formulation [1,11]. In a previous work it has been shown that Fe (III) EDTA-citrate chelates which are stable at high values of pH are promising catalysts for alkyl-mercaptans oxidation [5].

Therefore, in this paper we considered it would be interesting to investigate the oxidation of alkyl-mercaptans to alkyl-disulfides in the presence of Fe(III)EDTA-citrate chelate supported on a hydrotalcite-like compound (HTlc) playing the role of a solid base.

Experimental

The catalyst preparation utilised the following reagents without a previous purification: $Mg(NO_3)_2 \cdot 6H_2O$ (p.a) REACTIVUL min. 99.5 %; $Al(NO_3)_3 \cdot 9H_2O$ p.a. RIEDEL-DE HAËN AG min. 98.5 %; NaOH p. a. CHEMAPOL min. 98 %; Na_2CO_3 – p.a. CHIMOPAR min. 99.8 %, $Fe(NO_3)_3 \cdot 9H_2O$ p.a. (MERCK) min. 99%; $Na_2EDTA \cdot 2H_2O$ p.a. (MERCK) min. 99.2% ; citric acid anh. (REACTIVUL) min. 98%.

The preparation of the iron chelate Fe(III)EDTA-citrate (K) was performed according to the method previously described [5, 12].

The hydrotalcite support (HT) with the general formula $Mg_3Al(OH)_8(CO_3)_{0.5} \bullet 2H_2O$ (Al/(Al+Mg)=0.25) was prepared by co-precipitation at pH 10 and low super saturation according to the method described by A. Corma and R. M. Martin-Aranda [13,14]. Two solutions A and B were contacted at 25ºC by feeding with a flow rate of 60 $mL \cdot h^{-1}$ and were mixed under vigorous and continuous stirring. Solution A was prepared by solving $Mg(NO_3)_2 \cdot 6H_2O$ and $Al(NO_3)_3 \cdot 9H_2O$ in distilled water yielding a 1.5 M final concentration of Al+Mg. Solution B was prepared by solving NaOH and Na_2CO_3 enabling that the

mixture of A+B fulfills the following requirements: CO_3^{2-}/(Al+Mg)=0.666 and OH^-/(Al+Mg)=2.25.

The pH of the precipitates was maintained at 10, either by adjusting the flow rate of the alkaline solutions or by using 1 M NaOH or 1 M HNO_3 solutions. After addition of the reactants, the slurry was aged at 65^0C for 18 h in a thermostatic bath under mild stirring. A reflux unit was mounted on top of the vessel to prevent water evaporation. The resulting product was cooled at room temperature, filtered, washed thoroughly with a large amount of warm deionized water until neutral pH of the washing water was reached and subsequently dried at 90^0C for 18 h.

The catalyst consisting of Fe(III)EDTA chelate supported on HT was prepared by impregnation according to the method described in literature [15, 16]. The catalyst is further referred to as $K_{1.9}$/HT, where the index represents the iron concentration as determined by chemical analysis.

The solids were characterized by chemical analysis, XRD, and FTIR spectroscopy. X-ray diffraction analysis (XRD) was performed on a DRON-DART UM 2 diffractometer equipped with a monochromator graphite crystal ($\lambda_{CuK\alpha}$=1.5418 Å). The samples were scanned from 8^o to 70^o (2θ) in steps of 0.05^o with an acquisition time of 2 s at each point. The profile fitting calculations were performed using Jandel Scientific computer software and Voigt functions. FTIR spectra in the range 400-4000 cm^{-1} were recorded on a Perkin Elmer 1600 FTIR spectrometer using the KBr pellets technique.

The catalytic tests for alkyl-mercaptans (RSH) conversion were performed at ambiental temperature and pressure, under continuous stirring using as catalysts the solution of iron chelate (K), the parent hydrotalcite (HT), and the hydrotalcite-supported iron chelate $K_{1.9}$/HT . Synthetic samples of gasoline (100 ml) containing 200 ppm and 325 ppm alkyl-mercaptans (methyl- and *tert*-buthyl mercaptan) were submitted to oxidation under air flow (0.5L/h) in the presence of the above mentioned catalysts. Catalytic tests were carried out during 60 minutes, and the residual content of RSH was determined at 10 minutes intervals by titration with 0.01 N $AgNO_3$ alcoholic solution in the presence of dithizone according to the method described in a previous work [17].

Results and Discussion

XRD patterns presented in Fig. 1 show that the parent HT crystallizes in a hexagonal framework with rombohedral symmetry belonging to space group *R3m*. The parameters of the elementary cell were calculated according to the formulas: $\boldsymbol{a}= 2x\ d_{110}$, and $\boldsymbol{c}=1.5\ x\ (d_{003}+ 2d_{006})$. The structural data are presented in Table 1. The interlayer distance has been calculated using Miyata's evaluation of the brucite-type layer thickness 4.8 Å [18]. Since the XRD patterns of $K_{1.9}$/HT and $K_{3.5}$/HT were identical, in Fig. 1, only the spectrum of $K_{1.9}$/HT is presented. The XRD patterns show that both the parent HT and $K_{1.9}$/HT have a well crystallized hydrotalcite structure. The pattern of the sample containing the iron chelate does not present significant modifications compared to HT since the values of the structural parameters are very similar in the limits of experimental errors. The slight decrease of the basal spacing reflections illustrated by the lower ratios I_{003}/I_{110}, may be a

consequence of a new arrangement of the species in the interlayer space. The presence of diffraction lines corresponding to iron salt-like impurities has not been detected in the XRD pattern of $K_{1.9}$/HT. A slightly higher background of $K_{1.9}$/HT diffraction pattern could be a consequence of the high dispersion of the iron species, more likely on the outer surface of the hydrotalcite crystals than in the interlayer region.

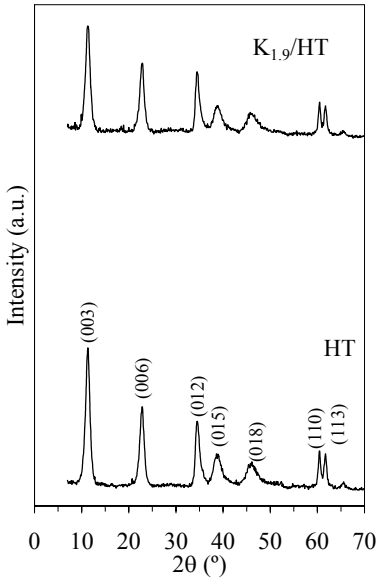

Fig.1. *XRD pattern of HT and $K_{1.9}$/HT*

Table 1. Structural data calculated from XRD analyses of HT and $K_{1.9}$/HT

Sample	***a*** (Å)	***c*** (Å)	I_{003}/I_{110}	Interlayer distance (Å)
HT	3.06	23.46	3.84	3.02
$K_{1.9}$/HT	3.06	23.44	3.47	3.01

The FTIR spectra of the catalyst samples, in the range of 400-4000 cm^{-1}, are shown in Fig. 2. The spectrum of HT used as support presents the characteristic adsorption bands for $Mg_3Al(OH)_8(CO_3)_{0.5}•2H_2O$ at 410, 629, 841, 1386, 1521, 1660 and 3562 cm^{-1} [14,15, 19]. In the spectrum of the pure iron chelate (K) the most intense adsorption bands appear at: 550 cm^{-1}; 830 cm^{-1}; 1060 cm^{-1}; 1320 cm^{-1}; 1580 cm^{-1}; 2280 cm^{-1}; 3300 cm^{-1} [5]. In the spectrum of the hydrotalcite-supported iron chelate the adsorption maximums are noticed at 610 cm^{-1}; 1050 cm^{-1}; 1340-1350 cm^{-1}; 1560 cm^{-1}, and 3400 cm^{-1}. The band corresponding to the vibration of the structural OH groups hydrogen bonded with interlamellar water molecules in HT are shifted from 3562 cm^{-1} towards 3400 cm^{-1}. Also the appearance of a shoulder of this band around 3300 cm^{-1} may be related to the presence of the complex. The bands in the region 600-1600 cm^{-1} are much broader than those observed in the spectrum of the pure hydrotalcite and they are also shifted to lower wavenumbers. This fact may be a consequence of the overlapping of the bands of the neat complex with those characteristics for HT.

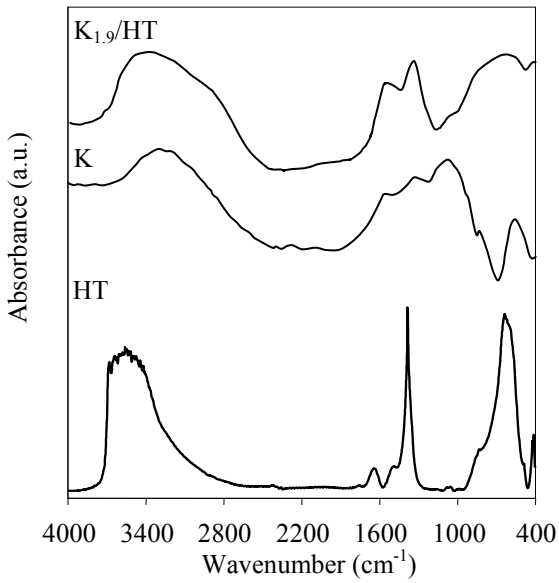

Fig. 2. *FTIR spectra of catalysts samples*

A first set of reactions concerned the catalytic activity for the oxidation of RSH to corresponding alkyl-disulfides. Samples of gasoline containing 325 ppm of RSH (MeSH, *t*-BuSH) were submitted to oxidation under air flow (0.5L/h) in the presence of different amounts of supported iron chelate catalyst, in order to find out the optimum value of the gravimetric ratio Fe/RSH necessary for reaching the highest conversion of RSH. The results obtained for $K_{1.9}$/HT were compared to those obtained in the tests performed in homogeneous system using an amount of iron chelate solution containing the same quantity of iron as in supported catalyst. The catalytic activity of the parent HT was also investigated under the same reaction conditions, using a mass of solid equal to the one utilised in the tests with $K_{1.9}$/HT. The conversion of RSH on HT did not exceed 14.2 in the case of MeSH and 10% in the case of *t*-BuSH, respectively, regardless the amount of solid used as catalyst. It may be assumed that on HT, the reaction takes place probably due to the basic sites of the solid, which play the role of enhancing the dissociation of RSH favouring their subsequent oxidation.

The results presented in fig. 4, show that the conversion of RSH to RSSR is slightly higher for the supported iron chelate catalyst than for the unsupported one. This fact may be a consequence of a better dispersion of the active iron chelate species on the surface of the supported catalyst. Therefore, the main advantage of using the hydrotalcite-supported iron chelate catalyst is related more to avoiding the use of the alkaline solution. The results show that at the same reaction time, and initial concentration of mercaptans the conversion to disulfides is different depending on the nature of the mercaptan. The conversion of MeSH is always higher than the conversion of t-BuSH. The lower reactivity of *t*-BuSH may be a consequence of its bigger molecular-size, which imposes diffusion constrains [3].

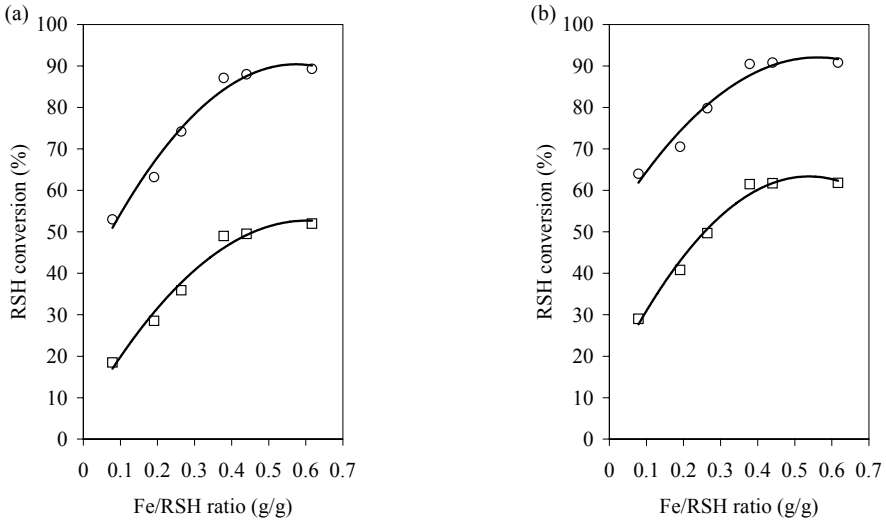

Fig. 4. *Dependence of RSH oxidation on the ratio Fe/RSH for (a) K, and (b) $K_{1.9}$/HT ; ○ – MeSH, □ -t-BuSH. Initial concentration of RSH = 325 ppm, Reaction time 30 minutes, Air flow (0.5 L/h)*

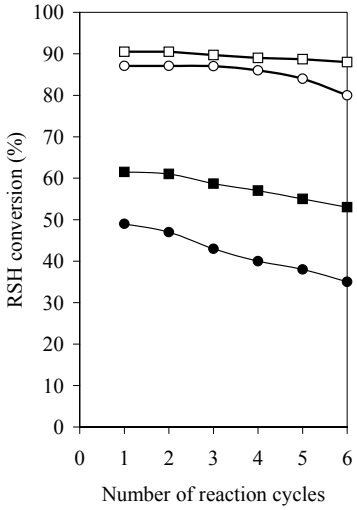

Fig. 5. *Conversion of mercaptans to disulfides as a function of the number of reaction cycles: ■ – conversion of t-BuSH on K1.9/HT ● – conversion of t-BuSH on K, □-conversion of MeSH on K1.9/HT, ○-conversion of MeSH on K. Initial concentration of RSH 325 ppm, gravimetric ratio Fe/RSH=0.4 g/g Air flow (0.5 L/h)*

The second set of experiments aimed to investigate the resistance of the catalyst under operating conditions and the possibility of using it in repeated reaction cycles. The duration of 1 cycle was 30 minutes. The catalyst used in one reaction cycle was separated from the reaction mixture and dried in the oven during 1 hour at 45°C. Afterwards it was introduced in the next reaction cycle. Since the previous tests showed that the increase of the

gravimetric ratio Fe/RSH above 0.4 g/g does not lead to significant enhancing of RSH conversion, these tests were performed using an amount of $K_{1.9}$/HT catalyst corresponding to this ratio. The results are presented in fig.5.

From fig. 5 it may be seen that the loss of the catalytic activity is lower in the case of MeSH conversion than in the case of *t*-BuSH. The more pregnant decrease of the activity for *t*-BuSH oxidation could be a consequence of the lower solubility of *tert*-buthyl-disulfide in the organic phase compared to that of the dimethyl disulfide. This fact could induce higher mass transfer limitations either at the liquid-liquid interface when using K catalyst or to a saturation effect due to the accumulation of disulfides on the surface of the solid catalyst $K_{1.9}$/HT and a subsequent screening of the active sites.

Conclusion

The above presented results shown that hydrotalcite-supported iron chelate Fe(III)EDTA-citrate are active catalysts for the conversion of mercaptans to disulfides. They present also a better stability during repeated reaction cycles compared to the stability of the complex used in liquid phase conditions. This fact may be related to the dispersion of the active phase at molecular level on the surface of the carrier, allowing a better contact between the reactants and the active sites. Due to its base properties, the hydrotalcite support favours also the dissociation of mercaptans, playing a role similar to the one of the alkaline solutions used in homogeneous conditions. It presents also the advantage that it can be easier separated from the reaction mixture and does not imply any corrosion effects.

REFERENCES

1. De-en Jiang, Biying Zhao, Yoichang Xie, Guangcheng Pan, Guopeng Ran, Enze Min, *Applied Catalysis A: General*, (2001), **219**, 69-78

2. Chatti, A. Ghorbel, P. Grange, J.M. Colin, *Catalysis Today*, (2002), **75,** 113–117

3. Liu Xiufan and Su Yixun, in *Proceedings of the International Conference on Petroleum and Petrochemical Processing*, *september 11-15*, (1991), **3**, Beijing, China

4. Philip, C.V.,.Brooks, D.W., *Inorg.Chem.*, (1974), **13(2)**, 384

5. Cruceanu A., PhD thesis, University "Politehnica" Bucharest, december 2001

6. Meuly W.C., Seldner, A., *U.S.P. 3.226.320* / 28 december 1965

7. Meuly, W.C., *U.S.P. 4.009.251* / 22 february 1977

8. Neyaglov, A.A., Digurov, D.G., Bukharkina, T.V., Mazgarov, A.M., Fakhriev, A.M., (1991) *Kinetica i Kataliz*, **32(4)**, 963-968

9. Neyaglov, A.A., Digurov, D.G., Bukharkina, T.V., Mazgarov, A.M., Fakhriev, A.M., (1991), *Kinetica i Kataliz*, **32(3)**, 541-547

10. Neyaglov, A.A., Digurov, D.G., Bukharkina, T.V., Mazgarov, A.M., Fakhriev, A.M., (1991) *Kinetica i Kataliz*, **32(3)**, 548 -554

11. Alcaraz, J.J., Arena, B.J., Gillespie, R.D., and Holmgren, J.S., (1998), *Catalysis Today,* **43**, 89-99

12. Angelescu, E., Popescu, D., Nastasi, A., Cruceanu, A., Petianu, E., *B.R. 110.12*/ 29.november 1995

13. Corma, A., Martin-Aranda, R. M., (1993), *Appl. Catal. A General*, **105**, 271-281

14. Angelescu, E., Pavel, O. D., Zăvoianu, R., Bârjega R., (2004) Revue Roumaine de Chimie, **49 (3-4)**, 367-375

15. Cavani, F., Trifiro, A., and Vaccari, A., (1991), *Catal.Today*, **11**, 173-301

16. Sels,. B.F., De Vos, D.E., Jacobs, P.A., *Catalysis Reviews*, (2001), **43(4)**, 443-488

17. Kunkel, R.K., Buckley, J.E., Gorin, G., (1959), *Anal.Chem*., **31**, 1098-1102

18. Miyata, S., (1975), *Clays Clay Miner*. **23,** 369-375

19. Parida, K., and Das, J., (2000), *J.Mol.Catal A: Chemical,* 151,185-192

VANADIUM-BASED CATALYSTS FOR PROPANE AMMOXIDATION REACTION

Mihaela Florea[*], R. Prada Silvy[*], P. Grange[**]

Amorphous high surface area vanadium aluminium oxynitrides (VAlON) prepared by nitridation of the amorphous oxide precursor exhibit high acrylonitrile yield in the propane ammoxidation at very low contact time, indicating the participation of ammonia dehydrogenated species in ammoxidation of alkanes. The productivity of the VAlON catalysts (l of ACN/ Kg catalyst.h) was remarkably improved as compared with the known oxide systems.

Introduction

Alkane transformation to high value chemical products constitutes an arduous and stimulating scientific and technological challenge. Among the most significant examples of industrial application in this field is the production of acrylonitrile (ACN) through the propane ammoxidation process. The advantages for replacing olefins by alkanes in the current ammoxidation process are essentially: the lower price of propane with respect to propylene, the risk of propylene shortage due to its increasing consumption and the increasing worldwide demand of nitriles and other derived products. However, two fundamental problems arise in the transformation processes of alkanes. i) alkane activation is difficult and requires severe operating conditions and very active, selective and stable catalysts and ii) products are generally less stable than reactants and they can be easily decomposed during the reaction leading to the formation of undesirable oxygenated C and N compounds [1].

Companies and research centers are independently developing new catalysts for the alkane ammoxidation process. The main identified factors for obtaining advantages over current propylene technology are i) maintain propane versus propylene cost advantages higher than 50%, ii) productivity levels comparable to those obtained with propylene, iii) operation temperatures no higher than 500°C and iv) maximize co-products formation, such as acetonitrile (AcCN) and hydrogen cyanide (HCN), which have a high value in the chemical market. It is thus clear that the key to successful commercialization of propane

[*] University of Bucharest, Faculty of chemistry, B-dul Regina Elisabeta, 4-12, 030016, Bucharest, fax: 40 21 3159249, email: mihaela.florea@chem.unibuc.ro
[**] Université Catholique de Louvain, Catalyse et chimie des matériaux divisés, Croix du Sud 2, Boite 17, 1348 Louvain-la-Neuve, Belgium, fax : 32 10 473649

Analele Universităţii din Bucureşti – Chimie, Anul XIV (serie nouă), vol. I-II, pg. 49-56

ammoxidation technology is the development of a new generation of catalysts capable of activating alkane molecules under moderate reaction conditions and promoting the production of other co-products of commercial interest.

The type of catalyst support and its acid–base character has a marked influence on the vanadium phase structure, surface dispersion, reducibility and catalytic properties. In fact, basic or amphoteric supports promote the formation of bidimensional vanadate surface dispersion, whereas acidic supports lead to the formation of tri-dimensional V_2O_5 species.

Lemonidou and co-workers [2] studied the effect of different catalyst supports on the vanadium reducibility and catalytic properties for the propane oxidative dehydrogenation (ODH) reaction. They observed that a V_2O_5/TiO_2 catalyst is the most active of the studied series of catalysts, while V_2O_5/Al_2O_3 is most selective in propylene formation. The authors also observed that the reduction temperature corresponding to the different V-supported catalysts varies according to the following sequence: V/ZrO_2 < V/TiO_2 <V/Al_2O_3 < V/MgO. The addition of basic promoters to the V-supported catalysts hinders the reducibility of the metal and enhances the catalytic activity. Other researchers have observed selective propylene formation over V-based catalysts supported on basic or amphoteric oxides rather than on acidic supports [3-6].

Typical propane ammoxidation catalysts are essentially constituted by combination of metallic mixed oxides. These catalysts have been classified according to two main categories i) Vanadium-molybdate catalysts, represented by $VMo_xM_yO_z$ where "M" is most often Bi or Te, with scheelite-type structure [7,8] and ii) Vanadium-antimonates which possess a rutile-type structure represented by the $VSb_xM_yO_z$ formula, where "M" are elements used as promoter such as W, Te, Nb, Sn, Bi, Cu, Al or Ti [9,10]. Other catalytic systems based on Ga-Sb oxides as well as vanadyl pyrophosphates were also investigated [11]. However, they were not so promising for the propane ammoxidation reaction.

Thus, we have been working on the development of new catalytic systems for alkane activation reactions. Metallic oxynitrides are materials that have shown excellent catalytic properties for different types of reactions [12,13]. These bi-functional catalytic systems are essentially constituted of metallic «redox» sites and basic sites with different strength distribution, which allow the activation of the alkane molecules and the subsequent nitrogen insertion reaction at relatively moderate reaction temperatures. In this article, we show the catalytic behavior of vanadium aluminum oxynitride catalysts (VAlON in the following) in the ACN production, as compared with metallic oxide propane ammoxidation catalysts reported in the literature.

Experimental

Vanadium aluminum oxide, V/Al atomic ratio of 0.25, was prepared by co-precipitation of ammonium vanadate and aluminum nitrate solutions followed by steps of drying (60°C-120°C) and calcination (500°C). The oxide precursor was submitted to nitridation treatment in NH_3 flow = 5 ml/min at 500 °C for 5hr. The system was subsequently cooled down to room temperature under a flow of pure nitrogen. More specific details about the catalyst preparation procedure have been reported elsewhere [13].

The principle of the chemical analysis of total nitrogen content is based on the reaction of the nitrogen species from the catalyst with a strong base (KOH) at 450°C and the formation of ammonia which is then titrated with a standard solution of sulphuric acid 10^{-2} N (Grekov method). The superficial nitrogen species were quantified by the Kjeldahl method. The alkaline attack was realized using a KOH saturated solution at 100°C. The titrated ammonia corresponds to the superficial NH_x (NH and NH_2) species. Bulk nitrogen does not react under these conditions.

The BET surface area corresponding to oxynitride catalysts before and after reaction was evaluated using a Micromeritics Flow Sorb II 2300 apparatus.

XRD lines were recorded using a Siemens D-5000 powder diffractometer equipped with a Ni-filtered Cu Kα radiation (λ = 1.5418 Å).

Catalytic tests were performed in a fixed bed quartz micro-reactor at atmospheric pressure and temperature of 500 °C, 0.1 g of catalyst and W/F= 8 g.h/mol of C_3H_8. Feed composition was 1.25:3:1 of C_3H_8: O_2: NH_3. The activity results are reported after 24 hours on stream. Feed and products were analysed on-line using a gas chromatograph, equipped with FID and TCD detectors and an on-line mass spectrometer was used to check the NO_x formation. The principal reaction products were: acrylonitrile (ACN), acetonitrile (AcCN) and carbon oxides (CO_x). Propane conversion is defined as the % ratio between the mole of propane consumed per mole of propane in the feed; the ACN selectivity as mole of ACN in the product per mole of propane consumed; and the ACN yield as mole of ACN in the product per mole of propane in the feed.

Results and discussions

Sample with V/Al atomic ratio of 0.25 was prepared by the co-precipitation method followed by nitridation in the presence of ammonia at 500°C for 5 hours. The sample is X-ray amorphous before and after the catalytic test. Table 1 compiles the values of the surface areas and the nitrogen content of the oxynitride powders before and after propane ammoxidation. A specific surface area of 154 m^2/g and the total nitrogen content of 3.1 wt% was obtained for the oxynitride sample after the nitridation process.

Table 1 Surface area and nitrogen content of VAlON catalyst (V/Al = 0.25)

VAlON	Surface area (m^2/g)	N_T^* (wt%)	N_K^* (wt%)	XRD
before the catalytic test	154	3.15	1.8	Amorphous
after the catalytic test	133	3.05	2.1	Amorphous

*N_T = total nitrogen content

*N_K = nitrogen determined by Kjeldahl method.

The surface area value corresponding to the V-Al oxide precursor was 250 m^2/g. After the nitridation process, the surface area of the solid decreased to 154 m^2/g, which represents a surface area loss of about 39%. After reaction, the surface area of the VAlON catalyst

decreased by about 13%. Assuming that during the reaction a continuous replacement of the surface nitrogen by ammonia exists, the slight decrease of surface may be explained. However, the nitrogen content of the samples before and after reaction remains almost the same. Evidence of nitrogen species on the vanadium aluminium oxynitrides was reported elsewhere [12].

In the literature, different nitrogen species are discussed to be active in the ammoxidation reaction depending on the nature of the catalyst. These nitrogen species have been identified on the catalyst surface during the catalytic reaction. NH_2^- groups would be active in nitrogen insertion on Ga-Sb oxides [14]. NH_4^+, NH_{3ads}, NH_2^- and NH groups are discussed to be active on vanadyl pyrophosphate [15]. If we compare the performance in propane ammoxidation of the vanadium aluminium oxynitride catalyst (acrylonitrile yield of 29.5%) with the catalytic results obtained on the vanadium aluminium oxide catalyst (acrylonitrile yield of 1.5%[16]), we can conclude that the catalytic activity is strongly related to the nitrogen species from the oxynitrides and that these species play a very important role in the acrylonitrile formation.

Nevertheless, no nitrogen insertion was found in [16] for the vanadium aluminium oxide system because once the oxide precursor is calcined and the $AlVO_4$ crystalline phase is formed, the nitrogen insertion in the network is almost impossible [12].

The effect of the reaction temperature and of the feed composition on the activity properties of VAlON system is shown in Figures 1 and 2. Optimal catalytic activity is achieved when the C_3:O_2:NH_3 molar ratio in the feed is 1.25:3.0:1.0, respectively, and the reaction temperature is 500°C.

For the formation of unsaturated nitriles, such as acrylonitrile from propane, the hydrocarbon activation is an important step, which proceeds at rather high temperatures compared with the formation of acrylonitrile from propylene. In order to identify the optimal range of temperature for propane ammoxidation over vanadium–aluminium oxynitrides, catalytic tests were carried out in the range of 400–550°C.

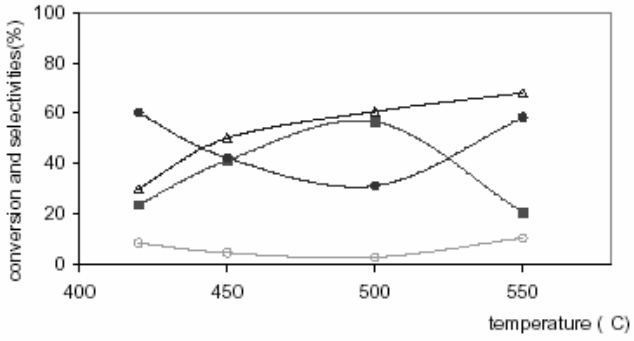

Fig. 1. *Catalytic behavior over VAlON catalyst (V:Al = 0.25) as function of the reaction temperature: GHSV = 16.800 m l/g h, C_3H_8:O_2:NH_3 = 1.25:3:1 (△) propane conversion; (■) ACN selectivity; (○) AcCN selectivity; and (●) CO_x selectivity*

Figure 1 shows the conversion of propane and product selectivities as a function of the reaction temperature over the vanadium–aluminium-based catalyst. The conversion of propane increased continuously with reaction temperature, while the selectivity to acrylonitrile increased with the temperature up to 500 °C and then decreased. Under these conditions, the maximum in selectivity to acrylonitrile corresponding to 55% was obtained at 500 °C. The selectivity to COx exhibited an opposite variation, namely, it progressively decreased up to 500 °C, while above this temperature most of the propane was oxidized. After 500 °C, traces of heavier products such as butanedinitrile were also detected.

The influence of the gas feed composition on propane ammoxidation was investigated under reaction conditions in which the catalyst showed the highest ACN selectivity value (T = 500 °C, GHSV = 16.800 ml/g h). The results are depicted in Figure 2.

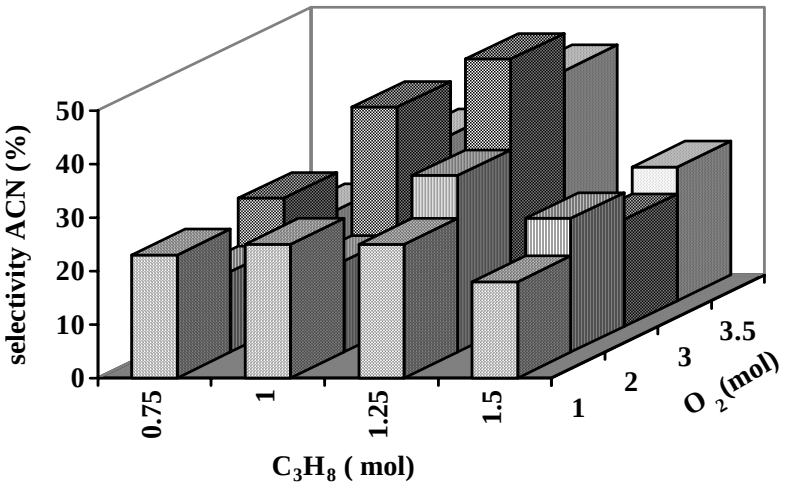

Fig. 2. *Catalytic behaviour over VAlON catalyst (V:Al = 0.25) as function of propane and oxygen molar ratio: GHSV = 16800 ml/g h, C3H8:O2:NH3 = X:Y:1*

The catalytic tests were performed by changing the contact time of one reactant and keeping the others constant. The total flow and the space velocity were kept constant by changing correspondingly the flow of helium used as diluent gas. These variations allowed the optimization of the gas composition of the mixtures subjected to the reaction.

Higher oxygen contents favor the oxidation of ammonia and under these conditions the V–NH_x species are transformed into V–O electrophilic ones, as already suggested [15]. However, a contact time of oxygen up to 3 mol of oxygen led to a large coverage of the catalyst surface with NH_x species, and for this value, the nitrogen content on the corresponding catalyst is about 3.2%. Under these conditions, the selectivity to acrylonitrile achieved 46.5%. It worth to note that even at higher contact time of oxygen, the formation of propylene was not observed.

Propane can also be a limiting reagent in the propane ammoxidation over VAlON catalysts and it seems that the propane:oxygen and propane:ammonia ratios have a significant influence on the catalyst selectivity. When very low contact times of propane are employed propylene is formed. Under these conditions, the conversion of propane reached 75% and the main reaction products were carbon oxides.

Thus, a proper feed composition provides a correct equilibrium between the active nitrogen and oxygen species. However, the activity of the VAlON catalyst is maximal when the molar ratio among C_3:O_2:NH_3 reactants is 1.25:3:1. This optimal molar ratio corresponds to a space time (W/F) of 7.69 g h/mol C_3, 3.11 g h/mol of O_2 and 10.2 g h/mol NH_3.

A series of transient experiments were conducted varying the O_2:NH_3 ratio in order to investigate the effect of the oxidation/reduction reaction environment on the catalytic activity of the VAlON system. The results are presented in Figure 3.

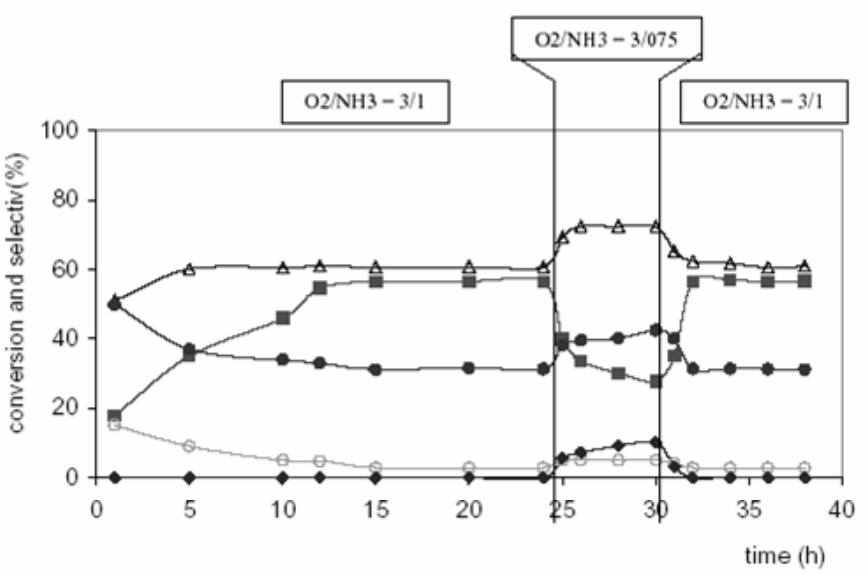

Fig. 3. *Catalytic behavior over VAlON catalyst (V:Al = 0.25) function of time on stream and function of O_2:NH_3 ratio: GHSV = 16800 ml/g h; C_3H_8:O_2:NH_3 = 1.25:3:X (X = 0.75 and 1), 500 °C (△) propane conversion; (■) ACN selectivity; (○) AcCN selectivity; and (●) CO_x selectivity, and (♦) propylene selectivity).*

After 24 h on stream, the O_2:NH_3 ratio was varied from 3:1 to 3:0.75 for 5 h. Subsequently, the reaction conditions used were the same as initially. Under these conditions, decreasing the O_2:NH_3 molar ratio had the following effects: (i) propane conversion increased, (ii) ACN selectivity decreased, (iii) CO_x selectivity increased, (iv) AcCN selectivity underwent a slight increase, and (v) propylene formation was detected. By changing the O_2:NH_3 ratio and returning to the initial conditions, the catalyst recovered the same catalytic activity and

selectivity, leading to the same selectivity to acrylonitrile, namely 56%. At the same time, propylene disappeared from the reaction products. Thus, a proper feed composition provides a correct equilibrium between the active nitrogen and oxygen species. These data obtained from transient experiments, clearly demonstrate that the catalytic behavior of the surface does not only depend on the presence of a particular surface species, but also depends on the nature of the changes in the surface reactivity induced by the adsorption of the reactants. It is also necessary to pay a special attention to the surface restructuring phenomena during the catalytic.

Comparative test conditions and activity results corresponding to the best performing propane ammoxidation catalysts vs VAlON system are shown in Table 2. Main observations are: i) all catalysts show differences in feed gas composition, reaction temperature and space velocity for achieving optimal ACN yield, ii) vanadium-molybdates system exhibits higher propane conversion at lower reaction temperature than V-Sb-W-Al-O and VAlON systems whereas, VAlON catalyst shows slightly higher ACN selectivity than Mo-V-Nb-Te-O systems, iii) ACN productivity is higher for the VAlON system than that obtained for Mo-V-Nb-Te-O (26 times) and for the V-Sb-W-Al-O (4 times) catalyst formulations and iv) propylene and HCN formation were reported for all Mo-V-Nb-Te-O and V-Sb-W-Al-O catalyst formulations. These products were not detected during catalytic reaction with the VAlON system, which suggests differences in reaction mechanism.

Table 2. Acrylonitrile productivity for different catalytic systems used in propane ammoxidation

Catalyst	Conv C_3H_8 (%)	select ACN (%)	Yield ACN (%)	W/F (g.h/moles C_3H_8)	Productivity (l ACN/kg.h)
Mo-V-Nb-Te-O	89.1	60.0	53.5	384.6	31.16
V-Sb-W-Al-O	77	48	37	53	164
V-Sb-O	30	26.6	8	2036	0.9
Fe-Sb-O	22	23	5	740	1.51
Ca-Bi-Mo	15	63	9.5	12	177
VAlON	59	50	29.5	8	812

Conclusion

In conclusion, the results of this work allow us to propose a new category of highly active catalysts for the alkane ammoxidation process based on metallo oxynitride materials. This novel catalytic system shows high ACN yield and competitive advantages in acrylonitrile productivityc per amount of catalyst and per time as compared with conventional vanadium-molybdates and vanadium-antimonates propane ammoxidation catalysts.

Acknowledgements

The authors thank the "Direction Générale des Technologies, de la Recherche et de l'Énergie" de la Région Wallonne (GREDECAT) and "La Communaute Française (ARC)" Belgium for financial support.

REFERENCES

1. Bowswell., C, (1999) "The technology Frontier: Alkane Activation" Chemical Market Reporter, 20.
2. Wiame, H., Cellier, C. and Grange, P. (2000) Journal of Catalysis **190**, 406.
3. Grzybowska-Swierkosz, B. (1997) Appl. Catal. A **157**, 409.
4. Luján Ferreira, M. and Volpe, M. (1999) J. Molec. Catal. A **149**, 33.
5. Luján Ferreira, M. and Volpe, M. (2000) J. Molec. Catal. A **164**, 281.
6. Khodakov, A., Olthof, B., Bell, A. and Iglesia, E., (1999) J. Catal. **181**, 205.
7. Kim, Y.C., Ueda, W. and Moro-oka, Y. (1990) Stud. Surf. Sci. Catal, **55**, 491.
8. Kim, J.S. and Woo, S. I. (1994) Appl. Catal. A **110**, 207.
9. Nilsson, R., Lindblad, T. and Andersson, A. (1994) J. Catal, **148**, 501.
10. Ratajczak, O., Zanthoff, H.W. and Geisler, S. (2000) Stud. Surf. Sci. Catal. **130**, 1685.
11. Davydov, A.A., Budneva, A.A. and Sokolovskii, V.D. (1979) Kinet. and Katal. **20**, 179.
12. Wiame, H., Bois, L., L'haridon, P., Laurent, Y. and Grange, P. (1997) Solid State Ionics **101-102,** 755.
13. Florea, M., Prada Silvy, R., Grange, P. (2003) Catal. Lett. **87**, 53.
14. Osipova, Z. G. and Sokolovskii, V. D. (1979) Kinet. and Katal. **20** 420.
15. Centi G. and Perathoner, S. (1993) J. Catal, **142**, 84.
16. Nilsson, J., Landa-Cànovas, A.R., Hansen, S. and Andersson, A. (1996) J. Catal, **160**, 244.

OXIDATIVE DEHYDROGENATION OF *N*-BUTANE OVER A MgO-SUPPORTED MAGNESIUM VANADATE CATALYST

I.-C. Marcu,[*] Adriana Urdă, I. Săndulescu

abstract : The catalytic and non-catalytic oxidative dehydrogenation of *n*-butane were investigated. It was found that in the non-catalyzed reaction the *n*-butane conversion not exceeds 4% at 550°C and the selectivities to butenes are significant only at temperatures below 450°C. Oxidative dehydrogenation was examined in the presence of mixed V-Mg-oxide catalyst comprising 24.5% V_2O_5. It was observed that the catalyst is active and quite selective for butenes and butadiene at reaction temperatures in the range 450 – 550°C. The selectivity to butenes decreased and the selectivity to butadiene increased with increasing conversion at 550°C. The low apparent activation energy observed (7 kcal.mol^{-1}), suggests that the rate-limiting step of the reaction is the reoxidation of the catalytic site by diffusion of the lattice oxygen or directly by gas phase oxygen.

keywords: V-Mg-oxide catalyst, oxidative dehydrogenation, *n*-butane.

Introduction

Vanadium-magnesium-oxides (V-Mg-O) are among the most selective and active catalysts for the oxidative dehydrogenation of *n*-butane to butene and butadiene, the orthovanadate phase being the selective phase [1]. Unfortunately, the selectivity and yield obtained in all literatures are too low to make the process commercially feasible [1-5].

In the present study, the catalytic oxidative dehydrogenation of *n*-butane is investigated over a range of temperatures and contact times for a stoichiometric butane/air ratio. MgO-supported magnesium vanadate is used as catalyst. The non-catalytic oxidative dehydrogenation of *n*-butane is also investigated.

Experimental

Catalyst preparation and characterization

The catalyst was prepared following a method described by Chaar et al. [1]. An appropriate amount of MgO powder was impregnated with a solution containing 1 wt % of ammonium vanadate and 0.5 wt % of ammonium hydroxide at 70°C. The resulting suspension was

[*] Department of Chemical Technology and Catalysis, Faculty of Chemistry, University of Bucharest, 4-12, Blv. Regina Elisabeta, 030018 Bucharest, Romania. Corresponding author: E-mail: marcu.ioan@unibuc.ro

Analele Universităţii din Bucureşti – Chimie, Anul XIV (serie nouă), vol. I-II, pg. 57-63

evaporated with stirring until a paste was obtained. The paste was dried for 18 h at 120°C. The resulting solid was calcined at 600°C for 4 h and then pelletized, crushed and sieved to the desired particle size. The catalyst composition used in this work was determined at 24.5 wt % V_2O_5 by means of inductively coupled plasma (SPECTROFLAME-ICP). The surface area of the sample was measured using the BET technique and the crystal phases were identified by X-ray diffraction using a Brüker D5005 diffractometer and Cu Kα radiation. Characterization of the catalyst has been performed before and after catalytic test. After catalytic test, the catalyst was recovered by cooling them down in the flow of reactants.

Catalytic test

The oxidative dehydrogenation of *n*-butane was carried out in a fixed bed quartz tube down-flow reactor operated at atmospheric pressure and in the temperature range of 400 – 550°C. The conditions of the catalytic test were described elsewhere [6]. A gas feed with an air to *n*-butane ratio equal to 5 and an hourly space velocity (VVH) of 1000 h^{-1} with respect to *n*-butane were used. When the effect of the VVH on the catalytic properties of the catalyst was studied, this was varied in the range 500 – 2000 h^{-1}. Quartz chips were used to fill the dead volumes before and after the catalyst bed to minimize potential gas-phase pyrolysis reactions at higher reaction temperatures. In the non-catalytic experiments, the catalyst bed was replaced with quartz chips having the same particle size. The major products formed under these reaction conditions were 1- and 2-butenes, butadiene, CO, CO_2, and cracking products (methane, ethane, ethylene and propylene).

Results and discussion

Catalyst characterization

The specific surface area of the solid as prepared was slightly over 20 $m^2.g^{-1}$. In the XRD pattern of this material, presented in figure 1.a, only the peaks indicating the presence of MgO are evidenced. A diffuse band between 20 and 40° is also observed, indicating a much less crystallized or more dispersed form of orthovanadate. Before the catalytic test, this solid was treated in the reactor at 600°C in the flow of reactants for 6 hours. The specific surface area of the resulted catalyst was only 12 $m^2.g^{-1}$ and the XRD pattern of this material (fig. 1.b) clearly shown the presence of the crystalline Mg orthovanadate ($Mg_3(VO_4)_2$). Neither pyro- ($Mg_2V_2O_7$) nor meta-vanadates (MgV_2O_6) are observed in this pattern. This activated catalyst was tested in the oxidative dehydrogenation reaction.

After catalytic test, the specific surface area remained almost the same and the XRD pattern of the solid was not affected by the test.

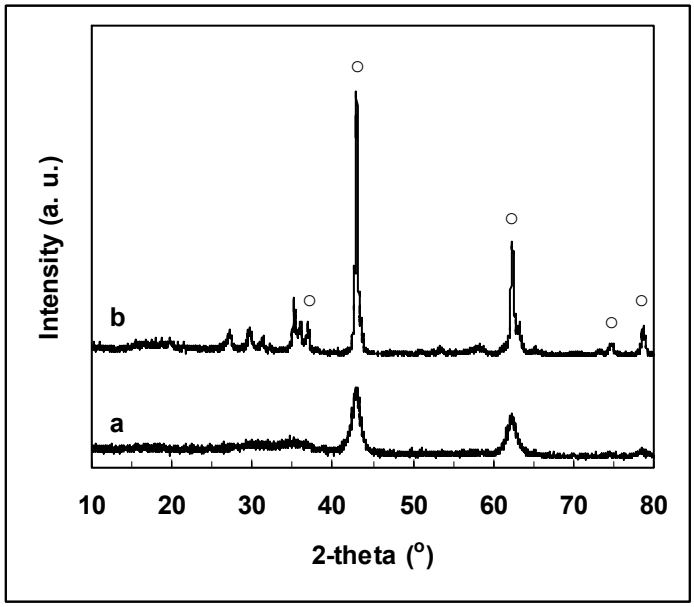

Fig. 1. *XRD patterns of the catalyst (a) as prepared and (b) after activation in the flow of reactants (○ - peaks corresponding to MgO phase).*

Non-catalytic oxidative dehydrogenation

The non-catalytic oxidative dehydrogenation of *n*-butane was investigated using a residence time of 0.6 s. The residence time was calculated by dividing the volume of the quartz chips bed replacing the catalyst (2 cm^3) by the volumetric flow rate of the feed

Fig. 2 shows the conversion of *n*-butane and the distribution of products as a function of reaction temperature. The conversion of *n*-butane is very low, at 550°C only 4% of butane being converted. The selectivity to butenes is high (~ 90%) at 410°C, but decreases to 30% as the temperature is increased to 550°C. Butadiene was not detected. The selectivity to cracking products is low at low temperatures and increases up to 54% at 550°C. The selectivity to combustion products (CO_x) is quite low and increases slightly in the range of temperatures used.

Summarizing, the non-catalytic oxidative dehydrogenation reaction of *n*-butane is not important in our conditions and the selectivities to butenes are significant only at temperatures below 450°C. Lemonidou et al. [7] shown that this reaction is very important in the range of temperatures of 530 – 580°C but using an empty reactor. When the reactor was fulfilled with inert quartz particles, only 2.5% of *n*-butane was converted at 580°C.

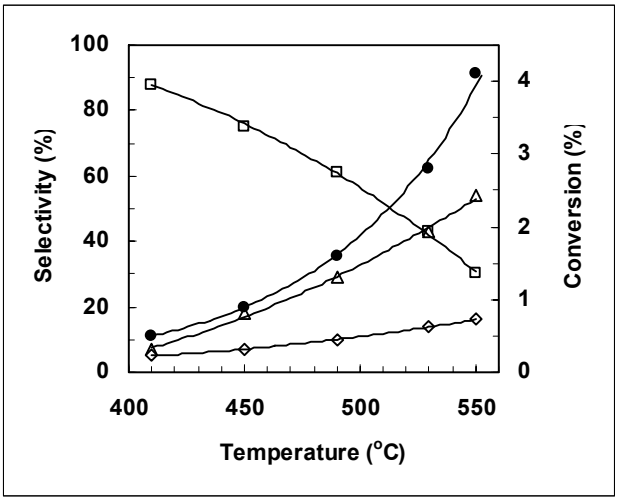

Fig. 2. *Effect of reaction temperature on the non-catalytic oxidative dehydrogenation of n-butane: n-butane conversion (●) and selectivities for butenes (□), CO_x (◇) and cracking products (△).*

Catalytic oxidative dehydrogenation

The results obtained in the presence of the MgO-supported magnesium vanadate catalyst are shown in figure 3. As expected, an increase in the temperature resulted in an increase in the conversion: from 13% at 450°C to 24% at 550°C. The selectivity for butadiene actually increased (from 17 to 32%), while this of the butenes decreased (from 39 to 31%), but the total dehydrogenation selectivity (TDS) remained almost the same between 490 and 550°C. There was a slight increase in the selectivity for the cracking products and, contrarily to results obtained by Chaar et al. [1], the selectivity for the combustion products decreased with increasing temperature. The same tendance was observed in the tests with a void post-catalytic volume reported by Lemonidou et al. [7].

The effect of the VVH on the conversion and on the total dehydrogenation selectivity at 550°C is shown in figure 4. The conversion decreased linearly when the VVH with respect to *n*-butane was increased from 500 to 2000 h^{-1} and the total dehydrogenation selectivity increased. These results are in agreement with the fact that the conversion of *n*-butane and the selectivity to butenes and butadiene are inversely related.

The influence of the conversion on the product distribution is depicted in figure 5. While the selectivity to butenes decreases with the conversion from 46 to 28%, the selectivity to butadiene increased from 25 to 33%. The selectivity to butenes decreased due to the formation of butadiene and carbon oxides in a consecutive reaction. The selectivity to cracking products decreases with increasing conversion, probably due to subsequent oxidation to carbon oxides. Finally, Fig. 5 also illustrates the well-known fact that butenes are primary products, with a high selectivity at low conversion (low contact time), while the secondary product butadiene appears at higher contact times.

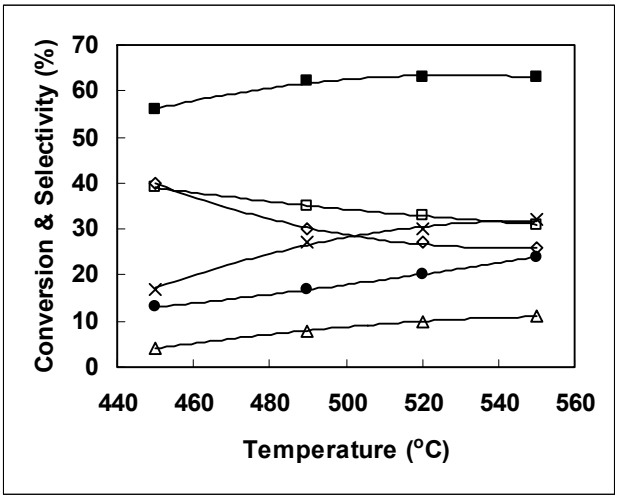

Fig. 3. *Effect of reaction temperature on the oxidative dehydrogenation of n-butane over $Mg_3(VO_4)_2$/MgO: n-butane conversion (●), total selectivity for dehydrogenation products (TDS) (■) and selectivities for butenes (□), butadiene (x), CO_x (◇) and cracking products (Δ).*

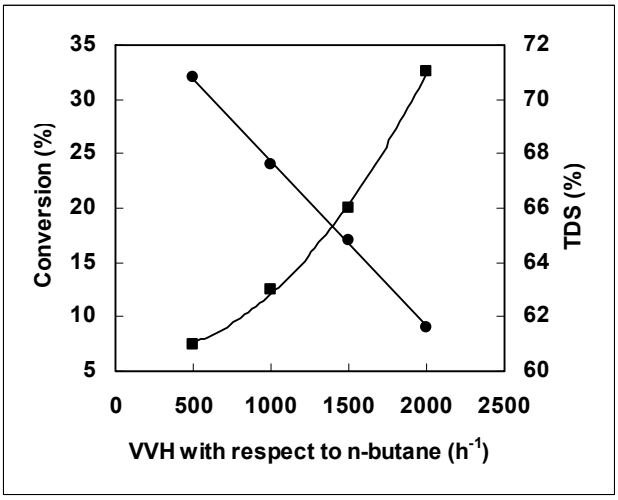

Fig. 4. *Effect of VVH on the conversion (●) and on the total selectivity for dehydrogenation products (TDS) (■) in the oxidative dehydrogenation of n-butane over $Mg_3(VO_4)_2$/MgO catalyst at 550°C.*

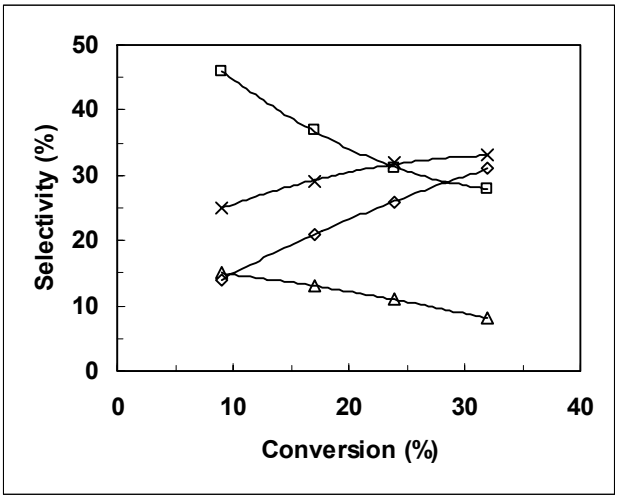

Fig. 5. *Effect of conversion on the selectivities in butenes (□), butadiene (x), CO_x (◇) and cracking products (Δ) in the oxidative dehydrogenation of n-butane over $Mg_3(VO_4)_2$/MgO at 550°C.*

The apparent activation energy for the reaction of *n*-butane was calculated from the Arrhenius plot over the range from 450 – 550°C (figure 6).

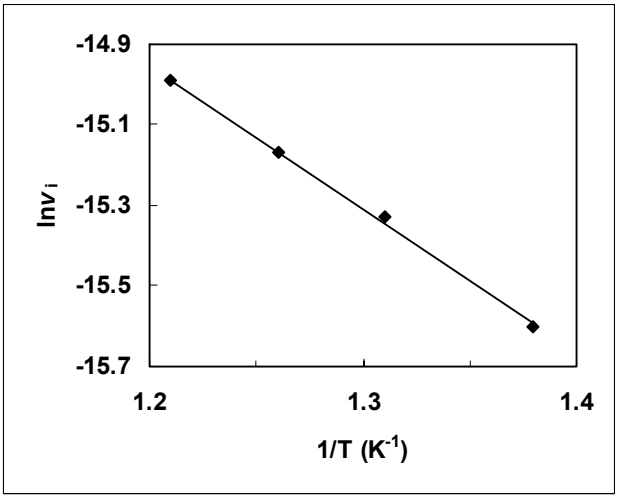

Fig. 6. *Arrhenius plot for the n-butane conversion on $Mg_3(VO_4)_2$/MgO catalyst.*

The obtained value is low, namely 7 kcal.mol^{-1}. Taking into account that the Mars – van Krevelen mechanism is the reaction mechanism in this case [8, 9], this low value of the apparent activation energy suggests that the rate-limiting step of the reaction is the reoxidation of the catalytic site by diffusion of the lattice oxygen or directly by gas phase oxygen, like in the case of titanium pyrophosphate (TiP_2O_7) catalyst in the same range of

temperatures [10]. Patel et al. [11], reported, for the same reaction in the same range of temperatures, an apparent activation energy equal to 22 kcal.mol^{-1}, but they worked with a rich-oxygen reaction mixture. This means that, when the oxygen content in the feed is not sufficient for the reoxidation of the catalytic site, like in our case, this becomes the rate-limiting step of the reaction.

Conclusion

In the non-catalyzed oxidative dehydrogenation, the *n*-butane conversion not exceeds 4% at 550°C and the selectivities to butenes are significant only at temperatures below 450°C. Butadiene was not detected.

MgO-supported $Mg_3(VO_4)_2$ catalyst is active and quite selective for butenes and butadiene at reaction temperatures in the range 450 – 550°C. The maximum yield was obtained at 550°C and a VVH of 500 h^{-1} with respect to *n*-butane, with selectivities in butenes and butadiene of 28% and 33%, respectively, for 32% conversion.

The apparent activation energy for *n*-butane conversion on $Mg_3(VO_4)_2$/MgO catalyst was 7 kcal.mol^{-1}. This low value suggests that the rate-limiting step of the reaction is the reoxidation of the catalytic site by diffusion of the lattice oxygen or directly by gas phase oxygen.

REFERENCES

1. Chaar, M.A., Patel, D., Kung, M.C., and Kung, H.H. (1987) *J. Catal.,* **105,** 483.
2. Blasco, T., López Nieto, J.M., Dejoz, A., and Vazquez, M.I. (1995) *J. Catal.,* **157,** 271.
3. López Nieto, J.M., Dejoz, A., Vazquez, M.I., O'Leary, W., and Cunningham, J. (1998) *Catal. Today,* **40,** 215.
4. Lemonidou, A.A., Tjatjopoulos, G.J., and Vasalos, I.A. (1998) *Catal. Today,* **45,** 65.
5. Téllez, C., Abon, M., Dalmon, J.A., Mirodatos, C., and Santamaria, J. (2000) *J. Catal.,* **195,** 113.
6. Marcu, I.C., Sandulescu, I., and Millet, J.M.M. (2002) *Appl. Catal. A*, **227**, 309.
7. Lemonidou, A.A., and Stambouli, A.E. (1998) *Appl. Catal. A*, **171**, 325.
8. Kung, H.H. (1994) *Adv. Catal.,* **40,** 1.
9. Mamedov, E.A., and Cortes-Corberan, V. (1995) *Appl. Catal. A*, **127**, 1.
10. Marcu, I.C. (2002) **PhD Thesis No. 64-2002**, University Lyon I.
11. Patel, D., Kung, M.C., and Kung, H.H. *in* M.J. Philips and M. Ternan, Eds., **Proceedings 9th International Congress on Catalysis**, (1988) vol. 4, p. 1554, Chem. Institute of Canada, Ottawa.

[1] HYDROTALCITE-LIKE COMPOUNDS, SOLID-BASE CATALYSTS FOR CYANOETHYLATION REACTION

O.D. Pavel[*], Ruxandra Bîrjega[**], E. Angelescu[*], S. Popoiu[***]

abstract: The layered double hydroxide (LDH) with chemical composition $LiAl_2(OH)_7 \cdot 2H_2O$ was prepared via a wet chemical route of gel to crystallite conversion. This solid-base compound and the mixed oxides resulting by LDH calcination were characterised by XRD, FT-IR and porous structure and then tested in the cyanoethylation of ethanol with acrylonitrile reaction.
The catalitic activity was compared with those obtained using catalyst samples $Li/Al(OH)_3$, Li/Al_2O_3, Na/Al_2O_3, K/Al_2O_3 prepared by wet impregnation.

keywords: Li-Al hydrotalcite, mixed oxides Me^I/Al_2O_3 (Me^I=Li, Na, K), cyanoethylation reaction

Introduction

Much attention has been paid over a recent years to the establishments of ecologically acceptable processes in the chemical synthesis. Therefore, the use of basic solid catalysts as hydrotalcite-like compounds (HT) and admixture of oxides obtained by calcinations of hydrotalcite (CHT) is an area of growing interest due to the following advantages: easy separation of catalysts from the reaction mixture, reusable catalysts, easy modification of the basic strength sites and their pore structure [1, 2, 3, 4].

Hydrotalcites consist of brucite-like layers having positive charge with anionic species in the interlayer, forming neutral materials with the general formula: $[M^{2+}_{1-x}M^{3+}_x(OH)_2]^{x+}[A^{n-}_{x/n}]\cdot mH_2O$ where M^{2+} and M^{3+} are respectively divalent and trivalent metal like Mg^{2+} and Al^{3+}, A^{n-} is an anion and x can have values between 0.2-0.33 [5].

The possibility of preparing hydrotalcites with nominal composition $[M^{1+}_{1-x}M^{3+}_x(OH)_2]^{(2x-1)+}[A^{n-}_{2x-1/n}]\cdot mH_2O$ is limited only to Li^+ which has an anionic radius comparable to that of M^{2+} even the HT structure presents important differences in comparison with Mg-Al hydrotalcites [2]. With other monovalent cations, the corresponding double hydroxycarbonates of aluminium are dawsonite-type compounds [6].

[*] University of Bucharest, Faculty of Chemistry, Department of Chemical Technology and Catalysis 4-12 Regina Elisabeta, Bucharest 3, 030018, Romania
[**] S.C. ZECASIN S.A., 202 Splaiul Independentei, Bucharest 6, Romania
[***] PETROM S. A. INCERP – Research, no. 291 A, Blv. Republicii, Ploiesti, Romania

Analele Universităţii din Bucureşti – Chimie, Anul XIV (serie nouă), vol. I-II, pg. 65-72

In the conventional (HT) the M^{2+} and M^{3+} occupy the some set of octahedral sites and there is no evidence for ordering of the cations. In the Li-Al (HT), the structure is constituted by the layer containing the cations in which Al octahedral are arranged as in gibbsite and the octahedral vacancies are filled by lithium ions [7].

Mg-Al hydrotalcites [8] and modified Mg-Al HT with Y, Gd, Sm, Dy or La ions [9, 10] and the corresponding mixed oxides obtained by calcinations of HT precursors act as base solid catalysts for the cyanoethylation of ethanol with acrylonitrile under mild reaction conditions and there are reusable without an appreciable loss of activity and selectivity. This conjugated addition gives β-ethoxypropionitrile which can be converted to a carboxylic acid by hydrolysis and into corresponding amine by reduction, giving compounds of industrial interest for drug intermediates [9, 10].

Combination of different elements for HT synthesis, changing the element ratios in the brucite-like layer, selection of different anionic species and modified HT by addition of alkaly cations, can tune up the basicity of HT, the interlayer distance and the catalytic properties.

Here we report the results of preparation of Li-Al HT and the corresponding mixed oxides obtained by calcinations of HT precursors and their structural properties in correlation of their activity and selectivity in the cyanoethylation of ethanol with acrylonitrile. The catalytic performances of the modified $Al(OH)_3$ and Al_2O_3 by addition of Li, Na, K ions (5% w/w) have been also studied in the cyanoethylation reaction.

Experimental

Catalysts preparation.

A layered double hydroxide with chemical composition $LiAl_2(OH)_7 \cdot 2H_2O$ was prepared by a wet chemical route of gel to crystallite conversion at 80ºC involving the reaction of hydrated alumina gel Al_2O_3 yH_2O ($80<y<120$) with LiOH ($Li_2O/Al_2O_3>0.5$) in presence of hydrophilic solvents such as ethanol under refluxing conditions.

The hydrated alumina gel were obtained by addition of concentrated ammonia solution (25% w/w) to an aqueous solution of $Al(NO)_3 \cdot 9H_2O$ till the pH was 8.0. The $Al(OH)_3$ gel was filtered, washed free of anion using hot and demineralized water, then was dried at 90ºC for 12 hours.

To obtain Li-Al HT the $Al(OH)_3$ gel was suspended in a conical flask containing an ethanolic solution of lithium hydroxide (four-fold excess of Li over the aluminum content Li/Al=4 in 50 ethanol and 50 % water). The reaction vessel was filted with a water-cooled condenser an alkali guard tube to prevent the contamination of CO_2 and refluxed for 8 hours under continuously magnetic stirring. The solid product obtained was washed free of unreacted LiOH (pH≈8-8.5) then filtred and dried at 90ºC for 24 hours. The mixed oxides were obtained by calcinations the dried hydrotalcite Li-Al at 460ºC for 18 hours under nitrogen flow. In order to check whether the catalysts Li/Al_2O_3 obtaining by wet impregnation present different activity and selectivity in the cyanoethylation of ethanol with acrylonitrile by comparison of dried and calcinated Li-Al HT were prepared samples

containing 5% Li (w/w) by wet impregnation of $Al(OH)_3$ and respectively γ-Al_2O_3 with aqueous solution of Li(OH). Also samples with 5% Na and respectively K on alumina. After impregnation the samples were dried at 70ºC for 12 hours and then calcined at 460ºC, 3 hours in air flow.

Catalysts characterization

The X-ray diffractions (XRD) patterns were recorded on a computer controlled DRON-3 X-ray diffractometer equipped with a graphite monochromator using the CuK_α radiation (λ=1.5418 Å) in a 2θ range of 7-90^o, a step width of 0.05^o and an acquisition time of 2s on each step.

Surface area were determined from N_2 adsorption-desorption isotherms, using BET equation.

FT-IR spectra was recorded by spectrometer BioRad FTS 135 using KBr pellet techniq. The specter was recorded between 400 – 4000 cm^{-1}.

Catalytic measurements

A typical procedure for the cyanoethylation of ethanol with acrylonitrile: into a reaction vessel equipped with a reflux condenser were successively placed the catalyst (0.0711g) ethanol (0.03 mmol; 1.7 ml) and acrylonitrile (0.01 mmol; 0.65 ml). The resulting mixture was stirred and heated on a silicon oil bath and refluxed for 5 hours. The conversion and selectivity of acrylonitrile into β-ethoxypropionitrile were determined by GC analysis using a Thermoquest equipment with a FID detector and a capillary column (30 m length; i.d. 0.324 mm) with DB-5 stationary phase.

Results and disscusion

The porous structure of catalysts containing lithium are reported in Table 1.

Table 1. Porous structure of calcinated catalysts containing lithium

Sample	$Li_2O{\cdot}2Al_2O_3$	$Al(OH)_3$+LiOH	Al_2O_3+ LiOH
Surface area ($m^2{\cdot}g^{-1}$)	163	196	178
Pore volume ($m^3{\cdot}g^{-1}$)	0.1587	0.2487	0.2336
Mean pore size (Å)	22	36	27

Figure 1 presents the XRD patterns of the Li based catalysts samples prepared as below along with their corresponding calcinated samples. The XRD patterns shows:

- The Li based catalyst has the structure of a layered double hydroxide of $LiAl_2(OH)_7{\cdot}2H_2O$ type (JCPDS 40-0710). (denoted HT Li/Al dried (1))
- Its calcinated form (HT Li/Al calc. (2)) presents a mixture of very fine particles of a poor crystallized γ-Al_2O_3 phase and large crystallites of a Li_2CO_3-zabeyelite phase (JCPDS 22-1141).
- The Li based catalyst prepared by impregnation on a boehmite type AlO(OH) presents the structure of this boehmite phase with very broad peaks ($Li/Al(OH)_3$).

- Its calcinated form ($Li/Al(OH)_3$ (3)) shows the formation of the structure of a layered double hydroxide of $LiAl_2(OH)_7{\cdot}2H_2O$. The LDH phase is poor crystallized and presents broader peaks characteristic of a material with very small crystallites. An amorphous mixed oxides phase is to be presume as the background is very high and the peak intensities of the Li/Al-LDH phase are lower.

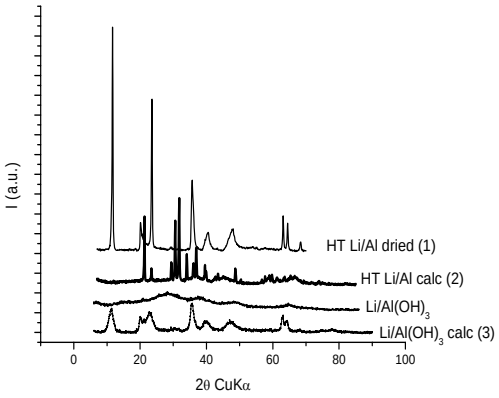

Fig. 1. *The XRD patterns of the Li based catalysts samples along with their corresponding calcinated samples.*

The XRD patterns of the Li, Na and K supported on γ-Al_2O_3 (Li,Na,K/Al_2O_3 (4,5,6)) are shown in figure 2. The patterns shows the preservation of the a γ-Al_2O_3 phase with no by-products originated from deposed phase, except for Li case. For Li on a γ-Al_2O_3 very fine particle of Li_2CO_3-zabeyelite phase (JCPDS 22-1141) are detected. The results account for the a highly dispersion of the active phase on the γ-Al_2O_3 support, probably due to the mesoporous properties of the γ-Al_2O_3 selected.

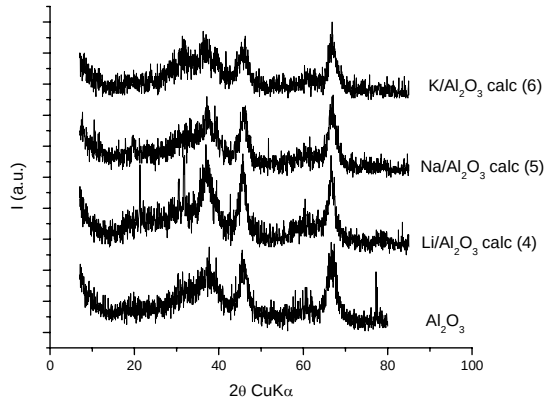

Fig. 2. *The XRD patterns of the Li, Na and K supported on γ-Al_2O_3*

The FT-IR spectra of $LiAl_2(OH)_7{\cdot}2H_2O$ HT is shows in figure. 3.

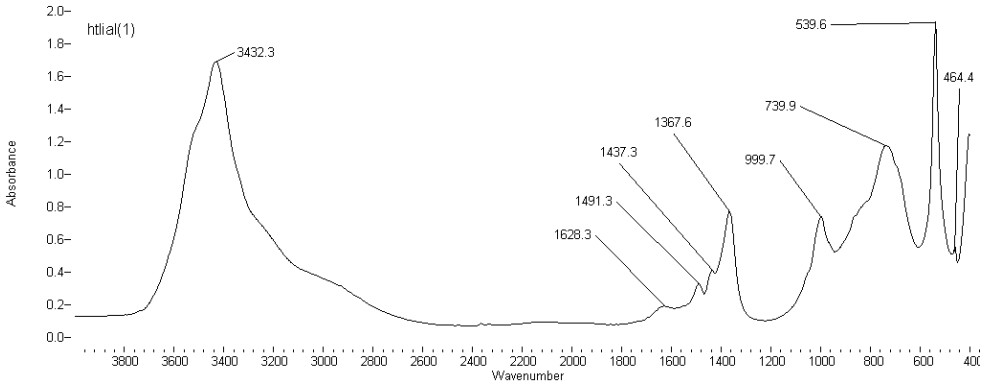

Fig. 3. *The FT-IR spectra of $LiAl_2(OH)_7{\cdot}2H_2O$ HT*

The IR absorption spectra for the sample heated to 100ºC shows a broad absorption band centered at 3432 cm^{-1} awing to the O-H stretching frequencies from hydrogen bonded as well bridged hydroxy groups. Sharp peaks at 1000, 740 and 539 cm^{-1} are characteristics of AlO_6 octahedra.

For the sample heated to 250ºC the band at 3432 cm^{-1} is reduced in intensity because the hydroxy groups are removed.

The peak at 1367 cm^{-1} vanishes, a doublet appears at 1550 cm^{-1} and a new peak was observed at 1200 cm^{-1}. Also the number of peaks between 1000 and 500 cm^{-1} reduced to one centered around 550 cm^{-1}.

The results of the thermal analyses are giving in figure 4.

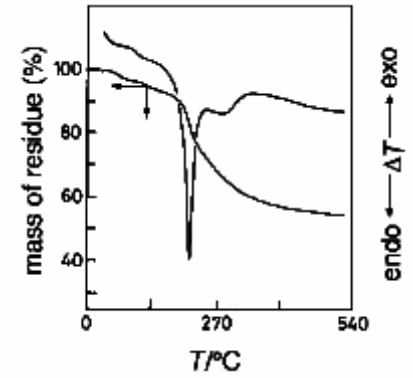

Fig. 4. *DTA traces of $LiAl_2(OH)_7$*

It has shown that for the dried Li-Al HT a total mass loss of ca. 51-54% up to 540ºC is in a good agreement with data previously reported [11, 12].

The mass loss (5-8%) below 100ºC is due to the loss of physically adsorbed water.

Between 100 and 200ºC a 16% mass loss accompanied by a very strong endothermic peak in the DTA is due to the removal of the structural water.

Between 200 and 500ºC the mass loss (ca. 30%) is for the dehydroxylation of surface; DTA shows a broad and shallow endothermic effect centered around 270ºC. Probable the following reaction occurs:

$$1)LiAl_2(OH)_7 \cdot 2H_2O \xrightarrow{150^0 C} LiAl_2(OH)_7 + 2H_2O \quad \Delta m = 16\%$$

$$2)LiAl_2(OH)_7 \xrightarrow{200-400^0 C} LiAl_2O_3(OH) + 3H_2O$$
$$3)4LiAl_2O_3(OH) \xrightarrow{400-500^0 C} 2Li_2O \cdot 2Al_2O_3 + 2H_2O \qquad \Delta m = 35.6\%$$

The Li content, determined by wet chemical analysis using atomic absorption spectroscopy (AAS) for the dried and respectively calcinated sample were 3.84% an respectively 5.62% (w/w), in good agreement with these thermal transformations.

Figure 5 shows the catalytic activity of these solid-base catalysts represented as the acrylonitrile conversion.

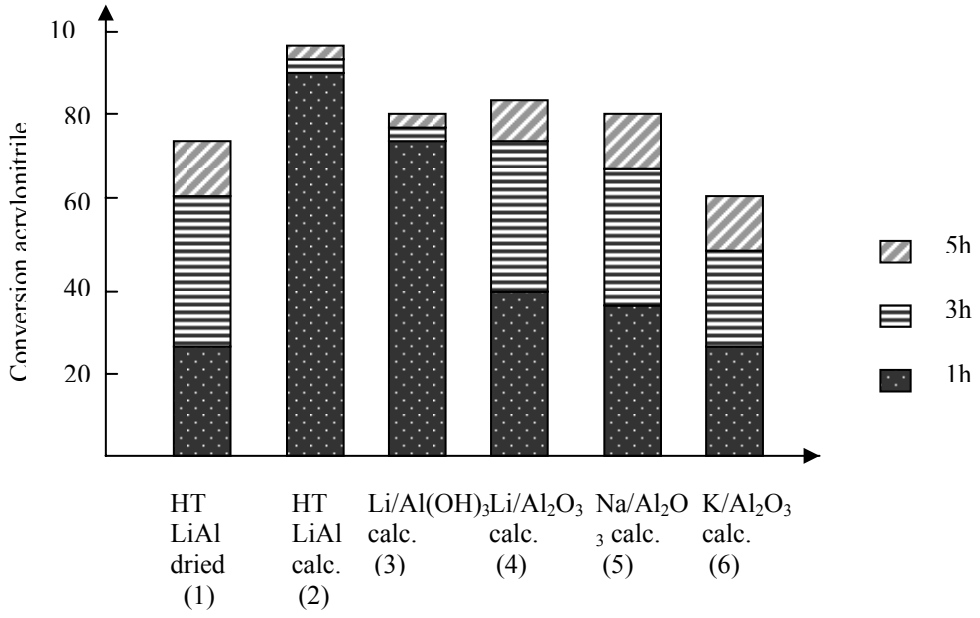

Fig. 5. *The variation of acrylonitrile conversion against the reaction time*

Although there are no significant difference of porous structure between the catalysts containing lithium a very important parameter of catalytic activity appeared to be the nature of precursors. The dried $LiAl_2(OH)_7$ sample shows a low activity even after five hours reaction time. High activity is characteristic of the calcined Li-Al LHD ($Li_2O \cdot 2Al_2O_3$) which provides 97% acrylonitrile conversion and 93% after one hour reaction time.

A similar behavior is shown for the sample obtained by impregnation of $Al(OH)_3$ with LiOH solution even the total conversion after five hours did not exceed 79%.

Low reaction rate is proper for the catalyst obtained by impregnation of Al_2O_3 with LiOH solution even the final conversion after five hours rises up to 84%. A similarly behaviors were shown the catalysts Na-Al_2O_3 and K-Al_2O_3. The activity of the catalysts which decreased with increasing the strength basicity of alkaline oxides suggested that the cyanoethylation reaction is catalyzed by the week and medium basic sites.

For all catalysts the selectivity of β-ethoxypropionitrile was 100%.

Because the preparation of precursors $LiAl_2(OH)_7$ and $LiOH/Al(OH)_3$ for catalysts (2) respectively (3) used $Al(OH)_3$ and aqueous LiOH solution and quite similar condition of preparation justify the high initial rate of reaction is due to some amount of $LiAl_2(OH)_7$ in the catalyst (2) composition (as is attested by the XRD measurements). The high activity of catalyst (2) obtained by calcinations of $LiAl_2(OH)_7$ precursor is probable a result from of highly disorder structure, small size crystals, accessibility of the active basic sites and the defect sites induced by lithium insertion in Al_2O_3 structure. All these elements could lead to a synergistic effects.

Conclusions

Li-Al LDH is an effective precursors for the manufacturing of mixed oxides catalysts in the reaction of cyanoethylation of ethanol with acrylonitrile.

These results show that the main parameter of catalitic activity is the nature of precursors. The high activity of calcined catalyst is a result from a highly disordered structure, small size crystals, defect sites and a weak and medium basicity of solid.

REFERENCES

1. A. de Roy, C. Forano, K.L.Malki, J.P.Besse **Synthesis of Microporous Materials**, vol. 2, Expanded Clays and Other Microporous
2. F. Cavani, F. Trifiro, A. Vaccari (1991) Catal. Today 11, 173
3. J. Palomeque, J. Lopez, F. Figueras (2002) J. Catal. 211, 150-156
4. K. Yamaguchi, K. Ebitani, K. Kaneda (1999) J. Org. Chem. 64, 2966-1968
5. F. Cavani, F. Trifiro, A. Vaccari (1991) Catal. Today 11, 173
6. M. J. H. Hernandez-Moreno, M. A. Ulibarri, J. L. Rendon and C. J. Serna (1985) Phys. Chem. Minerals 12, 34
7. C. J. Serna, J. L. Rendon, J. E. Iglesias (1982) Clays and Clay Minerals 30, 180
8. P. S. Kumbhar, J. Sancez-Valente, F. Figueras (1989) Chem. Commun., 1091
9. E. Angelescu, O. D. Pavel. M. Che, R. Birjega, G. Costentin (2004)5, 647-651
10. E. Angelescu, R. Birjega, O. D. Pavel, M. Che, G. Costentin, S. Popoiu, Stud. Surface Sci. and Catal., in press
11. K. R. Poppelmeier, S. J. Hwu (1987) 26, 3297
12. N. Nayak, T. R. N. Kutty, V. Jayaraman, G. Periaswamy (1997) J. Mater. Chem. 7 (10), 2131

CORRELATION BETWEEN TEXTURAL PARAMETERS AND CATALYTIC ACTIVITY IN OXIDATIVE DEHYDROGENATION OF n-BUTENES OVER Bi-Mo-Fe-O CATALYSTS

I. Săndulescu[*], **I. V. Nicolescu**

abstract: The mechano-topochemical method for preparation of Bi-Mo-O and Bi-Mo-Fe-O catalysts improved the activity and selectivity in oxidative dehydrogenation of n-butenes, compared with the catalysts prepared by classical methods. Addition of Fe_2O_3 to the binary catalytic system increases the catalytic performances of Bi-Mo-O oxides. Between the textural characteristics of catalysts and kinetic parameters of oxidative dehydrogenation reaction there are some correlations, which could be taken in consideration for selecting such catalysts.

keywords: oxidative dehydrogenation, n-butenes, Bi-Mo-Fe-O catalyst

Introduction

Oxidative dehydrogenation of n-butenes to butadiene is now an industrial process, which has replaced entirely the classical process of dehydrogenation. This one because the introduction in system of an hydrogen acceptor, which is oxygen, displaces so strongly the reaction equilibrium, that practically the conversion might not be related to equilibrium conditions. Therefore, the butadiene yield increases to about 65-70% and selectivity to 90-95%, per run, at 400-460^{o}C. Since the reaction is highly exothermic, a great deal of conventional fuel is saved [1-3].

The importance of the problem for the industrial practice, the diversity of literature concerning the catalytic systems and preparation methods have conducted to a large number of researches regarding correlations between the nature of active phases, catalyst composition, textural parameters and activity in oxidative dehydrogenation of n-butenes in butadiene [4-7].

In this paper, the activity and selectivity of catalytic systems Bi_2O_3-MoO_3 (Bi/Mo = 0.5:1.0) and Bi_2O_3-MoO_3-Fe_2O_3 (Bi/Mo/Fe = 0.5:1.0:1.2) are compared, and some correlations between textural parameters and the absolute rate of oxidative dehydrogenation over both systems are established.

[*] University of Bucharest, Faculty of Chemistry, Blvd. Regina Elisabeta 4-12, Bucharest, Romania

Analele Universităţii din Bucureşti – Chimie, Anul XIV (serie nouă), vol. I-II, pg. 73-80

Experimental

Catalysts Bi_2O_3-MoO_3 (Bi/Mo = 0.5:1.0) and Bi_2O_3-MoO_3-Fe_2O_3 (Bi/Mo/Fe = 0.5:1.0:1.2) were prepared and characterized [8].

Catalysts were prepared by „mechano-topochemical" method, which consists in a mechanical mixing of components (in solid phase, as crystals-hydrates) with an alkaline component – ammonium carbonate, also in solid state. We used bismuth nitrate, $Bi(NO_3)_3 \cdot 4H_2O$, ammonium paramolibdate $(NH_4)_6(Mo_7O_{24}) \cdot 4H_2O$ and respectively $Fe(NO_3)_3 \cdot 9H_2O$.

The solid-solid interface reaction took place in a dense fluid medium made up of crystal water according to a topochemical reaction mechanism [9].

Catalytic tests of oxidative dehydrogenation of n-butenes were carried out in a dinamic reactor in fixed bed of catalyst. n-Butenes used were 97.8% purity, with 61.4% 1-butene and 36.4% 2-butenes. The hydrogen acceptor was atmospheric oxygen and the diluent was steam.

The activity and selectivity of both catalysts were determined under the following conditions : temperature 400-520^oC ; volumetric flow rate 600h^{-1} for n-butenes ; molar ratio n-butene : air : steam = 1 : 3.5 : 7.5.

The textural properties of catalyst were determined.

Results and discussion

The „mechano-topochemical" method, in this case, allowed us to obtain catalytic systems more active than the same ones prepared by other methods. Therefore, in the case of Bi_2O_3-MoO_3-Fe_2O_3 (Bi/Mo/Fe = 0.5:1.0:1.2) catalyst, in table 1 comparative results obtained for the three different methods of preparation are presented.

A - mechano-topochemical method;

B – mixing equivalent quantities of oxide components, in order to obtain the desired atomic ratio, followed by thermal treatment;

C – mixing equivalent quantities of some metallic compounds (bismuth nitrate, iron nitrate, molybdenic acid), followed by thermal treatment.

Table 1. The influence of preparation method on activity of ternary system Bi/Mo/Fe = 0.5 : 1.0 : 1.2. Reaction temperature 440^oC; volumetric flow rate of n-butenes 600 h^{-1}; molar ratio n-butenes : air : steam = 1.0 : 3.5 : 7.5.

Preparation method	n-Butenes conversion (wt %)	Butadiene yield (wt %)	Butadiene selectivity (wt %)
A	49.4	42.6	86.2
B	56.2	49.8	88.4
C	67.2	62.0	92.3

In the following experiments, we used only catalysts prepared by mechano-topochemical method.

By comparing the binary and ternary systems, the introduction of iron shifts the optimum range reaction temperature to smaller values.

In fig. 1, we present comparatively the two catalysts. In the case of binary catalyst, activity increases with increasing temperature up to 480°C, at higher values the butadiene yield being practically constant. The selectivity to butadiene decreases, but until 480°C it is over 90% [9].

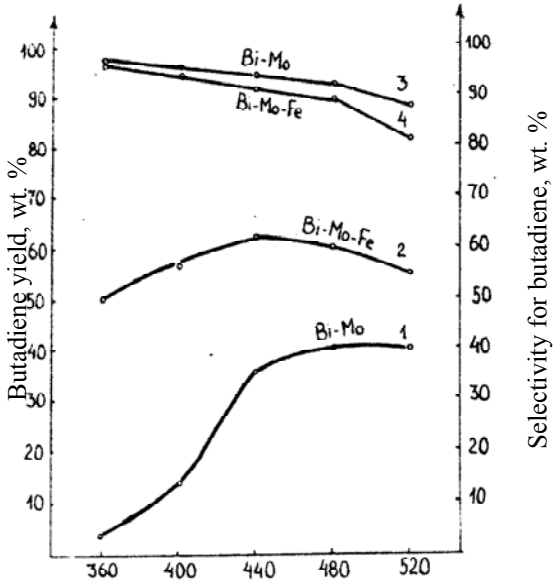

Fig. 1. *The activity and selectivity of Bi/Mo and Bi/Mo/Fe catalysts as a function of reaction temperature; 1,2 – yields; 3,4 – selectivities.*

For the ternary system, optimum of reaction temperature is 440°C, where the yield to butadiene is over 60%, but above this temperature, it decreases. In the same time, the selectivity to butadiene is over 90% until 480°C. Notice that for the ternary system the best results are obtained between 420 and 440°C.

For establishing the optimum contact time for oxydehydrogenation reaction, the volumetric flow rate of n-butenes varied between 200 and 1200 h^{-1}, and a total flow rate between 2400 and 14400 h^{-1}. This means that the contact time for n-butenes was from 18 to 3 seconds, and for the whole mixture between 1.5 and 0.25 s.

Figure 2 shows the variation of catalyst performances versus volumetric flow rate of n-butenes, for the ternary catalyst. It can be seen that oxydehydrogenation reaction takes place with increasing reaction rates in the range of 400-900 h^{-1}.

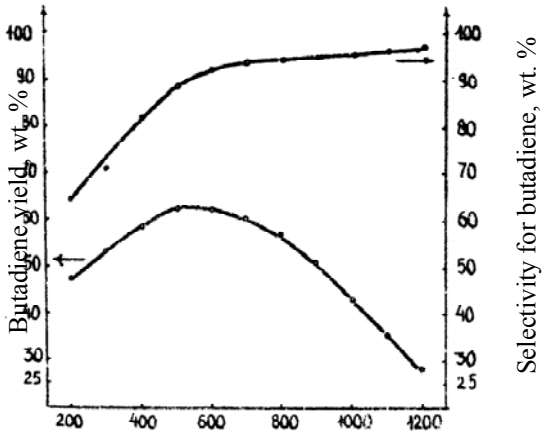

Fig. 2. *The Influence of volumetric flow rate on the oxydehydrogenation in the case of ternary catalyst Bi/Mo/Fe = 0.5 : 1.0 : 1.2.*

The main textural characteristics for the binary and ternary catalysts are shown in table 2.

Table 2. The main textural characteristics for the binary and ternary catalysts.

Catalytic system	Real density (g/cm^3)	Apparent density (g/cm^3)	Surface area (m^2/g)	Total pore volume (cm^3/g)	Macropores volume (cm^3/g)	R_m (Å)
Bi/Mo = 0.5 : 1.0	5.81	3.58	2.4	0.13545	0.12155	3400
Bi/Mo/Fe = 0.5 : 1.0 : 1.2	5.40	2.90	3.4	0.1604	0.1474	400 and 25000

Figure 3 shows pores distribution by radius for the binary Bi/Mo = 0.5 : 1.0 and ternary Bi/Mo/Fe = 0.5 : 1.0 : 1.2 systems. Fe_2O_3 addition changes the distribution of the medium pores and of the macropores. The ternary catalyst Bi/Mo/Fe = 0.5 : 1.0 : 1.2 exhibits a heterogeneous porous structure with medium pores and macropores having radii of 400 and, respectively, 25000 Å.

Now we intend to set out some correlations between activity, expressed as local reaction rate, and the textural parameters of catalysts, such as macroporosity, the pore radius, retention time of the reactant inside the macropores [10].

It is known that in general reaction rate equation, the retention time $d\tau$ of the reactant flow rate V_0 (cm^3/s) within the reactor volume dV_r (reactor cross section infinitely small) is given by:

$$d\tau = \frac{dV_r}{V_0}$$

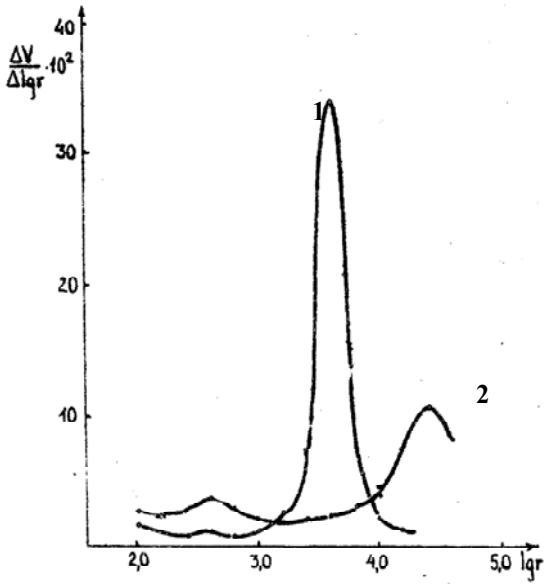

Fig. 3. *Pore distribution by the radius; 1 - Bi/Mo = 0.5 : 1.0; 2 - Bi/Mo/Fe = 0.5 : 1.0 : 1.2.*

By the substitution of the term that stands for the reaction volume, dV_r , with the macropores volume V_M, granting that the reactant flows through them, one obtains:

$$d\tau = \frac{dV_r}{F_{A_0}} = \frac{V_M}{F_{A_0}} = \tau_M$$

$$S_M = \frac{2V_M}{r_M}$$

$$-r_A = F_{A_0} \cdot X_A$$

$$F_M^{'} = -r_A \tau_M \; ; \quad F_M^{'} = \frac{-r_A}{F_{A_0}} V_M$$

where: F_A – feeding flow rate (mol/g·s);

X_A – moles butenes transformed per second and gram of catalyst;

τ_M – retention time of the reactants in the macropores;

S_M – internal surface area of the macropores;

r_M – mean radius of macropores;

F_M – moles butenes transformed as a function of retention time inside the macropores

r_A – total reaction rate (moles/g·s).

Figure 4 shows the variation of the apparent reaction rate with the feeding rate for the catalysts Bi_2O_3-MoO_3 (Bi/Mo = 0.5:1.0) and Bi_2O_3-MoO_3-Fe_2O_3 (Bi/Mo/Fe = 0.5:1.0:1.2), taking into account the global flow rate of the reactants.

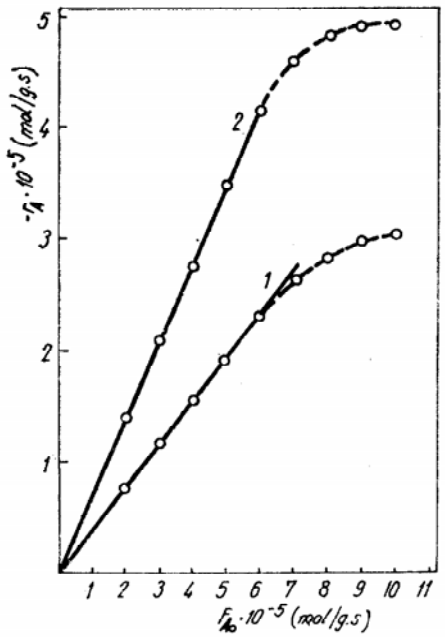

Fig. 4.*Variation of the apparent reaction rate with reactant flow at reaction temperature of 440°C;*

1 - Bi/Mo = 0.5 : 1.0; 2 - Bi/Mo/Fe = 0.5 : 1.0 : 1.2.

We notice a linear dependence between the reaction rate and the reactant flow rate up to a certain value. The linear range corresponds to our experiment conditions. Apparent reaction order calculated from slope, has fractionary values close to zero, which show that the mechanism is more complex when reaction mixtures of 1- and 2-butenes are used.

Figure 5 shows the flow rate of reaction products plotted against the retention time of the reactants inside the macropores, for the same catalysts. In both cases a linear dependence is noticed up to retention time ranging from 1.0 to 1.5 s. These experimental data suggest certain dependences between the kinetic parameters of the reaction and some textural characteristics of the catalysts that could be meaningful when criteria for selecting the catalysts are involved.

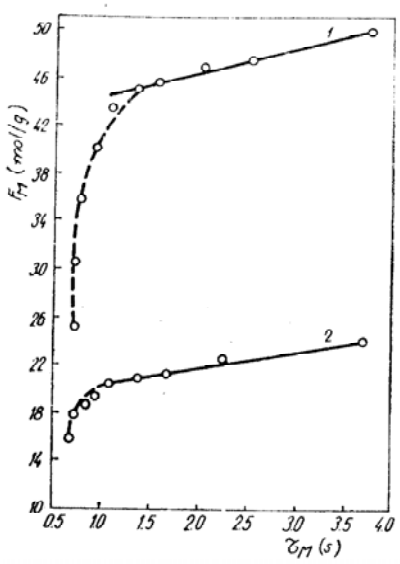

Fig. 5.*Variation of the reaction products flow with the retention time of the reactants inside the macropores. Reaction temperature 440oC. 1 - Bi/Mo = 0.5 : 1.0; 2 - Bi/Mo/Fe = 0.5 : 1.0 : 1.2*

In conclusion, the new mechano-topochemical method for catalyst preparation highly improves the activity and selectivity against the same catalysts prepared by classical methods. The interface reaction of the solid hydrated particles provides a better interaction among the components of the reaction mixture, thus favoring the formation of active catalyst phases. Addition of Fe_2O_3 to the binary catalytic system Bi-Mo-O substantially increases their activity. There are some interdependences between the kinetic parameters of reaction and some textural characteristics of the catalysts, which could be considered as criteria for selecting a particular catalyst.

REFERENCES

1. Qiu, F. Y., Weng, L. T., Sham E., Ruiz P. and Delmon, B. (1989) *Appl. Catal.,* **51,** 235-253.
2. Nedelcu, Gh. and Nicolescu, I. V. (1990) *Rev. Chim. Bucuresti.,* **41(11-12),** 881-884.
3. Morselli L., Trifiro, F. and Urban, L. (1982) *J. Catal.,* **75,** 112-121.
4. Yang, B. L., Kung, M. C. and Kung, H. H. (1984) *J. Catal.,* **89,** 172-176.
5. Lambert, J. C. and Germain, J. E. (1982) *Bull. Soc. Chim. France,* **I(1-2)**, I-33-38.
6. Nedelcu, Gh. and Nicolescu, I. V. (1991) *Rev. Chim. Bucuresti.,* **42(1-3)**, 21-26.
7. Yang, B. L. and Cheng, D. S. (1991) *Appl. Catal.*, **70**, 161-173.
8. Moisin, Ana Maria, Chirtoc, V., Sandulescu, I. And Nicolescu I. V. (1975) *Z. Phys. Chem.. (Frankfurt),* **95,** 159-164.
9. Nicolescu, I. V., Sandulescu, I., Grigoriu , I., Crisan, T., Angelescu, E. and Pascu, S. (1977) Rom. Patent, 62701.
10. Nicolescu, I. V. and Sandulescu, I. (1971) *Anal. Univ. Bucuresti, Chimie,***20(4)**, 27-31.

11. Sandulescu, I. and Nicolescu, I. V. (1973) *Anal. Univ. Bucuresti, Chimie*,**22(2)**, 555-561.

12. Nicolescu, I. V. and Sandulescu, I. (1979) *Rev. Roum. Chimie*, **26(2)**, 217-228.

CONVERSION OF C_6 HYDROCARBONS ON Zn/H(Na,K)L ZEOLITE

Adriana Urdă[*], I. Săndulescu[*], Mariana Carată[**]

abstract: Aromatization of C_6 hydrocarbons (hexane isomers and cyclohexane) was performed on a Zn/H(Na,K)L zeolite. Increasing temperature favors aromatization reactions, but leads to intense cracking. Zinc modifier promotes direct dehydrogenation leading to benzene, but reactions that lead to aromatics also take place on the acid sites remained in the zeolite. Cyclohexane is the reaction intermediate in the direct dehydrogenation pathway.

Keywords: L zeolite, Zn/L, hexane conversion, cyclohexane conversion

Introduction

Valorization of saturated hydrocarbons by transforming them into more valuable products is a topic widely covered in literature, aromatization of light alkanes being one of the processes that apply this concept [1-3]. Many types of zeolite structures were tested for this purpose, with ZSM-5 being most frequently used because of its acidic properties, pore structure and shape selectivity [2,4-6].

L zeolite has a structure composed of cylindrical 12-membered rings, with a pore diameter of 7.1 Å that allows an easy access of hydrocarbon molecules to the active centers [7]. KL zeolite modified with platinum was extensively studied for the aromatization of n-hexane with good selectivity for benzene, as an alternative method for obtaining aromatic hydrocarbons from alkanes and naphtha [3,8-18]. The high selectivity for benzene was attributed either to the structural parameters of this zeolite, or to its basic properties related to the alkaline cation [10]. Meanwhile, there is a consensus that the reaction mechanism is monofunctional and implies dehydrocyclization on the platinum clusters inside the zeolite channels, the zeolite support being non-acid in order to avoid secondary acid-catalyzed reactions [16-18].

For ZSM-5 zeolites, modification with Zn or Ga strongly increases the selectivity for aromatics, due to a change in the reaction pathways [1,2,4,19]. The modifiers promote dehydrogenation reactions leading to aromatics, instead of acid-catalyzed hydrogen transfer reactions that, besides aromatics, lead to large amounts of alkanes remaining in the reaction products. Due to the zinc beneficial effect in these processes, we intended to observe the role of zinc as modifier in aromatization of some C_6 hydrocarbons on L zeolite. We studied

[*] University of Bucharest, Faculty of Chemistry, Department of Chemical Technology and Catalysis, Bd. Regina Elisabeta 4-12, Bucharest 3, Romania

[**] Institute of Physical Chemistry, Romanian Academy, Splaiul Independenței 202, Bucharest 6, Romania

Analele Universității din Bucureşti – Chimie, Anul XIV (serie nouă), vol. I-II, pg. 81-88

the activity of a LTL zeolite and that of Zn-modified LTL catalysts in the aromatization of n-hexane, 2-methylpentane, 3-methylpentane and cyclohexane. The catalyst was selective for obtaining a liquid fraction rich in aromatic hydrocarbons and C_5-C_8 oligomers.

Experimental

The LTL zeolites were analyzed and characterized at the "L.V. Pisarzhevsky" Institute of Physical Chemistry from the Ukrainian Academy of Sciences from Kiev, Ukraine. The as-synthesized parent sample, NaKL, had the following composition: $K_6Na_3[Al_9Si_{27}O_{72}]\cdot 21H_2O$. This parent sample was exchanged in the ammonium form and calcined at 450^{o}C for 2 h. Upon calcination, the composition was determined by atomic absorption spectroscopy to be $H_{3.33}Na_{2.79}K_{2.98}[Al_9Si_{27}O_{72}]\cdot 21H_2O$.

The calcined sample was obtained by impregnation of the parent zeolite with a $Zn(NO_3)_2$ solution, so that the final catalyst to have a 2.8% Zn concentration. The two catalyst samples were calcined in steps up to 550^{o}C.

All catalytic tests were performed in a fixed bed glass reactor, at atmospheric pressure and temperatures between 400 and 525^{o}C; the LHSV of reactant was $2h^{-1}$. Before the catalytic tests, the catalyst was heated at 550^{o}C in airflow, and then the temperature was lowered to the reaction temperature. After the reactor, reaction products were cooled and the liquid and gaseous fractions separately collected and analyzed by gas chromatography. Hexane (Merck, 99%), 2-methylpentane (Fluka AG, 99%), 3-methylpentane (Fluka AG, 99%) and cyclohexane (Merck, 99.7%) were used as raw materials. Total conversion was calculated as the amount of feed transformed into products divided by the amount of feed introduced into the reactor. Selectivity for aromatics was calculated as the amount of aromatics formed in the reaction divided by the amount of feed transformed into products.

Results

The effect of temperature on the activity and selectivity for aromatics in the conversion of n-hexane on Zn/H(Na,K)L zeolite is shown in fig. 1 and table 1. The conversion has low values on the entire temperature range (400-525^{o}C) that increase slowly with temperature up to 10%. The selectivity for aromatics also increases with temperature, reaching a maximum of 45% at 500^{o}C. This increase is expected since many of the reactions that might lead to aromatic hydrocarbons (cyclization and dehydrogenation) are endothermic. At 525^{o}C, the slightly lower value for the selectivity for aromatics could be due to more intense cracking reactions and coking.

A very small volume of gas fraction is obtained at all temperatures, suggesting that cracking does not play an important role in the process. Due to its low Si/Al ratio and to the presence of Na and K in the structure, the acidity of this zeolite is smaller that in other zeolites used in hydrocarbon conversions, such as ZSM-5, so cracking is low in our catalyst.

Among gaseous hydrocarbons (table 1), propene and butenes have almost equal shares, larger than ethene's one, showing that cracking leads mainly to C_3H_8 + C_3H_6 and C_4H_8 + C_2H_6 hydrocarbons. Hydrogen was also observed in the reaction products, proving dehydrogenation reactions that presumably take place on zinc oxide.

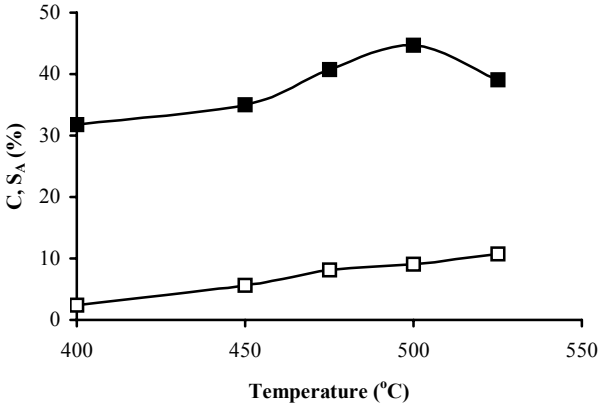

Fig. 1. *Influence of temperature on the activity and selectivity for aromatics in n-hexane aromatization on Zn/H(Na,K)L zeolite (LHSV = 2 h^{-1}; □ – n-hexane conversion; ■ – selectivity for aromatics.*

Table 1. Composition of reaction products in the aromatization of n-hexane on Zn/H(Na,K)L zeolite (LHSV = 2h^{-1})

Products	400°C	450°C	475°C	500°C	525°C
Hydrogen	0.4	0.1	0.1	0.2	0.3
Methane	2.6	0.2	1.1	1.0	1.1
Ethane	9.2	0.5	2.1	0.8	2.6
Ethene	2.6	0.4	1.8	0.9	2.6
Propane	19.9	1.6	6.4	0.7	1.4
Propene	12.0	10.3	8.9	3.4	3.7
Butanes	1.3	0.2	0.4	0.2	0.3
Butenes	7.9	10.8	10.0	2.6	2.8
Oligomers	12.3	30.4	28.6	45.4	46.2
Benzene	11.9	28.7	8.9	9.8	4.2
Toluene	4.0	4.9	2.1	4.1	2.5
Ethylbenzene + Xylenes	13.4	9.1	12.1	12.9	10.2
C_{9+} aromatics	2.5	2.8	17.5	18.0	22.1

The main reaction products are oligomers, consisting in C_5-C_8 hydrocarbons among which hexane isomers, cyclohexane, methylcyclopentane and cyclohexene were identified. On acidic zeolites, aromatics are usually formed from alkanes by a succession of reactions on the acid sites, starting with cracking or dehydrogenation in order to obtain an alkene. This initial step is followed by oligomerization or alkylation of the alkene with an alkane, cyclization and dehydrogenation, leading to an aromatic hydrocarbon. If the catalyst is bifunctional (with a dehydrogenation component besides the acid function) and the starting alkane has at least six carbon atoms, then direct dehydrogenation is also possible. From the data in table 1, the first pathway seems to be active on Zn/H(Na,K)L. The large concentrations of C_5-C_8 oligomers that are formed, particularly at higher temperatures, show that the first succession of reactions is favored in these conditions. At lower temperatures, benzene is formed in large amounts, at 450°C being the main aromatic in the reaction products. This fact suggests that direct dehydrogenation also plays an important role, the presence of cyclohexane, methylcyclopentane and cyclohexene in the products supporting this hypothesis. As temperature increases, ethylbenzene, xylenes and C_{9+} aromatics become increasingly important, their formation being favored in the relatively large (7.1 Å diameter) circular pores of the zeolite.

Because the maximum selectivity for aromatics was obtained at 500°C, the rest of the catalytic tests were performed at this temperature.

The influence of the starting hydrocarbon was investigated on the Zn/H(Na,K)L zeolite, using n-hexane, 2-methylpentane (2MeP), 3-methylpentane (3MeP) and cyclohexane (CH) as feed. 2MeP and 3MeP were tested because their formation was observed in the first series of experiments, and CH was tested in order to confirm the direct dehydrogenation pathway to benzene, that has CH as an intermediate. Results are shown in fig. 2 and table 2.

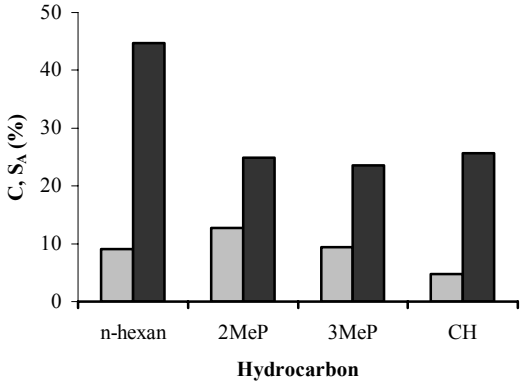

Fig. 2. *Influence of hydrocarbon nature on the activity and selectivity for aromatics in C_6 hydrocarbons aromatization on Zn/H(Na,K)L zeolite (LHSV = 2 h^{-1}; ■ – conversion; ■ – selectivity for aromatics.*

Among hexane isomers, results are similar, with a slightly higher conversion for 2MeP. The selectivity for aromatics has much lower values for 2MeP and 3MeP compared to n-hexane, probably because they can not be directly dehydrogenated to benzene and, in order to transform in aromatics, they have to pass through an isomerization step at one time of the reaction. For 2MeP and 3MeP, benzene is the main aromatic hydrocarbon, that can be formed by either isomerization to hexane and then dehydrogenation, or by cyclization to methylcyclopentane then isomerization to cyclohexane and dehydrogenation.

Oligomers were again present in high concentrations in the reaction products. Isomerization of hexane, 2MeP and 3MeP takes place on the acid sites that still exist in the zeolite, and the composition of hexane isomers is similar in the catalytic tests. The similarity of reaction products distribution among C_6 aliphatic hydrocarbons suggests that reaction pathways are the same, leading to the same intermediates and products. Both direct dehydrocyclization and the cracking - oligomerization - dehydrocyclization succession seem to be co-operating for these hydrocarbons.

CH has a more stable molecule and is less reactive on acid sites than hexanes, so its conversion has lower values than those obtained for the other hydrocarbon feeds. The fact that benzene concentration is double compared to that obtained for hexanes and that hydrogen is present in larger amounts confirm that in this case conversion takes place mainly by direct dehydrogenation.

Table 2. **Composition of reaction products in the aromatization of some C_6 hydrocarbons on Zn/H(Na,K)L zeolite (LHSV = 2h^{-1})**

Products	n-hexane	2MeP	3MeP	CH
Hydrogen	0.2	0.5	0.3	1.6
Methane	1.0	0.7	1.9	3.3
Ethane	0.8	2.1	4.0	4.9
Ethene	0.9	1.9	3.8	2.7
Propane	0.7	1.2	0.9	0.5
Propene	3.4	8.5	8.7	5.5
Butanes	0.2	0.9	1.3	6.0
Butenes	2.6	8.9	9.4	12.0
Oligomers	45.4	50.9	46.2	37.2
Total aromatics	44.8	24.4	23.5	26.3
Benzene	9.8	12.9	11.6	19.7
Toluene	4.1	2.1	1.9	2.2
Ethylbenzene + Xylenes	12.9	9.4	5.9	2.2
C_{9+} aromatics	18.0	-	4.1	2.2

The influence of the promoted catalyst is discussed compared to the parent zeolite, H(Na,K)L. The results are shown in figs. 3-5 for n-hexane, 2MeP and CH feeds.

For all starting hydrocarbons conversion values are similar on the two catalysts, but the selectivity to aromatics is intensified when zinc is present in the catalyst, confirming its

promoting role. This finding is in line with literature data that prove the positive influence of zinc promoter in aromatization reaction on other zeolites.

On the parent zeolite, aromatic hydrocarbons are formed in very small amounts, and they consist in benzene, toluene and no xylenes except for the reactions with n-hexane. On the zinc-modified catalyst mainly benzene and xylenes concentrations increase.

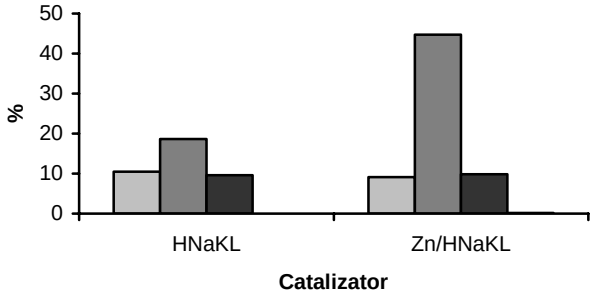

Fig. 3. *Catalytic activity and reaction products composition in n-hexane aromatization on H(Na,K)L and Zn/H(Na,K)L catalysts. LHSV = 2 h^{-1}, T = 500°C. ■ –conversion; ■– selectivity for aromatics, ■-benzene concentration.*

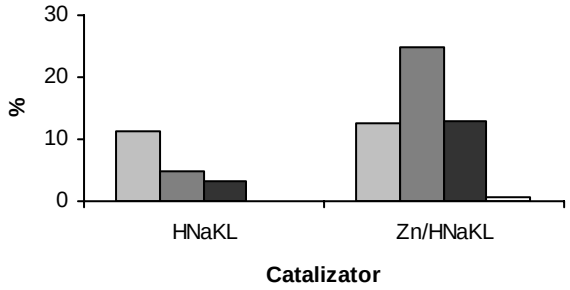

Fig. 4. *Catalytic activity and reaction products composition in 2MeP aromatization on H(Na,K)L and Zn/H(Na,K)L catalysts. LHSV = 2 h^{-1}, T = 500°C. ■ –conversion; ■– selectivity for aromatics, ■-benzene concentration, □- hydrogen concentration.*

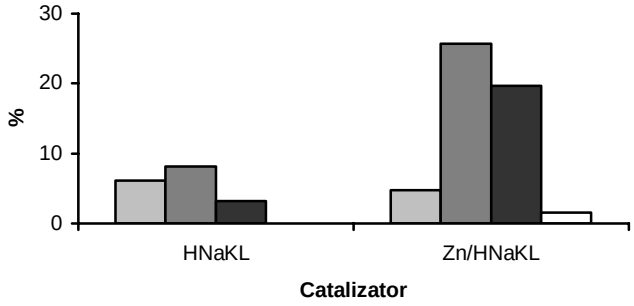

Fig. 5. *Catalytic activity and reaction products composition in CH aromatization on H(Na,K)L and Zn/H(Na,K)L catalysts. LHSV = 2 h^{-1}, T = 500°C.* ■ *–conversion;* ■*– selectivity for aromatics,* ■*-benzene concentration,* □*-hydrogen concentration.*

Benzene is formed probably by dehydrocyclization, while xylenes result from coupling two butene molecules. Other differences are the higher hydrogen and methane concentrations in reaction products on zinc-modified catalyst. The higher hydrogen amount proves that zinc promotes dehydrogenation reactions and it correlates with the higher selectivity for aromatics and higher benzene concentration in the reaction products.The fact that methane is formed in larger amounts on zinc-modified zeolites was also observed in aromatization reactions on ZSM-5 [19], and it was explained by the hydrogenolysis activity of zinc ions.

Conclusion

The Zn/H(Na,K)L catalyst showed a good selectivity to aromatics compared to the parent HNaKL zeolite, the main aromatic hydrocarbon being always benzene. This proves that zinc promotes direct dehydrogenation reactions, but is not involved in the activation of the initial hydrocarbon. Increasing temperature favors the aromatization process, but at high temperatures cracking becomes dominant. The presence of acid sites in the zeolite promoted reactions that lead to large amounts of C_5-C_8 hydrocarbons, including cyclohexane, methylcyclopentane and cyclohexene.

REFERENCE

1. Seddon, D. (1990) *Catalysis Today* **6**, 351-371
2. Ono, Y. (1992) *Catal. Rev. – Sci. Eng*. **34(3)**, 179-324
3. Meriaudeau, P. and Naccache C. (1992) *Catal. Rev. – Sci. Eng*. **39(1,2)**, 5-127
4. Kanai, J. and Kawata, N. (1988) *J. Catal*. **114**, 284-290
5. Meriaudeau, P. and Naccache C. (1990) *J. Mol. Catal.*. **59**, L31-L36
6. Trombetta, M., Gutierrez, A. A., Ramirez, S. J. and Busca, G. (2000) *Appl. Catal. A: General* **198**, 81-93

7. Baerlocher, Ch., Meier, W. M. and Olson D. H. (2001) **Atlas of zeolite framework types**, 5th edition, Elsevier, Amsterdam, 170-171

8. Bulow, M., Struve, P., Finger, G., Redszus, C., Erhardt, K., Schirmer, W. and Karger, J. (1980) *J. Chem. Soc., Faraday Trans*. **176**, 597-605

9. Haag., W. O., Lago, R. M. and Weisz P. B. (1981) *Faraday Disc. Chem. Soc*. **72**, 317-325

10. Besoukhanova, C., Guidot, J. and Barthomeuf, D. (1981) *J. Chem. Soc., Faraday Trans. I* **77**, 1595-1604

11. Sharm, S. B., Miller, J. T. and Dumesic, J. A. (1994) *J. Catal*. **148**, 198-204

12. Mojet, B. L., Kappers, M. J., Muijsers, J. C., Niemansverdriet, J. W., Miller, J. T., Modica, F. S. and Koningsberger D. C. (1994) *Stud. Surf. Sci. Catal*. **84B**, 909-912

13. Vaarkamp, M., Mojet, B. L., Kappers, M. J., Miller, J. T. and Koningsberger D. C. (1995) *J. Phys. Chem*. **99**, 16067-16075

14. Miller J. T., Agrawal, N. G. B., Lane G. S. and Modica F. S. (1996) *J. Catal*. **163**, 106-116

15. Menacherry, P. V., Fernandez-Garcia, M. and Haller, G. L. (1997) *J. Catal*. **166**, 75-87

16. Jacobs, G., Padro, C. L. and Resasco, D. E. (1998) *J. Catal*. **179**, 43-56

17. Jacobs, G., Ghadiali, F., Pisanu, A., Borgna, A., Alvarez, W. E. and Resasco, D. E. (1999) *Appl. Catal. A: General* **188**, 79-98

18. Jentoft, R. E., Tsapatsis, M., Davis, M. E. and Gates, B. C. (1998) *J. Catal*. **179**, 565-578

19. Urdã, A., Tel'biz, G. and Sãndulescu, I. (2001) *Stud. Surf. Sci. Catal*. **135**, 4017-4024

THE CATALYTIC SYNTHESIS OF METHYL-ISOBUTYL KETONE FROM ACETONE. THE STUDY OF THE INFLUENCE OF ZINC ADDITION THROUGH IMPREGNATION ON THE BEHAVIOUR OF THE CATALYST PD / ZN- H-ZSM 5

D. Bombos[*1], Mihaela Bombos[2], Fanica Bacalum[2], I. Stanciu[2], Camelia Bala[3], N. Naum[4]

abstract: Methyl-isobutyl –ketone (MIBK) was obtained in vapor phase, from acetone and hydrogen in a single step, using Pd/H-ZSM-5 as a catalyst. The experiments were performed in a continuous fixed bed reactor at 5 atm, 170 ^{o}C, hydrogen/acetone molar ratio measured at reactor outlet (MRHA) 0.4 and acetone WHSV 0.3 h^{-1}. Acetone conversions up to 50 % and MIBK yield up to 45 % were obtained. The experimental data showed that the presence of zinc oxide, in an amorphous form, decrease the Pd/Zn- H-ZMS-5 catatalyst's activity in the process of reductive condensation of acetone. The selectivity for methyl-isobutyl ketone also presents a decrease when zinc in an amorphous form is added. This behavior is due probably to the decrease in the activity of the acid catalyst centers in the presence of zinc oxide in an amorphous form.

Introduction

Methyl-isobutyl –ketone is a chemical product of industrial interest obtained from acetone. It is mainly used as a solvent for polishes and dyes or for obtaining other chemical products (stabilizers, etc.) Due to its volatility, which is lower than that of acetone, MIBK is considered a solvent with higher performances.

The conventional technology of MIBK synthesis from acetone consists of a sequence of three steps and it has been the only one used until late 1960's. In this technological variant, acetone is condensed, in the first stage, to DAA (diacetonealcohol) in a basic catalysis in liquid phase. In the second stage, DAA is dehydrated to MO (mesityl oxide) with an acid catalyst such as the phosphoric or the sulphuric acid, and during the third stage MO is hydrogenated to MIBK. Recently, an one-stage process for manufacturing MIBK has been introduced, a process which uses bifunctional catalysts containing a metal (Pd usually) deposited on a solid acid support. The process presupposes the reversible condensation of

[*1] Polytehnica University Bucharest, Department of Chemical Engineering, Bucharest, Romania
[2] National Research Institute for Chemistry and Petrochemistry, ICECHIM, Bucharest, Romania
[3] Laboratory for Quality Control & Process Monitoring, Dept. of Analytical Chemistry, Faculty of Chemistry, University of Bucharest, Sos. Panduri 90, Bucharest-5, Romania
[4] Oil-Gas University, Ploiesti, Romania

Analele Universităţii din Bucureşti – Chimie, Anul XIV (serie nouă), vol. I-II, pg. 89-94

acetone to MO on the acid centers and, in succession, the hydrogenation of MO to MIBK on the metallic centers.

An important number of studies have been published, which deal with the direct synthesis of MIBK from acetone and hydrogen on Pd-based catalysts deposited on ion-exchange resins [1], zeolites [2,3], zirconium phosphate [4] or niobic acid [5]. The direct synthesis of MIBK from acetone on catalysts of Ni deposited on magnesium oxide or alumina has been presented recently [6,7].

In this paper we present some of the results obtained in the research regarding the single-stage MIBK synthesis from acetone and hydrogen in the presence of a Pd catalyst deposited on a ZMS-5 zeolite in the form proton modified with zinc during the process of crystallization and of the same catalyst which also contains zinc oxide in an amorphous form at different concentrations.

Experimental

The tested catalyst is mainly made of palladium deposited on a H-ZMS-5 zeolite modified with zinc in the process of crystallization, made by ZECASIN S.A. The zeolite powder was bound in an amorphous alumina matrix, as extrudated composite pellets containing 30 % alumina. The catalytic pellets were dried and calcined at 550 ^{0}C and then impregnated with a water solution of palladium chloride, dried and calcined at 450 ^{0}C. To prevent the possible interactions of the acid centres with the metallic centres, the palladium chloride impregnation was performed on the surface area of the catalytic pellet by spraying. The activity of this catalyst remains virtually constant during the time of the experiment, according to the data presented in a previous paper [2].

Adding zinc oxide in different concentrations in the Pd catalyst deposited on an H-ZMS-5 zeolite modified with zinc in the crystallization process had the purpose of studying the influence of zinc oxide in an amorphous form on the activity of this catalyst in the process of acetone reductive condensation. Thus, to emphasize the fact that zinc oxide modifies its acidity in the presence of water only when it is in an amorphous form, catalysts containing amorphous zinc oxide were prepared, through the impregnation with a zinc salt of the Pd/Zn H-ZMS-5 catalyst, using different concentrations of this metal (3% and 5% respectively).

The deposit of zinc in an amorphous form was obtained through the impregnation of the catalyst with a water solution of zinc nitrate (the method of "filling the pores"), followed by drying and by calcination at 450 ^{0}C. The activation of the catalyst was made through the reduction in a stream of hydrogen at 180 ^{0}C.The reagents used in this experiment were analytically pure acetone and electrolitically pure hydrogen.The palladium content of the catalysts was determined through colorimetric methods applied to a water solution obtained by the dissolving of palladium. The specific surface area of the zeolite catalyst was determined through measurements of porosimetry with mercury and nitrogen absorption and the concentration of the acid centres of the zeolite catalyst was determined through the

method of programmed thermodesorption of ammonia (data presented in a previous paper [2]).

The experimental program of testing the bifunctional catalysts prepared according to the above described procedure was performed in a continuous fixed bed catalytic reactor. A mobile metallic jacket for thermocouple was also placed in the axis of the bed, in order to measure the reaction temperature. The process was carried out in isothermal conditions, the temperature being measured with a mobile thermocouple, the sheath of which was axially placed in the central zone of the catalyst layer. The composition of the reaction mixture was determined through gas chromatography on a HP 5890 chromatograph equipped with an HP - INNOWAX capillary column of 30 m in length and 0.25 mm in diameter.

Results and discussions

For the domain of variation of the reaction parameters within the experimental framework, the main reaction product was MIBK and the secondary products identified in small amounts diisobutyl ketone (DIBK), 2-methyl-pentane (2-MP), isopropyl-alcohol (iPA), di-isopropyl-ether (DIPE), MO and traces of advanced condensation products.

The influence of the zinc content, added through impregnation, on the performances of the process is presented in figure 1.

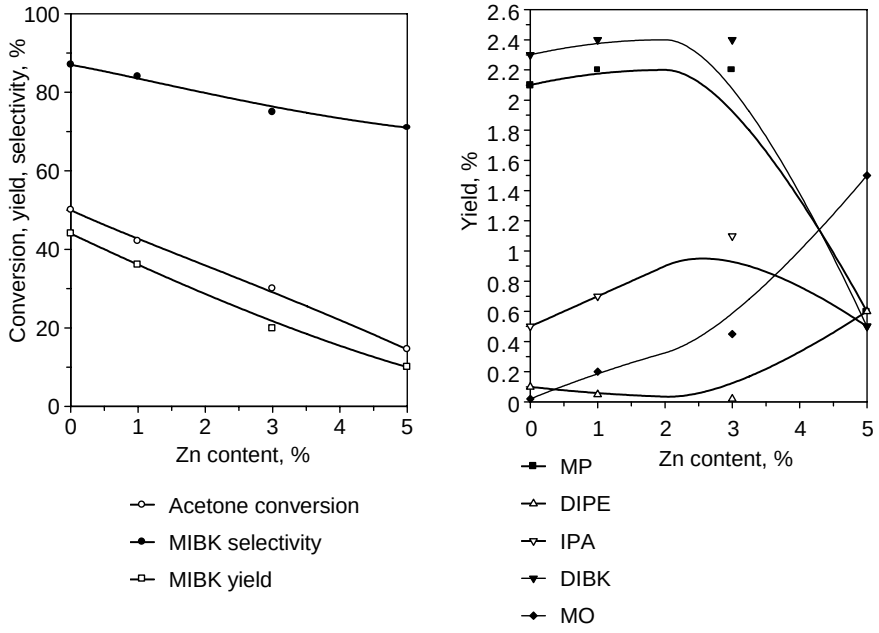

Fig.1. *Influence of zinc content added by impregnation on the process performances Catalyst 0.3% Pd/Zn-HZSM-5, T=170°C, P=5 atm., WHSV =0.3 h^{-1}, MRHA=0.4*

One can notice a high decrease of acetone conversion in relation to the zinc content of the catalyst (added through impregnation) for the same values of the operating parameters. The selectivity for methyl-isobutyl ketone also presents a decrease when zinc in an amorphous form is added. The output in methyl-isobutyl presents a decrease directly proportional to the catalyst's zinc content added through impregnation.

Thus, increasing the catalyst's zinc content three times leads to a decrease in the methyl-isobutyl ketone output by half, and increasing the catalyst's zinc content five times leads to a five-time decrease in the methyl-isobutyl ketone output. The output in 2-metyl pentane and diisobutyl ketone is relatively constant when the catalyst's zinc content is increased up to 3 %, the increase in the catalyst's zinc content to 5 % triggering an important decrease in the output in these chemical compounds.

It should also be noted the formation of the mesityl oxide in the reaction product in the case of the catalyst promoted with amorphous zinc oxide. An increase in the content of the catalyst's zinc oxide (in an amorphous form) results in an increase in the mesityl oxide output.

The variation of the performances of acetone conversion process depending on the reaction time is presented in figure 2 for a 3 % zinc content in an amorphous form and in figure 3 for a 5 % zinc content in an amorphous form.

It can be seen that the activity of the Pd / Zn H – ZMS –5 catalyst impregnated with zinc oxide decreases in time, for the catalyst which contains 3 % Zn, as well as for the catalyst which contains 5 % Zn added through impregnation, decrease highlighted by the variation of acetone conversion in time. The selectivity for methyl-isobutyl ketone and the output in methyl-isobutyl-ketone also decrease in time.

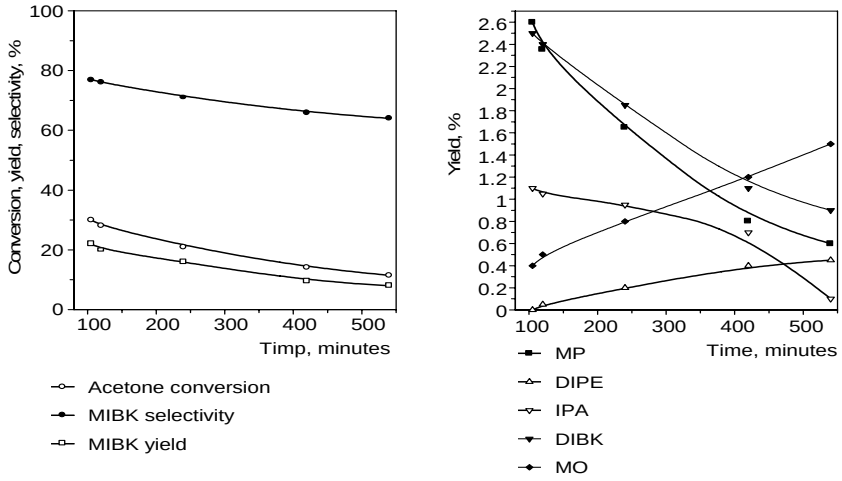

Fig.2. *Variation of acetone conversion process performances vs. running time*
Catalyst 0.3% Pd/Zn-HZSM-5 impregnated with 3% Zn
T=170°C, P=5 atm., WHSV =0.3 h^{-1}, MRHA=0.4

The output in 2-metyl pentane also decreases in time, while the outputs in diisopropyl ether and isopropylic alcohol tend to remain constant in time. The output in diisobutyl ketone slowly decreases for the 5 % zinc catalyst and it presents a variation with a maximum point for the 3 % zinc catalyst.

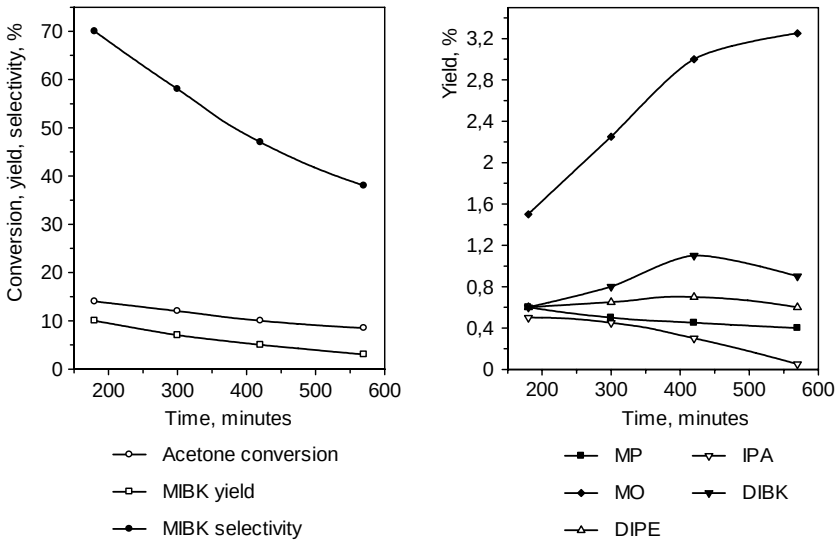

Fig.3. *Variation of acetone conversion process performances vs. running time*
Catalyst 0.3% Pd/Zn-HZSM-5 impregnated with 5% Zn
T=170°C, P=5 atm., WHSV =0.3 h^{-1}, MRHA=0.4

The output in mesityl oxide increases with testing time, for the catalyst impregnated with 3 % zinc, as well as for the catalyst impregnated with 5 % zinc, output values in mesityl oxide being bigger for the catalyst containing 5 % zinc for the same amount of working time.

The decrease of acetone conversion in the case of the catalysts promoted with amorphous zinc oxide is due to the negative effect of amorphous zinc oxide on the metallic centers and probably on the acid centers as well. Thus, the presence of mesityl oxide in the reaction product, irrespective of the catalyst's zinc content, indicates a decrease in the activity of the metallic centers.

The scientific literature does not indicate any poisonous or deactivating effect of zinc on the palladium based catalysts used for hydrogenation (assertion also backed up by the behavior of the Pd/Zn H ZMS-5 catalyst on the reductive condensation of acetone). In these circumstances, the deactivation of the metallic centers in the presence of amorphous zinc oxide is probably due to the decrease in the desorption speed of the water formed in the reaction of acetone condensation in the presence of amorphous zinc oxide, water which negatively influences the palladium catalytic activity. Although the zinc oxide presents certain acidity after calcinations, we did not notice any improvement in the activity of the

catalyst's acid centers after zinc impregnation, improvement which would have determined an increase in the output in condensation products and implicitly in the acetone conversion. This behavior is probably due to the same reason, that is, the interaction between the reaction water and the amorphous zinc oxide. The decrease in the activity of the catalyst impregnated with amorphous zinc oxide in time, is probably due to the accumulation of water in the pores, due to its reduced desorption speed in the presence of zinc oxide.

Conclusions

The study of the influence of amorphous zinc addition on the activity of a bifunctional catalyst in the process of acetone reductive condensation was carried out through the impregnation with a zinc salt of a Pd catalyst deposited on a ZMS-5 zeolite in an acid form which contains zinc bound in a crystalline network.

The decrease in the Pd/Zn- H-ZMS-5 catalyst's activity in the presence of zinc oxide in an amorphous form in the process of reductive condensation of acetone is due to the decrease in the activity of the acid catalyst centers.

The variation in time of the performances of the catalysts containing zinc oxide in an amorphous form emphasized the fact that zinc oxide modifies its activity in the presence of water only when it is in an amorphous form.

REFERENCES

1. Grigoriev A. A., Guseva S. I., Katzman E. A., *Himicheskii Prom*., no. 7, pg. 392 (1988).
2. D. Bombos, G. Bozga, M. Bombos, A. Stefan, I. Stanciu, *Chemical Papers,* 54 (3), 171-176, 2000.
3. Huang T., Haag W., U. S. Pat. 4339606 (jul. 1982).
4. Watanabe Y., Okada M., Izumi Y., Mizutani Y., *Bull. Chem. Soc. Jpn*., **50**, 1539(1977).
5. Higashio Y., Nakayama T., *Catal. Today* , **28**, 127(1996).
6. Gandia L., Montes M., *Appl. Catal. A: General*, 101, L1(1993).
7. Narayanan S., Unnikrishnan R., *Appl. Catal. A: General,* 145,231(1996).

NONIONIC EMULSIFIERS BASED ON STABILIZED POLIOXIETHYLENE-SORBITANS

D. Bombos[*], M. Andrei[**], Maria Mihailescu[**], Irina Tamas[**], C. Teodorescu[**]

abstract: In the present work is studied the synthesis of a nonionic emulsifier and its use for the preparation of emulsified fuels. The nonionic emulsifier is an ester and it was prepared in two ways: the addition of chemical compounds containing active hydrogen (esters obtained out of fatty acids and sorbitol) to an oxyran (ethylene-oxide); the transesterification of the ethoxylated sorbitol with the methylic ester of a fatty acid (oleic acid). The products obtained were further purified through a patented procedure, to obtain stabilized compounds. The ester of oleic acid with sorbitol was obtained by the transesterification of the sorbitol with methyl oleat. The product content of oxiethylenic groups was 20-40 relative to a sorbitol molecule. The synthesized emulsifiers were tested for the preparation of emulsified oil-in-water fuels used for burning processes improvement and implicitly reductions of pollutants.

Introduction

The policondensation of a compound containing hydroxilic groups (alcohol, poliol, alkylphenol, carboxylic acid) with ethylene oxide can be schematically represented through the following chemical reactions:

$$R - OH + CH_2 - CH_2 \text{ (O)} \text{-------->} RO - CH_2CH_2 - OH \quad (1)$$

$$RO - CH_2 - CH_2 - OH + n\,(CH_2 - CH_2 \text{ (O)}) \text{------>} RO - (CH_2 - CH_2 - O)_{n+1} H \quad (2)$$

The policondensation reactions can occur non-catalytically, at a high temperature and pressure, or catalytically, in the presence of alkaline hydroxids or strong acids, at moderate temperatures and pressures. The usage of acid catalysts is limited by the production of polialkylglycolls which have small molecular weights and a very large distribution of the molecular weights.

[*] PETROL-GAZE University, Department of Chemical, Ploiesti, Romania
[**] ZECASIN S.A., Spl. Independentei 202, 060021, Bucharest, Romania

Analele Universităţii din Bucureşti – Chimie, Anul XIV (serie nouă), vol. I-II, pg. 95-101

One of the domains in which the transesterification with a single development is applied is the synthesis of the esters obtained out of fatty acids and polihydric compounds. Thus, the polihydric compounds such as glycerine, diglycerine, poliglycerine, xylitol, sorbitol, mannitol, saccharose and other poliglycoside, lead, by the partial esterification with fatty acids, to products presenting tensioactive properties. The hydrophilicity of these esters can be enhanced through the ethoxylation of the unesterified hydroxilic groups.

The sorbitol esters are very important due to fact that sorbitol is easily available (it is obtained by the simple reduction of glucose) and also due to the fact that sorbitol has a relatively higher thermic stability than saccharose. Sorbitol can be converted into monoesters or polyesters through the reaction with acid chlorides of the fatty acids in mild conditions, in the presence of pyridine. In industry, the esterification is produced using fatty acids or their methylic esters.[1] Along with the sorbitol which does not react, the reaction product contains monoesters or diesters obtained of fatty acids and sorbitol. Triesters are only formed in small percents.

A process for the synthesis of nonionic tensioactives was implemented using as raw material the saccharose instead of the sorbitol.[2] The ethoxylation at 120^0C took place in a first stage, followed by the transesterification of the fatty acid esters at 100^0C in the presence of a catalyst like potassium bicarbonate or at 180^0C in the presence of a catalyst like hydrochloric acid. Optionally a solvent can also be used and the transesterification can take place in the presence of an enzyme.[3]

In the majority of cases, emulsions are prepared with the aid of one or more emulsifiers, usually with different HLB values. The emulsifier is either dissolved or pre-emulsified in the oil or water phase, and this solution is then worked into the external phase, or the external phase is slowly added to the emulsifier–oil mixture. Whether an ionic or nonionic emulsifier is used for emulsifying depends on the system. Nonionic emulsifiers are also often used to prepare o/w emulsions.

The usage of nonionic emulsifiers for the preparation of emulsions based on oil-based products is recent. Thus, in a recent paper [4] it has been studied the behaviour of 13 nonionic surfactants for the preparation of bituminous o/w emulsions. It has been noticed that the emulsifiers used to prepare oil in water (o/w) emulsions are soluble in the aqueous phase and they have an HLB ranging from 9,6 to 17,6 and that the emulsifiers used to prepare water in oil (w/o) emulsions have an HLB ranging from 4,7 to 6,7, being soluble in the oily phase.

A different paper [5] describes a composition and a method for obtaining a w/o emulsion. This invention is related to a composition of the emulsifier forming a w/o emulsion with an exceptional stability as far as stocking is concerned. The emulsifier is a mixture made of dibehenilfumarate, the distearic ester of PEG 1500 and the stearic acid's monoethanolamine. The emulsifier thus prepared even manages to stabilize emulsions with a high content of water (50-90%).

The hydrophobic/hydrophilic properties of the emulsions prepared with such emulsifiers can be controlled by the selection of the fatty acid type, by the degree of ethoxylation and through cosurfactants addition respectwely.

Experimental

The reaction of ethoxylation was conducted in liquid phase, in a stirred reactor equipped with a heating coil using isothermic and isobaric conditions. The stirrer is acted by means of magnetic coupling. The heating agent is supplied by a thermostat, the temperature in the reactor being measured with a thermocouple and the pressure with a manometer. The stirring speed is adjusted using a potentiometer. The supply of oxiran is taken from a gas cylinder coupled with a calibrated vessel equipped with level-indicating glass.
The reactor's inertisation as well as the oxiran dosage is made using nitrogen. The succesive operations of voiding – inertisation of the reactor in order to eliminate the air, are performed with an air pump.
The reaction took place under a nitrogen layer between 110-130^{0}C temperatures. The process of ethoxylation is performed semicontinuously, the compound which is to be ethoxylated being introduced in the first stage, and then the ethylene oxide being gradually added with controlled rate, using in this aim the calibrated vessel with level-indicating glass. The catalyst used, the potassium hydroxide, is added as an aqueous solution, by dosing it in small amounts, before the feed of the ethylene oxide.
The reaction product was purified in a laboratory column-like reactor, with a view to retaining the alkaline metallic ions on the strong acid, cation-exchanger resin (PUROLITE CT 175).
The process of transesterification was performed in a three-necked glass flask under continuous mechanical mixing. The heating was provided with the help of an electric calotte equipped with a potentiometer for the adjusment of the heating rate.
The reaction of the sorbitol with the fatty acid esters was performed at 110-130^{0}C temperature, in the presence of an alkaline catalyst at atmospheric pressure or under a slight vacuum. The catalyst used was the potassium hydroxide with a concentration of max. 1% relative to the sorbitol, dissolved in methanol.
The experimental program performed with the purpose of determining the emulsifying characteristics of nonionic, sorbitol-based emulsifiers, took place on a micropilot, colloidal mill of the EMULBITUME type.
The raw materials used for the synthesis of the etoxilated products were: the ethylene oxide, the sorbitol and the methyl-oleate of analytical purity.

Results and discussions

The plot of Fig. 1 represents the specific ethylene oxide consumption in time during sorbitol ethoxylation at 110^{0}C and 4 atm.

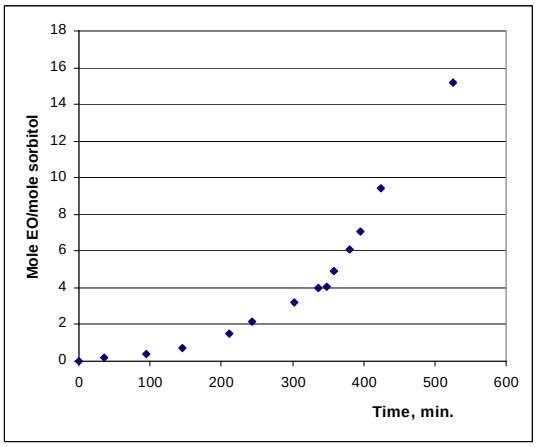

Fig. 1. *Specific ethylene oxide (EO) consumption in time during sorbitol ethoxylation (t = 110℃, p = 4 atm, KOH:Sorbitol = 0.6:100)*

As one can see from Figure 1, the reaction present an induction period when the process follow with low rate, behaviour probable due to relative high acidity of sorbitol. The influence of the catalyst's concentration on the reaction of sorbitol ethoxylation was emphasized in Figure 2, and the influence of the pressure on the ethoxylation process was evidenced Figure 3.

In Figure 4 is graphically represented the variation of the specific etylene oxide consumption in respect with time, for the ethoxylation of sorbitan di-oleate, comparing it to the ethoxylation of sorbitol, in the same working conditions.

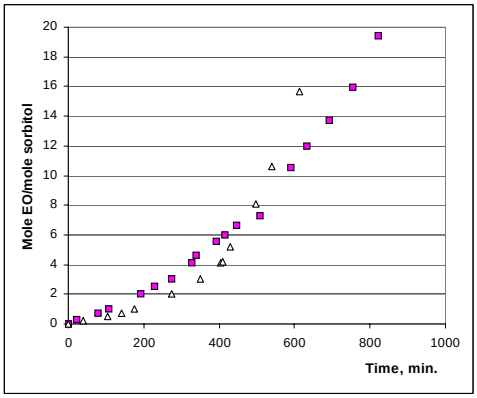

Fig. 2. *Effect of catalyst concentration on specific consumption of EO (sorbitol ethoxylation) (t = 100℃, p = 4 atm, (□) KOH:Sorbitol = 0.2:100, (Δ)KOH:Sorbitol = 0.4:100)*

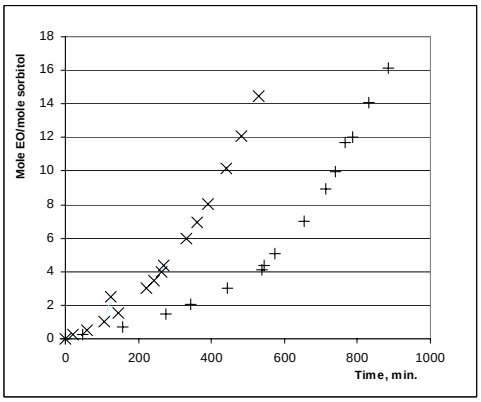

Fig 3. *Pressure effect on specific consumption of EO (sorbitol ethoxylation) (t = 110℃, KOH:Sorbitol = 0.2:100, (+) p = 3 atm, (×) p = 4 atm)*

In Figure 5 we comparatively present the ethoxylation of sorbitol for two different temperatures (100^0C and 110^0C).

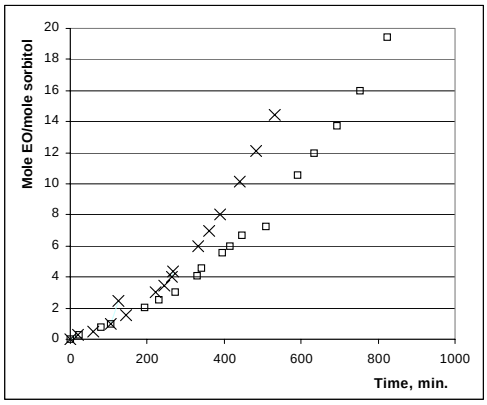

Fig. 4. *Temperature effect on specific consumption of EO (sorbitol ethoxylation) (p = 4 atm, KOH:Sorbitol = 0.2:100, (□) t = 100℃, (+) t = 110℃)*

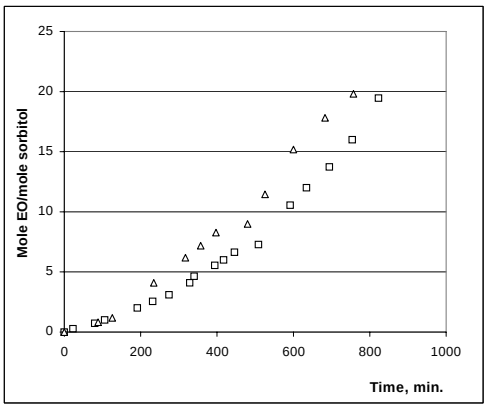

Fig. 5. *Time variation of specific EO consumption for different substrates (□) sorbitol, (Δ) sorbitan dioleate*

The experimental program of transesterification included 6 experience (see table1) using sorbitol or sorbitol ethoxylated with 20 molecules of ethylenoxide. The reaction temperature varied between 120-210^0C. The analysis of reaction progress was performed by measuring the saponification value.

The experimental observations evidenced the fact that the rise of the temperature over 135 ^{0}C favors the dehydration-condensation reactions conducting to caramel type by-products, this diminishing the selectivity in ester.

The tendency of the sorbitol condensation to caramel through shutting off the hydroxilic groups decrease if the ethoxilation stage is realized before the transesterification stage.

Table 1. Transesterification of sorbitol and ethoxylated sorbitol with methyl oleate

Nr crt	Sort of sorbitol	Temp. [^{0}C]	Pressure	Catalyst concentration [%]	R_m * E / S	Time of reaction [h]	Saponification value [mgKOH/g]
1.	Not-etoxylated	130	vacuum	0,8	4	16	244,2
2.	Not-etoxylated	120	vacuum	0,8	3	16	189,9
3.	Not-etoxylated	135	vacuum	0,8	2	16	179,9
4.	Not-etoxylated	120	vacuum	0,8	2	16	68,7
5.	Etoxylated	210	atmospheric	0,4	2	8	63,9
6.	Etoxylated	170	atmospheric	0,4	2	8	62,4
	Etoxylated						

R_m^* E / S –Molar ratio between sorbitol and ester

This emulsifiers were tested in the preparation of fuels emulsions in the following conditions:
- temperature of the organic phase : 80^0C
- temperature of aqueous phase : 40 ^{0}C
- content of the emulsifier : 1%
- weight ratio between organic phase and aqueous phase: 3/1
- rotation speed of atomix: 6000 rpm

The main characteristics of fuel emulsions obtained are :
- type of the emulsions: oil in water
- viscosity at 25^0C: 3,6-3,8^0E;
- stability: emulsion stable at 30 days after preparation.

Conclusions

The conclusions of this work can be drawn in the following points:

- the ethoxylation process of sorbitol present an induction period when the reaction follow with low speed, behaviour probable due to relative high acidity of sorbitol; after formation of the monoethoxylat intermediary product, the raw material acidity lowed and the process speed is stabilized at higher values.

- the increase of the catalyst's concentration increase the reaction rate without significant influence of the process rate in the induction period.

- the workin pressure influence in an important measure the reaction rate due to increase of the ethylenoxide concentration in liquid phase.

- the sorbitan di-oleate is ethoxylated with the higher rate than sorbitol in the same reaction conditions; the induction period is shorter than in the sorbitan di-oleate ethoxylation.

- the thermal stability of sorbitol is lower at temperature higher than 120^0C.

- the yield of the transesterification process is favorized by performing the process in vacuum.

- the fuels emulsions stability obtained with derivatives of ethoxylated oleic acid have the same stability as the cationic emulsions.

REFERENCES

1. *Ullmann"s Encyclopedia*, Sixth Edition, 2002, WILEY-VCH.

2. F.I. Talens si colab. , *J. Dispersion Science and Technol*. , 19(4), 423 - 433 (1998).
3. Clarient GmbH, US 6,465,036 / 2002, (F.X.Scherl).
4. Al. Sabagh Ahmed, Al treilea Congres Mondial de Emulsii 24 - 27 sept. 2002 , Lyon, Franta.
5. Akzo Nobel, US 6,486,120 / 2002, (N. Porta, H.J. Weissen).

SKELETAL ISOMERISATION ON SULFATED ZIRCONIA MODIFIED BY Ce^{IV} AND Sn^{IV} CATIONS

Mihaiela Ropot[*], Ruxandra Barjega[**], Floreta Constantinescu[***]

abstract: Sulfated zirconia and modified sulfated zirconia $Zr_{0.85}Me^{IV}_{0.15}O_2/SO_4^{2-}$ (M = Ce^{IV}, Sn^{IV}) have been studied as catalysts for skeletal isomerisation of n-butane. The correlation between the structure, porosity, the solid-acid character of these samples and their catalytic performances were reported.

key words: Modified sulfated zirconia; n-butane isomerisation.

Introduction

Sulfated metal oxides, particularly sulfated zirconia have been widely studied in the past 20 years because they present catalytic properties for various carbenium ion type reaction such as the skeletal isomerisation of lower alkanes at low temperature [1-5].

Many studies have been devoted to the investigation of the influence of preparation and of the nature of precursors, on the structural properties and the catalytic performances of sulfated zirconia, which were claimed to have superacidic properties [6-7]. Now it is accepted that this catalyst is not a superacid solid but is merely a strong solid acid; it was shown that its acid sites are not stronger than the Brönsted sites in promoted zeolites and the Lewis sites in γ-Al_2O_3 [8,9].

Different promoted sulfated zirconia with Fe, Co, Cr, W, Ni, Pt or with different oxides such as Al, Ce, Ga, In, Tl, Mo, W were also used as active contact masses in skeletal isomerisation of n-butane [10]. Many studies have come to the conclusion that the skeletal isomerisation of lower alkanes occurs via a bimolecular mechanism while for those with more than five carbons a monomolecular mechanism would be involved [11].

In both cases, however, the dehydrogenation function related to the redox character of the catalyst seems to be important.

The aim of this paper is to prepare high-dispersed composites $Zr_{0.85}Me^{IV}_{0.15}O_2/SO_4^{2-}$ (M = Ce^{IV}, Sn^{IV}) and to study the promoting effect of these sulfated zirconia catalysts in the skeletal isomerisation of n-butane. The presence of the modified cations in the zirconia

[*] University of Bucharest, Faculty of Chemistry, 4-14 Regina Elisabeta, Bucharest 3, 70346, Romania

[**] S.C. ZECASIN S.A., 202 Splaiul Independentei, Bucharest, Romania

[***] SNP – PETROM, Research Institute for Petroleum Processing and Petrochemistry, 291 A, Republicii Blvd., Ploiesti 2000, Romania

Analele Universităţii din Bucureşti – Chimie, Anul XIV (serie nouă), vol. I-II, pg. 103-110

lattice may induce the changes in the concentration and strength of acid sites and also in the redox ability of these catalysts. The correlation between the structural, the acid properties of the catalysts and their catalytic performances are also discussed.

Experimental

Catalysts preparation.

The $Zr(OH)_4$ and $Zr_{0.85}Me^{IV}_{0.15}(OH)_4$ were obtained by hydrolysis of ethanol solutions of $ZrCl_4$ and admixture of this compound and $Ce_2(NO_3)_2 \cdot 6H_2O$ or $SnCl_4$; these solutions were dropped under vigorous stirring, at room temperature in an aqueous hydrazine hydrate 20 % (w/w) solution. During the precipitation the pH remained 9. The precipitates were maturated 72 hours at 60 ^oC, the pH being unchanged. Then the product was filtered and washed with distilled water to remove all chlorine ions. Finally the gels were dried for 12 hours at 110 ^oC. Sulfated samples were prepared by impregnation of the dried gels for 24 hours with a 1N H_2SO_4 solution (15 ml/g of hydrous zirconium oxides), followed by filtration and drying at 110 ^oC for 12 hours. The solids were calcinated in an air stream (20 cm^3/min.) at 600 ^oC for 2 hours.

Catalysts characterization.

Differential thermal analysis were carried out on dried $Zr(OH)_4$ and $Zr_{0.85}Me_{0.15}(OH)_4$ and also on the sulfated samples. Both TG/DTA data were obtained simultaneous at a heating rate of 10 ^oC/min by using MOM-Q 1500 D equipment. The specific surface areas of the catalysts were determined by nitrogen adsorption isotherms at liquid nitrogen temperature, using a BET and Dubinin-Raduskyedici equations. The sulfated samples were examined by X-ray diffraction (XRD) using a Ni-filtered CuKα radiation with a goniometer speed of 1 ^oC/min. from 10 ^oC to 80 ^oC. For quantitative analysis a step scanning technique was applied in the 2θ range of 27-37^o, with a step of 0.02^o for 20 s. at each step. SiO_2-α-quartz was used as internal standard. The acidity of the samples was measured by ammonia TPD in the range of 100-500 ^oC.

The experiments were carried out in conventional equipment using a quartz microreactor, at the heating rate of 10 ^oC/min. in nitrogen flow; the microreactor was coupled at a GL chromatograph with TC detector. Catalytic tests were performed in a quartz microflow reactor with fixed bed at atmospheric pressure using 0.5 g of catalyst (0.4-0.5 mm fraction). The reactant flow was an admixture of argon and n-butane in a molar ratio 2:1. W/F = 16.8 mol n-$C_4H_{10} \cdot g_{cat} \cdot h^{-1}$ was used. On-line analysis of the products was made in a ThermoQuest Trace GC 2000 Gas Chromatography with FID detector and a capillary column with stationary phase GS-Alumina, 30m x 0.53 mm I.D.

Results and discussion

Thermogravimetric results are shown in the table 1.

Table 1. TG/DTA results for unsulfated and sulfated samples

Sample	Exothermic peak (°C)	Total weight loss (wt %)	Q[a] (u.c)
$Zr(OH)_4$	420	1.68	3.11
$Zr(OH)_4/SO_4^{2-}$	615	3.72	3.60
$Zr_{0.85}Ce_{0.15}(OH)_4$	380	3.77	5.95
$Zr_{0.85}Ce_{0.15}(OH)_4/SO_4^{2-}$	600	1.73	3.59
$Zr_{0.85}Sn_{0.15}(OH)_4$	430	4.35	7.92
$Zr_{0.85}Sn_{0.15}(OH)_4/SO_4^{2-}$	600	3.80	7.69

[a] Crystallization surface effect/g dehydrated sample

The catalytic precursor samples $Zr(OH)_4$ or $Zr_{0.85}Me^{IV}_{0.15}(OH)_4$ exhibit, between 130-330 °C, a wide and intensive endothermic peak assigned to the loss of hydration and constitution water. The hydrous oxides show an intensive exothermic peak at 380-420 °C, which is likely, related to the crystallization of ZrO_2. For the sulfated samples, the exothermic peak is shifted to a higher temperature; this is wider and of much lowers intensity. These results seem to be possible that M^{IV} ions are substituted in the ZrO_2 lattice. Over 600 °C the TG curve indicates a small but continuous weight loss of sample corresponding to the partial decomposition of the sulfate groups. At 850 °C another exothermic peak of lower intensity suggested that a change of crystalline structure. The surface area of sulfated zirconia and sulfated-doped zirconia samples are shown in table 2.

Table 2. Surface area and sulfur content of the sulfated zirconia catalysts.

Sample[a]	Surface area (m^2/g)	Pore volume 0-300 Å (cm^3/g)	Pore volume 0-100 Å (cm^3/g)	Sulfur content (wt %)
ZrO_2/SO_4^{2-}	110	0.1864	0.1715	2.23
$Zr_{0.85}Ce_{0.15}O_2/SO_4^{2-}$	107	0.1343	0.1222	2.08
$Zr_{0.85}Sn_{0.15}O_2/SO_4^{2-}$	126	0.1905	0.1657	2.64

[a] calcinated at 600 °C for 2 hours.

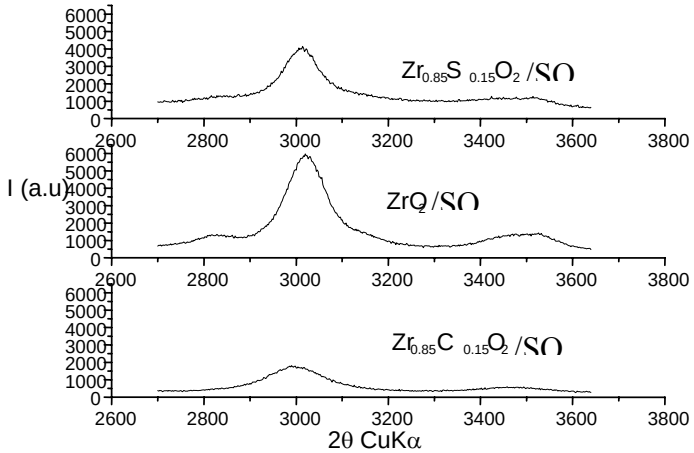

Fig. 1. *XRD patterns of the samples in the 2θ range 27-37°.*

All the catalysts present a high surface area and the pore volume distribution indicates that the adsorbents posses a well-defined mesopore structure with a maximum corresponding to pores with 50-75 Å diameter. XRD patterns of the sulfated samples are presented in the figure 1.

The volume fraction of the tetragonal phase could be determined from the empirical formula of Porter and Heuer [12] or using a similar empirical equation proposed by Toraya et al. [13]

The results presented in table 3. are similar, the differences might be accounted to the low monoclinic phase content.

Table 3. The content of the tetragonal phase of the samples and their lattice parameters of the main tetragonal phase.

Samples	V_t(%) [2]	V_t(%) [3]	a(Å)	c (Å)	c/a	V(Å^3)	D*(Å)
ZrO_2/SO_4^{2-}	86	81	5.09	5.20	1.022	134.5	85
$Zr_{0.85}Sn_{0.15}O_2/SO_4^{2-}$	91	86	5.10	5.22	1.024	135.9	90
$Zr_{0.85}Ce_{0.15}O_2/SO_4^{2-}$	100	100	5.14	5.21	1.015	137.7	54

* D is the average crystallite size along (1,1,1) direction calculated by Sherrer's formula $D=0.91\lambda/(\beta\cos\theta)$ were λ is the wavelength (Cu K_α), $\beta$the correct half-width obtained using α-quartz as reference and the Warren formula and θ the diffraction angle [8].

The volume fraction of the tetragonal phase were correlated with the values of the temperatures for the exothermic peak from DTA profiles which increased with the percentage of the volume of the tetragonal phase as a result of the stabilizing role played by the cationic doping, explained partially by a bulk free energy effect.

As figure 1 shows, it should be pointed out that, for the $Zr_{0.85}Ce_{0.15}O_2/SO_4^{2-}$sample, because of the line broadening due to the fine crystallite size, some uncertainties in discriminating between the tetragonal (*t)* and the cubic (*c*)- phases subsist. However, as the full-width at half-maximum (half-width) of the $2\theta = 34.69^o$ is considerable larger the half-width of the $2\theta = 29.98^o$ we should assume that the $2\theta = 34.69^o$ peak is actually, the convolution of the 0,0,2 and 2,0,0 tetragonal peaks. The fitting of the profiles reveals improved standard fitting errors by assuming a tetragonal symmetry in stand of a cubic one. It is to be emphasised that for this sample the axial *c/a* ratio of the unit cell is the lowest one, quite close to the unit, revealing that for the ceria-zirconia sample the tetragonal phase has the lowest oxygen displacements from the ideal fluorite positions [14] as a result of the stabilising role played by cerium in the structure. In fact it has been reported [15,16] for zirconia-ceria materials with ceria amounts > 50% XRD patterns with a cubic structure and a lattice parameter moving as the cerium amount increases towards the lattice parameter of the fluorite-type structure of CeO_2.

Table 3 shows some interesting results. Sample $Zr_{0.85}Ce_{0.15}O_2/SO_4^{2-}$ has the largest lattice volume as a result of the Ce^{4+} incorporation in the framework (larger ionic radius in comparison with Zr^{4+}, 1.01Å versus 0.80Å). The lowest axial ratio along with the lowest crystallite size for the ceria-zirconia sample is a clear mark of a stabilised tetragonal phase. For the $Zr_{0.85}Sn_{0.15}O_2/SO_4^{2-}$ one expected the lowest volume as the ionic radius are lowest one (0.71 Å). For this sample an overlapping effect occurred in connection with the transition of the tetragonal phase to the monoclinic phase. This sample has the largest crystallites size and the largest axial ratio too, indicating a higher transformability of the

tetragonal to the monoclinic phase. A crystallite effect size is reported in the literature [14, 17].

Table 4 contains the correlation between the X-ray crystallite size, the BET surface areas and levels of the X-ray background as a measure of the X-ray amorphous material content.

We calculated the surface area derived from the average crystallite size, D (m), determined by XRD, assuming a spherical particle:

$$A_{XRD}[m^2 / g] = 6/(\rho D) \qquad (1)$$

where $\rho[gm^{-3}]$ is the density of the crystallite, which we evaluated also as an X-ray density using the crystallographic data and the chemical compositions already determined.

In the evaluation of the background in the 2θ range 27-37^o a correction was applied which takes into account the differences in the mass absorption coefficients μ for the $Cu_{k\alpha}$ wavelength. The background level estimated as a constant will ascertain for the differences of the amorphous and very fine crystallites content of these samples.

Table 4. The correlation between the XR crystallite size, the BET surface areas and levels of the XR background.

Sample	$A_{XRD}(m^2.g^{-1})$	$A_{BET}(m^2.g^{-1})$	Background level (a.u)
ZrO_2/SO_4^{2-}	78	110	620
$Zr_{0.85}Sn_{0.15}O_2/SO_4^{2-}$	71	126	827
$Zr_{0.85}Ce_{0.15}O_2/SO_4^{2-}$	116	107	382

The results from table 4 lead to the following observation:

- only for the ceria-zirconia sample the BET surface area and XRD area are in good agreement. This result is consistent with the low amorphous amount and the formation only of a pure tetragonal phase for this sample.
- there is a linear correlation between the BET area and the background level attesting for the connection between the amorphous or very fine particles amount and the BET areas.
- the appearance of a larger amounts of an amorphous material is due to the transition from the tetragonal phase to a monoclinic phase accompanied by a volume expansion.
- the highest BET area along with the largest amorphous amount for $Zr_{0.85}Sn_{0.15}O_2/SO_4^{2-}$ is suggested by a larger unit cell volume than for the zirconia sample and the largest crystallites sizes, too. For larger crystallites it seems, that is a higher probability to contain embryonic nuclei which, when they reached a critical size, favour the transition to a monoclinic phase

Temperature-programmed desorption of ammonia has been used as a measure of total acidity and acid strength distribution in solids. The results are shown in table 5.

Table 5. Acidity and acid strength distribution of the catalysts.

Sample	Total acidity (100 ºC) mmol $NH_3 \cdot g^{-1}$	Desorbed NH_3 mequiv. $NH_3 \cdot g^{-1}$			Number of strong acid sites/$g_{cat.}$
		Weak acid sites 100-175ºC	Medium acid sites 175-300ºC	Strong acid sites 300-500ºC	
ZrO_2/SO_4^{2-}	0.70	0.11	0.24	0.35	$2.11 \cdot 10^{20}$
$Zr_{0.85}Sn_{0.15}O_2/SO_4^{2-}$	0.76	0.14	0.29	0.33	$1.99 \cdot 10^{20}$
$Zr_{0.85}Ce_{0.15}O_2/SO_4^{2-}$	0.53	0.17	0.20	0.16	$9.64 \cdot 10^{19}$

The ZrO_2/SO_4^{2-} and respectively $Zr_{0.85}Sn_{0.15}O_2/SO_4^{2-}$ samples have the same concentration of strong acid sites even the last one has a grater amount of the weak and medium acid sites. The $Zr_{0.85}Ce_{0.15}O_2/SO_4^{2-}$ sample exhibits a lower total acidity and also a lower concentration of strong acid sites.

The figure 2 shows the variation of the catalytic performances of unpromoted ZrO_2/SO_4^{2-} at different temperature of reaction. The increase of the reaction temperature corresponds to a high activity, which is associated to a lower selectivity.

The activity of sulfated zirconia and promoted samples decreases during the first 30 minutes then it trends to a constant value. (Figure 3). The decrease of catalytic activity in time is due to the fact that by-products are formed as result of the simultaneous secondary reactions, mainly at higher temperature, responsible for their catalytic deactivation. This can also show from the results give in the table 6.

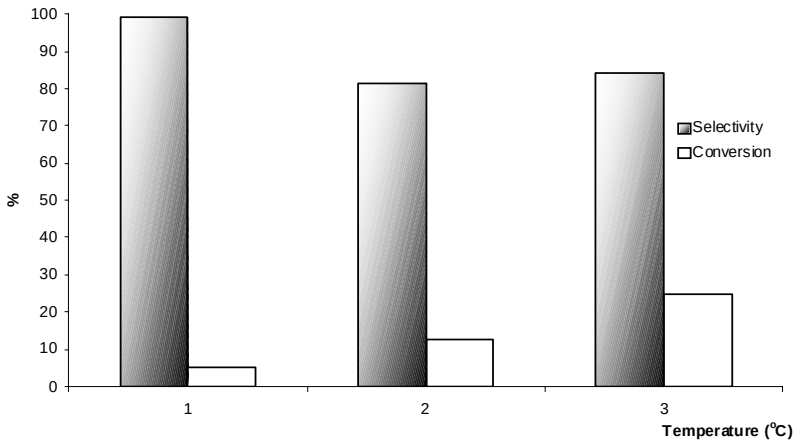

Figure 2. Conversion and selectivity for ZrO_2/SO_4^{2-} at different temperatures. (1): 100°C, (2):150°C, (3) 250°C.

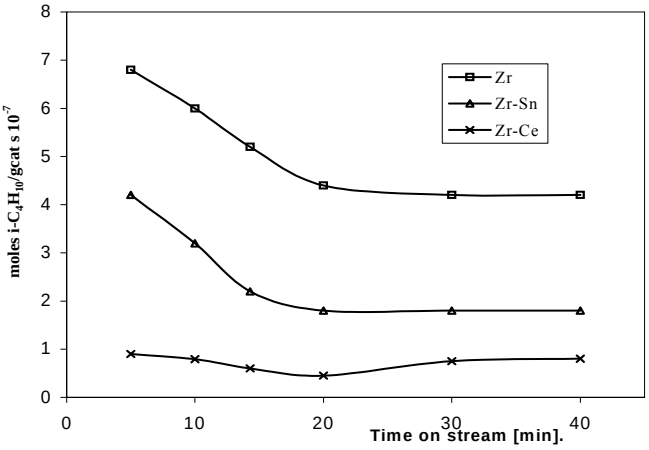

Fig, 3. The activity of sulfated zirconia at 250 °C.
0,5 g catalysts; reactant flow = 5 ml/min.; Ar/n-C_4H_{10} = 2/1 molar ratio

Table 6. The activity of the catalysts in the skeletal isomerisation of n-butane; temp. = 250°C, 0.5 g catalyst; reactant flow = 5 ml/min, Ar/n-C_4H_{10} = 2/1 molar ratio;

Sample *	Time on stream [min.]	wt %					Conversion n-C_4H_{10} (%)	Selectivity iso-C_4H_{10} (%)
		C_2+C_3	iso C_4H_{10}	n-C_4H_{10}	C_4H_8	C_4^+		
SZ	5	4.72	28.76	57.14	6.06	3.32	42.86	67.10
	30	2.61	18.83	74.58	2.75	1.23	25.42	74.07
SZ-Sn	5	1.20	15.26	81.55	1.59	0.40	18.45	82.71
	30	0.46	8.20	90.60	0.52	0.22	9.40	87.23
SZ-Ce	5	0.61	6.24	92.49	0.46	0.20	7.51	83.08
	30	0.18	3.62	95.83	0.24	0.13	4.17	86.81

*SZ = ZrO_2/SO_4^{2-}; SZ-Sn = $Zr_{0.85}Sn_{0.15}O_2/SO_4^{2-}$; SZ-Ce = $Zr_{0.85}Ce_{0.15}O_2/SO_4^{2-}$

Even the activity of promoted catalysts is lesser than for unpromoted ones, the isobutane selectivity is higher for the samples modified by Ce^{4+} and Sn^{4+}. The cracking effect of ZrO_2/SO_4^{2-} is diminished in the same way as the dehydrogenation effect. There have been given for the formation of Zr^{3+} species located on the crystallite surfaces by decomposition of same sulfate groups during the calcination of the catalysts. The redox properties of the catalysts may strongly depend on the surface concentration of these ions having a lower oxidation state. Doping the ZrO_2/SO_4^{2-} lattice with different tetravalent ions, which can also change their oxidation state, we are able to discreetly modify the redox properties of these catalysts. The correlation of these results shown that the doping of zirconia lattice with Ce^{4+} and respectively Sn^{4+} ions has as effect the stabilization of the tetragonal phase, an increase of the surface area and the modification of the crystallite dimensions. The catalytic activity depends on both, the concentration of the strong acid sites and the electron acceptance ability of the solid as a result of the enhancement of the redox properties.The presence of Sn^{4+}ions seem to modified the redox sites population without affecting essentially the acidity of the solid, which has a lower activity than unpromoted sulfated zirconia but higher selectivity in isobutane formation. As already was shown the first step of reaction implies the abstraction of hydrogen from hydrocarbon substrate and for this purpose the acid sites as well as the redox properties of the catalyst are manly responsible. This step is the cause

of the activity of these catalysts and also of their deactivation, because dehydrogenated species lead to polymerisation. Even the dehydrogenated function of the promoted catalysts is lower than the unpromoted sample, the doped ions may diminish the polymerisation function and enhance the consumption of olefins by a bimolecular mechanistic pathway of skeletal isomerisation of n-butane.

Conclusions

The preparation of the doped sulfated zirconia by soft chemistry as well described leads to the synthesis of a stable ZrO_2 tetragonal phase; these solids have a particular texture characterised by a pore diameter in the mesoporous range. The synthesised composites $Zr_{0.85}Me^{IV}_{0.15}O_2/SO_4^{2-}$ (M = Ce^{IV}, Ti^{IV}, Sn^{IV}) having the same sulfur content have lower activity than undoped sulfated zirconia, but they are more selectiv in skeletal isomerisation of n-butane.

REFERENCES

1. Hino M., Kobayashi S. and Arata K., (1979)*J. Am. Chem. Soc.,* **101**, 6439.
2. Hino M. and Arata K., (1980) *J. Chem. Soc., Chem. Commun.,* 851.
3. Arata K., *Adv. Catal*., (1990), **37**, 165.
4. Tanabe K. and Yamaguchi T. (1990)*, Stud. Surf. Sci. Catal*., **44**, 99.
5. Tanabe K., Hattori H. and Yamaguchi T., (1990) *Crit. Rev. Surf. Chem.,* **1***,* 1.
6. P. Moles, *Spec. Chem., 12*, 382 (1992).
7. B. H. Davis, R. A. Keogh, R. Srinivasan, *Catal. Today, 20,* 219 (1994).
8. Yin-Yan Huang, Bi-Ying Zhao, You-Chang Xie, *Appl. Catal., 75-83,* 171 (1998).
9. V. Adeeva, J. W. de Hann, J. Janchen, G. D. Lei, V. Schunemann, L.J.M. van de ven, W.M.H. Sachtler, R. A van Santen, *J. Catal., 151*, 365 (1995).
10. X. Song, A. Sayari, *Catal. Rev.-Sci. Eng., 38(3)*, 329-412 (1996).
11. E. Iglesia, S.L. Soled, G.M. Kramer, *J. Catal, 144*, 283 (1993).
12. D.L.Poster and A.H.Heuer , *J.Am.Ceram.Soc.,*62 [5-6], 298-305 (1968).
13. H.Toraya,M.Yoshimara,S.Somaya, *J.Am.Ceram.Soc.,67,* C-119 (1984).
14. W.Stichert and F.Schűth ,*Chem.Mater.,10,* 2020-2026 (1998).
15. S.Rossignol,Y.Madier,D.Duprez, *Catalysis Today*,*50,* 261-270 (1999**).**
16. S.Rossignol,F.Gerard and D.Duprez, *J.Mater.Chem.,*9, 1615-1620 (1999**).**
17. R.C.Garvie,*J.Phys.Chem. 82,* 216-224 (1978).

PARTICLE-INDUCED X-RAY EMISSION (PIXE): A PRACTICAL APPROACH TO DETERMINE THE MANGANESE ACCUMULATION BY YEAST MITOCHONDRIA[a]

Ileana C. Farcasanu[*], Fumitaka Nishiyama[**], Tokichi Miyakawa[***]

abstract: In this study, particle-induced X-ray emission (PIXE) is used to monitory the Mn^{2+} accumulation by yeast mitochondria, under conditions of Mn^{2+} stress. We found that mitochondria accumulates the cation, leading to a steady-state level in the first 20 minutes of incubation under high Mn^{2+}.

Introduction

Manganese is an essential metal for all organisms and has been implicated in regulation of growth and metabolism of fungi, mainly due to its influence on several key enzymes. Mn^{2+} has been proposed as an important cell regulator [1] and it may, under some circumstances, substitute for calcium [2]. In yeast, it appears to be preferentially located in the vacuole, where it is bound to polyphosphate; this organelle is thought to be the main determinant for Mn^{2+} detoxification [3-7]. Mn^{2+} is also present in other sucellular compartments. Thus, the cytosol contains Mn^{2+} as well as Mn^{2+}-dependent enzymes, which include pyruvate decarboxylase, glutamine syntethase, and arginase [8]. In the Golgi apparatus, Mn^{2+} activates glycosyltransferases that are involved in the processing of secreted proteins [8,9]. In the mitochondria, Mn^{2+} is required by mitochondrial superoxide dismutase (SOD), by enzymes of the citric acid cycle [8] as well as by proteases involved in mitochondrial protein import. As most of the trace metals, manganese in toxic when present in high concentrations, having growth-inhibitory and mutagenic properties in yeast [10].

---

[a] This work was performed at Hiroshima University, Japan

[*] Bucharest University, Faculty of Chemistry, Department of Organic Chemistry and Biochemistry, Sos. Panduri 90-92, Bucharest, Romania. Tel.: 40-21-4103178/ext.135. E-mail: ifarcasanu@chem.unibuc.ro. Corresponding author

[**] Department of Power Engineering and Applied Physics, Graduate School of Engineering, Hiroshima University, Japan.

[***] Department of Molecular Biotechnology, Graduate School of Advanced Sciences of Matter, Hiroshima University, Japan.

Analele Universităţii din Bucureşti – Chimie, Anul XIV (serie nouă), vol. I-II, pg. 111-115

The bakers' yeast *Saccharomyces cerevisiae* represents an ideal eukaryotic system in which to unravel metal trafficking pathways. This organism has been extremely powerful for elucidating the manganese acquisition pathway and a number of candidates for manganese trafficking have already been identified. The transport of manganese (and calcium) into the secretory pathway is accomplished by a Golgi-localized P-type ATPase known as Pmr1p [11-14]. Atx2p is another manganese homeostasis factor that localizes to intracellular vesicles [15] whereas the uptake of manganese into yeast vacuoles is accomplished by vacuolar Ccc1p [16, 17]. Ahp1p is another protein involved in trafficking manganese, apparently transporting this cation from cytosol to mitochondria [18].

When studying metal trafficking, assessment of intracellular distribution of cations can be enlightening. Particle-induced X-ray emission (PIXE) is a multielement analysis technique that is useful for applications in biological sciences. PIXE was used to monitory the uptake or efflux rates of individual trace elements [19,20] as well as the intracellular distribution of manganese [18]. In this article, we use PIXE to monitory the manganese accumulation by yeast mitochondria, under conditions of manganese stress.

Experimental

Yeast strains, growth conditions, and isolation of mitochondria

The brewer's yeast *Saccharomyces cerevisiae*, strain W303 1A (*MAT* **a** *trp1 leu2 ade2 ura3 his3 can1-100*) was used for our experiments. Cells were grown in synthetic medium containing 0.67% yeast nitrogen base without amino acids, amino acids mixture, 0.1% glucose, and for mitochondria proliferation, 3% glycerol. Cell growth was assessed by measuring OD_{600}. For isolation of mitochondria, 100 ml-cultures were used (cell density, $5x10^7$ cells/ml). Mitochondria were isolated from a homogenate of yeast spheroplasts as described by Yaffe [21], including the purification in a Percoll gradient step. Succinate dehydrogenase (SDH) was used as a mitochondrial marker and its activity was measured using the method described by Munujos *et al*. [22]. Mitochondrial extracts were obtained by permeabilizing organelle membranes with digitonin (1mg/mg protein).

Mn^{2+} determination. Yeast cells were grown $5x10^7$ cells/ml, then Mn^{2+} was added to the desired concentration. Cells were incubated with Mn^{2+} for various times. Mn^{2+}-loaded cells were rapidly harvested and transferred to centrifuge tubes that contained 6 ml silicone oil (550; Dow Corning) on top of which had been layered 8 ml of 10 mM MES-Tris buffer (pH 8) with 20 mM EDTA, vortexed briefly and let 10 seconds for phase separation. Cells were harvested by centrifugation through the silicone layer, while the externally-bound ions remained complexed with EDTA. The buffer and the silicone oil were aspirated off, and cells were used to isolate the mitochondria that were subjected to PIXE analysis for Mn^{2+} determination.

Preparation of PIXE samples. 5 μl of purified mitochondria were placed on polycarbonate membranes (Nucleopore Corp., U. S. A., pore size 0.1 μm, thickness ~ 6 μm) and let dry overnight in a desiccator containing silicagel. The Mn^{2+} in the mitochondrial material was determined using a Van de Graaff accelerator (Nissin High Voltage Co. Ltd., model AN-2500). The proton energy used was 2 MeV. The Mn^{2+}

determined was expressed as μg/mg total cellular protein. Proteins were measured using the method described by Bradford [23]. All measurements were done three times, and the results were similar. Unless otherwise stated, all manipulations were done at 4°C.

Results and discussion

The number of individual mitochondria per yeast cell varies from 1-2 in early logarithmic phase on glucose. When grown on nonfermentable carbon sources (*e.g.*, glycerol, ethanol, lactic acid, etc.) the number of mitochondria is higher compared to the same stage of growth on glucose. In this study, we chose glycerol as a carbon source for the yeast cells used to determine the mitochondrial accumulation of Mn^{2+}. Glycerol induces mitochondria proliferation and the yield in mitochondria isolation can be therefore increased.

Mn^{2+} concentration in conventional yeast media is about 3 μM [24], but *S. cerevisiae* cells are viable in environments containing much higher levels. Thus, the wild-type strain W303 1A that was used in our experiments could grow on glycerol agar plates containing $MnCl_2$ up to concentrations as high as 8-10 mM (data not shown). We also determined the growth of yeast cells in liquid glycerol media containing various concentrations of $MnCl_2$ (Fig. 1).

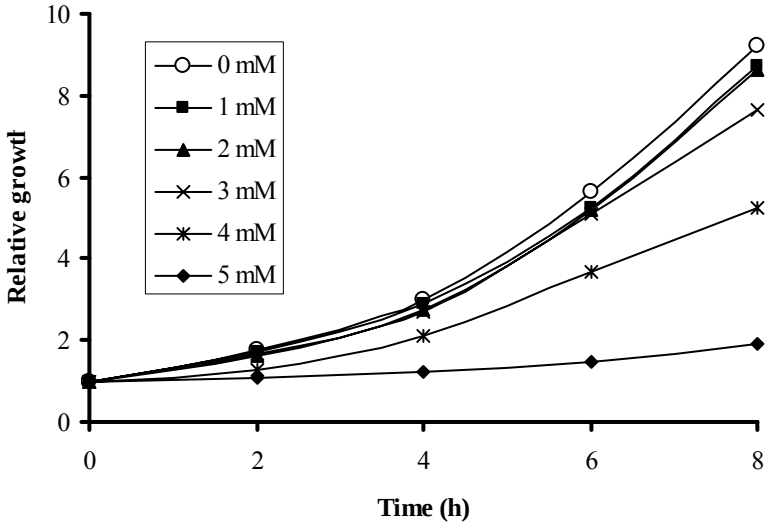

Fig.1. ***Influence of Mn^{2+} on growth.*** *Yeast cells were grown in synthetic media containing 3% glycerol up to 1 x10^6 cells/ml, before various concentrations of $MnCl_2$ were added. Growth was assessed by measuring OD_{600}.*

We found that Mn^{2+} did not impair cell growth at concentrations up to 3 mM. At 4 mM, Mn^{2+} reduced growth rate considerably, but the cells could still undergo division. At 5 mM,

Mn^{2+} induced growth arrest (Fig. 1). To determine the Mn^{2+} accumulation by mitochondria, we used the 3 mM $MnCl_2$ concentration in the incubation medium. At this concentration, Mn^{2+} accumulation did not interfere with mitochondria integrity and proliferation (as seen by microscopic analysis and SDH activity, data not shown), and at the same time it was high enough to allow detection of Mn^{2+} dynamics in mitochondria. We found that Mn^{2+} accumulated in the mitochondria in the first 20 minutes of exposure of cells to the cation, before reaching a saturation level (Fig. 2A).

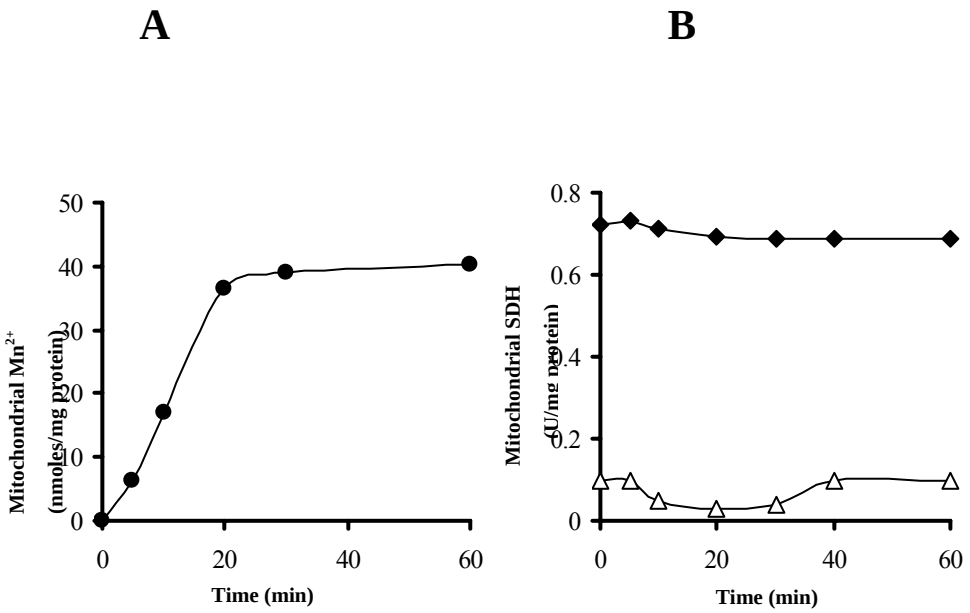

Fig. 2. ***A. Mn^{2+} accumulation in yeast mitochondria.*** *Yeast cells were grown in synthetic media containing 3% glycerol to 5 x10^7 cells/ml, before $MnCl_2$ was added (3 mM final concentration). Mitochondria were isolated and their Mn^{2+} content was determined by PIXE.* ***B. Succinate dehydrogenase (SDH) activity*** *was monitored as a mitochondrial marker. SDH activity was measured in mitochondrial extracts (closed diamonds) and non-mitochondrial extracts (opened triangles).*

The activity of mitochondrial enzyme succinate dehydrogenase was measured as mitochondrial marker in the extracts obtained from the same pool that was used for Mn^{2+} detection by PIXE (Fig. 2B, closed diamonds). The non-mitochondrial fraction was also tested for SDH activity and was found to be almost free of mitochondrial contamination (Fig. 2B, opened triangles). The mitochondrial fractions used for Mn^{2+} detection were also tested for contamination by other subcellular components, but we practically found no activity of vacuolar or cytosolic enzymatic markers (data not shown). Although we cannot completely rule out the possibility of contamination with other subcellular compartments, we consider that the approach we used offers a possibility to monitor cation accumulation by yeast mitochondria.

REFERENCES

1. Wiliams, R. J. P. (1982) *FEBS Lett.* **140**, 3-10
2. Loukin, S and Kung, C. (1995) *J. Cell Biol.* **131**, 1025-37
3. Okorokov, L. A., Lichko, L. P., Kadomtseva, V. M., Kholodenko, V. P., Titovski, V. T., and Kulaev, I. S. (1977) *Eur. J. Biochem.***75**, 373-7
4. Lichko, L. P., Okorokov, L. A., and Kulaev, I. S. (1980) *J.Bacteriol.* **144**, 666-71
5. Okorokov, L. A., Kulakovskaya, T. V., Lichko, L. P., and Polorotova (1985) *FEBS Lett.* **192**, 303-6
6. Kihn, J. C., Dassargue, C. M., and Mestdagh, M. M. (1988) *Can. J. Microbiol.* **34**, 1230-4
7. Paidhungat, M. and Garrett, S. (1998) *Genetics*, **148**, 1787-98
8. Wedler, F. C. (1994) *Manganese in Health and Disease* ed. Klimis-Tavantzis D. J., CRC Press Inc., Boca Raton FL, 1-38
9. Dürr, G., Strayle, J., Plemper, R., Elbs, S., Klee, S. K., Catty, P., Wolf, D. H., and Rudolph, H. K. (1998) *Mol. Biol. Cell* **9**, 1149-62
10. Putrament, A., Baranovska, H., Ejehart, A., and Jachymezyc W. (1977) *Mol. Gen. Genet.* **151**, 67-76
11. Rudolph, H. K., Antebi, A., Fink, G. R., Buckley, C. M., Dorman, T. E., LeVitre, J., Davidow, L. S., Mao, J. I., and Moir, D. T. (1989) *Cell* **58**, 133-45
12. Antebi, A., and Fink, G. R. (1992) *Mol. Biol. Cell* **3**, 633-54
13. Mandal, D., Woolf, T. B., and Rao, R. (2000) *J. Biol. Chem.* **31**, 23933-8
14. Sorin, A., Ross, G., and Rao, R. (1997) *J. Biol. Chem.* **272**, 9895-901
15. Lin, S. J., and Culotta, V. C. (1996) *Mol. Cell. Biol.* **16**, 6303-12
16. Lapinskas, P. J., Lin, S. J., and Culotta, V. C. (1996) *Mol. Microbiol.* **21**, 519-28
17. Li, L., Chen, O. S., Ward, D. M., and Kaplan, J. (2001) *J. Biol. Chem.* **276**, 29515-19
18. Farcasanu, I. C., Hirata, D., Tsuchiya, E., Mizuta, K., and Miyakawa, T. (1999). *Biosci. Biotechnol. Biochem.* **63**: 1871-81
19. Farcasanu, I. C., Hirata, D., Tsuchiya, E., Nishiyama, F., and Miyakawa, T. (1995) *Eur. J. Biochem.* **232**: 712-17
20. Farcasanu, I.C., Mizunuma, M., Hirata, D., and Miyakawa, T. (1998) *Mol. Gen. Gen.* **259**: 541-8
21. Yaffe, M. P. (1991) *Methods Enzymology* **194**, 627-4
22. Munujos, P., Coll-Canti, J., Gonzales-Sastre, F., and Gella, F. J. (1993) *Anal. Biochem.* **72**, 506-9
23. Bradford, M. M. (1976) *Anal. Biochem.* **72**: 248-54
24. Sherman, F., Fink, G. R., and Hicks, J. B. (1986) *Methods in yeast genetics.* Cold Sprig Harbor Laboratory Press, Cold Spring Harbor, New York

COORDINATION OF Co(II), Ni(II), Cu(II), Zn(II), Cd(II) AND Hg(II) WITH THE NEW SCHIFF-BASE DERIVED FROM 4,5-DIHYDROXIPHTALALDEHIDE AND 2-AMINOTHIAZOLE

Monica Iliş[*], Angela Kriza, Veronica Pop, Anca Nicolae[**]

abstract: A series of new complexes of type $[ML_2].xH_2O$ (where x = 0 for M = Zn(II), Cd(II) and Hg(II); x = 1 for M = Co(II), Ni(II) and Cu(II); LH_2 is a Schiff-base derived from 4,5-dihydroxiphtalaldehide and 2-aminothiazole) have been prepared. The compounds were characterized by elemental analysis, IR and UV-VIS spectra, magnetic moments and thermal behaviour have been discussed.

Introduction

A great number of complexes of different transitional metallic ions with bidentate Schiff-bases, derived from 2-aminothiazole and from different type of carbonylic compounds, have been reported. Heterocyclic ligands containing nitrogen and sulf donor atoms have been extensively studied due to their biological applications, in particular as pesticides and drugs [1-4]. In order to obtain more information about the preparation conditions, the properties and the stereochemistry of the metallic chelates with Schiff-bases, derived from 2-aminothiazole, a new series of complexes of type $[ML_2].xH_2O$ (x = 0 for M = Zn(II), Cd(II) and Hg(II); x = 1 for M = Co(II), Ni(II), Cu(II); LH_2 is a Schiff-base derived to 2-aminothiazole and 4,5-dihydroxiphtalaldehide, has been prepared.

Materials and Methods

The chemicals were purchased from Aldrich and all manipulations were performed using materials as received. The IR spectra were recorded on a BIO-RAD FTIR 135 spectrophotometer using KBr pellets. Electronic spectra have been obtained by diffuse reflectance technique, using MgO as standard, with a UV-VIS Carl Zeiss Jena spectrophotometer. The magnetic moments have been measured by the Faraday method. Thermal decomposition was studied with a MOM Q-1500 D derivatograph. Metallic ions were estimated by the AA 6 DA – VARIAN TECHTRON atomic absorbtion spectrophotometer and nitrogen has been determined by the Kjeldahl method.

The Schiff-base (LH_2) was prepared by mixing the methanolic solutions of 4,5-dihydroxiphtalaldehide and 2-aminothiazole (molar ratio 1:1) and refluxing for 2 h, on a water bath, filtered, washed with methanol, dried and recrystallized from methanol, with melting point at 210^{o}C.

[*] Department of Inorganic Chemistry, Faculty of Chemistry, University of Bucharest
[**] Department of Organic Chemistry, Faculty of Chemistry, University of Bucharest

Analele Universităţii din Bucureşti – Chimie, Anul XIV (serie nouă), vol. I-II, pg. 117-121

The compounds were prepared by mixing, at room temperature, with stirring the methanolic solutions of Schiff-base derived from 4,5-dihydroxiphtalaldehide and 2-aminothiazole and the salt of the appropriate metallic ion, in molar ration 2:1. The pH of the resulting solution was adjusted to about 7 by adding aqueous solution of Na_2CO_3. By changing the pH, coloured precipitates have been obtained. The precipitates were filtered, washed with methanol and were dried in vacuum.

Results and Discussion

The Co(II), Ni(II), Cu(II), Zn(II), Cd(II) and Hg(II) compounds with the Schiff-base derived from 4,5-dihydroxiphtalaldehide and 2-aminothiazole, were obtained as powers with high melting points and low solubility in organic solvents. Anal. for $C_{22}H_{16}O_7N_4S_2Co$: calc. (%) N 9.80, Co 10.31, found (%) N 9.60, Co 10; for $C_{22}H_{16}O_7N_4S_2Ni$: calc. (%) N 9.81, Ni 10.28, found (%) N 9.50, Ni 9.98; for $C_{22}H_{16}O_7N_4S_2Cu$: calc. (%) N 9.73, Cu 11.04, found (%) N 9.21, Cu 10.74; for $C_{22}H_{14}O_6N_4S_2Zn$: calc. (%) N 9.73, Zn 11.35, found (%) N 9.32, Zn 11.00; for $C_{22}H_{14}O_6N_4S_2Cd$: calc. (%) N 8.99, Cd 18.05, found (%) N 8.62, Cd 17.45; for $C_{22}H_{14}O_6N_4S_2Hg$: calc. (%) N 7.88, Hg 28.21, found (%) N 7.42, Hg 27.98.
The elemental analysis for all these complexes are in agreement with the proposed formula $[ML_2].xH_2O$ (where x = 0 for Zn(II), Cd(II) and Hg(II); x = 1 for Co(II), Ni(II) and Cu(II)).
In order to get data concerning the ligand mode coordination to metallic ions, the IR spectra, on the 400-4000 cm^{-1} range, for free ligand and for complexes, have been carried out (Table 1).

Table 1. The characteristic frequencies in IR (cm^{-1}) for the ligand and complexes

Compound	$\nu_{C=N}$	ν_{C-O} phenolic	ν_{C-N} exocyclic	ν_{-CHO}	ν_{C-S}	ν_{H-OH}
LH_2: $C_{11}H_8O_3N_2S$	1595	1141	1290	1634	730	-
$[CoL_2].H_2O$	1586	1148	1272	1633	732	3415
$[NiL_2].H_2O$	1579	1154	1281	1635	733	3407
$[CuL_2].H_2O$	1589	1158	1280	1636	738	3447
$[ZnL_2]$	1588	1152	1274	1633	734	-
$[CdL_2]$	1587	1143	1273	1636	733	-
$[HgL_2]$	1578	1148	1276	1635	732	-

In the spectrum of the free ligand, the sharp band at 1595 cm^{-1} can be assigned to the $\nu_{C=N}$ vibration. In the spectrum of the complexes, this band is found at the lower values ($\Delta\nu$ = 9-17 cm^{-1}). The lowering of the $\nu_{C=N}$ frequency in the complexes, indicates the coordination of the azomethine nitrogen atom at the metallic ion [5].
The coordination through the azomethinic nitrogen atom is supported by the shift of ν_{C-N} (exocyclic) frequency to lower wave number ($\Delta\nu$ = 9-18 cm^{-1}) in the IR spectra of complexes compare to IR spectrum of the free ligand.
The infrared spectrum of the free ligand shows a band at 1141 cm^{-1} assigned to the vibration frequency of the phenolic C-O group. In the spectrum of the complexes, this band undergoes a positive shifts (with 7-17 cm^{-1}) indicating that the Schiff-base is bonded to the metallic ions through the oxygen phenolic atoms [6-8].
The ν_{C-S} and ν_{-CHO} are not affected by coordination to metallic ion.

In addition, all IR spectra belonging to the Co(II), Ni(II) and Cu(II) compounds present an absorption band at 3415, 3407 and 3417 cm^{-1}, confirming the existance of water molecules in the structure of the crystalline lattice [9]. The presence of the crystallizations water was indicated by the thermogravimetric analysis.

The information reffering to the geometry of these complexes are obtained from the electronic spectra and from the value of the magnetic moments (Table 2).

Table 2. Electronic spectra and magnetic moments of the $[ML_2].xH_2O$ complexes

Compound	ν (cm^{-1})	Assignments	μ_{eff} (MB)
LH_2	22220	$\pi\rightarrow\pi^*$	
	16660	$n\rightarrow\pi^*$	
$[CoL_2].H_2O$	21000	$\pi\rightarrow\pi^*$	2.30
	15607	$n\rightarrow\pi^*$	
	14129	$^4A_2\rightarrow{}^4T_1(P)$	
	12195	$^4A_2\rightarrow{}^4T_1(F)$	
$[NiL_2].H_2O$	22190	$\pi\rightarrow\pi^*$	dia.
	15200	$n\rightarrow\pi^*$	
	14814	$^1A_{1g}\rightarrow{}^1B_{2g}$	
	12658	$^1A_{1g}\rightarrow{}^1A_{2g}$	
$[CuL_2].H_2O$	20000	$\pi\rightarrow\pi^*$	1.82
	16100	$n\rightarrow\pi^*$	
	15873	$d_{xy}\rightarrow d_{xz}$	
	14285	$d_{xy}\rightarrow d_{z2}$	
$[ZnL_2]$	21255	$\pi\rightarrow\pi^*$	dia.
	18867	TS	
	15900	$n\rightarrow\pi^*$	
$[CdL_2]$	21390	$\pi\rightarrow\pi^*$	dia.
	18181	TS	
	16000	$n\rightarrow\pi^*$	
$[HgL_2]$	21000	$\pi\rightarrow\pi^*$	dia.
	18230	TS	
	16000	$n\rightarrow\pi^*$	

In the electronic spectrum of the ligand there are two absorption bands assigned to $\pi\rightarrow\pi^*$ and $n\rightarrow\pi^*$ transitions [10, 11]. These transitions are found also in the spectra of the complexes, but they are shifted towards lower frequencies, confirming the coordination of the ligand at the metallic ions.

In the electronic spectrum of $[CoL_2].H_2O$ complex two new absorption bands at 14129 cm^{-1} and 12195 cm^{-1}, are observed. These bands are assigned to $^4A_2\rightarrow{}^4T_1(P)$ and $^4A_2\rightarrow{}^4T_1(F)$ transitions, respectively [12]. These transitions indicate a square-planar geometry of the complexes. The observed magnetic moment, 2.30 MB [13] is in agreement with this structure.

The electronic spectrum of $[NiL_2].H_2O$ complex shows two new bands at 14814 cm^{-1} and 12658 cm^{-1}, which are attributed to $^1A_{1g}\rightarrow{}^1A_{2g}$ and $^1A_{1g}\rightarrow{}^1B_{2g}$, respectively [12]. These transitions and the magnetic moments ($\mu_{eff} = 0$) suggest a square-planar stereochemistry [14].

In the electronic spectrum of the $[CuL_2].H_2O$ complex was noticed the presence of a two new bands at 15873 cm^{-1} and 14285 cm^{-1}, assigned to the $d_{xy}\rightarrow d_{xz}$, respectively $d_{xy}\rightarrow d_z2$ transitions [12]. These transitions, as well as the measured value of the magnetic moment

(1.82 MB) suggest a square-planar stereochemistry of the compound. We assumed for the Zn(II), Cd(II) and Hg(II) complexes a tetrahedral geometry [12].
The thermal behaviour of the compounds of Co(II) and Ni(II) was studied by thermogravimetric analysis. The heating rate was 10°C/min, while the temperature interval was 20-1000°C. The weight losses are presented the Table 3.

Table 3. Thermal behaviour of the prepared compounds

Compound	Decomposing stages	Temperature range (°C)	Thermal effect	Weight losses (%)	Residue (%)
$[CoL_2].H_2O$	1	50-180	exo-	3.50	3.15
	2	240-420	exo-	83	85.93 (Co_3O_4)
$[NiL_2].H_2O$	1	80-180	endo-	3.45	3.15
	2	290-540	exo-	85	86.91 (NiO)

The studied of Co(II) and Ni(II) compounds are decomposing in two successive stages. The first stage of decomposition consisted in elimination of the crystallization water; the last stage is exotherme and corresponds to the burning of the organic components. From the weight losses registered in TG and TDG of the Ni(II) compound, the following process of decomposition may be presented:

1. $NiC_{22}H_{16}O_7N_4S_2(s) \xrightarrow{80\text{-}180^oC} NiC_{22}H_{14}O_6N_4S_2(s) + H_2O(g)$

2. $NiC_{22}H_{14}O_6N_4S_2(s) + 29O_2(g) \xrightarrow{290\text{-}540^oC} NiO(s) + 22CO_2(g) + 2SO_2(g) + 4NO_2(g) + 7H_2O(g)$

The above-mentioned data suggest the following structural formula (Figure 1):

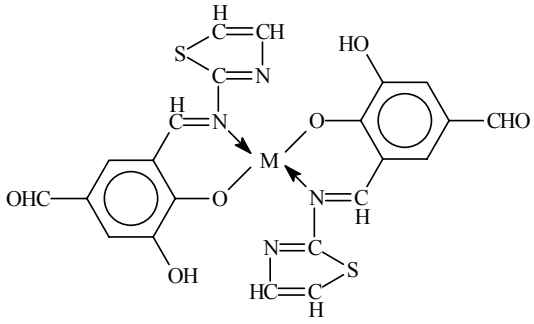

Fig 1. *The proposed structure for compounds*

Conclusions

In this article we present the results of a study of the new complexes of Co(II), Ni(II), Cu(II), Zn(II), Cd(II) and Hg(II) with Schiff-base derived from 4,5-dihydroxiphtalaldehide and 2-aminothiazole. The complexes were characterized as square-planar species of Co(II),

Ni(II), Cu(II), and as tetrahedral species of Zn(II), Cd(II) and Hg(II) based on the chemical analysis, thermal behaviour, spectrometric and magnetic measurements.

REFERENCES

1. Dash C., Pradhan J., (1991) Indian J,Chem. Sect.A, Inorg., Bio-Inorg.,Phys., Theor.Anal.Chem., **70**, 7601
2. Rosamma T., Parameswaran G., (1992) J.Indian Chem.Soc., **69**, 3117
3. Bhaskare C.K., Hankare P.P., (1995) J.Indian Chem.Soc., **72**, 9585
4. Zaidi A. Aftab S., Zaidi A. Rehan S., Shaher S.A., Tabrez A., (1987) Indian J.Chem Sect.A, **26**, 8715
5. Percy G.C., Thornton D.A., (1972) J.Inorg.Nucl.Chem., **34**, 3357
6. Lewis J.W., Sandorfy H., (1982) Can.J.Chem., **60**, 1737
7. Gillard R.D., McCleverts J.A., (1987) **Comprehensive Coordination Chemistry**, Eds. Wilkinson, Pergamon Press, Oxford
8. Bhardway S., Ansari M.N., Jain M.C., (1987) Indian J.Chem., **28A**, 81
9. Nakamoto K., (1978) **Infrared and Raman Spectra of Inorganic and Coordination Compounds**, 3rd Ed., John Wiley, New York
10. Ito M., Hata M., (1955) Bull.Chem.Soc.Jpn., **28**, 260
11. Friedel R.A., Orchin M.,)1958) **Ultraviolet Spectra of Aromatic Compounds**, John Wiley, New York
12. Level A.B.P., (1984) **Inorganic Electronic Spectroscopy**, Elsevier Publishing Company, Amsterdam
13. Sacconi L. et al., (1968), J.Am.Chem.Soc., **84**, 3246
14. Holm R.M., (1961) J.Am.Chem.Soc., **83**, 468

TEMPLATE SYNTHESIS AND STRUCTURAL CHARACTERISATION OF FIVE DIFFERENT Co(II) COMPLEXES WITH THE SAME LIGAND

Angela Kriza[*], Mariana Loredana Dianu[*], G. Dianu[*], N. Stanica[**]

abstract: A range of Co(II) complexes with Schiff bases obtained through condensation of salicylaldehyde with 2-aminothiazole has been synthesised. The stoechiometric formulas of the obtained complexes are: $[Co(SATZ)_2X_2]$; $[Co(SATZ)_2]Cl_2$ where: SATZ = saliciliden 2-aminothiazole; X = Cl^-, CH_3COO^-. Elemental analysis, molecular weight, magnetic susceptibility, molar conductivity determination, electronic and IR spectra were carried out. It has been found out that the ligand is NO bidentate, and the complexes are octahedric, except $[Co(SATZ)_2]Cl_2$ which has a tetrahedral geometry.

Introduction

The importance for biological systems of 2-aminothiazole and its derivatives is well known /1, 2/. It is also known that the thiazolic ring is part of B_1 vitamin, and of some antibacterial drugs, those contain sulphathiazole. Even a range of penicillin contains in the molecule the hydrogenate thiazolic ring /3/.

The 2-aminothiazole and its derivative complexes with transitional metal ions, which are also interesting from biological point of view, have been synthesised and studied by some specialists /4-7/.

Upon these, we tried to obtain a range of Co(II) complexes with Schiff bases through condensation of 2-aminothiazole with salicyl aldehyde. We must underline the fact that, this ligand can coordinate the metal ion through the N and S atoms from the thiazolic ring, but also through the N (azomethinic) and O (phenolic) atoms.

Experimental

All chemicals used are of p.a. produced by Merck.

[*] Departament of Inorganic Chemistry, University of Bucharest, Dumbrava Rosie str. 23, R-70254, Bucharest, ROMANIA

[**] „ I.G. Murgulescu" Institute of Physical Chemistry, Spl. Independentei 202A, Bucharest, ROMANIA

Analele Universităţii din Bucureşti – Chimie, Anul XIV (serie nouă), vol. I-II, pg. 123-128

The electronic spectra were determined with a UNICAM UV-VIS 3-100, and the IR spectra with a spectrophotometer BIO-RAD FTS-135. The molar conductivity measurements were obtained through a conductivity bridge Elico CM-82.

Ligand synthesis

The Schiff base was obtained by mixing the salicyl aldehyde and 2-aminothiazole solutions in methanol, in molar ratio of 1:1. The obtained solution was refluxed for 6 hours and concentrated through distillation until the volume decreased to one third. The precipitate formed of light-brown colour was filtered off, washed with methanol and dried in vacuum over phosphorus pentaoxyde.

Complexes synthesis $[Co(SATZ)_2(ac)_2]$ (I), (II)

A solution of 0,005 molls of salicylaldehyde in 50 ml of methanol is added by continuously stirring to that obtained of 0,005 molls of 2-aminothiazole and 100 ml methanol. After 20 minutes the solution is added through the same procedure at 0,0025 molls of $Co(CH_3COO)_2.4H_2O$ dissolved in 50 ml of methanol. The solution colour is reddish. The mixture is refluxed for 3 hours and concentrated through until the volume is decreased to one third. After 24 hours a brick-reddish precipitate appears (compound I); this is filtered, washed with methanol and dried over in vacuum. Diethyl ether is added to the solution obtained through filtering. A brown-yellowish precipitate is obtained (compound II); this is filtered, washed with diethyl ether and dried over in vacuum.

Compound I is soluble in chloroform, acetone, benzene, half-soluble in ethanol, methanol and carbon tetrachloride and hard soluble in diethyl ether and toluene.

Compound II is half soluble in chloroform, acetone, benzene, hard soluble in benzene and not soluble in methanol, ethanol, toluene and carbon tetrachloride.

Analysis for I: calculated: Co 10,11; C 28,82; N 9,6; found: Co 12,03; C 27,45; N 10,9 and for II: calculated: Co 10,11; C 28,82; N 9,6; found: Co 11,4; C 26,77; N 11,1.

Obtaining of the $[Co(SATZ)_2]Cl_2$ (III) and $[Co(SATZ)_2Cl_2]$ (IV) complexes

A solution of 0,005 molls salicylaldehyde in 50 ml methanol is added through stirring to the solution obtained from 0,005 molls 2-aminothiazole and 100 ml methanol. After 20 minutes this solution is added through the same procedure to 0,0025 molls $CoCl_2.6H_2O$ dissolved in 50 ml of methanol. The colour of the obtained solution is green-yellowish. The solution is refluxed for 4 hours and is concentrated until the volume decrease to one third. Even after 24 hours, any precipitate is not observed. Thus, diethyl ether is added to the clear solution and two layers are observed. The alcoholic layer is light-brown coloured and the etheric one is green. After separating the two layers, through evaporation from the alcoholic solution a blue precipitate is obtained. This is recrystalised from methanol. A light blue precipitate is obtained (compound III).

From the green ether solution through concentration, a brown-yellowish precipitate is obtained through concentration (compound IV). This is filtered washed with diethyl ether and dried over in vacuum.

Compound (III) is soluble in chloroform, benzene, acetone, half soluble in methanol and hard soluble in soluble in ethanol and diethyl ether.

Compound (IV) is soluble in ethanol and methanol, half soluble in chloroform, benzene, acetone and diethyl ether, hard soluble in the other usual solvents.

Analysis for III: calculated: Co 10,99; C 22,39; N 10,45; Cl 13,24; found Co 11,73; C 20,44; N 11,72; Cl 15,32 and for IV: calculated: Co 10,99; C 22,39; N 10,45; Cl 13,24; found Co 11,54; C 24,32; N 9,33; Cl 14,71.

Obtaining of the $[Co(SATZ)_2Cl_2]$ (V) complex

The synthesis described above is repeated, until the separation of the two layers, ether and alcoholic. The alcoholic solution is evaporated and precipitate obtained is redisolved in acetone. After concentration of the solution, a green compound is obtained through evaporation (compound V), which is filtered, washed with acetone and dried over in vacuum. Analysis for V: calculated: Co 10,99; C 22,39; N 10,45; Cl 13,24; found Co 12,04; C 23,89; N 9,71; Cl 13,98.

Results and discussion

The molecular weight, magnetic susceptibility and molar conductivity determinations of the products are shown in Table 1. The molar conductivity determination in DMF 10^{-3} M indicates for compounds (I), (II), (IV), (V), low values between 15-25 $\Omega^{-1}cm^2mol^{-1}$, this showing the non-electrolytic nature of those compounds. The value of molar conductivity of the compound (III) solution indicates an 1:2 electrolyte.

Table 1. Molecular weight and conductivity determination (DMF 10^{-3}M)

No.	Compound Formula	M calc./det.	Λ ($\Omega^{-1}cm^2mol^{-1}$)	μ (B.M.)
(I)	$[Co(SATZ)_2(ac)_2]$	582,93/567,14	12,4	5,44
(II)	$[Co(SATZ)_2(ac)_2]$	582,93/571,18	21,5	5,51
(III)	$[Co(SATZ)_2]Cl_2$	535,93/504,22	275,4	4,45
(IV)	$[Co(SATZ)_2Cl_2]$	535,93/509,93	24,5	4,76
(V)	$[Co(SATZ)_2Cl_2]$	535,93/512,4	18,5	5,04

The main band from the ligand and complex compounds IR spectra are presented in table 2.

Table 2. Spectral IR data of the ligand and of metal complexes with Co(II) (cm^{-1})

SATZ	(I)	(II)	(III)	(IV)	(V)	Assignments
3414	3333	3304	3308	3336	3284	ν_{O-H} phenolic
3111	3093	3122	3159	3114	3116	ν_{C-H} heterocyclic
2923	2910	2936		2905	2922	ν_{C-H} aromatic
1646	1627	1614	1629	1619	1604	$\nu_{C=N}$ azomethine
	1608	1580				ν_{COO}- asymmetric
1535	1531	1540	1538	1527	1533	$\nu_{C=N}$ heterocyclic
1493	1478		1501	1512	1506	$\nu_{C=C}$ heterocyclic
1453	1454	1429	1429	1482		$\nu_{C=C}$ aromatic
	1439	1405				ν_{COO}- symmetric
1273	1316	1291	1305	1298	1288	ν_{C-N} exocyclic
1109	1148	1151	1152	1149	1163	ν_{C-O} phenolic
759	743			756		χ_{C-H} heterocyclic
702		713	702	730	724	χ_{C-H} aromatic
675	666	671	683	680	679	ν_{C-S} heterocyclic

In the ligand IR spectra, at 3414 cm^{-1}, a strong absorption band appears, assigned to the phenol O-H bond vibration which is shifted to lower frequencies in the complexes IR spectra. Also the absorption band characteristic for C-O bond, appears in the ligand IR spectrum at 1109 cm^{-1}. In the complexes IR spectra this band appears between 1148-1163 cm^{-1}, shifted toward higher frequencies. These data indicates the O atom implication in coordination. The ligand shows in the IR spectra, a band of medium intensity, at 1646 cm^{-1}, attributed to the stretching frequencies ν(C=N) (azomethine). In the complex compounds IR spectra, this band appears between 1604-1629 cm^{-1}, shifted to lower frequencies, which indicates the implication of the azomethinic group nitrogen atom in coordination of the metal atom, with the forming of a chelate ring of six members. This fact is sustained also by the shift of the ν(C-N) (exocyclic) stretching frequency from 1273 cm^{-1}, in the ligand spectrum, toward higher frequencies, in the complexes spectra inside the 1288-1316 cm^{-1} domain /8/. The small shifts of the stretching frequencies of C=N /9/ and C-S /4, 10/ bonds from the thiazolic ring in the complexes IR spectra, compared with the ligand, demonstrates that the N and S atoms from the thiazolic ring are not involve in the coordination. In the (I) and (II) complexes IR spectra, two absorption bands appears at 1608, 1580 and 1439, 1405 cm^{-1}. These could be ascribed to the stretching of the acetate groups (antisymmetric) respectively (symmetric). The difference between the two frequencies is of 139 cm^{-1}, for complex (I) and of 175 cm^{-1} for complex (II) afford us to considerate that the acetate groups are monodentate. The difference between two frequencies of acetate groups is too big to consider them to function in a bidentate way. As a conclusion, we can say that the ligand, saliciliden 2-aminothiazole is bidentate, of NO type, the phenolic oxygen and azomethinic nitrogen atoms taking part to the coordination of the metal ion. The N and S thiazolic atoms don't participate to this coordination.

In Table 3, spectral UV-VIS data for ligand and complexes are presentate.

Table 3. Spectral UV-VIS data for ligand and complexes (cm^{-1})

No.	Compound	Absorption band	Assignments
	SATZ	46082	$\pi \rightarrow \pi^*$
		37593	$\eta \rightarrow \pi^*$
(I)	$[Co(SATZ)_2(ac)_2]$	46340	$\pi \rightarrow \pi^*$
		39270	$\eta \rightarrow \pi^*$
		27027	$^4T_{1g} \rightarrow {}^4A_{2g}$
		22220	$^4T_{1g} \rightarrow {}^4T_{1g}(P)$
(II)	$[Co(SATZ)_2(ac)_2]$	47619	$\pi \rightarrow \pi^*$
		39840	$\eta \rightarrow \pi^*$
		25000	$^4T_{1g} \rightarrow {}^4A_{2g}$
		22321	$^4T_{1g} \rightarrow {}^4T_{1g}(P)$
(III)	$[Co(SATZ)_2]Cl_2$	46790	$\pi \rightarrow \pi^*$
		38461	$\eta \rightarrow \pi^*$
		21276	$^4A_2 \rightarrow {}^4T_1(P)$
(IV)	$[Co(SATZ)_2Cl_2]$	44440	$\pi \rightarrow \pi^*$
		35087	$\eta \rightarrow \pi^*$
		21739	$^4T_{1g} \rightarrow {}^4A_{2g}$
		19762	$^4T_{1g} \rightarrow {}^4T_{1g}(P)$
(V)	$[Co(SATZ)_2Cl_2]$	45662	$\pi \rightarrow \pi^*$
		35971	$\eta \rightarrow \pi^*$
		20920	$^4T_{1g} \rightarrow {}^4A_{2g}$
		18656	$^4T_{1g} \rightarrow {}^4T_{1g}(P)$

In the UV-VIS spectra of the $[Co(SATZ)_2(ac)_2]$ complex compounds the absorption bands from 27027 and 25000 cm^{-1} are generated by the electronic transition. Also, the bands from 22220 and 22321 cm^{-1}, that appears in the electronic spectra of complexes (I) and (II) are ascribed to the $^4T_{1g} \rightarrow {}^4T_{1g}(P)$ (ν_2) transition, these data indicates that those complexes have distorted octahedral geometry (Figure 1 a,b).

The absorption band at 21276 cm^{-1} of the $[Co(SATZ)_2]Cl_2$ (III) UV-VIS spectrum, could be ascribed to the electronic transition $^4A_2 \rightarrow {}^4T_1(P)$ /9/ and also to the low symmetry components may be due to spin-orbital coupling. As a conclusion, we could say that this blue complex has a tetrahedral geometry (Figure 1 c).

The absorption bands from 21739 and 19762 cm^{-1}, that appears in the complex (IV) electronic spectrum are ascribed to the $^4T_{1g} \rightarrow {}^4A_{2g}(\nu_3)$ electronic transition and $^4T_{1g} \rightarrow {}^4T_{1g}(P)$ (ν_2). The same type of transition has as a result the appearance of the absorption bands from 20920 and 18656 cm^{-1} from the complex (V) electronic spectrum. This is giving us the opportunity to say that these complexes have a distorted octahedral geometry (Figure 1 d,e).

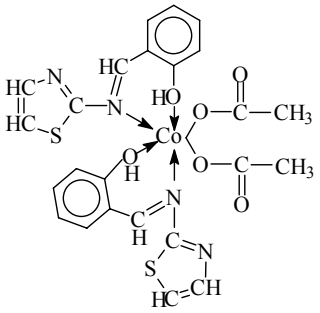

(a)

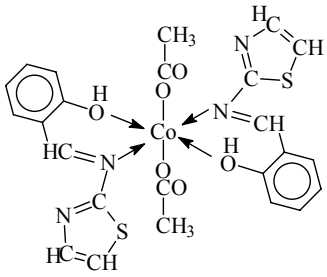

(b)

↔

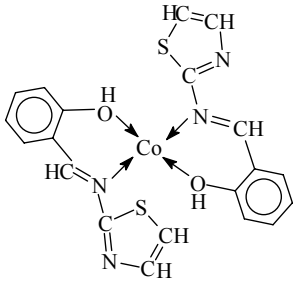

(c)

(d) ↔ (e)

Fig. 1 *The geometric formulas of Co(II) complex compounds.*

Conclusions

As a conclusion, five Co(II) complexes compounds with saliciliden 2-aminothiazole have been synthesised, the ligand is acting as a bidentate by coordinating to the metal ion through the nitrogen (azomethine) and oxygen (phenol) atoms. The complexes (I) and (II) have a distorted octahedral geometry and they can be cis-trans isomers, complex (III) shows a tetrahedral geometry, and complexes (IV) and (V) have also a distorted octahedral geometry and they possible be cis-trans isomers.

REFERENCES

1. M., Van Bensichem; N., Farrell; (1992) *Inorg. Chem.;* **31**, 639
2. N., Farrell; Y., Qu; L., Feng; B., Van Houten; (1990) *Biochemistry;* **29**, 9522
3. N., Farrell; Y., Qu; M.P., Hacker; (1990) *J. Med. Chemistry;* **33**, 2179
4. N., Farrell; T.M.G., Carneiro; (1987) *Inorg. Chim. Acta;* **126**, 137
5. S.K., Srivastava; K.A., Gupta; (1985) *Acta Chim. Hung.;* **118(3)**, 249
6. T.R., Goudar, G.S.. Nadagouda, (1988) *J. Indian Chem. Soc.;* **65**, 5009
7. S.D., Dhumwad, K.B., Gudasi; (1995)T.R., Goudar; *Indian J. Chem.;* **34A**, 38
8. N.V., Murthy, P., Liangaiahi, V., Malla Reddy; (1983) *J. Indian Chem. Soc.;* **60**, 529
9. V.K., Revankar; V.H., Arali; V.B., Mahale; (1990) *Indian J. Chem;* **29A**, 38
10. M.R., Chaurasia; P., Shukla; (1983) *J. Indian Chem. Soc.;* **60**, 1011

COMPLEXES OF Cu(II) AND Mn(II) WITH ACYLATED AMINOACIDS DERIVED FROM GLYCINE AND α-ALANINE

Maria Negoiu[*], T. Rosu*, Ioana Saramet[**], C.A. Matei[***]

abstract: a series of complexes of Cu(II) and Mn(II) with 4-(4'-halobenzenesulfonyl)-benzoyl glycine and 4-(4'-halobenzenesulfonyl)-benzoyl α-alanine with formula $[M(L\text{-}H)_2(H_2O)_2]$ have been synthesized and characterized as mononuclear species on the basis of elemental chemical analysis, electronic and infrared spectra and molar conductibility measurements. The IR spectra indicated the presence of aminoacid derivative as coordinated through nitrogen atom and the oxygen from the carboxylic group. The experimental data suggest that the ligands act as bidentate and adopt an octahedral stereochemistry.

keywords: aminoacids, copper(II), manganese(II), complexes

Introduction

Interactions between transitional metal ions and aminoacids are very interesting in the biological applications.

Complexes of some metal ions with aminoacids can be used as models to study the pharmaco-dynamic effects of drugs or for increasing the biocompatibility and minimize toxic effects of some metal ions [1,2]. The Cu(II) complexes with gluconic acid is the main drug used in the treatment of infectious, inflammatory and virological conditions, while a number of complexes based on Mn(II) are used in treating allergies, heart diseases and anaemia [3-8].

In this paper we proposed to prepare a series of Cu(II) and Mn(II)complexes with acylated aminoacids derived from glycine and α-alanine:

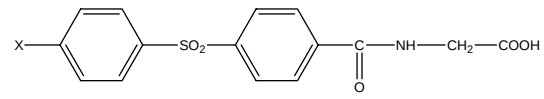

X = Br (**L**[1]), Cl (**L**[2])

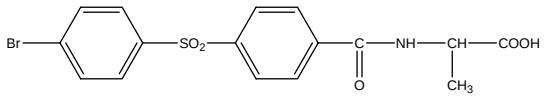

(**L**[3])

[*] University of Bucharest, Inorganic Chemistry Department, 23 Dumbrava Rosie st., Bucharest, sector 2, Romania

[**] University of Medicine and Pharmacy, Organic Chemistry Department, 6 Traian Vuia st., Bucharest, Romania

[***] University of Petrosani, Faculty of Mines, 20 Universitatii st, Petrosani, Romania

Analele Universităţii din Bucureşti – Chimie, Anul XIV (serie nouă), vol. I-II, pg. 129-133

Experimental

Materials and Methods

All reagents were of analytical grade and were used without further purification. The chemical analyses were performed by using the well-known micro methods. The diffuse reflectance spectra were recorded in the range 350 – 800 nm on VSU2-Carl Zeiss Jena spectrophotometer, using MgO as standard. The IR spectra were recorded in the 400 – 4000 cm^{-1} range with a BIO-RAD FTS 135 spectrophotometer using KBr pellets.

Molar conductivities were measured in freshly prepared solutions 10^{-3} M in DMF at room temperature with a digital conductivity meter Consort C 533.

Synthesis of Ligands

Ligands were prepared using the reaction between 4-bromo and 4-chlorobenzene sulphonyl benzoic acids with tionyl chloride in DMF [9,10].

The acid chloride obtained in this reaction was treated further with aminoacids following the Steiger procedure [11].

Synthesis of Complexes

A solution of sodium hydroxide 30% was added over the aqueous solution of anhydrous $MnSO_4$ (2 mmole in 20 ml H_2O) or cooper acetate monohydrated (2mmole in 20 ml H_2O) until a precipitate was formed. The precipitate was filtered off and was treated further with hot aqueous aminoacid solution (4 mmole in 40 ml H_2O). The M(II): aminoacid ratio was 1:2. The resulting mixture was refluxed for one hour and then the solution was cooled down. Pink pale crystals in the case of Mn(II) complexes and blue-violet crystals in the case of Cu(II) complexes separated out the solution. These crystals were filtered, washed with water and dried over P_4O_{10}. The pH value must be adjusted to 6-7 using 0.1N solution of NaOH.

Elemental analysis results and conductibility measurements values are:

$[Cu(L^1\text{-}H)_2(H_2O)_2]$: Found (%): C:39.85; H:2.50; Cu:7.01; Require(%): C: 40.10;H:2.60; Cu:7.09; $\Lambda_M=5.3\Omega^{-1}cm^2mol^{-1}$

$[Cu(L^2\text{-}H)_2(H_2O)_2]$: Found (%): C:43.50; H:2.50; Cu:7.70; Require(%): C:44.02;H:2.60; Cu:7.81; $\Lambda_M=4.10\Omega^{-1}cm^2mol^{-1}$

$[Cu(L^3\text{-}H)_2(H_2O)_2]$: Found (%): C:40.75; H:2.85; Cu:6.50; Require(%): C:41.10;H:3.05; Cu:6.88; $\Lambda_M=2.90\Omega^{-1}cm^2mol^{-1}$

$[Mn(L^1\text{-}H)_2(H_2O)_2]$: Found (%): C:40.30; H:2.80; Mn:5.79; Require(%): C:40.68; H:2.93; Mn:6.19; $\Lambda_M=6.10\Omega^{-1}cm^2mol^{-1}$

$[Mn(L^2\text{-}H)_2(H_2O)_2]$: Found (%): C:45.10; H:3.14; Mn:6.50; Require(%): C:45.22;H:3.26; Mn:6.88; $\Lambda_M=5.40\Omega^{-1}cm^2mol^{-1}$

$[Mn(L^3\text{-}H)_2(H_2O)_2]$: Found (%): C:41.85; H:3.10; Mn:5.82; Require(%): C:42.05; H:3.28; Mn:6.00; $\Lambda_M=4.50\Omega^{-1}cm^2mol^{-1}$

Results and Discussions

The results of the elemental chemical analysis of complexes obtained indicate a molar ratio of M(II):LH=1:2.

The values of molar conductivity for Mn(II) and Cu(II) complexes suggest that they are in non-electrolytes form in solution. To establish the structural formula of these complexes IR and UV-VIS spectra were recorded. The positions and assignments of the absorption bands in the UV-VIS spectra are presented in Table 1.

Table 1. Electronic Spectra Data

Compound	λ(nm)	Transitions
$C_{15}H_{12}BrNO_5S(L^1)$	230	$n\rightarrow\pi^*$
	262	$\pi\rightarrow\pi^*$
$[Cu(L^1\text{-}H)_2(H_2O)_2]$	235	$n\rightarrow\pi^*$
	270	$\pi\rightarrow\pi^*$
	415	TS
	620	$d\text{-}d(^2Eg\rightarrow{}^2Tg)$
$[Mn(L^1\text{-}H)_2(H_2O)_2]$	220	$n\rightarrow\pi^*$
	250	$\pi\rightarrow\pi^*$
	340-350	$^6A_{1g}\rightarrow{}^4T_{1g}(P)$

The UV-VIS spectra of Cu(II) complexes with the three ligands show two absorption bands assigned to intraligands transitions and a large band around 620 nm (≈16000 cm^{-1}). The presence of the later band support an octahedral stereochemistry for these complexes.

The UV-VIS spectra of Mn(II) complexes show two bands corresponding to the ligand and a weaker band around 340-350 nm that can be attributed to the d – d spin forbidden transition $^6A_{1g}\rightarrow{}^4T_{1g}(P)$. It is possible that this absorption band appears because of linear combinations of forbidden transitions: $^6A_{1g}\rightarrow{}^4T_{1g}(P)$ and $^6A_{1g}\rightarrow{}^4A_{2g}(F)$ [12].

The study of IR spectra can give valuable information regarding the ligands and the nature of the donor atoms. The bands assignments were done in agreement with the literature data [13-15] and are given in table 2.

Table 2. IR Spectral Data (cm^{-1})

Compound	$\nu s_{(COO-)}$	$\nu as_{(COO-)}$	δ_{NH}	$\nu_{OH(H2O)}$	ν_{M-N}	ν_{M-O}
$[Cu(L^1\text{-}H)_2(H_2O)_2]$	1400	1600	1520	3220	450	495
$[Cu(L^2\text{-}H)_2(H_2O)_2]$	1402	1605	1510	3250	440	490
$[Cu(L^3\text{-}H)_2(H_2O)_2]$	1405	1600	1515	3400	445	495
$[Mn(L^1\text{-}H)_2(H_2O)_2]$	1400	1610	1520	3240	430	490
$[Mn(L^2\text{-}H)_2(H_2O)_2]$	1403	1605	1525	3300	435	490
$[Mn(L^3\text{-}H)_2(H_2O)_2]$	1405	1600	1530	3280	430	495

The IR spectra of complexes show the characteristic bands of the aminoacids that are slightly shifted or weaker in case of the amino and deprotonated carboxyl groups.
The M-N and M-O stretching frequencies appear in the IR spectra between 430 - 450 cm^{-1} and 490-495 cm^{-1}. The stretching vibrations of the group OH corresponding to the coordinated water are located in the 3200-3400 cm^{-1} range. The uncoordinated COOH

group (ν_{CO2H}=1730 - 1775 cm^{-1}) could not be detected in the IR spectra, this fact indicating the coordination of the ligands to metal ions through the carboxilate anions.

All complexes show in the IR spectra a large absorption band in the 3200-2500 cm^{-1} range, a characteristic of transitional metal complexes with Aminoacids.

The correlation of all experimental data suggest that the geometry of Cu(II) and Mn(II) complexes prepared is octahedral.

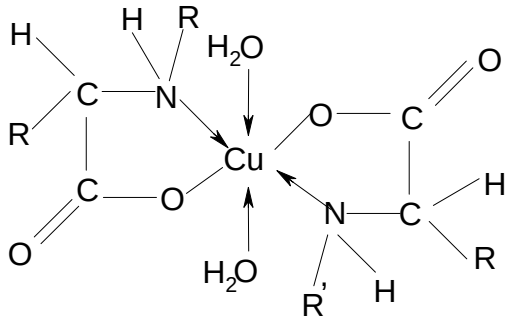

Conclusions

Six new Cu(II) and Mn(II) complexes of 4-(4'-halobenzenesulfonyl)benzoyl glycine and 4-(4'- halobenzenesulfonyl)benzoyl α-alanine have been synthesized and characterized on the basis of their elemental analysis, electronic and infrared spectra, as well as by molar conductivity measurements. The correlation of the experimental data allowed the assignment of an octahedral stereochemistry to all the reported complexes.

REFERENCES:

1. Grecu,I., Sandulescu, R. and Neamtu M. (1986) *Rev. Chim.* **37(7)**, 589-595.
2. Asma,I.El-Said., Amna, S.A.Zidan., Mahmoud,S.El-Meligy., Aref, A.Aly and Omar, F.Mohamened (2001) *Synth.React.Inorg Met-Org Chem.* **31(4)**, 633-648.
3. Grecu,I., Neamtu, M. and Enescu, L. (1982) **Implicatii biologice si medicale ake chimiei anorganice**, Ed Dacia, Cluj-Napoca.
4. Anjaneyulu, Y. and Rao, R. P. (1986) *Synth. React. Inorg.Met-Org.Chem* **16**(21), 257-272.
5. Gupta, M. and Srivastrava, M. N. (1985) *Polyhedron* **4**(3), 475-479.
6. Gupta, M and Srivastrava, M. N. (1991) *Bull. Soc.Chim Fr.*, 859-863.
7. Saxena, V.K., Gupta, M. and Srivastrava, M. N. (1996) *Synth. React. Inorg. Met-Org.Chem* **26**(10), 1661-1676.
8. Ullah, M.R. and Bhattacharya, P.K. (1990) *Indian J. Chem. Sect A* **29A**(2), 150-153.
9. Schiketanz, I., Istrati, D., Draghici, C. and Balaban, A. T. (1999) *Rev. Roum. Chim.* **44**, 137.

10. Schiketanz, I., Draghici, C., Saramet, I. and Balaban, A. T. (2002) The Journal Arkivoc (Archive for Organic Chemistry) 64-72.

11. Steiger, R.E. (1994) *J. Org. Chem*. **9**, 396.

12. Lewis, J. and Wilkins, R.G. (1960) **Modern Coordination Chemistry Principles and Methods**, Interscience Publ.Inc., New York, 287.

13. Nakamoto, K. (1986) **Infrared and Raman Spectra of Inorganic and Coordination Compounds**, Wiley, New York, 201-206.

14. Balaban, A.T., Banciu, M. and Pogany I. (1983) **Aplicatii ale metodelor fizice inn chimia organica**, Ed. Stiintifica si Enciclopedica Bucuresti.

15. Schiketanz ,I; Draghici, C; Saramet, I and Balaban,A.T(2002) Rev. Roum. Chim. **47** (3-4) 235-238.

COMPLEXES WITH AMIDES. Part 3. SYNTHESIS, SPECTROSCOPIC AND THERMAL CHARACTERIZATION OF A Cu(II) COMPLEX WITH 2-IODOANILIDE-3-CHLOROBENZO[b]THIOPHENE-2-CARBOXILIC ACID

Rodica Olar[*], Mihaela Badea[*], Codruta Paraschivescu[**], Dana Marinescu[*], I. Baciu[**]

abstract: A new complex of Cu(II) with 2-iodoanilide-3-chlorobenzo[b]thiophene-2-carboxilic acid (L) [$CuL(CH_3COO)_2$] (**2**) has been synthesised and characterised. The bonding and stereochemistry of the complex have been characterised by IR and electronic spectroscopy. The results concerning the thermal behaviour of the complex are reported. The amide ligand behaves as unidentate and coordinates through the amidic oxygen atom while the acetate acts as chelate. The copper (II) ions adopt a square-pyramidal stereochemistry.

Introduction

Copper as a component of numerous enzymes is involved in energy production, is necessary for neurotransmission in the brain and is active in cell protection from the damage generated by the free radicals. The copper deficiency is associated with the anaemia and bone demineralisation [2]. For understanding the biological role of this biometal, many current studies are concerned on the complexes with amides. We have prepared and characterised complexes of this type with polyfunctional amides [1,3].

Moreover many copper complexes, including amide complexes, are reported to be anti-inflamatory [4-6], analgesic [7] or antitumor agents [8]. Also the copper species exhibit numerous biological activities as antiviral [9], antifungal [10,11] and antibacterial [12-14] etc. Having in view that the benzothiophene derivatives are the components of some dies and drugs used for the osteoporosis and inflammatory diseases [15] we report herein the synthesis and characterisation of new complex of copper (II) with 2-iodoanilide-3-chlorobenzo[b]thiophene-2-carboxilic acid (**1**). The complex was formulated as mononuclear specie according to analytical and spectral data as well as thermal behavior.

[*] Department of Inorganic Chemistry, Bucharest University, 90 Panduri, 050663 Bucharest, Romania
[**] Department of Organic Chemistry, Bucharest University, 90 Panduri, 050663 Bucharest, Romania

Analele Universităţii din Bucureşti – Chimie, Anul XIV (serie nouă), vol. I-II, pg. 135-140

Experimental part

IR spectra were recorded in KBr pellets with an UR 20 Zeiss Jena instrument, *electronic spectra* were obtained by diffuse reflectance technique, using MgO as standard, with a VSU-2P Zeiss Jena instrument. *Thermal decomposition* was studied with a MOM (Budapest) derivatograph, type Paulik-Paulik-Erdey, in a static air atmosphere with a sample weight of 38.6 mg over the temperature range 20-800^{o}C at a heating rate of 10^{o}C min^{-1}.

The ligand (**1**) was prepared as reported in literature and were recrystallised from EtOH prior to use. The melting point (165.5-166) and ^{1}H NMR ($CDCl_3$) data (δ: 8.38 (1H), 7.35-7.85 (m, 7H), 6.90(1H)) agree with literature data [16]. Copper (II) acetate monohydrate (Merck) was of analytical grade. The chemical analyses were performed by usual micromethods.

The complexes were prepared by adding the ligand (2 mmoles) dissolved in minimal quantities of ethanol into the copper (II) acetate (4 mmoles) solution in 50 mL ethanol. Reaction mixture was heated and stirred for 4 hours. After concentration until the solution volume was reduced to about 15 mL, the resulting precipitate was filtered off, washed several times with a small volume of ethanol and air dried.

2-iodoanilide-3-chlorobenzo[b]thiophene-2-carboxilic acid (L**, 1**): IR data (cm^{-1}, KBr): 3200-3600 m (ν_{NH}), 1670 s ($\nu_{C=O}$, AI), 1530 s (δ_{NH} +δ_{C-N}, AII), 1500, 1450, 1320 s (δ_{C-N}+ δ_{NH}, AIII), 780 m (γ_{CH}).

Compound $[CuL(CH_3COO)_2]$ (**2**): Analysis found: Cu, 10.62; N, 2.60; S, 5.45 %; requires for $CuC_{19}H_{15}NClIO_5S$: Cu, 10.67; N, 2.35; S, 5.38 %; IR data (cm^{-1}, KBr): 3336m,3298m (ν_{NH}), 1655 m ($\nu_{C=O}$, A I), 1636 m ($\nu_{COO\ as}$), 1526 vs (δ_{NH} +δ_{C-N}, AII), 1433 s ($\nu_{COO\ s}$), 1294m (δ_{C-N}+ δ_{NH}, AIII), 750 m (ν_{CH}), 422 w (ν_{Cu-O}).

Results and discussion

In this paper we report the preparation and physico-chemical characterization of a new complex (**2**) of Cu(II) with N-(2-chloro-pyrid-3-yl)-4-chlorobenzamide (L, **1**). The molar ratio M:ligand was 1:1 and the isolated complex has the formula $[CuL(CH_3COO)_2]$ as indicate the chemical analyses and the thermogramm (figure 1).

Thermal behaviour of complexes was investigated by thermal gravimetric analysis and the final residues were examined by X-ray diffraction on powder. The majority of intermediate products formed during thermolysis were not possible to identify because the steps were not distinct. By thermogravimetric analysis it was proved that (**2**) it is anhydrous specie and the oxidative degradation of this compound was made in four steps in range 180 - 770 ^{o}C with CuO as final residue. The first endoothermic step corresponds to the ligand decarbonilation. The second one consists in transformation of acetate in carbonate according to the mass loss (table 1). In the next two steps occur the oxidative degradation of the residual ligand and the carbonate decomposition.

Table 1. Thermal behaviour data (in static air atmosphere) for the complex

Step	Thermal effect	Temperature interval / ºC	Δm_{exp} / %	Δm_{calc} / %
1.	Endothermic	180-220	4.66	4.70
2.	Exothermic	220-280	9.82	9.74
3.	Exothermic	280-440	42.66	42.69
4.	Exothermic	440-770	29.53	29.66
		Residue (CuO)	13.33	13.21

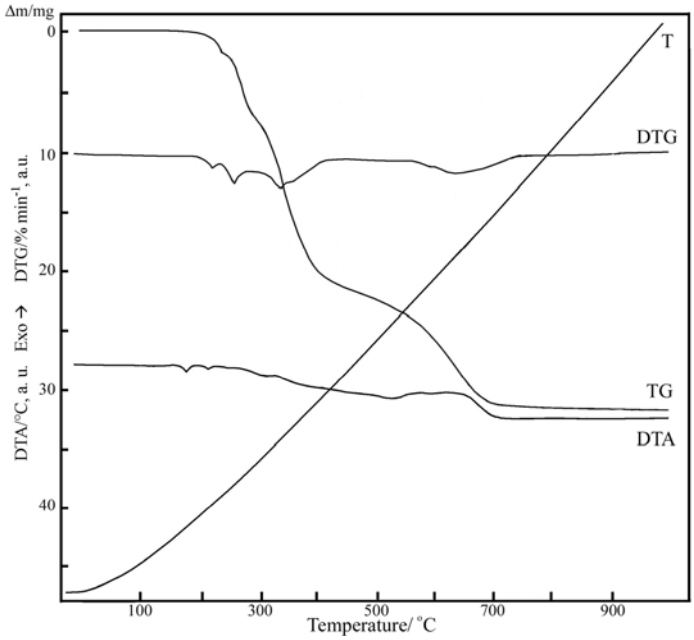

Fig. 1. *The TG, T, DTG and DTA curves of complex (2)*

The most important IR absorption bands for the ligand and complex are given in the experimental part. The presence of sharp strong bands in the 1670-1690, 1560-1580 and respectively 1290-1310 cm^{-1} range is suggestive for amide group [17-20]. All the three combined amide bands are shifted by 15-25 cm^{-1} to lower wawenumbers in the spectrum of complex (**2**). These modifications indicate that the ligand (**1**) is coordinated as unidentate through oxygen of amidic moiety [17-20]. Two bands at 1636 and 1433 cm^{-1} may be assigned to the coordinate acetate in chelate mode ($\Delta\nu = 103cm^{-1}$) [21]. The band that appears at 422 cm^{-1} could be assigned to ν(Cu-O) stretching vibrations [22].

Electronic spectrum of the complex (Fig.2) shows a broad band centred at 13160 cm^{-1}. The band position and the presence of the greater intensity absorption to higher energy agree with a square-pyramidal coordination [23].

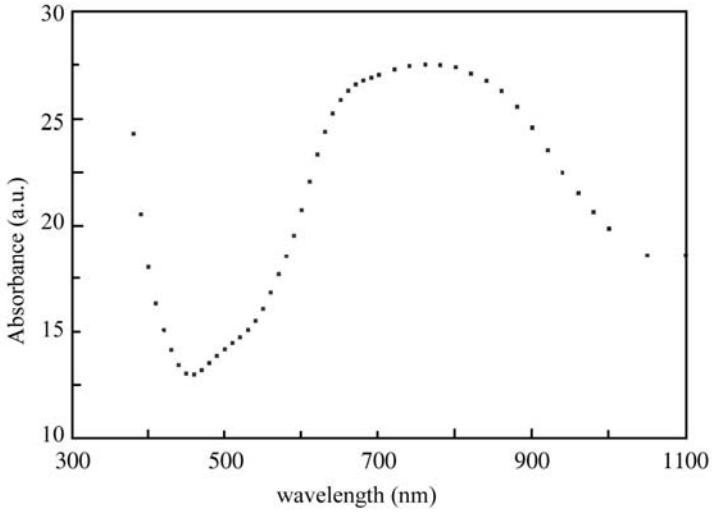

Fig. 2. *Diffuse reflectance spectra of [CuL(CH$_3$COO)$_2$] (2)*

By the present, the DMF solutions of the ligands and new complexes were tested for the activity against pathological microorganisms *Proteus*, *Escherichia Coli* and *Staphilococcus* but they show no important modifications in culture area. The works are in progress in our laboratory to perform the testes of compounds against other microorganisms cultures.

Taking into account the complex stoichiometry and the spectral features, it seems most probably a mononuclear structure for complex (**2**) with amide acting as unidentate (fig.3).

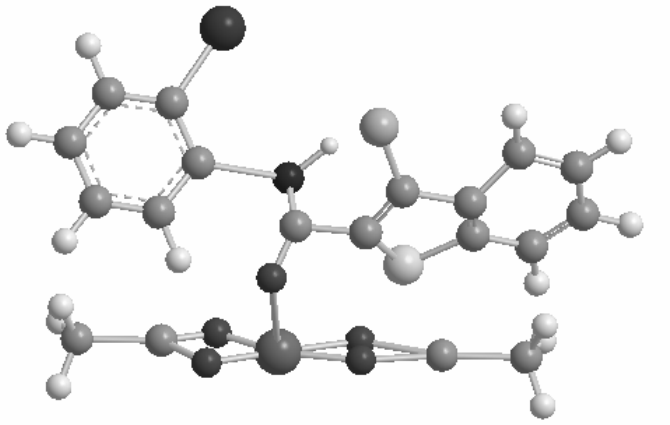

Fig. 3. *The proposed coordination for copper complex*

Conclusion

The copper (II) complex with 2-iodoanilide-3-chlorobenzo[b]thiophene-2-carboxilic acid has been synthesised.

Thermal decomposition of complex gave the possibility to establish the composition of complex and also the intervals of thermal stability.

The bond and stereochemistry were characterised by means of IR and electronic spectroscopy. The modifications evidenced in the IR spectrum were correlated with the presence of 2-iodoanilide-3-chlorobenzo[b]thiophene-2-carboxilic as unidentate coordinated through amidic oxygen while the acetate acts as bidentate. The diffuse-reflectance spectrum in the VIS-near-IR region shows a single band in agreement with a square- pyramidal surrounding.

REFERENCES

1. Marinescu, D., Olar, R., Simonescu, C.M., Ivan, L., Grandclaudon, P., Meghea, A. and Stanica N. (2002) *Rev. Roum. Chim*. **47,** 437-41.

2. R. Olar (2001) **Chimie bioanorganica. Biometale**, Ed. Universitatii din Bucuresti, Bucuresti, 37-39.

3. Cristurean, E., Olar, R., Simonescu, C.M., Ivan, L., Couture, A. and Stanica, N. (2000) *Sci. Bull. „Politehnica" University of Bucharest, Series B* **62**, 55-62.

4. Z. Korolkiewicz, Z., Hac, E., Gagalo, I., Gorczyca, P. and Lodzinska, A. (1989) *Agents Actions* **26**, 355-9.

5. Kovala-Demertzi, D. (2000) *J. Inorg. Biochem*. **79(1-4)**, 153-7.

6. Bonomo, R.P., Bruno, V., Conte, E., De Guidi, G., La Mendola, D., Maccarrone, G., Nicoletti, F., Rizzarelli, E., Sortino, S. And Vecchio, G. (2003) *J. Chem. Soc. Dalton Trans*. 4406-15.

7. Jacka, T., Bernard, C.C.A. and Singer G. (1983) *Life Sci*. **32**, 1023-8.

8. Singh, N.K., Singh, S.B., Singh, N and Shriviastav A. (2003) *Biometals*. **16(3)**, 471-7.

9. Ranford, J.D., Sadler, P.J. and Tocher, D.A., (1993) *J. Chem. Soc. Dalton Trans*. 3393-9.

10. Carcelli, M., Mazza, P., Pelizzi, C., Pelizzi, G. And Zani, F. (1995) *J. Inorg. Biochem*. **57(1)**, 43-62.

11. Ramadan, A.M. (1997) *J. Inorg. Biochem*. **65(3)**, 183-9.

12. Blasco, F., Ortiz, R., Perello, L., Borras, J., Amigo, J. and Debaerdemaeker, T. (1994) *J. Inorg. Biochem*. **53(2)**, 117-26.

13. Blasco, F., Perello, L., Latore, J., Borras, J. and Garcia-Granda, T. (1996) *J. Inorg. Biochem*. **61(2)**, 143-54.

14. Zoroddu, M.A., Zanetti, S., Pogni, R. and Basosi, R. (1996) *J. Inorg. Biochem*., **63(4)** 291-300.

15. Bradly, D.A., Godfrey, A.G. and Schmid, C.R. (1999) *Tetrahedron Lett*. **40**, 5155-9.

16. Baciu, I. and Paraschivescu, C. (2002) **Colloque Franco-Roumain de chimie appliqué**, Ed Alma Mater, Bacău and Tehnica-Info, Chisinau, 49-50.

17. R.C. Paul, A.K. Moudgil, S. L. Chadha and S.K. Vasisht, I*nd. J. Chem.*, **1978,** *8*, 1017-1019.

18. H.O. Desseyn and M.A. Herman, *Spectrochim. Arta*, **1967,** *23A*, 2457-2463.

19. D.G. Brewer, P.T.T. Wong and M.C. Sears, *Can. J. Chem.*, **1969,** *46*, 3137-3141.

20. M.C. Sears, W.V.F. Brooks and D.G. Brewer, *Can. J. Chem.*, **1970,** *48*, 3786-3789.

21. Deacon,G.B. and Philips, J.R. (1970) *Coord. Chem. Rev.* **5**, 217-262.

22. Nakamoto, K. (1986) **Infrared and Raman Spectra of Inorganic and Coordination Compounds**, Wiley, New York, 227-230.

23. A.B.P. Lever, (1984) **Inorganic Electronic Spectroscopy**, Elsevier, Amsterdam, London, New York, 554-572.

CONTROLLED SYNTHESIS III. REACTION OF Sn(IV) AND Zr(IV) WITH ISATINS

Carmen Pârnău*, Angela Kriza, Niculae Popa, Silvia Udrea

abstract: New metal chelates of Sn(IV) and Zr(IV) with isatins have been synthesized and characterized. Following the synthesis conditions, two types of complexes were obtained: $[M(HL^I)_2Cl_2]Cl_2$; $[ML^{II}_2Cl_2]Cl_2$ and $[ML^I_2Cl_2]$, where: HL^I = isatin; L^{II} = N-metil-isatin; M=Sn(IV), Zr(IV). The complexes were characterised by elemental analysis, IR and NMR spectroscopy, diffuse reflectance data and molar conductivity measurements. The experimental data suggest that the ligands acts as bidentate (OO), and in function of reaction system, can coordinates in two different forms.

Introduction

Isatin (1H-indol-2,3-dione) is a syntetically versatile substrate, where it can be used for synthesis of a large variety of heterocyclic compounds, such as indoles and quinolines, and a raw material for drug synthesis. Isatin has also been found in mammalian tissues [1]. There has been considerable interest show in the coordination chemistry of metal ions and isatins [1÷11], but less attention has been paid to complexation of main group metal ions. Isatin (1H-indol-2,3-dione, fig. 1) was first obtained by Erdman and Laurent in 1841 as a product from the oxidation of indigo by nitric and chromic acids.

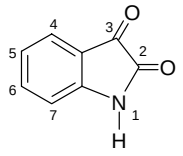

Fig. 1: *Structure of 1H-indol-2,3-diona*

Our interest in this category of ligands is justified by their already proved medical and biological implications [2÷12]. On the other hand, a great deal of our precedent work is focussed on the complex compounds generated by Group 14 metal halides [13÷19], also important in some biological processes.

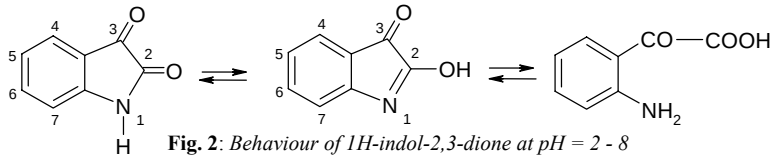

Fig. 2: *Behaviour of 1H-indol-2,3-dione at pH = 2 - 8*

* University of Bucharest, Faculty of Chemistry, Department of Inorganic Chemistry, Dumbrava Roşie 23

Analele Universităţii din Bucureşti – Chimie, Anul XIV (serie nouă), vol. I-II, pg. 141-146

Isatin, due to its cis α-dicarbonyl moiety, is a potentially good substrate for the synthesis of metal complexes, either alone or deprotonated [1].

Experimental

Materials and methods

All reagents used were of analytical grade and were used without further purification. $SnCl_4$ (Riedel), $ZrCl_4$ (Merck), isatin and *N*-methylisatin (Aldrich, 98%) and other chemicals employed were used as supplied by commercial sources. Solvents were purified by usual methods. *Chemical analysis* were performed by using the well-known micromethods. *The diffuse reflectance spectra* were recorded in range 250-800 nm using MgO as standard. *The IR spectra* were recorded in range 400-4000 cm^{-1} with a BIO-RAD FTS 135 spectrophotometer, using KBr pellets. ^1H NMR data were recorded on Bruker Avance WH 2790 spectrometer in dmso-d_6 using TMS as standard. *Molar conductivities* were measured in freshly prepared 10^{-3} mol·dm^{-3} solutions in DMF at room temperature with a digital conductivity meter Consort C 533.

Synthesis of complexes $[M(HL^I)_2Cl_2]Cl_2$ or $[ML^{II}_2Cl_2]Cl_2$; $[MCl_2L^I_2]$

All complexes were prepared by the following general procedure: a hot anhydrous ethanol solution of the ligand was added to the clorides (1:2 molar ratio) of Sn(IV), Zr(IV) dissolved in anhydrous ethanol.

$[M(HL^I)_2Cl_2]Cl_2$; **$[ML^{II}_2Cl_2]Cl_2$** MCl_4 (0,002 mol in 50 mL anhydrous ethanol) was treated with 0,004 mol ligand (HL^I = isatin; L^{II} = *N*-methylisatin) dissolved in 50 mL anhydrous ethanol. The mixture was stirred during 1 h under nitrogen atmosphere and than was refluxed on a steam bath for 6 h. The solvent excess was distilled.

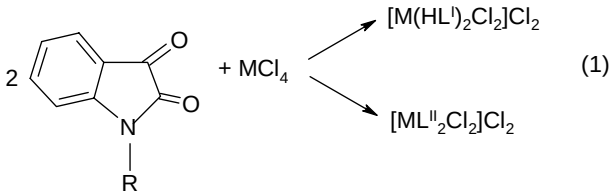

$[ML^I_2Cl_2]$ The ligand in 50 mL anhydrous ethanol was added drop wise to MCl_4 under nitrogen atmosphere; then, under nitrogen atmosphere and continuous stirring, sodium methoxide was added (M:ligand:CH_3ONa 1:2:2). The reaction mixture was refluxed on a steam bath for 8 h.

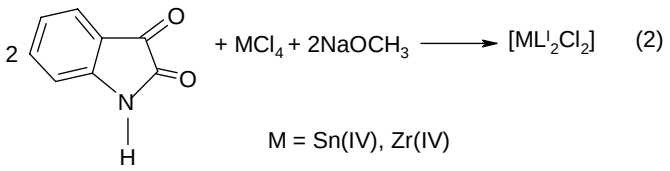

The complexes were crystallized upon concentration. The compounds were filtered, washed with anhydrous ethanol and dried over P_2O_5 in vacuum.

$[M(HL^I)_2Cl_2]Cl_2$ $SnCl_4C_{16}H_{10}O_4N_2$ *Requires*: Sn 21.40; Cl 25.60; N 5.05%. *Found for brick solid:* Sn 21.46; Cl 25.68; N 4.80%. $ZrCl_4C_{16}H_{10}O_4N_2$ *Requires*: Zr 17.30; Cl 26.93; N 5.31%. *Found for brick solid:* Zr 17.36; Cl 27.00; N 5.20%. **$[ML^{II}_2Cl_2]Cl_2$** $SnCl_4C_{18}H_{14}O_4N_2$ *Requires*: Sn 20.37; Cl 24.37; N 4.80%. *Found for pink solid:* Sn 20.42; Cl 24.40; N 4.52%. $ZrCl_4C_{18}H_{14}O_4N_2$ *Requires*: Zr 16.43; Cl 25.57; N 5.04%. *Found for pink solid:* Zr 16.56; Cl 25.68; N 5.95%. **$[ML^I_2Cl_2]$** $SnC_{16}H_8O_4N_2Cl_2$ *Requires*: Sn 24.45; Cl 14.67; N 5.78%. *Found for beige-maron solid:* Sn 24.67; Cl 14.63; N 5.70%. $ZrC_{16}H_8O_4N_2Cl_2$ *Requires*: Zr 20.12; Cl 15.63; N 6.16%. *Found for beige-maron solid:* Zr 20.18; Cl 15.98; N 6.05%.

Results and Discussion

The analytical data show different stoichiometries in dependence of organic anion and in function of reaction system (*i.e.* CH_3ONa), ligands can coordinates in two diferent forms.

The complexes were isolated as sparingly soluble, coloured products from the reaction medium. These chelates are powders stable towards air and moisture. They decompose at >260 °C and are insoluble in most common organic solvents but soluble in dmf and dmso.

On the basis of *chemical analysis* the minimal formula correspond to $[M(HL^I)_2Cl_2]Cl_2$ and $[ML_2Cl_2]$, M=Sn(IV), Zr(IV).

The conductivity values for the $[ML^I_2Cl_2]$ complexes (6.5-8.9 $\Omega^{-1}.cm^2.mol^{-1}$) indicate that the complexes are non-electrolytes in solution. For the $[M(HL^I)_2Cl_2]Cl_2$ and $[ML^{II}_2Cl_2]Cl_2$ the conductivity values (65-82 $\Omega^{-1}\cdot cm^2\cdot mol^{-1}$) indicate that the complexes are electrolytes in dmf solutions.

Table 1. Infrared spectra (cm^{-1})

Compound	ν_{NH}	$\nu_{C=O(2)}$	$\nu_{C=O(3)}$	$\nu_{C=N*}$	ν_{C-O}	ν_{M-O}
HL^I	3190 br	1730 s	1620 vs	-	-	-
$[Sn(HL^I)_2Cl_2]Cl_2$	-	1720 m	1609 m	-	-	420 w
$[Zr(HL^I)_2Cl_2]Cl_2$	-	1718 m	1603 m	-	-	430 w
$[SnL^I_2Cl_2]$	-	1721 m	-	1582 s, sh	1249 s, sh	527 w
$[ZrL^I_2Cl_2]$	-	1700 m	-	1575 s,sh	1228 s, sh	500 w
L^{II}	-	1744 s	1725 vs	-	-	-
$[SnL^{II}_2Cl_2]Cl_2$	-	1730 m	1609 m	-	-	427 w
$[ZrL^{II}_2Cl_2]Cl_2$	-	1720 m	1606 m	-	-	430 w

The *infrared spectrum of isatin* shows two strong bands at 1730 and 1620 cm^{-1} corresponding to the carbonyl stretching vibrations (see table 1).

A broad band occurs at 3190 cm^{-1} due to the N-H stretching, and it is accompanied by many sub-bands; the several bands in the region 1400-1100 cm^{-1} are associated with N-H in-plane bending. The $\nu_{C=O}$ values are not modified by N-alkylation.

All the bands assigned to stretching vibration modes ν_{NH} and $\nu_{C=O(3)}$ in the free isatin disappear in the spectra of the compounds $[ML^{I}_{2}Cl_2]$, but new bands are recorded at 1585-1575 and 1250-1230 cm^{-1}, respectively. These new bands, assigned to the $\nu_{C=N}$* (new azomethine bond) and ν_{C-O} vibration modes respectively, suggest the enolysation of NH hydrogen of isatin and the coordination at tin/zirconium through the oxygen of the C-O group.

The formation of M-O bonds is further supported by the appearance of ν_{M-O} in the regions 400-500 in the spectra of chelates.

The highest energy $\pi \rightarrow \pi^*$ band at 35780 cm^{-1} (279 nm) in the *UV-VIS spectra* of ligands, in ethanol, is at higher energy in the spectra of complexes, suggesting it likely arises from one of the functional groups that coordination rather the aromatic ring.

The diffuse reflectance spectra were recorded in range 250-800 nm (MgO). In the spectra of ligands the band at 27820 cm^{-1} (359 nm) is very broad and likely involves $n \rightarrow \pi^*$ transitions for the C=O functions. The Sn(IV) and Zr(IV) chelates are diamagnetic with no ligand field transition. The lowest energy bands of the complexes $[ML^{I}_{2}Cl_2]$ at 430-441 nm are assigned to charge transfer transitions of hydroxilato donor (see fig.3).

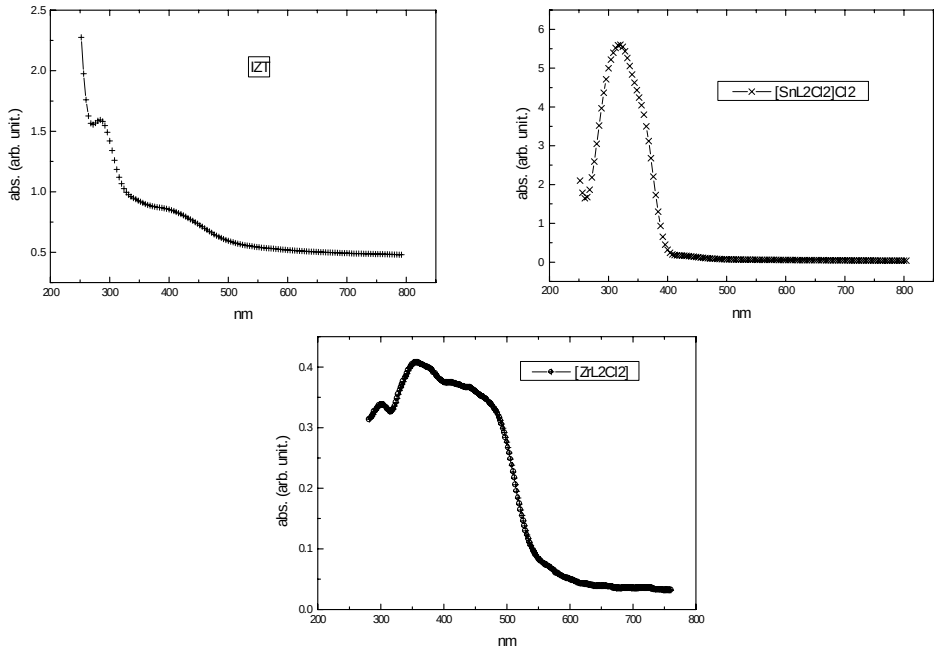

Fig. 3: *The diffuse reflectance spectra: isatin (HL^{I}), $[SnL^{II}_{2}Cl_2]Cl_2$ and $[ZrL^{I}_{2}Cl_2]$*

Supplementary data have been obtained by *^{1}H NMR spectroscopy*, recorded for the ligands and for their complexes of Sn(IV). The ^{1}H NMR spectrum of isatin shows the signals of the aromatic nucleus at δ 6.86 (d), 7.00 (t), 7.47 (d) and 7.53 (t) (DMSO-d_6), corresponding to H-7, H-5, H-4 and H-6 respectively. N-alkylation not alter this pattern (see table 2). The only ^{1}H NMR signal displaying a down field shift in complex compounds $[Sn(HL^I)_2Cl_2]Cl_2$ is those associated with the hydrogen (NH) of the isatin. This behavior is related with a decrease of the electron density and a deshielding of the NH proton, as a result of the participation of the adjacent carbonyl group in coordination. This behavior is in good agreement with IR spectra of complexes where the maximum of the $\nu_{C=O(2)}$ vibration mode appears at lower frequencies as in the corresponding free ligand. This ^{1}H NMR signal (NH) disappear in the spectrum of $[SnL^I_2Cl_2]$.

Table 2. ^{1}H NMR spectra (δ, ppm)

Compound	N-H	H-4	H-5	H-6	H-7
HL^I	11.03s	7.50d	7.07t	7.60t	6.92d
$[Sn(HL^I)_2Cl_2]Cl_2$	11.63s	7.53d	7.10t	7.62t	6,93d
$[SnL^I_2Cl_2]$	-	7.50d	7.07d	7,60t	6.92d
L^{II}	-	7.59d	7.12t	7.61t	6.91t
$[SnL^{II}_2Cl_2]Cl_2$	-	7.56d	7,10t	7.61t	6.93t

The correlation of the experimental data allows assigning a octahedral stereochemistry to all the reported complex compounds. The proposed structural representations are presented in figure 4.

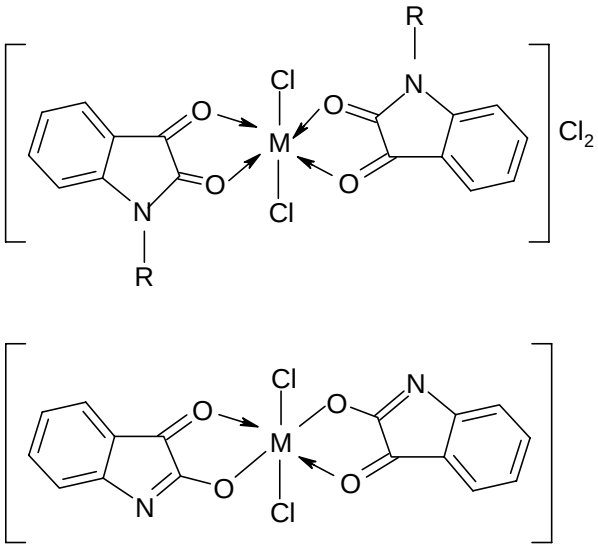

Fig. 4: *Propose structures of complex compounds $[M(HL^I)_2Cl_2]Cl_2$, $[ML^{II}_2Cl_2]Cl_2$ and $[ML^I_2Cl_2]$; M=Sn(IV), Zr(IV)*

Conclusion

We report here the synthesis and the characterization of new complexes of Sn(IV) and Zr(IV) with "isatins". The syntheses were conducted in conditions allowing the bidentate in dependence of organic anion and in function of reaction system (*i.e.* CH_3ONa, stability of Sn/Zr(IV)). The synthesized compounds were characterized by elemental analysis, IR, ^1H NMR and electronic spectroscopy, as well as by conductance measurements. The correlation of the experimental data allows assigning a octahedral stereochemistry to all the reported complex compounds.

REFERENCE TITLE

1. da Silva, J. F. M., Garden, S. J. and Pinto, A. C. (2001) *J. Braz. Chem. Soc.* **67(3)**, 273.
2. Popp, F. D. and Pajouhesh, M. (1988) *J. Pharm. Sci.* **17**, 1052.
3. Taha, F. I. M. and Khatab, M. A. (1970) *UAR J. Chem.* **13**, 227.
4. Popp, F. D., Parson, D. and Doningan, B. E. (1980) *J. Heterocyclic Chem.* **17**, 1329.
5. Kontz, F. (1973) *Sci. Pharm*. **41**, 123.
6. Casas, J. S., Garcia-Tasende, M. S. and *all* (1996) *J. Inorg. Biochem*, **62**, 41.
7. Agrawal, K. C. and Sartorelli, A. C. (1978) *Prog.Med.Chem.*, **15**, 321.
8. Casas, J. S., Castineiras, A. and *all* (1994) *Inorg. Chem. Acta*, **221**, 61.
9. Medvedev, A.E., Sandler, M. and Glover, V. (1998) *Life Sci.*, **62**, 2391.
10. Boon, R. (1997) *Antiviral Chem. Chemother.*, **8**, 5.
11. Pandeya, S.N. and Dimmock, J.R. (1993) *Pharmazie*, **48**, 659.
12. Casas, J. S., Castineiras, A. and *all* (2000) *J. Chem. Soc., Dalton Trans.*, 4056.
13. Kriza, A., Pârnău, C. and Popa, N. (2001) *Rev. Chim.* **52(6)**, 346.
14. Kriza, A. and Pârnău, C. (2001) *Acta Chim. Slov.* **48(3)**, 445.
15. Kriza, A., Pârnău, C. and Popa, N. (2002) *Anal. Univ. Buc.*, Ser. Chim. **XI(I)**, 191.
16. Kriza, A., Pârnău, C., Zălaru F. and Kriza A. F. (2002) *Anal. Univ. Buc.*, Ser. Chim. **XI(II)**, 37.
17. Kriza, A., Pârnău, C., Popa, N. and Roşu T. (2004) *Anal. Univ. Buc.*, Ser. Chim. **XIII(I,II)**, 155.
18. Cristurean, E., Pârnău, C., Badea, M. and Olar R. (2004) *Anal. Univ. Buc.*, Ser. Chim. **XIII(I,II)**, 179.
19. Pârnău, C., Kriza, A., Pop, V. and Udrea S. (2005) *J. Indian Chem. Soc.*, **82**, 1.

SYNTHÈSE ET CARACTÉRISATION SPECTRALE D'UNE NOUVELLE SÉRIE D'ACÉTYLACÉTONATES MIXTES DU COBALT(II)

Ileana Şerban[*], Mirela Călinescu*, A.M. Stadler**

abstract : Metal complexes of the type : $[Co(acac)(Aacac)(H_2O)_2]$, $[Co(Aacac)_2(H_2O)_2]$, $[Co(Aacac)_2(py)_2]$, $[Co(acac)(Aacac)(bipy)]$, $[Co(Aacac)_2(bipy)]$ and $[Co(acac)(Aacac)(phen)]$, where acac = acetylacetone, Aacac = allylacetoacetate, py = pyridine, bipy = 2,2'-dipyridil and phen = 1,10-phenantroline have been prepared and studied by elemental and thermogravimetric analyses, molar conductance measurements, IR and UV-VIS spectra. All the complexes have a distorted octahedral environment for the cobalt(II) ion.

Introduction

On accorde actuellement une attention de plus en plus grande à la préparation et à la possibilité de mettre en pratique des propriétés multiples des acétylacétonates métalliques. On connaît qu'ils ont déjà un très large domaine d'applicabilité comme catalyseurs dans des synthèses organiques [1-3], pour dépositions de films minces sur diverses surfaces [4-6], pour leurs propriétés magnétiques spéciales [7] et leurs propriétés conductrices [8].

Les travaux actuels montrent le souci des chimistes d'optimiser les conditions de synthèse des composés et de caractériser aussi finement que possible leur structure, leur microstructure et leur composition.

Parallèlement à la recherche et à la caractérisation de nouveaux composés, des études sont entreprises sur la mise en forme de ceux déjà connus.

Le but de ce travail et de préparer et d'étudier une nouvelle série d'acétylacétonates mixtes de cobalt(II) qui contiennent, outre l'acétylacétone, d'autres ligands tels que : allylacétoacétate, pyridine, 2,2'-bipyridine et 1,10-phénantroline.

Partie expérimentale

Matériaux et méthodes. Les sels métalliques et les ligands utilisés sont livrés par Merck ou Flucka. Les solvants organiques ont été purifiés par les méthodes usuelles. Le métal a été

[*] Département de Chimie Inorganique, Université de Bucarest, 23 Dumbrava Rosie, Bucarest, Roumanie
**Université de Strassbourg, France

Analele Universităţii din Bucureşti – Chimie, Anul XIV (serie nouă), vol. I-II, pg. 147-152

déterminé gravimétriquement en le précipitant sous forme de phosphate par $(NH_4)_2HPO_4$ [9].

La détermination de C, H et N a été effectuée par combustion, avec un analyseur Carlo Erba 1106.

Les courbes thermopondérales ont été enregistrées dans un intervalle de température compris entre la température ordinaire et 1000^0C, sous atmosphère statique d'air, à l'aide d'une thermobalance de type MOM Q-1500, avec une vitesse de chauffe de 5^0C.

La conductibilité molaire a été mesurée en solutions acétoniques de concentration 10^{-4}M, sur un conductomètre Phillips PR 9500.

Les spectres infrarouge (4000-400 cm^{-1}) ont été enregistrés sur un spectrophotomètre Perkin Elmer FT-IR 1600, en pastille de KBr.

Les spectres UV-VIS (10000-50000 cm^{-1}) ont été obtenus en réflexion diffuse, en MgO, à l'aide d'un spectrophotomètre Spekord M-40.

Préparation des combinaisons complexes

La méthode générale de synthèse pour les complexes s'appuie sur celle utilisée dans la littérature pour préparer l'acétylacétonate de Co(II) [10].

$[Co(acac)(Aacac)(H_2O)_2]$ (**1**), a été préparé de la manière suivante: l'hydroxyde de sodium (0,08 g) dissous dans 1 ml d'eau a été ajouté lentement à un mélange formé par acétylacétone (0,1 ml, 1 mmole) et allylacétoacétate (0,14 ml, 1mmole). Il se forme une solution jaunâtre qui est ajoutée, sous agitation à la température ambiante, à une solution aqueuse de sel métallique (0,238 g, 1mmole de $CoCl_2 \cdot 6H_2O$ en 1,5 ml d'eau). Le précipité lavé avec de l'eau et de l'alcool et séché à l'air donne une poudre fine, violette claire.

$[Co(Aacac)_2(H_2O)_2]$ (**2**). En remplaçant l'acétylacétone par allylacétoacétate dans le rapport molaire Co : Aacac = 1 : 2, on obtient dans les mêmes conditions un précipité rose-violet. En le séchant à 150^0C, il perd de l'eau et peut former rapidement, par dissolution dans la pyridine, un adduct rouge-violet qui s'est avéré être $[Co(Aacac)_2(py)_2]$ (**3**).

[Co(acac)(Aacac)(bipy)] (**4**). On utilise les mêmes quantités que pour le composé (**1**), en ajoutant de plus 2,2'-dipyridine (0,158 g, 1mmole) en alcool éthylique. On évapore à moitié du volume initial, lorsqu'il se sépare des cristaux transparents qui sont lavés avec de l'alcool et séchés à l'air.

$[Co(Aacac)_2(bipy)]$ (**5**). Aux quantités correspondantes au composé (**2**), on ajoute une solution alcoolique de 2,2'-bipyridine (0,158 g, 1mmole). Le précipité jaune-orange formé est filtré, lavé avec de l'eau et de l'alcool et séché à l'air.

[Co(acac)(Aacac)(phen)] (**6**). La même méthode de synthèse. On ajoute au mélange utilisé pour le composé (**1**) de la phénantroline (0,198 g, 1mmole). Il se forme un précipité orange qui est traité de la même manière que les composés précédents.

Résultats et discussion

Les synthèses des complexes listés dans le tableau 1 ont été effectuées par la réaction directe entre les constituants de chaque composé, à froid, dans des quantités correspondantes aux rapports stoéchiométriques.

Tous les composés se présentent sous forme de poudres fines, colorées, solubles dans des solvants organiques usuels (chloroforme, acétone, chlorure de méthylène, DMF et DMSO). Cette bonne solubilité atteste le fait que les composés obtenus sont des monomères.

Les valeurs de la conductivité molaire en acétone montrent le caractère de non-électrolytes de tous les composés.

Dans le tableau 1 sont portées quelques propriétés physiques des composés obtenus, telles que : les points de fusion, les couleurs et les résultats de l'analyse élémentaire.

Tableau 1. Quelques caractéristiques physiques des combinaisons complexes

Composés	P.f. (^{0}C)	Couleur	Co% Calc/exp	C% Calc/exp	H% Calc/exp
1	187	Violette	17,48/17,01	42,85/42,30	5,95/5,58
2	182	Rouge-violette	15,52/14,80	44,34/43,70	5,80/5,90
3	151	Rouge-violette	11,82/11,32	57,72/57,00	5,61/5,42
4	150	Rouge	12,98/12,31	58,02/57,80	5,26/5,10
5	159	Orange	11,85/11,39	57,9457,61	5,23/5,08
6	119	Jaune-orange	12,25/11,92	60,01/59,20	4,99/4,68

La concordance assez bonne entre les valeurs théoriques et celles expérimentales démontre la valabilité des formules brutes proposées.

L'étude de la décomposition thermique des complexes obtenus a permis de mettre en évidence la présence de l'eau de coordination dans les complexes **1** et **2**. Les courbes thermogravimétriques (ATG) et l'analyse thermodifférentielle (ATD) pour ces deux composés ont relevé le fait que la perte de l'eau débute vers 170^{0}C et finit à 210^{0}C et se traduit en ATD par un signal endothermique. Pour tous les complexes, la perte des ligands organiques se produit dans une seule étape, par un processus fortement exothermique, qui commence à environ 250-300^{0}C. Vers 700-800^{0}C il n'y a que d'oxyde métallique comme dépôt. Les résidus de la thermolyse ont fait, par ailleurs, dans certains cas, l'objet d'analyse du métal.

Spectres en IR. Les fréquences caractéristiques dans les spectres infrarouge des complexes pour les groupements susceptibles d'être impliqués dans la coordination sont portées dans le tableau 2. Pour comparaison, on a enrigé dans le même tableau les positions de ces bandes indiquées dans la littérature pour l'acétylacétone et allylacétoacétate.

Dans les spectres en IR de tous les complexes synthétisés on observe trois bandes intenses situées dans les régions 1600-1630 cm^{-1}, 1500-1535 cm^{-1} et 1230 -1260 cm^{-1}.

Tableau 2. Absorptions caractéristiques en IR pour acac, Aacac et les combinaisons complexes (cm^{-1})*

Composé	ν(OH)	ν(C=O)	ν(C=C)	ν(C-O)	Réf.
acac	2900 m	1720 ti 1660 ti	1590 m	1230 m	11-13
Aacac	2920 m	1707 ti 1650 ti	1640 i (vinyle group) 1590 m	1235 m	13-15
$[Co(acac)(Aacac)(H_2O)_2]$	3400 m	1626 i	1530 m	1254 m	
$[Co(Aacac)_2(H_2O)_2]$	3360 m	1626 i	1529 m	1254 m	
$[Co(Aacac)_2(py)_2]$	-	1620 i	1525 m	1253 m	
[Co(acac)(Aacac)(bipy)]	-	1625 i	1500 m	1251 m	
$[Co(Aacac)_2(bipy)]$	-	1625 i	1500 m	1250 m	
[Co(acac)(Aacac)(phen)]	-	1620 i	1510 m	1250 m	

ti = très intense ; i = intense; m = moyenne

Les spectres infrarouge de l'acétylacétone et de l'allylacétoacétate présentent deux bandes d'absorption très intenses, à 1720-1707 cm^{-1} et 1660-1650 cm^{-1}, attribuées à la vibration de valence du groupement >C=O dans la forme cétonique, respectivement dans la forme énolique [11-15]. La deuxième bande est élargie par la superposition de la vibration de déformation en plan du groupement OH de la forme énolique [13].

La vibration de valence symétrique de la liaison >C=C< donne une bande d'intensité moyenne, située à 1590 cm^{-1} [13,16]. De plus, dans le spectre IR de l'allylacétoacétate la vibration ν(C=C) du groupement vinyle donne une bande intense, à 1640 cm^{-1} [14,15]. Ce groupement peut-être aussi identifié par les bandes dues aux vibrations des liaisons C-H : ν(C-H), à 3085 cm^{-1} et γ(C-H), à 914 cm^{-1} [14].

L'abaissement de la fréquence ν(C=O) dans les spectres IR de tous les complexes est d'accord avec la coordination de l'acétylacétone et de l'allylacétoacétate par l'atome d'oxygène carbonylique [16-18]. La déprotonation du groupement OH et la coordination de l'oxygène énolique sont attestées par la disparition de la bande due à la vibration ν(OH) et le déplacement de la vibration ν(C-O) vers des fréquences plus élevées [18]. Les bandes attribuées aux vibrations ν(C-H) et γ(C-H) de l'allylcétoacétate ne subissent pas de déplacement dans les spectres IR des complexes, ce qui indique que le groupement vinyle n'est pas impliqué dans la coordination.

La présence de l'eau dans les complexes **1** et **2** est prouvée par l'apparition des bandes dans la région 3300-3400 cm^{-1}.

Les observations présentées ci-dessus montrent que l'acétylacétone et l'allylacétoacétate agissent comme ligands monobasiques bidentés, en se coordinant par les atomes d'oxygène.

Les spectres IR des complexes **3-6** contiennent aussi d'autres bandes, dans les régions 1460-1570 cm^{-1} et 1250-1335 cm^{-1}, dues à la présence des hétérocycles aromatiques [19]. Leur position, légèrement déplacée par rapport à celle rencontrée dans les ligands libres (py, bipy, phen) indique la coordination de ceux-ci à l'ion métallique.

Spectres électroniques. Les spectres en ultraviolet-visible de tous les complexes synthétisés présentent quatre bandes, dans les régions 15380-15600 cm^{-1}, 19200-19400 cm^{-1} et à environ 26000 cm^{-1} et 33000 cm^{-1}. Les deux dernières bandes sont caractéristiques aux ligands, tandis que les premières deux correspondent à des transitions *d-d* en symétrie octaédrique, avec $^4T_{1g}$ le fondamental orbital [20] :

15380-15600 cm^{-1} $^4T_{1g} \rightarrow {}^4A_{2g}$ (ν_2) et 19200-19400 cm^{-1} $^4T_{1g} \rightarrow {}^4T_{1g}(P)$ (ν_3)

Bien que la symétrie ne soit pas parfaitement octaédrique, l'absence d'un nombre supplémentaire de bandes ne permet pas d'apprécier la distorsion du champ des ligands.

La bande ν_1 n'apparaît pas dans le visible, mais sa position peut-être prévue sachant que pour les complexes octaédriques du cobalt(II) le rapport ν_2/ν_1 = 2,0-2,1 [20]. En ces conditions, ν_1 se situe à environ 7690-7800 cm^{-1}. Comme la différence entre les transitions ν_2 et ν_1 est égale à 10Dq, il en résulte pour Dq des valeurs comprises entre 770 et 780 cm^{-1}. En connaissant que ν_3 - ν_2 = 15B – 12Dq, on a pu déterminer aussi les valeurs de B, comprises, pour tous les complexes, entre 875 et 890 cm^{-1}. Tous ces résultats sont en bon accord avec les données de littérature pour des complexes analogues [20].

Les déterminations chimiques et spectrales nous ont permis d'attribuer aux complexes les formules structurales suivantes (Fig. 1) :

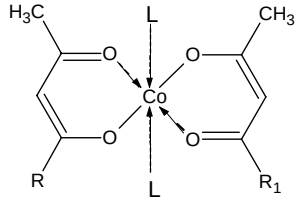

(1) *R : -CH_3 ; R_1 : -O-CH_2-CH=CH_2 ; L: H_2O*

(2) *R = R_1: -O-CH_2-CH=CH_2 ; L: H_2O*

(3) *R = R_1: -O-CH_2-CH=CH_2 ; L: Py*

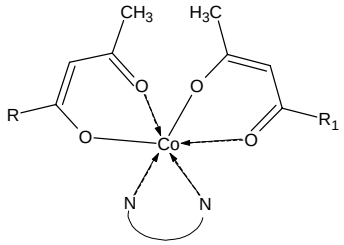

(4) *R : -CH_3 ; R_1 : -O-CH_2-CH=CH_2 ;* N N *: bipy*

(5) *R = R_1: -O-CH_2-CH=CH_2 ;* N N *: bipy*

(6) *R : -CH_3 ; R_1 : -O-CH_2-CH=CH_2 ;* N N *: phen*

Fig. 1. *Formules structurales proposées pour les complexes*

Conclusions

On a préparé six nouvelles combinaisons complexes du Co(II) en utilisant comme ligands acétylacétone, allylacétoacétate, pyridine, 2,2'-dipyridine et 1,10-phénantroline. Sur la base de la composition chimique et des résultats des analyses spectrales, on a pu conclure que la symétrie de tous les complexes est pseudo-octaédrique. Certains d'entre eux, dû à la présence de l'allylacétoacétate, sont susceptibles d'être copolymérisés avec d'autres ligands pour former des films.

BIBLIOGRAPHIE

1. Cullen,W.R. et Wickenheiser,E.B. (1989) *J. Organomet. Chem.* **370**, 141-154
2. Bennett,M.A., Chung,G., Hockless,D.C.R. et Neuman,H. (1999) *J. Chem. Soc. Dalton Trans.* **3**, 3451-3460
3. Taqui Khan,M.M., Srinivas,D., Kureshy,R.I. et Khan,N.H. (1990) *Inorg. Chem.* **29**, 2320-2324
4. Kodas,T.T. et Conita,P.B. (1990) *Acc. Chem. Res.* **23**, 188-194
5. Levis,F.D. et Salvi,G.D. (1995) *Inorg. Chem.* **34**, 3182-3189
6. Song Gao,B.Q.M. et Guang-Xian Xu,T.Y. (2001) *Polyhedron* **20**, 1-7
7. Sano,Y., Tanaka,M, Koga,N., Matsuda,K., Iwamura,H., Rabu,P. et Drillon,M. (1997) *J. Amer. Chem. Soc.* **119**, 8246-8250
8. Hanack,M., Dotz,A. et Fay,R. (1986) in : T.A. Skotheim(Ed): **Handbook of Conducting Polymers,** Marcel Dekker, New York
9. Macarovici,C.Gh. (1979) **Analiza Chimica Cantitativa**, Ed.RSR, Bucuresti, 223,350-352
10. Sharps,R.P. (1995) **Comprehensive Organometallic Chemistry**, vol. 8, Eds. E.W. Abel, F.G.A. Stone and G. Wilkinson, Pergamon, Oxford, 227
11. Nakamoto,K. (1978) **Infrared and Raman Spectra of Inorganic and Coordination Compounds**, 3rd Ed. Wiley-Interscience Publication, New York, 254
12. Athappan,P. et Rajagopal,G. (1995) *Trans. Met. Chem.* **20**, 356-360
13. Tayyari,S.F. et Milani-nejad,F. (2000) *Spectrochim. Acta A Mol. Biomol. Spectrosc.* **56(14)**, 2679-2691
14. Attygalle,B.A. (1994) *Pure Appl. Chem.* **66**, 2323-2326
15. Akarsu,M., Sayilkan,H., Şener, Ş., Sayilkan,F. et Arpaç,E. (2003) *Turk. J. Chem.* **27**, 477-486
16. Veeraraj,A., Sami,P. et Raman,N. (2000) *Proc. Indian Acad. Sci. (Chem. Sci.)* **112(5)**, 515-521
17. Nijse,J.F.W., Van Steenbergen,M.J., Kooijman,H., Talsma,H., Kroon-Batenburg,L.M.J., Van de Weert,M., Van Rijk,P.P., Witte,A., Van het Schip,A.D. et Hennink,W.E. (2001) *Biomaterials* **22**, 3073-3081
18. Yung,M.W., Oh,J.K., Yang,J.C. et Shul,Y.G. (1999) *Bull. Korean Chem. Soc.* **20(12)**, 1394-1398
19. Balaban,A.T., Banciu,M. et Pogany,I. (1983) **Aplicatii ale metodelor fizice in chimia organica**, Ed. Stiintifica si Enciclopedica, Bucurest, 23
20. Lever,A.B.P. (1984) **Inorganic Electronic Spectroscopy,** 2nd Ed. Elsevier, Amsterdam-Oxford-New York-Tokio, 280-287

COMPLEX COMBINATIONS OF Cu(II) WITH MIXED LIGANDS

T. Rosu[*], Maria Negoiu[*], V. Circu[*]

abstract: This paper describer the synthesis and characterization of several Cu(II) complexes using 2,2'- bipyridin as a primary ligand and L-tyrosine, L- tryptophan and L- histidine as secondary ligands Complex combinations were characterized through EPR spectra, IR-spectroscopy, electronic spectra, thermogravimetrycal analysis and elemental analysis. Analyzing the result we were able to determine the geometry of complex combinations that we obtained.

Introduction

Complex combinations of metal ions with aminoacids are important because of their biological applications. In 1965 Szazuchin O. and his team studied the synthesis of complex combinations of Zn(II) and Ni(II) with aminoacids: D-penicilamine and L-cysteine. These complex combinations have biological and therapeutical activities [1a].

Protein phosphorylation is recognized as an important step in information transfer and control of various biological processes such as enzyme activity[1b,2a]. X-ray structural studies have revealed that Serina phosphorylation of the active and less active forms of an allosteric enzyme muscle phosphorylase induces a conformational transition due to electrostatic or hydrogen bonds involving the phosphate moiety and histidine and arginine residues [2b,3] A classical example of electrostatic interactions that play a vital role in enzyme activity is that revealed for a zinc enzyme carboxypeptidase A. In its complex with a substrate,glycyl-L-tyrosine, it fixes the substrate by electrostatic interactions between the carboxylate group of the substrate and the arginine guanidinium group of the enzyme [4]. Ternary Cu(II) complexes containing aromatic heterocycles such as phen and aromatic amino acids such as phenylalanine (Phe) and L- tyrosine (Tyr) have been show to by stabilized by calculating the ring stacking equilibrium constant for a hypothetical equilibrium involving ternary species with without stacking interactions [5]. X-ray crystal structure analysis of Cu(histamine)(L-Tyr) [6], Cu(phen)(L-Trp) [7], (Trp=tryptophane), Cu(bpy)(L-Trp) ,(bpy = 2,2'-bipyridine), $[Cu(bpy)(L\text{-}Tyr)ClO_4].2H_2O$ [8] etc. revealed that the intramolecular stacking exists in the complex in the solid state.

This paper describer the synthesis and characterization of several Cu(II) complexes using 2,2'- bipyridin as a primary ligand and L-tyrosine, L- tryptophan and L- histidine as secondary ligands. We using this type of ligands to prove, by spectral measurements, that

[*] Department of Inorganic Chemistry, Faculty of Chemistry, University of Bucharest

Analele Universităţii din Bucureşti – Chimie, Anul XIV (serie nouă), vol. I-II, pg. 153-159

only complexes with a certain geometry can show π-π stacking intramolecular interactions. Characterization of the new prepared complexes was made by EPR spectra, IR-spectroscopy, electronic spectra, thermogravimetrycal analysis and elemental analysis.

Experimental

Reagents

The required chemicals were purchased from Merck and Chimopar Bucharest and all manipulations were performed using materials as received.

Physical measurements

The content of metallic ions was determined by atomic absorption spectroscopy with AAS 1N spectrometer Carl Zeiss Jena ; C, H, and N were analyzed with a Carlo Erba elemental analyzer. Elemental analyses were performed after drying the complexes at

60^0C. Electronic spectra were recorded by the diffuse-reflectance technique, using MgO as diluting matrix, on a JASCO V-550 spectrophotometer.IR spectra were recorded with a BioRad FTS 135 spectrophotometer in the 4000-400cm^{-1} region using KBr pellets. All the complexes were studied by thermogravimety (TG) in static air atmosphere, with a sample heating rate of 10 ^{0}C/min. using DuPont 2000 ATG thermo balance. EPR spectra were obtained with an ART-6, model IFA-Bucharest, X-band spectrometer (9.01 GHz) on line with a PC equipped with a 100KHz field modulation unit, on polycrystalline powders and solutions at room temperature and 77K.

Synthesis of complexes

Synthesis of [Cu(bpy)(L-Tyr)NO_3].3H_2O**,(1)**

$Cu(NO_3)_2$.3H_2O (1,21g, 5 mmol) and bpy (0,78g, 5mmol) were dissolved in 0,2 M HCl (25ml) by heating, and after cooling a solution of L-Tyr (0,91g, 5mmol) in 1 M NaOH (10 ml) was added. The mixture was concentrated in vacuo and kept at room temperature. The blue crystals which separated were collected and recrystallised from water. Anal. Calc. for $C_{19}H_{24}N_4O_9Cu$: C, 44,18; H, 4,65; N, 10,85; Cu, 12,40. Found: C, 44,87; H, 4,08; N, 10,15; Cu, 12,20%.

Synthesis of [Cu(bpy)(L-Trp)NO_3].H_2O**(2)** and [Cu(bpy)(L-histidine)NO_3].2H_2O**(3)**

These complexes were prepared by the method described above but using 1,02g

L-Trp (5 mmol) and 0,78g histidine (5mmol). The light-blue crystals which separated were collected and recrystallised from water.Anal. Calc. for [Cu(bpy)(L-Trp)NO_3].H_2O, $C_{21}H_{21}N_5O_6Cu$: C, 50,09; H, 4,17; N, 13,91; Cu, 12,72. Found: C, 50,83; H, 3,74; N, 13,78; Cu, 12,47%, and calc. for [Cu(bpy)(histidine)NO_3].2H_2O, $C_{15}H_{19}N_7O_7Cu$: C, 40,67; H, 4,23; N, 17,29; Cu, 13,55. Found: C, 40,89; H, 3,86; N, 16,93; Cu, 13,32%.

Results and Discussion

These complexes have a low solubility in chloroform, acetone,ethanol and water but they are insoluble in dimethylformamide (DMF).

The IR spectral data

In IR spectra of newly prepared complexes there are 3 bands assigned to NO^{3-} ion bound to Cu(II) center: 1451 – 1456 cm^{-1}(ν_1), 1378-1393 cm^{-1}(ν_2), 1016-1040 cm^{-1}(ν_3) ranges.The splitting of the bands situated at higher wave numbers (ν_1-ν_2) is about 60 – 70 cm^{-1} indicating the coordinate of nitrate ion in a monodentate fashion [9].
Also, the $\nu_{COO^-(s)}$ bands shifts towards lower wave numbers while the $\nu_{COO^-(as)}$ frequencies shift towards higher wave numbers compare to the positions of these bands in the IR spectrum of free aminoacid.

The $\delta_{NH(1)}$ and $\delta_{NH(2)}$ frequencies shift towards higher wave numbers in the IR spectra of the complexes together with the vanishing of the ν_{NH} frequencies. This behavior suggests the coordination of the aminoacid through $–NH_2$ and $–COO^-$ group in a bidentate fashion

Table 1. IR Spectral Data for the Ligands and their Complexes (cm^{-1}).

Compound	$\nu_{coo(s)}$	$\nu_{coo(as)}$	ν_{NH}	$\delta_{NH(1)}$	$\delta_{NH(2)}$	ν_{C-N-C}	$\nu_{C:::N}$	ν_{NO3}
L- Tyrosine	1415	1583	3121	1662	1535	-	-	-
2,2'- bipyridina	-	-	-	-	-	-	1572	-
$[Cu(bpy)(L\text{-}Tyr)NO_3].3H_2O$	1380	1621	-	1705	1578	-	1528	1456
								1393
								1040
L-Tryptophan	1393	1608	3103	1645	1520	1108	-	-
$[Cu(bpy)(L\text{-}Trp)NO_3].H_2O$	1344	1630	-	1683	1568	1104	1530	1451
								1382
								1020
L-histidine	1387	1610	3112	1638	1517	1115	1580	-
$[Cu(bpy)(histidin)NO_3]2H_2O$	1339	1652	-	1672	1560	1110	1580	1453
							1541	1378
							1534	1024

The $\nu_{C:::N}$ frequency of 2,2'-bipyridine ligand shifts with 30 – 40 cm^{-1} towards lower wave numbers in the IR spectra of complexes compare to the IR spectrum of free ligand, thus indicating the coordination to Cu(II) through the two sp^2 hybridized nitrogen atoms. In the IR spectra of Cu(II) complexes with L-histidine as a secondary ligand there is an additional $\nu_{C:::N}$ frequency in the 1531-1535cm^{-1}range. This behavior indicates the coordination of L-histidine ligand through the sp^2 hybridized nitrogen atom.

The electronic absorption data

The electronic spectroscopy data for the complexes in solid state are presented in table2.

The UV-VIS spectra of $[Cu(bpy)(L\text{-}Tyr)NO_3].3H_2O$ and $[Cu(bpy)(L\text{-}Trp)NO_3].H_2O$ complexes show two distinct bands at 11435 cm^{-1} and 14980 cm^{-1} for the former one and at 11790 cm^{-1} and 15120 cm^{-1} for the later complex. The position of these two bands is a strong indication of a square-pyramidal geometry [10].

Table 2. Electronic Spectral Data for Complexes in Solid State (cm^{-1}).

Compounds	Assignment d-d (cm^{-1})			Geometry
	$z^2 \rightarrow x^2 - y^2$	$xy \rightarrow x^2 - y^2$	$xz;yz \rightarrow x^2 - y^2$	
$[Cu(bpy)(L\text{-}Tyr)NO_3].3H_2O$	11435	-	14980	Square-pyramidal
$[Cu(bpy)(L\text{-}Trp)NO_3].H_2O$	11790	-	15120	Square-pyramidal
$[Cu(bpy)(histidin)NO_3]2H_2O$	13125	16300	17230	Octahedral

The UV-VIS spectrum of $[Cu(bpy)(L\text{-histidine})NO_3].2H_2O$ complex shows two absorption bands at 16300 cm^{-1} and 17230 cm^{-1} and a third weak absorption band at 13215 cm^{-1}, suggesting a distorted octahedral geometry.

The coordination of sp^2 hybridized heterocyclic nitrogen atom of histidine in the axial position (for Cu(II) complexes with histidine) increases the splitting between d_z^2 and $d_{x^2-y^2}$ orbitals as well as between d_{xz},d_{yz} and $d_{x^2-y^2}$ orbitals [11].

EPR spectra

EPR spectra in X-band for Cu(II) complexes **1, 2, 3** were recorded using ethanolic solutions at 77K.

Table3. EPR parameters of the complexes

Compounds	$g_\perp$	$g_{//}$	$A_{//}$	$A_\perp$
$[Cu(bpy)(L\text{-}Tyr)NO_3].3H_2O$	2,03	2,18	152	13,8
$[Cu(bpy)(L\text{-}Trp)NO_3].H_2O$	2,02	2,20	150	14,5
$[Cu(bpy)(histidin)NO_3]2H_2O$	2,09	2,29	185	17

The frozen ethanolic solution spectra of $[Cu(bpy)(L\text{-}Tyr)NO_3].3H_2O$ and $[Cu(bpy)(L\text{-}Trp)NO_3].H_2O$ are identical, Fig 1, with $g_\perp$ =2,03, $g_{//}$ =2,18 and $A_{//}$ =152 Gauss, respective $g_\perp$ =2,02, $g_{//}$ =2,20 and $A_{//}$ =150 Gauss. The seven lines of hypersuperfine structure of EPR spectra indicates the presence of 3 nitrogen atoms around the Cu(II) ion [11]. The frozen ethanolic solution spectra of $[Cu(bpy)(L\text{-histidine})NO_3].2H_2O$ indicates that there are 4 nitrogen atoms around Cu(II) ion [11]. The splitting parameters $g_\perp$ and $g_{//}$ values depend on the ground level occupied by the paramagnetic electron of Cu(II). Thus, if the ground state of Cu(II) is $B_{1g}(d_{x^2-y^2})$ then the two parameters are related by the following relationship: $g_{//} > g_\perp > 2{,}002$ and the complex shows an axial distortion [12].

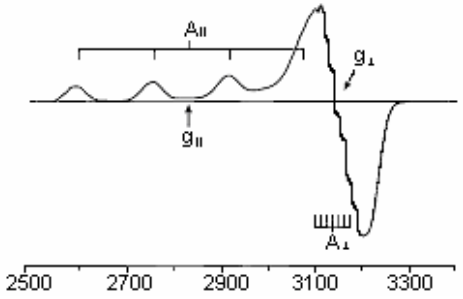

Fig. 1. *Frozen solution EPR-spectra of $[Cu(bpy)(L\text{-}Tyr)NO_3].3H_2O$ recorded at 77 K in ethanol.*

Thermal Decomposition

The complexes of this study were investigated by thermogravimetry (TG). Experimental data for thermo gravimetrical analysis are presented in table 4. The TG and DTG indicate a lost of weight from 90^o –110^{o}C corresponding to 3 molecules of water per mol of complex combination (1), one molecule of water per mol of complex combination (2), and 2 molecules of water per mol of complex combination (3).

Table 4. Experimental data for thermo gravimetrical analysis

Compounds	Temperature range (^{o}C)	Eliminated fragment	Weight lose exp.%	calc.%
[Cu(bpy)(L-Tyr)NO_3].3H_2O	90-110	3H_2O	10,08	10,46
	365-560	bpy ; Ph-OH	47,86	48,25
	650-670	-$C_3NO_2H_5$	16,33	16,86
	785	CuO (residue)	15.89	15,50
[Cu(bpy)(L-Trp)NO_3].H_2O	93-108	H_2O	3,20	3,57
	340-580	bpy ; heterocycle	53,28	54,07
	610-635	-$C_3NO_2H_5$	16,76	17,29
	775	CuO (residue)	16,31	15,90
[Cu(bpy)(histidin)NO_3]2H_2O	98-109	2H_2O	7,25	7,62
	275-380	bpy	33,69	33,05
	490-680	heterocycle; -$C_3NO_2H_5$	31,97	32,62
	745	CuO (residue)	16,27	16,94

The GT and DGT curves for (1) and (2) complex combinations are similar with the exception of the temperature of lost of weight,Fig. 2(a). Thus, the second step has two consecutive effects which indicates the loss of one molecule of *bpy* and the heterocyclic fragment of aminoacid molecule while the third step corresponds to the loss of -$C_3NO_2H_5$ fragment of the aminoacid molecule.

For complexe (3), Fig. 2(b), the second step of decomposition corresponds to the loss of the primary ligand, *bpy*,in the 200 – 380^{o}C range which is much smaller than the corresponding temperature range of complexes (1) and (2). The third step of decomposition cumulates two consecutive effects that correspond to the loss of secondary ligand. For all complexes the last decomposition step corresponds to the loss of NO_3^- group in the 675-785^{o}C range.

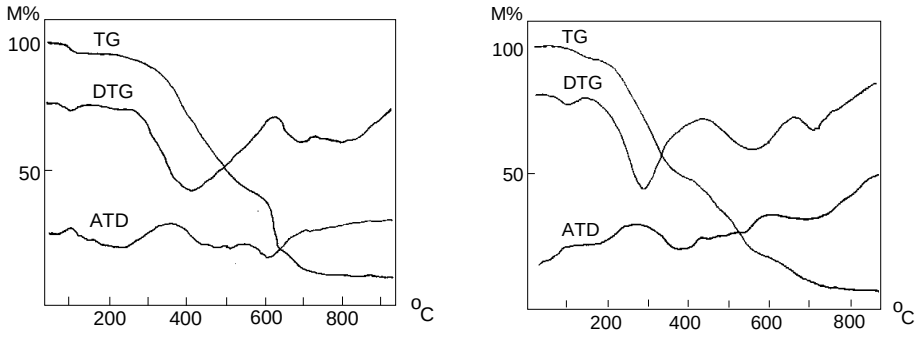

(a) **(b)**

Fig. 2. *TG, DTG and ATD curves for* ***(a)*** *-[Cu(bpy)(L-Trp)NO_3].H_2O ;* ***(b)*** *-[Cu(bpy)(L-histidine)NO_3].2H_2O*

The values of temperature that characterizes the weight loss indicate that the stability of complexes decreases following the sequence: **(1)** ≅ **(2)** > **(3).** The final residue, for all complexes , was analyzed by IR spectroscopy and was identified as CuO, and %M corresponds to the calculated one.

The physico-chemical data led to the conclusion that the[$Cu(bpy)(L\text{-}Tyr)NO_3].3H_2O$ and [$Cu(bpy)(L\text{-}Trp)NO_3].H_2O$ complexes have a square-pyramidal geometry similar to that of [$Cu(bpy)(L\text{-}Tyr)ClO_4].2H_2O$ [8] complex which suggests that the NO_3^- ion has no influence upon coordination geometry. The solid-state structure of [$Cu(bpy)(L\text{-}Tyr)ClO_4].2H_2O$ [8] complex shows π-π intermolecular stacking (3,02A) . For both prepared complexes the geometry is identical and the metallic center is surrounded by similar ligands which might suggest that the π-π stacking interactions are favored.

.

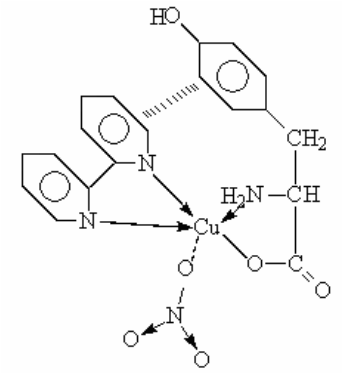

(1)

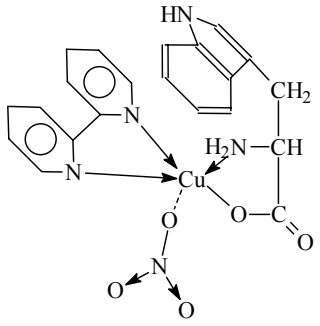

(2)

The UV-VIS spectra of complexe **(3)** containing hisitidine as a secondary ligand show medium intensity absorption bands specific to an octahedral geometry. The coordination of sp^2 hybridized nitrogen atom of aminoacid heterocycle in the axial position of Cu(II) complexes with hisitidine leads to the conclusion that these complexes have an axial distortion [11].

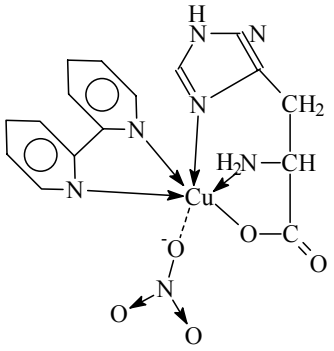

(3)

For complexe **(3)** the intermolecular π-π stacking interactions may lack due to the formation of a co-ordinative bond between Cu(II) ion and sp^2 hybridized nitrogen atom of aminoacid heterocycle.

The presence of intermolecular interactions can give rise to an increase of thermal stability of the complex [8]. Thus, the decomposition temperatures of $[Cu(bpy)(L\text{-}Tyr)NO_3].3H_2O$ si $[Cu(bpy)(L\text{-}Trp)NO_3].H_2O$ complexes confirm a greater stability than the prepared complexe with an octahedral distorted geometry.

As a conclusion one might say that the presence of π-π stacking interactions is possible unless a co-ordinative bond is formed between Cu(II) ion and sp^2 hybridized nitrogen atom of the aminoacid heterocycle.

REFERENCE

1. (a) Szazuchin, O. Navarin, S.M. (1965)., *Antibiotiki,* **6** , 56; (b) Perutz , M.F. (1988) *Nature (London),* **336**, 202-203.
2. (a) Da Silva, J.J.R.F. Williams, R.J.P. (1991) **The Biological Chemistry of The Elements,** Claredon Press, Oxford, 440; (b) Sprang, S. R.. Acharya, K. R. Goldsmith, E. J. Stuart, D. I.. Varvill, K Flettrick, R. J.. Madsen, N. B Johnson, L. N. (1988) *Nature (London),* **336** 215-221.
3. Hurley, J. H. Dean, A. M.. Sohl, J. L Koshland, D. E. Jr. and Stroud, R. M. (1990) *Science (Washington),* **249** 1012.
4. (a) Lipscomb, W. N(1970). *Acc. Chem. Res*., **3**, 81; (b) Christianson, D. W.. Lipscomb, W. N (1989) *Acc. Chem. Res***., 22,** 62.
5. Yamauchi, O. Odani, A. (1985) *J. Am. Chem. Soc.,* **107 ,**5938.
6. (a) Yamauchi, O. Odani A., Kohzuma, T. Masuda, H. Toriumi, K.. Saito, K (1989) *Inorg. Chem.,* **28,** 4066; (b) Sigel, H. Tribolet, R. Yamauchi, O. (1990) *Comments Inorg. Chem.,* **9** ,305.
7. (a) Aoki, K. Yamazaki, H. (1987) *J. Chem. Soc., Dalton Trans.,* 2017; (b) Masuda, H. Matsumoto, O. Odani, A. Yamauchi, O. (1988) *Nippon Kagaku Kaishi*, 783.
8. (a) H. Masuda, T. Sugimori, A. Odani, O. Yamauchi, (1991) *Inorg. Chim. Acta,* **73,***180*; (b) Yamauchi, O. Odani, A. Masuda, H. (1992) *Inorg. Chim. Acta, 198-200*
9. Nakamoto, K. **Infrared Spectra of Inorganic and Coordination Compounds**, Ed. (1986)J. Wiley and Sons , New York , 256-257.
10. Lever, A. B. P. (1984) **Inorganic Electronic Spectroscopy,** 2nd Edn, Elsevier Science, New York,
11. (a) Abragam, A. Bleanei, B. (1970),**Electron Paramagnetic Resonance of Transition Ions,**Clarendon Press, London, 492; (b) Mabbs, F.E. Collison, D. ,(1992)**Electron Paramagnetic Resonance of d Transition Metal Compounds,** Elsevier, Amsterdam; (c) Hathaway B. J. (1987) Comprehensive Coordination Chemistry, Pergamon Press, U.K**., 5,** 652.
12. (a) Bleaney, B. Bowers, K. D..Pryce, M.H.L(1955) *Proc. Roy. Soc.* **A 228,** 166. (b) Hayes, W. Wilkens, J. (1964)*Proc. Roy. Soc.* **A 281**, 32
13. Linert, W. Jamenson, R.F. Taha, A. (1993) *J. Chem. Soc., Dalton Trans.,* 318.

POLAROGRAPHIC BEHAVIOR OF PALLADIUM ION IN PARTIAL AQUEOUS MEDIUMS

V. Dumitrescu[*], N. Dumitrescu[*], M. Calugareanu[*]

abstract : There was studied the polarographic behavior of palladium ion in presence of the reagent 1,10-phenantroline and the solvent hexamethylphosphotriamide (HMPA). The method can be used for quantitative determinations of palladium into the domain $5 \cdot 10^{-5}$ M-$2 \cdot 10^{-4}$ M. Polarograms were well defined and reproductible.

keywords: polarographic determination palladium

Introduction

Polarographic determination of many species can be achieved using aqueous or non-aqueous mediums. A large variety of inorganic and organic substances that are not soluble in water requires a proper solvent or a mixture of solvents so that the polarographic waves should be well defined for a quantitative determination. In this study is presented a method of polarographic determination of palladium in presence of 1 , 10-phenantroline and HMPA solvent.

HMPA is a colorless liquid miscible which water in any ratio and with other polar non-polar organic solvents. HMPA has been used in polarographic determination of Pd^{+2} complex with *p*-nitrosodimethylaniline [1,2].

In the specialty literature a series of electrometric determination of Pd^{+2} is mentioned [3-14].

In this paper the solvents influence on polarographic waves and the optimal conditions for quantitative determination of palladium were established.

[*] Departament of Analytical Chemistry, University of Bucharest, 90 road Panduri, Bucharest, ROMANIA

Analele Universităţii din Bucureşti – Chimie, Anul XIV (serie nouă), vol. I-II, pg. 161-165

Experimental

Apparatus and reagents

Polarographic determinations were accomplished with the aid of a polarograph LP72 and a recorder TZ213S. The electrochemical cell was composed of dropping mercury electrode as cathode and a electrode with large surface of mercury as anode. The glass capillary had a diameter of 0.07 mm and the dropping rate was 2 drops/second.
For the determinations the following (basic) solutions were used:

- $PdCl_2$ solution 10^{-3} M in 1% HCl ; $PdCl_2$ solution was provided by Fluka ;
- $(CH_3)_4NCl$ (tetramethylamonium chloride) 1M; $(CH_3)_4NCl$ was used as support electrolyte and was provided by Merck;
- gelatine solution 0,1% , used as a suppresor for polarographic maxims;
- 1,10-phenantroline solution 10^{-2} M in 50% ethanol provided by Merck;
- HMPA solution 99% provided by Merck;

All reagent used in our studies were of analytical purity. The solutions were obtained in bidistilled water. Sample volume was 5 ml.

Results and Discussion

I. The polarographic study of palladium ion in presence of HMPA (without reagent) was made using the following solutions: $(CH_3)_4NCl$ 10^{-1} M; gelatine 0.01%; HMPA 20%; Pd^{2+} $5\cdot10^{-5}$M-$2\cdot10^{-4}$M. The polarograms obtained were well defined and reproductible. We mention that these are the optimal conditions. The polarograms height increases with the increase of the concentration of the $PdCl_2$ solution. We made the logarithmic analysis of the polarographic wave. We also made the calibration curve. We made polarographic determinations of Pd^{2+} in presence of HMPA and 1,10-phenantroline reagent, using solutions with the same concentrations as we mentioned above and phenantroline 10^{-3}M and Pd^{2+} $2\cdot10^{-4}$M. In fig.1 the polarogram obtained is shown.

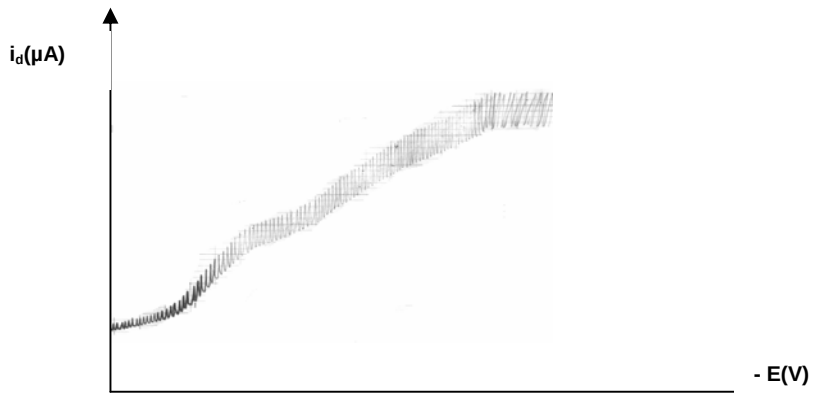

Fig. 1. *Polarogram for a solution containing the complex between Pd^{2+} and 1,10-phenantroline ın presence oţ HMPA*

The polarogram is also obtained in optimal conditions for polarographic determination of palldium. It shows two reduction steps. We discussed and analyzed during this study only the second polarographic wave, for which $E_{1/2}$= -1.32 V.

In these conditions (Pd^{2+}+HMPA+1,10-phenantroline) the influences of various components of the solution were studied.

a) Influence of suppresser

The presence of maxims on polarograms has a drawback of incorrect evaluation of parameters of polarographic wave. Removing of these maxims could be fulfilled by adding to the solution to be polarographically determined an active superficial substance in a low concentration.

Gelatine in different concentrations was used as a suppresser for polarographic maxims maintaining the concentrations of other substances constant.

The polarographic wave becomes less defined and its height decreases with the increase of gelatine concentration. It was established that 0.5 ml gelatine/5 ml sample was enough for obtaining well defined and reproductible polarograms.

b) Influence of reagent concentration

Concentrations of $(CH_3)_4NCl$ 10^{-1} M; gelatine 0,1%; HMPA 20%; Pd^{2+} $2\cdot10^{-4}$ M were kept at a constant value. It was observed that by adding 1,10-phenantroline with a higher concentration than 10^{-3} M the semiwave potential is constant. At smaller concentrations the polarographic wave is less defined and $E_{1/2}$ takes more positive values. At higher reagent concentrations the height of the polarographic waves decreases (we consider only the second polarographic wave).

In polarographic determination the optimal reagent concentration must be at least 20 times higher than that of Pd^{2+}.

c) Influence of support electrolyte

As a support electrolyte in our polarographic determinations a solution of tetramethylamonium chloride 10^{-1} M was used. At this concentration the polarographic waves are well defined and reproductible. Support electrolyte is in excess than the concentration of palladium.

d) Influence of the height of Hg column

This study was accomplished using the following solutions: Pd^{2+} $15\cdot10^{-5}$ M ; $(CH_3)_4NCl$ 10^{-1} M; gelatine 0,1%; HMPA 20%; 1,10-phenantroline 10^{-3} M, at different mercury column heights within 300-600 mm. It was noticed that the height of the polarographic waves increased with the increase of the mercury column height.

In Fig. 2 we show the dependence between log h and log $H^{1/2}$, where h is the limit current intensity and H is the mercury column height (for the second polarographic wave).

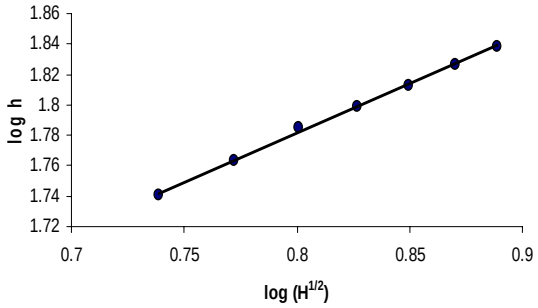

Fig.2: *Dependence log h = f(log $H^{1/2}$)*

We reached the conclusion that the dependence log h = f(log$H^{1/2}$) is linear which means that current intensity is a diffusion-controlled process.

In Fig. 3 is presented the logarithmic analysis of the second polarographic wave for a more accurate determination of semiwave potential.

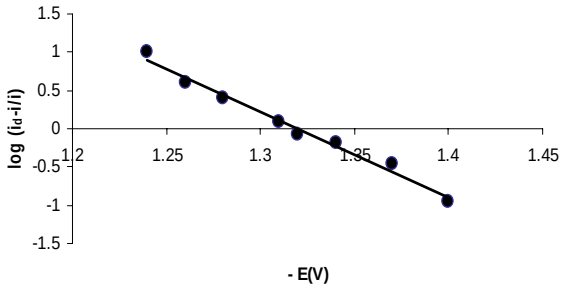

Fig. 3: *Diagram of logarithmic of the second polarographic wave*

From this representation we obtained $E_{1/2}$= - 1.32 V.

We also accomplished the quantitative determination of Pd^{2+} in presence of 1,10-phenantroline and HMPA. We established the optimal conditions for polarographic determination of Pd^{2+} : $(CH_3)_4NCl$ 10^{-1} M; gelatine 0,1%; HMPA 20%; 1,10-phenantroline 10^{-3} M. Palladium concentration was taken within the domain $5\cdot10^{-5}$ M-$2\cdot10^{-4}$ M.

In Fig. 4 the calibration curve for quantitative determination of palladium ion is given, taking into account the second polarographic wave.

It was ascertained that Pd^{2+} could be determined within the domain $5\cdot10^{-5}$ M-$2\cdot10^{-4}$ M.

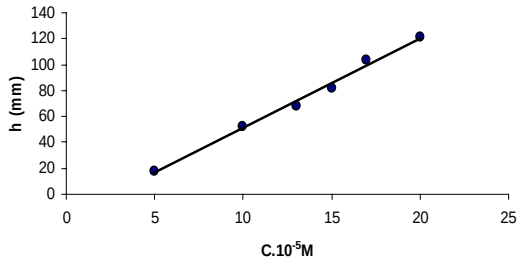

Fig.4: *Calibration curve for palladium polarographic determination in presence of 1,10 phenantroline and HMPA*

Conclusions

In this paper the condition of polarographic determination of palladium ion in presence of 1,10- phenantroline and HMPA solvent were established. This solvent influenced the diffusion current intensity and the value of the semiwave potential ($E_{1/2}$). This effect are due to the solvation modification of the ions and to different diffusion coefficients.
Polarograms were well defined and reproductible. The results lead us to the conclusion that this method can be applied to the quantitative determination of palladium ion with in the concentration domain $5 \cdot 10^{-5}$ M-$2 \cdot 10^{-4}$ M in presence of 1,10-phenantroline and HMPA solvent. In presence of 1,10-phenantroline reagent the semiwave potential takes more negative values than in its absence. The whole study was made for the second polarographic wave.

REFERENCES

1. Dumitrescu, V., David, V. and Cazacu, C. (**1998**) *Anal. Univ. Buc*. 47, 21-6
2. Dumitrescu, V., Dumitrescu, N., and Anghel D. **(2003)** *Anal. Univ. Buc.* XII (serie noua), vol. I-II, 61-68
3. Georgieva, M., Pihlar, B. (**1996)** *Anal. Lab*. 4(3), 108-4.
4. Kumar, A., Pandey, P., Mishra, N. and Narad, S. (**1996**) *Chem. Anal*. (Warsaw) 41(1), 121-4
5. Georgieva, M. and Pihlar, B. (**1996**) *Electroanalysis* (N.Y.) 8(12), 1155-9
6. Zhang, F.Y., Dong, A.j. and Sun, Q.Z. (**1997**) *Fenxi Huaxue* 25(1), 76-8.
7. Li, Y.P., Chen, W. S. and Wei, X. P. (**1997**) *Lihua Jianyan, Huaxue Fence* 33(10), 459-61.
8. Nadezhiana, L. S., Lobanova, O. A. and Pankina, I. A. **(1998)** *J. Anal. Chem*. 53(2), 151-3.
9. Dias, L. F., Nozaki, J. (**1998**) Anal. Lett. 31(14), 2489-97.
10. Sun, Q. Y., Wang, C. M., Li, L. X. and Li, H. X. (**1999)** Fresenius'*J. Anal. Chem*. 363(1), 114-7.
11. Aher, V. T., Palrecha, M. M., Kulkarni, A. V., Shah, G. C. and Mathur, P. K. (**1999**) Fresenius' *J. Anal. Chem*. 364(4), 362-3.
12. Sladkov, V. E., Prokhorova, G. V., Ivanov, V. M. *Chem. Abstract*, vol. 133, nr. 16, 232089d, **2000**.
13. Sung, Kim , Ki, W. C. *Talanta*, 57, 675-679, **2002**
14, Gevorgyan, A. M., Vanyukov, V. V., Olikhova S. V., Mukhamedgalieva, U. A., Vakhnenko, S. V., *Chem. Abstracts*, vol. 138, nr. 10, 146756r, **2003.**

DETERMINATION OF VITAMIN C IN DIFFERENT STAGES OF FRUITS GROWING

N. Rasanu[*], V. Magearu[**], Nicoleta Matei[*], Alina Soceanu[*]

abstract: Ascorbic acid (AA) is a powerful antioxidant naturally present in many foods, especially fruits and vegetables, which play an important role in the prevention of infectious diseases. It is important in processes of oxidation and reduction in human organism, participating in several metabolic reactions. A simple method for the ascorbic acid (Vitamin C) in some fruit type utilizing a titrimetric method with potassium bromide is described. To observe source of Vitamin C in these fruits and how easy it's losing once with the vegetation period, we determine Vitamin C concentration from: leaves, tails, green fruits, respectively from fruits. The precision of the determination of Vitamin C was evaluated and it was found that the recovery of ascorbic acid was 97%. The precision of the method is good and the recovery of the analyte is nearly quantitative.

Introduction

Vitamin C, the L-enantiomer of ascorbic acid, is a water-soluble vitamin used by the body for several purposes. Most animals can synthesize their own vitamin C, but some animals, including primates, guinea pigs, and humans, cannot. Vitamin C was first isolated in 1928, and in 1932 it was proved to be the agent, which prevents scurvy. Citrus fruits (lime, lemon, orange, grapefruit) and tomatoes are good common sources of vitamin C. Other foods that are good sources of vitamin C include papaya, broccoli, brussels sprouts, blackberries, strawberries, cauliflower, spinach, cantaloupe, and blueberries.

The amount of Vitamin C in fruit depends on the precise variety of the fruit, the soil and climate in which it grew, and the length of time since it was picked. As a participant in hydroxylation, vitamin C is needed for the production of collagen in the connective tissue. Some tissues have a greater percentage of collagen, including: skin, mucous membranes, teeth, bones [1].

Vitamin C is also required for synthesis of dopamine, noradrenaline and adrenaline in the nervous system or in the adrenal glands. It is a strong antioxidant. [2]

[*]Department of Chemistry, University "Ovidius" of Constantza, 124,Mamaia Blvd., 900527, RO,E-mail: nmatei@univ-ovidius.ro

[2**]Department of Analytical Chemistry, Bucharest University,4-12, Regina Elisabeta Blvd., 70346, Bucharest, RO

Analele Universităţii din Bucureşti – Chimie, Anul XIV (serie nouă), vol. I-II, pg. 167-172

Lack of ascorbic acid in the daily diet leads to a disease called scurvy, a form of avitaminosis that is characterized by: loose teeth, superficial bleeding, fragility of blood vessels, poor healing, compromised immunity, mild anaemia. The dietary amounts recommended by various authorities are 50-150 mg of ascorbic acid per day. High doses (thousands of mg) are used but may result in diarrhea. Any excess of vitamin C is generally excreted in the urine Vitamin C is needed in the diet to prevent scurvy. It also has a reputation for being useful in the treatment of colds and flu. The evidence to support this idea, however, is ambiguous. [3]

Vitamin C is an important anti-oxidant, helps protect against cancers, heart disease, stress, it is part of the cellular chemistry that provides energy, it is essential for sperm production, and for making the collagen protein involved in the building and health of cartilage, joints, skin, and blood vessels. Vitamin C helps in maintaining a healthy immune system, it aids in neutralizing pollutants, is needed for antibody production, acts to increase the absorption of nutrients (including iron) in the gut, and thins the blood. Just to mention it's most important functions. [4]

Apple: *Malus pumila (M. domestica).* Apples vary from a 'fairly good' to a 'very good' source of vitamin C, as there are significant differences between the varieties. 'Crab apples', possibly *Malus sylvestris*, are listed as having very little vitamin C content (compared weight for weight to modern apples). Apples are a good source of the B vitamin 'biotin'. Apples are also a good source of a variety of minerals-magnesium, iron, chromium, and manganese. Apples (as distinct from the expressed juice) are a good source of soluble fiber, which has been shown to slow the release of sugars in the blood and also slightly drop blood cholesterol levels. Eating 100 grams of fresh red delicious apple with the skin on provides the total anti-oxidant activity equal to 1,500 milligrams of vitamin C. [5]

Apricot: *Prunus armeniac.* Apricot flowers are easily damaged by frost, and the plant really needs a hot, relatively dry growing season. Apricots can't be regarded as a significant source of vitamin C, but are a good source of vitamin A (as carotene)- one 35-gram apricot has 914 International Units of vitamin A, making them the third richest source of vitamin A of all the common commercial fruit. Canned apricots are also good source of Vitamin A, with one canned apricot having very approximately half the content of a fresh fruit. [6]

Cherry: *Prunus avium*. The first ancestral *Prunus* species probably arose in Central Asia, and gave rise to plums, apricots, peaches, almonds, and cherries. Sour cherries, *Prunus cerasus*, evolved from the sweet cherry, perhaps with infusion of genes from another Central Asian *Prunus* species. At 10 mg per 100 grams of flesh, both fresh sweet cherries and fresh sour cherries rank as a good source of vitamin C. But even *frozen* sour cherries have useful amounts-5mg/100gram. (there will almost certainly be differences between varieties). [7]

Though the literature is replete with the different types of methods for the analysis of such diversified products, efforts continue in the search of better methods. Such attempts to quantify ascorbic acid in these samples have resulted in a large number of methods: titrimetry, voltammetry, fluorometry, potentiometry, kinetic-based chemiluminiscence (CL), flow injection analyses, biosensors and chromatography with spectrometer detector. [8-13]

The aim of the present paper consist in determination of ascorbic acid concentration changes occurred along vegetation period in sour cherry - *Prunus cerasus,* apricot – *Prunus armeniac* and apple – *Malus pumila*.

Experimental

The titrimetric method

For determination of ascorbic acid we used titrimetric method with potassium brommat-bromide solution in the acid medium [14,15]. This method was optimized by the laboratory conditions. [16]

Ascorbic acid, $C_6H_8O_6$ is cleanly oxidized to dehydroascorbic acid by bromine. An unmeasured excess of potassium bromide is added to an acidified solution of the sample. The solution is titrated with standard potassium bromate to the first permanent appearance of excess bromine: this excess is then determined iodometrically with standard sodium thiosulfate. The entire titration must be performed without delay to prevent air-oxidation of the ascorbic acid.

The reagents

The reagents used have been: $Na_2S_2O_3$ 0,5N, $KBrO_3$-KBr 0,05N, $K_2Cr_2O_7$ 0,5N, H_2SO_4 1N, H_2SO_4 1:2, KI, starch indicator 1%. All reagents were of analytical-reagent grade and all solutions were prepared using distilled-deionized water.

Sample preparation

The biological samples consisted in apple, apricot and sour cherry harvested in May-August 2004.

To observe source of Vitamin C in these fruits and how easy it's losing once with the time and during the vegetation period, it has determined Vitamin C concentration from: tails, leaves, green fruits, respectively from fresh fruits.

The fruits were weighed, crushed, dissolved in water and transferred into a 100mL volumetric flask. After that, was filtered and for analysis we take a portion of this filtrate.

Results and discussion

The contents of L-ascorbic acid in different fruits were determined by titrimetric method and the results are given in Table 1 for apricot, in Table 2 for sour cherry and in the last for apple in Table 3.

It can observe that in leaves a height Vitamin C concentration exists, which tell us that Vitamin C provide from apricot leaves, respectively from apple leaves. In apricot flower exist a big ascorbic acid content and the possibility of saying that the vitamin come from flowers cannot be eliminated.

Table 1. **Vitamin C concentration in leaves and apricot.**

Data	Vitamin C content in apricot (mgAA/100g product)	
	Leaves	Fruits
10.05.2004	166.76	flowers 129.43
09.06.2004	109.6	67.18
16.06.2004	87.01	55.59
22.07.2004	31.20	green fruit 31.10
10.08.2004	30.18	fresh fruit 20.75*

**The vitamin C content in fresh apricot from literature is 8-20mgAA/100g products.[17]*

Table 2. Vitamin C concentration in tails, leaves and sour cherry.

Data	Vitamin C content in sour cherry (mgAA/100g product)		
	Tails	Leaves	Fruits
10.05.2004	165.40	151.64	flowers 143.2
09.06.2004	118.77	79.18	54.01
16.06.2004	112.30	75.42	green fruit 30.12
23.06.2004	77.53	61.55	fresh fruit 20.94*

**The vitamin C content in fresh sour cherry from literature is 10-20mgAA/100g products.[17]*

The source of Vitamin C in sour cherries it's coming from tails and the concentration of this vitamin in fruits it's decreasing once with growing fruits.

Table 3. Vitamin C concentration in leaves and apple.

Data	Vitamin C content in apple (mgAA/100g product)	
	Leaves	Fruits
10.05.2004	121.44	flowers 167.51
09.06.2004	59.91	49.49
16.06.2004	49.91	42.60
22.07.2004	38.91	Green fruit 25.21
17.09.2004	20.12	Fresh fruit 12.68*

**The vitamin C content in fresh apple from literature is 12mgAA/100g products.[17]*

After determinations, it can observe that in green apricot and green sour cherry is a higher concentration of vitamin C than in green apple and the same in the fresh fruit. The ascorbic acid contents its lower in fresh fruit than in other organs of fruit trees. Also, the ascorbic acid concentration obtained by volumetric method is in good agreement to the literature data.[17] After determinations, it can observe one variation of vitamin C concentration depending on vegetation period.

The precision of the determination of Vitamin C was evaluated under the optimum conditions mentioned in [18-21] It was found that the recovery of ascorbic acid was 97%. The precision of the method is good and the recovery of the analyte is nearly quantitative (>90%).

Also, the interferences are determined in [22] and it can be seen that citric acid, acetylsalicylic acid and sugar doesn't interfere in ascorbic acid determination if it is in the same concentration with the vitamin C or lower. The ascorbic acid concentration in fresh fruits determined with the titrimetric method described is in concordance with that showed in literature. [17]

Conclusions

As a result of this work, the titrimetric method was found to be advantageous comparatively to other methods reported in the literature: it is sensitive, economic, practical and less time-consuming.

The results obtained by the proposed procedure show that the method can be used for determination of Vitamin C in vegetable samples.

The method has been used for ascorbic acid determination on different type of fruits: green fruits, leaves fruit trees and fruits and also it have been used to show the distribution of this vitamin in different stages of fruits growing.

In this work a simple method for the ascorbic acid (Vitamin C) determination in some fruit type: apple, apricot and sour cherry utilizing a titrimetric method with potassium bromide were described.

The tails, leaves, flowers and fruits of apple, apricot and sour cherry were investigated. One can see that plants synthesized ascorbic acid in leaves to apricot and apple, respectively tails to sour cherry and the fruits absorb this vitamin.

REFERENCES

1. Tomas Perez-Riuz, Carmen Martinez-Lozano, Virginia Tomas, Jose Fenol, (2001), *Analyst*, 126, 1436
2. Mannino, S., Cosio, M. S., (1997), *Analyst*, 122, 1153
3. Murray K R., Granner DK., Mayes PA. et al, (1996), **Harper's Biochemistry**, 24th Edition, Lange Medical Book
4. Jing Yang, Katsuaki Kato, Kenji Noguchi et al, (2003), *Life Sciences*, **73**, 3245-56
5. http://www.produceoasis.com/Items_folder/Fruits/Apple.html
6. http://www.bouquetoffruits.com/fruit-facts/index.html
7. http://www.e-referate.ro/referate/biologie/0bo54.html
8. Bates C. J., (1999), **Vitamins: Fat and Water Soluble Analysis**, *Enciclopedia of Analytical Chemistry*, 1
9. Ruedas Rama, M. J., Ruiz Medina, A., Molina Diaz, A., (2004), *Microchemical Journal*, **78**, 157-162
10. Anthony B Shephard, Steven C Nichols, Alan Braitawaite, (1999), *Talanta*, **48**, 585-93
11. Anthony B Shephard, Steven C Nichols, Alan Braitawaite, (1999), *Talanta*, **48**, 595-06
12. Anthony B Shephard, Steven C Nichols, Alan Braitawaite, (1999), *Talanta*, **48**, 607-22
13. Aberasturi, F., Jimenez, A I, Jimenez, F., Arias, J. J., (2001), *Journal of Chemical Education*, **78,** (6), 793-95

14. Skoog, D. A., West, D. M., Holler, F. J., (1998), **Fundamentals of Analytical Chemistry**-Seventh Edition, 845

15. Dobrinas, S., Matei, N., Birghila, S., Popescu, V., Soceanu, A., (2004), *Environmental Engineering and Management Journal*, **3** (4), 689

16. Matei, N., Birghila, S, (2001), *Ovidius University Annals of Chemistry*, **12** (1), 47-9

17. Damaschin, F., Rudencu, T., (2001) **Elemente Minerale si vitamine,** Editura Medicala, Bucuresti

18. Matei, N., Magearu, V., (2004), *Analele Universitatii Bucuresti*, **XIII**, I-II, p. 65-8

19. Matei, N., Birghila, S., Dobrinas, S., Magearu, V., (2004), *Revista de Medicina si Farmacie*, **50**, 43-5

20. Matei, N., Birghila, S., Dobrinas S. et al, (2004), *Acta Chimica Slovenica*, **51**, 169-75

21. Birghila, S., Dobrinas, S., Matei, N., Magearu, V., Popescu, V., Soceanu, A., (2004), *Revista de Chimie*, **55**, (9), 683-5

22. Matei N, Magearu, V., Birghila, S., Dobrinas, S., (2004), *Rev. Chim.*, **55**, (5), 294

ACCUMULATION OF MANGANESE AND IRON IN CITRUS FRUITS

Alina Soceanu[*], V. Magearu[**], Viorica Popescu[*], Nicoleta Matei[*]

The aim of this work is to determine the metal contents from different components of a fruit (pulp, film and peel). The determinations of metal's traces are very important because they are involved in biological cycles and indicate high toxicity. Analyses were performed using the flame atomic absorption spectrometry (Shimadzu AA 6200), after the chemical mineralization of the sample with a Digesdahl device. The obtained values are in good agreement with the literature data.

Introduction

Plants can accumulate trace elements, especially heavy metals, in or on their tissues due to their great ability to adapt to variable chemical effects of the environment, thus plants are intermediate reservoirs for trace elements originated from the lithosphere, hydrosphere or the atmosphere.

In general heavy metals produce their toxicity by forming complexes or "ligands" with organic compounds. These modified biological molecules lose their ability to function properly, and result in malfunction or death of the affected cells. The most common groups involved in ligand's formation are oxygen, sulfur, and nitrogen. When metals bind to these groups they may inactive important enzyme systems, or affect protein structure [1].

Manganese (Mn) is a plant micronutrient that, depending on its content in the soil and on factors that control its availability such as pH, organic matter and microbial activity, can achieve levels which are toxic for the plants [2]. The critical level of foliar Mn concentration in plants to produce toxicity symptoms varies among species and even cultivars [3, 4].

Iron is closely concerned with chlorophyll formation but is not a constituent of it. Its role appears in connection to be that of a catalyst.

A point of great importance in connection with iron is its relative immobility in plant tissues. Its mobility seems to be affected by several factors, such as the presence of

[*] Department of Chemistry, University "Ovidius" of Constantza, Constantza, asoceanu@univ-ovidius.ro
[**] Department of Analytical Chemistry, Bucharest University, Bucharest

Analele Universităţii din Bucureşti – Chimie, Anul XIV (serie nouă), vol. I-II, pg. 173-177

manganese, potassium deficiency and high light intensity. There is evidence that the amount of chlorophyll is related to "active" (readily soluble) iron in plants. It will be seen that so-called iron deficiency in the plant may in fact usually mean iron immobility. Lack of mobility may also account for the fact that iron deficiency is first shown in the younger tissues.

In the last years a large number of analytical techniques for metal determination in plants have been reported, such as ICP-AES [5], X-ray fluorescence spectrometry [6,7], flame atomic absorption spectrometry [8], atomic absorption spectroscopy (GFAAS) [9], flow injection spectrometry [10] and ICP-MS [11].

Experimental

Reagents and solutions

All metal stock solutions (1000 mg/L) were prepared by dissolving the appropriate amounts of the spectral pure metals in dilute acids (1:1) and then diluting them with deionized water. The working solutions were prepared by diluting the stock solutions to appropriate volumes. The nitric acid 65% and hydrogen peroxide 25% solutions used were of ultra pure grade, purchased from Merck. All reagents were of analytical-reagent grade and all solutions were prepared using deionized water.

Sample preparation

The pulp, the film and the peel of oranges, lemons and grapefruits were investigated. The samples were washed with deionized water, dried and homogenized. 0.5-0.9 grams of each dry sample was submitted digestion with 8 mL HNO_3 and 10 mL H_2O_2 at 170^{o}C in a Digesdhal device provided by Hach Company [12]. After the complete digestion the samples solution were filtered, made up to 50 mL in volumetric flask with deionized water.

Sample analysis

Metals were determined by FAAS in air/acetylene flame using an aqueous standard calibration curve. Analyses were made in triplicate and the mean values are reported.

A Shimadzu atomic absorption spectrometer (Model AA 6200) equipped with air-acetylene flame was used for the determination of metals (Mn and Fe) in citrus fruits. Acetylene of 99.99% purity at a flow rate of 1.8-2.0 L/min was utilized as a fuel gas and also as a carrier gas for introducing aerosols. Metals were measured using monoelement hollow cathode lamps.

Results and discussion

The metals content is reglementate by international law.

In table1 are presented the maximum admissible concentrations in fruits according to Food Surveillance Information Sheet No.131 [13].

Table 1. The maximum admissible concentrations in fruits

No	Metal	The maximum admissible concentrations (mg/kg)
1	Mn	2
2	Fe	2.7

The characteristics of metal calibration are presented in table 2.

Table 2. Characteristics of metal calibration curves

No	Metal	λ, nm	Concentration range (ppm)	Correlation coefficient
1	Mn	279.5	0.008-1.600	0.9984
2	Fe	248.3	0.020-4.000	0.9976

The content of metals in citrus fresh fruits was determined by FAAS technique.

In figure 1 are presented the average values of Mn concentrations from citrus fruits.

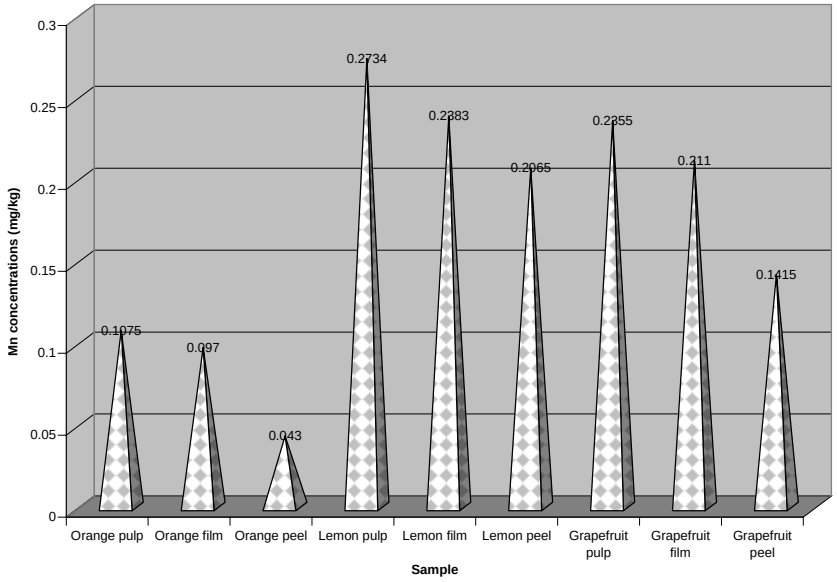

Fig. 1: *Mn concentrations in citrus fruits (mg/kg)*

We can observe that the highest value for Mn concentrations is that of lemon's pulp (0.2734 mg/kg) and the lowest is that of orange's peel (0.043 mg/kg). But it can be noticed that all values of Mn concentrations are under the maximum admissible value (2 mg/kg).
In figure 2 are presented the average values of Fe concentrations from citrus fruits.

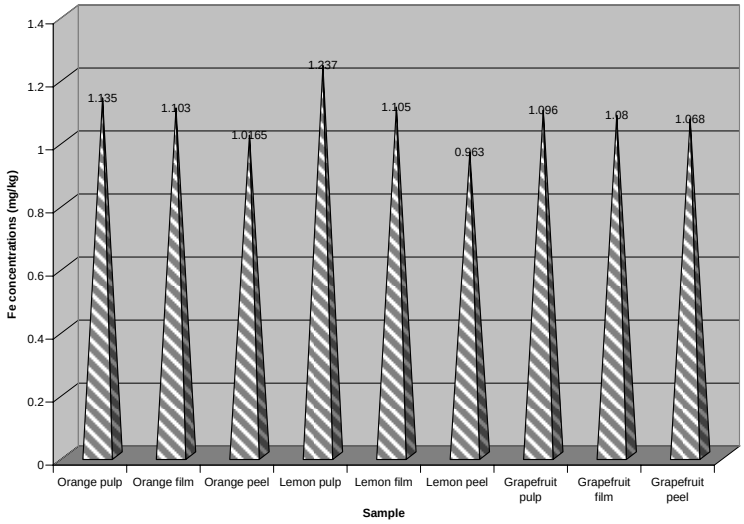

Fig. 2: *Fe concentrations in citrus fruits (mg/kg)*

All values for Fe concentrations are comparable and under the maximum admissible value (2.7 mg/kg).

Konstantin Lubenov [14].while analyzing Mn concentrations in some medicinal plants and their infusions by a kinetic spectrophotometric method find that most of the manganese in the infusions exists in a bound state, and only very low concentrations are in a free state.

Conclusions

1. This paper presents original studies concerning metals accumulation in citrus fresh fruits by FAAS.
2. It can be noticed that the highest value for Mn concentrations is that of lemon's pulp (0.2734 mg/kg) and the lowest is that of orange's peel (0.043 mg/kg).
3. All values of Fe concentrations are comparable and under the maximum admissible value.
4. The obtained concentrations of these elements in citrus fruits are situated within the limits imposed by the last regulations of the specialized international commissions such as EC's Scientific Committee for Food.

REFERENCES

1. Abdulla M., Chmielnicka J., *New aspects on the distribution and metabolism of essential trace elements after dietary exposure to toxic metals*, 25, (1990)

2. Foy C D, Chaney R L and White M C, The physiology of metal toxicity in plants, *Ann. Rev. Plant Physiol*. 29, 511-566, (1978)

3. Foy C D, Physiological effects of hydrogen, aluminium, and manganese toxicities in acid soils, *American Society of Agronomy*, Madison, 57-97, (1984)

4. Marschner H, **Mineral nutrition of higher plants**, Academic Press, London, UK, 889, (1995)

5. Perronnet K., Schwartz C., Morel J., *Plant and soil*, 294, 19,(2003)

6. Sarret G., Manceau A., Spadini L., Roux J. C., Hazemann J. L., Soldo Y., Eybert-Berard L., Menthonnex J.*J., Environ.Sci. Technol*., 32, 1648, (1998)

7. Belakova M., Havranek E., Bumbalova A., *Journal of Radioanal. and Nucl. Chem*., 201, (1998)

8. Doyle M.O., Otte M.L, *Environ. Pollut*., 96, (1997)

9. Basile A., Cogoni E., Bassi P., Fabrizi E., Sorbo S., Giordano S., Cobianchi C., *Annals of Botany*, 87, p. 537, (2001)

10. Silva F.V., Nogueira A.R.A., Souza G.B., Zagatto E.A.G., *Anal. Chim. Acta*, 370,, p.39, (1998)

11. Yi-Ching Li, Shiuh-Jen Jiang, Shu-Feng Chen, *Analytica Chimica Acta* 372, 365-372, (1998)

12. Chirila E., Carazeanu I., Bavaru A., Belc M., Proceedings of International Conference „Bramat 03", Brasov, Romania, IV, p.354, (2003)

13. Ministry of Agriculture, Fisheries and Food, Total diet study- aluminium, arsenic, cadmium, chromium, copper, lead, mercury, nickel, selenium, tin and zinc, *Food Surveillance Information Sheet*, 131, (1999)

14. Konstantin Lubenov , Determination of manganese in some medicinal plants and their infusions by a kinetic spectrophotometric method, *Chemical Speciation and Bioavailability*, 13, (2001)

ELECTROCHEMICAL DNA BASED BIOSENSOR FOR THE DETECTION OF GENOTOXIC COMPOUNDS IN FISH BILE SAMPLES

A.M. Tencaliec•, G. Bagni, M. Mascini**, V. Magearu***

abstract: A disposable electrochemical DNA based biosensor for the detection of genotoxic compounds in fish bile samples as marker of PAHs (polycyclic aromatic hydrocarbons) exposured at contaminated sites has been reported. The DNA biosensor is assembled by immobilising double stranded *Calf Thymus* DNA onto the surface of a disposable carbon screen-printed electrode. The oxidation signal of the guanine base, obtained by a square wave voltammetric scan, is used as analytical signal to detect the DNA damage; the presence of low molecular weight compounds with affinity for nucleic acids is measured by their effect on the guanine oxidation peak. Preliminary analysis of some PAH metabolites standard solutions were performed, in order to establish their behaviour with DNA based biosensor. Also, in order to highlight the differences between the not exposed bile and the injected bile, a deconjugation (or hydrolisis) process of the bile has been performed.The applicability of such a biosensor for analysing bile samples of fish from sites with high ecological risk was evaluated.

keywords: Electrochemical DNA biosensor, Genotoxic compounds, Screen-printed electrode

Introduction

Polycyclic Aromatic Hydrocarbons (PAHs) constitute a major environmental threat due to their carcinogenic properties. Increased prevalences of liver lesions and tumors have been observed in several fish populations in European and North American waters, and were linked to PAH pollution [1-4]. In order to quantitate PAH uptake by fish, biotransformation products (metabolites) can be determined in the bile fluid [5-9]. The Oslo & Paris Comission (OSPARCOM) has recently expressed its view that the determination of PAH metabolites in fish bile should be included in the new Joint Assessment and Monitoring Programme (JAMP) [10].

Analysis of PAH accumulation levels in fish tissue is usually not feasible due to rapid transformation (metabolism) into more polar and more easily excretable forms. The occurrence of biotransformation does, not, however, imply that PAHs are relatively

* University of Bucharest, Faculty of Chemistry, Department of Analytical Chemistry, Blvd.Regina Elisabeta 4-12, 703461, Bucharest, Romania
** Universita degli studi di Firenze, Dipartimento di Chimica, Via della Lastrucia 3, 50019 Sesto Fiorentino, Firenze, Italy

Analele Universităţii din Bucureşti – Chimie, Anul XIV (serie nouă), vol. I-II, pg. 179-186

harmless to metabolizing species. On contrary during metabolism some reactive intermediates can be formed that can bind to proteins and DNA [11,12].

Many studies have demonstrated that the presence of PAH metabolites in bile is well correlated with level of exposure [13-16], therefore bile PAHs metabolites can be determined as a biomarker of PAH exposure.

In recent years, the detection of DNA damage has been proposed as a useful tool for assessing biological effects of environmental pollutants. Consequently, a variety of DNA based assays are presently in use [17,18]. Nevertheless, the impact of PAH exposure at the level of individual genes and the subsequent utilization of these effects for biosensor development requires further attention.

The interactions between DNA and environmental pollutants can cause chemical or conformational modifications of nucleic acids and thus variation of the electrochemical properties of DNA. The presence of these compounds is measured by their effect on the guanine base: the changes in oxidation of the guanine peak, obtained by a square wave voltametric scan, is used as analytical signal [19].

In this paper, a rapid and low cost device, based on electrochemical DNA biosensor, is proposed as a screening tool for the detection of PAH exposure at contaminated sites. PAH exposure in marine organisms is often assessed by measuring the concentration of PAHs in their tissues. However fish caught at highly polluted sites often showed only trace levels of PAHs in the tissue, due to their ability to metabolise these compounds. Laboratory studies have demonstrated the presence of PAH metabolites in bile is well correlated with level of exposure [20 -23], as the gallbladder bile is major excretion route for PAH in fish. After biotransformation, PAH metabolites are excreted into the bile and concentrated. Thus, the bile can be used as an indicator of PAH exposure.

The developed DNA based biosensor is used as a rapid (8 minutes for each test) screening tool for the evaluation of an environmental sample.

Experimental

Material and methods

a. Apparatus and reagents

Electrochemical measurements were performed with a Palm Sens (Palm Instrument BV, Hoten Netherlands) which is controlled by a Pocket PC (fig. 1) and screen printed electrodes (SPE).

Fig. 1 *Palm Sens connected with Pocket PC*

The Palm Sens Instrument is used for sensors or cells with two or three electrodes and the dynamic range allows applications as micro as well as macroelectrodes.

The Pocket PC software provides easy control of Palm Sens.

The electrochemical cells produced at the University of Florence is presented in fig 2.

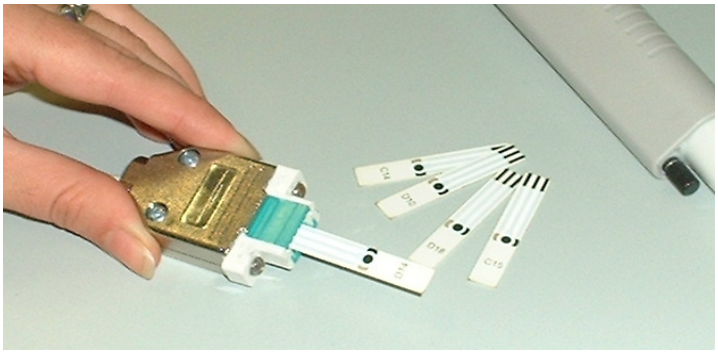

Fig. 2. *Electrochemical screen printed cell*

These planar electrochemical cells can be used as "drop and sensors" and only 10 μL of sample solution is required to perform the measurements. The cell consists of a circular graphite working electrode (diameter of 3 mm), a pseudo reference electrode and a graphite counter electrode (fig. 3). The procedure and the reagents to make screen printed electrodes were reported in literature [24]. Each electrode is disposable.

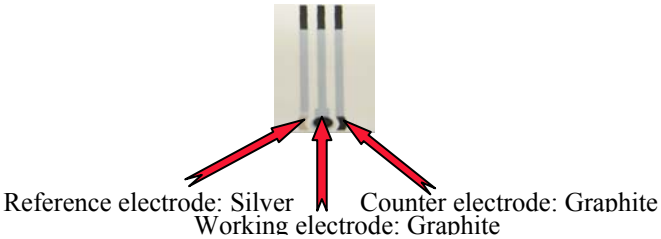

Fig. 3. *Screen printed electrode*

b. Samples preparation

In order to minimize the matrix effect of bile on the electrochemical measurements, different dilutions of fish bile samples have been investigated (1:250, 1:1000, 1:3000, 1:5000, 1:10000). In this study, it was used the 1:5000 dilution being considered the best one. Crude bile sample (10μL) was first diluted in acetate buffer solution (0.25M, pH 4.74) containing 20% ethanol for a final dilution factor of 1:250. The second dilution step involved in the use of acetate buffer solution containing 1% ethanol for final dilution factor 1:5000. Crude bile samples were stored at +20˚C. Glass vials were used for the preparation of all solutions.

c. DNA biosensor

The electrode surface was pretreated by applying a potential of + 1.6 V for 2 min. and a potential of 1.8 V for 1 min.

The biosensor was assembled by immobilizing double stranded calf thymus DNA at fixed potential (+ 0.5 V vs. Ag screen printed pseudo-reference electrode, for 300 s) onto the screen printed electrode surface. During the immobilization step, the strip was immersed in acetate buffer solution containing 50 ppm of double stranded calf thymus DNA. Then a washing step was performed by immersion of the biosensor in a clean acetate buffer solution for 30 s, at open circuit condition. The interaction step was performed just by placing 10 μL of the sample on the electrode surface of the DNA biosensor. After 2 min the biosensor was washed, immersed in acetate buffer and a square wave voltammetric scan was carried out to evaluate the oxidation of guanine peak on the electrode surface. The area of the guanine peak (around + 1 V vs. Ag screen printed pseudo-reference electrode) was measured. Potentially toxic compounds present in water were evaluated by changes of the electrochemical signal of guanine. We estimated the DNA modification with the value of the percentage of response decrease (S%) which is the ratio of the guanine peak area after the interaction with the analyte (GPAs), and the guanine peak area after the interaction with buffer solution (GPAb): $S\% = [100 - (GPAs/GPAb)] \times 100$.

The results of the test for one sample can be obtained within 8 min.

The supporting electrolyte for the voltammetric experiments and for any step in the biosensor set up was acetate buffer 0.25M pH 4.74, KCl 10 mM.

Square wave voltammetric parameters were: frequency = 200 Hz, step potential = 15 mV, amplitude = 40 mV, potential range 0.2 – 1.2 V versus Ag – pseudo-reference electrode.

Results and discussion

a. PAH metabolites response in standard solutions

The behaviour of some hydroxy-PAHs and dihydroxi-PAHs standard solutions was investigated with the DNA biosensor. A stock solution of each compound was previously prepared in ethanol or acetone.

Preliminary analysis of some PAH metabolites standard solutions were performed, in order to establish their behaviour with DNA-based biosensor.

In the fig. 5 the comparison between one metabolite for each PAH class is reported. S(%) values decreased increasing the standard concentration and increasing the number of the condensed aromatic rings. An exception is chrysene which, even if has 4 rings is less stronger than phenantrene (3 rings): this behaviour could be explained with different positions of fused rings that permits a less or strong interaction with DNA.

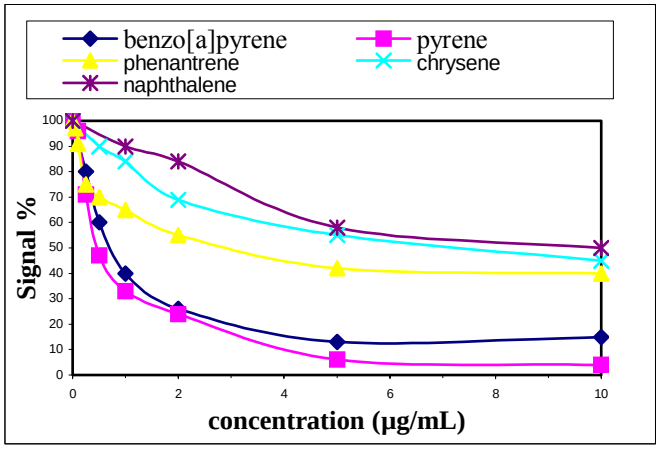

Fig. 4. *Comparison of the DNA biosensor response for one metabolite standard solutions for each PAH class.*

b. Analysis of fish bile samples with single PAH intraperitoneal injection dose before and after a deconjugation process.

A simulation experiment of acute exposure to PAH was performed in fish. A single PAH compound was injected intra peritoneally in Atlantic cod (*Gadus morhua*) in different doses depending to the ring number of the compound and the fish weight. The fish were sacrified five days after the exposure and the bile was sampled for the analysis.

The bile of fish exposed with single PAHs did not show very strong genotoxic effects on the DNA biosensor. In order to highlight the differences between the not exposed bile and the injected bile, a deconjugation (or hydrolisis) process of the bile has been performed.

It seems that the not strong genotoxic effect could be due to the metabolic pathways of the PAHs in fish. In the bile after the fish metabolism it didn't find that PAH or the hydroxy-PAHs and dihydroxydihydro-PAHs in a high percentage, but the PAHs conjugated with glucoronic acid and sulphatase that are not toxic and so they don't interact DNA.

Therefore, the next step of the study was the determination of the influence of deconjugation process of fish bile samples on the signal of guanine. To obtain this, the deconjugation process was performed and all the parameters were optimised. Different volumes of crude bile sample were mixed with different volumes of β-sulphatase enzyme (from *helix pomatia*, Sigma) or glucoronidase enzyme (from *helix pomatia*, Sigma) in a solution of 0.25M acetate buffer (pH 4.74) with 10mM KCl. The mixture was kept for 2 or 4 hours at 40°C. Then samples were centrifugated for 5 minutes at 12.000 r.p.m. and the supernatant was used to prepare final concentration 1:5000 with 0.25M acetate buffer (pH

4.7) with 10mM KCl, containing 1% of ethanol. Supernatants were analysed during the same day.

The results obtained with electrochemical DNA biosensor analysing fish bile samples with a single PAH injection dose using the deconjugation process are presented in the table 1 and in the fig. 5. Samples were diluted 1/5000 with acetic buffer 0.25M (pH 4.74) containing 1% EtOH. A normalisation of the signal related to the no exposure bile sample was performed: S*n* = (S*i* x 100)/S *no exposure*, where S*i* is the signal of different samples.

Table 1. The results for fish bile samples

Type of bile	Before deconjugation		After deconjugation with sulphatase	
	Signal %	sd	Signal %	sd
No exposure	100	6	100	5
Codliver oil	99	8	100	2
Naphtalene	88	5	93	4
Phenantrene	93	3	73	9
Fluorene	97	8	98	4
Dibenzothiophene	81	5	100	3
Fluoranthene	81	9	91	1
Chrysene	72	2	90	2
Pyrene	86	4	90	4
Benzo(a)pyrene	87	8	78	7

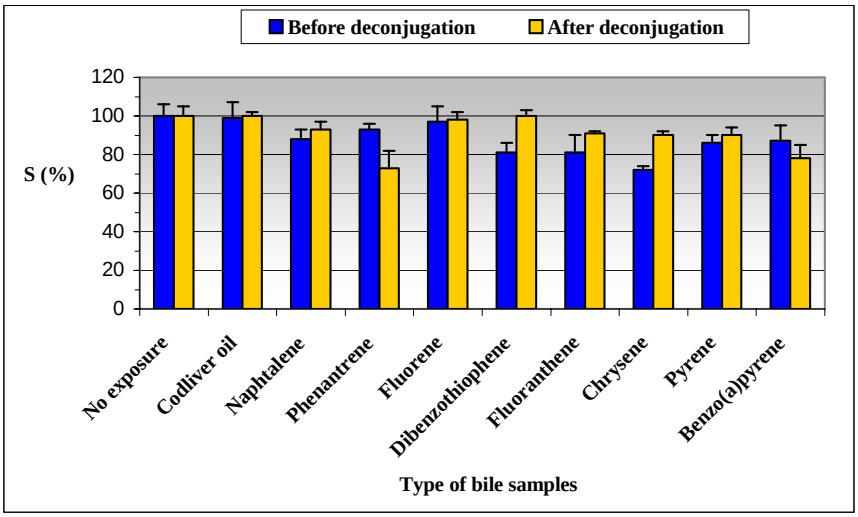

Fig. 5. *Comparison between before and after deconjugation process using normalisation method*

The simulation experiments of acute exposure showed that PAHs genotoxic effects were statistically different. This different carcinogenic power could be due to the ring number of compound, the molecular conformation and the presence of heteroatom. They were divided into two groups depending of the S% level. The compounds of the first group (naphtalene, phenantrene and fluorene) produced S% levels around 93%. The second group includes fluoranthene, chrysene, pyrene and benzo(a)pyrene and showed higher genotoxic effects

with S% levels around 82%. The dibenzotiophene effect cannot diffrence to the control sample; the presence of heteroatom could not facilitate the interaction with dsDNA.

Conclusions

In conclusion it can be seen that electrochemical DNA based biosensor permits the measurements of the overall PAH metabolites content of a sample. Moreover DNA biosensor give the global content of pollution and can be used as markers of recent exposure at contminated sites.

Nevertheless the DNA biosensor could be a very good test since can give rapid and easy informations to evaluate the presence of small compounds with the affinity for nucleic acids.

Electrochemical DNA based biosensors offer several advantages like an easy immobilization of the DNA layer, fast measurement, portable instrumentation suitable for measurements in situ, in field screening analysis of toxic compounds and cost effective, moreover the disposable single use biosensor avoids contamination among samples and allows constant sensitivity and reproducibility.

REFERENCES

1. Malins D.C., McCain B.B., Landhal J.T., Myers M.S., Krahn M.M., Brown D.W., Chan S. L., Roubal W.T., (1988) *Aquat. Toxicol*. **11**, 43-67.
2. Myers M.S., Landhal J.T., Krahn M.M., McCain B.B. (1991*) Environ Health Perspect*. **90**, 7-16.
3. Vethaak A.D., Jol J.G., Meijboom A., Eggens M.L., Rheinallt T., Wester P.W., Zande T., Bergman A., Dankers N., Ariese F., Baan R.A., Everts J.M., Opperhuizen A., Marquenie J.M. (1996*) Environ. Health Perspect.* **104**, 1218-1229.
4. Vethaak A.D., Wester P.W. (1996) *Diseases of Aquatic Organisms*, **26**, 99-116.
5. Krahn M.M., Myers M.S., Burrows D.G., Malins D.C. (1984) *Xenobiotica,* **14**, 633-646.
6. Johnston E.P. Baumann P.C. (1989) *Hydrobiologia*, **188/189**, 561-566.
7. Ariese F., Kok S.J., Verkaik M., Hoornweg G.Ph., Gooijer C., Velthorst N.H., Hofstraat J.W. (1993a) *Anal. Chem*., **65**, 1100-1106.
8. Van der Oost R., Van Schooten F.J., Ariese F., Heida H., Satumalay K., Vermeulen N.P.E. (1994) *Environ. Toxicol. Chem*., **13**, 859-870.
9. Vethaak A.D., Jol J.G. (1996), *Diseases of Aquatic Organims*, **26**, 81-97.
10. OSPAR/ICES, (1995) Report of the Workshop on Biological Effects Monitoring Techniques (Aberdeen, Oct 2-6 1995).
11. Conney A.H. (1982), *Cancer Res*., **42**, 4875-4880.
12. Cavalieri E.L., Rogan E.G., (1992) *Pharmac. Ther*., **55**, 183-199.
13. Aas E., Baussant T., Liewenborg B., Andersen O.K., (2000) *Aquatic Toxicology*, **51**, 241-258.
14. Aas E., Beyer J., Johnsson G., Reichert W.L. Andersen O.K., (2001) *Marine Environmental Research*, **52**, 213-229.

15. Myers M.S., Johnson L.L., Olson O.., Stehr C.M., Horness B.H., Collier T.K., McCain B.B., (1998) *Marine Pollution Bulletin,* **37**, 92-113.

16. Regoli F., Pellegrini D., Winston G.W., Gorbi S., Giuliani S., Virno-Lamberti, Bompadre S., (2002) *Marine Pollution Bulletin,* **44**, 912-922.

17. Gupta R.C., Reddy M.V., Randerata K., (1982), *Carcinogenesis,* **3**, 1081-1092.

18. Reichert W.L., Stein J.L., French B., Goodwin P., Varanasi U., (1992), *Carcinogenesis,* **13**, 1475-1479.

19. Lucarelli F., Authier L., Bagni G., Baussant T., Aas E., Marrazza G., Mascini M., (2003) *Anal. Lett*., **36**, 1887-1901.

20. Escartin E., Porte C., (1999) *Marine Pollution Bulletin*, **38**, 1200-1206.

21. Beyer J., Aas E., Borgenvik H.K., Ravn P., (1998) *Marine Environmental Research*, **46**, 233-236.

22. Aas E., Beyer J., Goksoyr A., (1998), *Marine Environmental Research*, **46**, 225-228.

23. Lin E.L.C., Cormier S.M., Torsella J.A., (1996) *Ecotoxicology and Environmental Safety*, **35**, 16-23.

24. Cagnini, I. Palchetti,I. Lionti, M.Mascini, A.P.F. Turner, (1995) *Sens. Actuators*, **B 24-25,** 85-95.

SULPHOSALICILIC ACID LOADED WOOL NEW CHELATING SORBENT FOR IRON (III)

Luminița Vlădescu*, Mihaela Costache and Irinel Adriana Badea

abstract: A new chelating material has been prepared based on bleached wool loaded with sulphosalicilic acid. The sorption capacity of the bleached wool for the organic reagent and the stability of the new material in acidic solutions have been established. The sorption capacity of the new material for iron (III) and the conditions for removal of them from the material have been established. The new material has been tested for the separation and concentration of iron (III) found at traces level in synthetic solutions and natural waters.

Introduction

Determination of trace metal ions by inductively coupled plasma-atomic emission spectrometry (ICP-AES) and inductively coupled plasma – mass spectrometry (ICP-MS) have been selected as techniques of choice. However, pre-concentration or selective separations of the analyte before its determination are frequently required in order to avoid interferences caused by the matrix. The selective and quantitative retention of metal ions has been investigated on a great number of materials. The most extensively studied materials are ion exchange resins both conventional and chelating, inorganic ion exchangers, solvent impregnated resins, controlled pore glass and foamed plastics [1÷3]. The potential of anionic chelating agents loaded on anion exchange resins and important aspects of organic reagents retention on non-ionic and anionic conventional exchangers have been discussed in literature [4,5]. New materials having the wool fibre as support have been reported in the literature [6]. The wool is almost solely made of keratin proteins and contain up to 22 different amino acids. The cationic groups of the lateral chains are placed on the arginine, lysine and histidine rests and the anionic ones on the glutamic acid and asparagine rests [7]. A new material based on wool loaded with Mordant Yellow 10 has been studied and reported in a previous paper [8]. Sulphosalicilic acid (further noted by SSA) is an organic compound, having similar structure to Mordant Yellow 10, and it forms with iron (III) stables complexes having the stoechiometry Fe(III) : SSA = 1 : 1, 1: 2 and 1 : 3 at pH : 2.50, 4.50 and 8.00 respectively [9]. As proteic support the bleached wool having the functional groups activated by chemical treatment has been used. Thus the optima

*Department of Analytical Chemistry , Faculty of Chemistry, University of Bucharest, 2-14 Bv. Regina Elisabeta, 030018 Bucharest, Romania

Analele Universității din Bucureşti – Chimie, Anul XIV (serie nouă), vol. I-II, pg. 187-192

working conditions for the preparation of a new chelating material based on natural wool loaded with Sulphosalicilic Acid are presented in this paper. The both SSA – loaded wool and the bleached wool activated in acidic conditions have been used for concentration and recuperation of iron (III) from diluted solutions.

Experimental

Reagents

The wool was obtained from S. C. LACECA S.A. (Romania) and was a Romanian type called Merinos of Bărăgan. Water was double distilled and all chemical reagents were of analytical reagent grade. Hydrochloric acid fuming 37%, hydrogen peroxide 30% (Perhydrol®), sodium hydroxide pellets, iron ICP standard (CertiPUR®) and sulphosalicilic acid were purchased from Merck. Diluted HCl solutions having the concentration of 0.100, 1.000, 4.000 and 6.000 $mol.L^{-1}$ have been prepared using HCl 37%. Stock solutions of sulphosalicilic acid 0.020 $mol.L^{-1}$ has been prepared. Aqueous stock solutions of iron (III) 0.020 $mol.L^{-1}$ (in HNO_3 0,0144 $mol.L^{-1}$) has been obtained by diluting Merck atomic absorption standard metal ion solutions with distilled water. CHEMIX DBS used as detergent has been obtained from CHIMOPAR (Romania). Chloroform has been purchased from Aldrich.

Apparatus

A spectroflame Spectro Analytical Instruments Model P inductively coupled plasma atomic emission spectrometer has been used. The spectrometric studies were performed on a Jasco V 530 spectrometer coupled with a PC running a Jasco software. An electronic analytical balance Kern 770 was used for weigh wool. A microwave oven MILESTONE MLS - 1200 MEGA has been used for the digestion of bleached wool samples activated in acid medium and loaded with iron (III).

Procedure

Bleaching of wool. Purification and activation

The wool has been bleached in the laboratory using a procedure as follow: 300 g of raw wool has been washed several times using a solution containing 6 g of detergent in 1000 mL water. Samples of washed wool weighing each 20 g have been immersed into chloroform for 75 minutes and then dried at room temperature. Thus grease has been removed from the wool. Samples of degreased wool weighing each 30 g have been treated with hydrogen peroxide 30% at pH 8.00 and 80°C during 60 minutes. After that the bleached wool obtained has been washed with distilled water until the pH of waste water was equal to the pH of distilled water. The bleached wool weighing each 0.5 g were mixed with 35 mL of HCl 1 $mol.L^{-1}$ and 15 mL distilled water and shaken with a mechanical shaker for about 2 h. After being stirred the wool has been decanted and washed with distilled water until the pH of waste water was equal to the pH of distilled water. The washed wool has been pressed with a glass rood and dried up in the same Erlenmeyer flask used for the mechanical stirring. Thus the bleached wool has been activated.

Preparation of sulphosalicilic acid-loaded wool

The bath method was used for retention of sulphosalicilic acid on the wool. A weighed amount (~ 0,5 g) of bleached wool activated by bath method using HCl solutions of different concentrations was treated with 50 mL of 0.02 mol.L^{-1} of SSA solution and shaken with a mechanical shaker for about 2 h. Then the loaded wool was filtered off in a fritted-glass funnel and washed with distilled water to remove the excess reagent. The supernatant solution and the rinsing water were collected in a 100 mL volumetric flask. The amount of SSA in supernatant solutions was determined by spectrometry (y = 0,000124 + 0,008752x, r = 0.9997). The SSA loaded on wool was determined by subtracting the quantity found in supernatant from the quantity used at the beginning of the shaking.

Acidity influence on the stability of the SSA-loaded wool

The bath method was used. An exactely weighed amount of SSA-loaded wool was treated with 50 mL of HCl solutions having different concentrations and shaken with a mechanical shaker for about 2 h. Then the loaded wool was filtered off in a fritted-glass funnel and washed with HCl solution of the same concentration as the solution used for the equilibration. The supernatant solution and the rinsing water were collected in a 100 mL volumetric flask. The amount of SSA in supernatant solutions was determined by spectrometry.

Sorption of metal ions on the SSA-loaded wool

Weighed amount of SSA-loaded wool was treated with 50 mL of iron (III) solutions having different concentrations and shaken with a mechanical shaker for about 2 h. Then the loaded wool was filtered off in a fritted-glass funnel and washed with small volumes of distilled water to remove the excess of metal ion. The supernatant solution and the rinsing water were collected in a 100 mL volumetric flask. The amount of iron (III) found in supernatant solutions has been determined by ICP – AES. The quantity of iron (III) sorption on SSA–wool was calculated by subtracting the quantity found in supernatant from the quantity used at the beginning of the shaking.

Results and discussion

Retention of sulphosalicilic acid in wool

As support for SSA-loaded wool the bleached wool has been used as this sort of wool loads a quantity of reagent greater than those fixed by the raw wool. After the activation stage ions from the fibre passed into solution, amine groups of wool became ammonium ions and are accessible to the organic reagent. The amount of SSA loaded on the bleached wool was determined by bath method. The results of sulphosalicilc acid retention in bleached wool are presented in Table 1. As it is shown the samples of bleached wool activated with HCl of 4 and 6 mol.L^{-1} load a quantity of SSA greater than bleached wool activated with 0.100 and 1,000 mol.L^{-1}.

Table 1. Retention of SSA in bleached wool shaken with HCl of various concentrations

No.	Quantity of wool (g)	HCl ($mol.L^{-1}$)	Quantity of SSA added (mg)	Quantity of in wool (mg)	SAA found in filtrate (mg)	Sorption Capacity (mmoli SSA /g wool)
1.	0.5502	0 (water)	230.0	15.4 ± 0.68	214.6 ± 1.32	0.028 ± 0.0030
2.	0.5598	0.10	230.0	40.3 ± 0.35	189.7 ± 1.68	0.072 ± 0.0050
3.	0.5498	1.00	230.0	53.3 ± 0.94	176.7 ± 1.59	0.097 ± 0.0020
4.	0.5465	4.00	230.0	95.6 ± 0.21	134.4 ± 1.09	0.175 ± 0.0001
5.	0.5524	6.00	230.0	99.4 ± 0.14	130.6 ± 0.29	0.280 ± 0.0003
6.	0.5396	6.00	230.0	149.9 ± 0.46	310.1 ± 0.83	0.652 ± 0.0002

Note : each result represents the mean from five determinations ± standard deviation

Stability of SSA - loaded wool in acid solutions

In order to investigate the stability of the SSA-loaded wool in presence of acidic solutions, different concentrations of aqueous HCl solutions were used. The results are present in Table 2. The results in Table 2 show a different stability of SSA–loaded wool in acidic solutions. The occurrence of SSA has been noticed in HCl solutions having a concentration greater than 0.400 $mol.L^{-1}$. It was observed that the organic reagent was quantitatively held by the wool in the presence of 0.120 $mol.L^{-1}$ acid solution. Some SSA was still retained on the wool even in 1.000 $mol.L^{-1}$ HCl solution due to the π- π interaction between the benzene ring of SSA and the structure of the wool fibre. The sorption of the organic reagent by its chelating groups has to be taken into consideration.

Table 2. Stability of the SSA-loaded wool in acidic solutions

No.	Quantity of wool (g)	Concentration of HCl ($mol.L^{-1}$)	Concentration of SSA in filtrate solution mmol/100 mL
1.	0,5025	0,001	0
2.	0.5012	0,010	0
3.	0.5004	0,100	0
4.	0,5010	0,120	0
5.	0.5017	0,400	0.0015 ± 0.00021
6.	0,5002	1,000	0.0420 ± 0.00006

Note: each result represents the mean of five determinations ± standard deviation

Sorption of metal ions on the SSA-loaded wool

Both bleached wool activated with HCl of 4 and 6 $mol.L^{-1}$ and the SSA–loaded wool have been used for the sorption of iron (III) from synthetic samples. The results regarding the capacity of two kinds of wool to fix the iron (III) are presented in Table 3.

Table 3. Capacity of bleached wool and SSA–wool to fix the iron (III)

No.	Quantity of wool (g)	Quantity of Fe^{3+} added (mg)	Quantity of Fe^{3+} found		Sorption Capacity mmol iron (III)/ g wool
			in filtrate (mg)	in wool (mg)	
1	*0.5415*	*27.9*	*26.7* ± 0.17	*1.2* ± 0.05	*0.039 (a)** ± 0.0016
2	0.0230	27.9	22.3 ± 0.35	5.6 ± 0.06	0.199 (b) ± 0.0007
3	0.5064	27.9	21.9 ± 0.41	6.0 ± 0.08	0.212 (b) ± 0.0002
4	0.5023	27.9	22.1 ± 0.24	5.8 ± 0.02	0.206 (b) ± 0.0009

Note : each result is the mean from five determinations ± standard deviation

*after digestion of wool samples in a microwave four and determination of iron (III) by ICP–AES

The results obtained show that both bleached wool activated with HCl and the SSA–loaded wool fix the iron (III) from diluted solution. The sorption capacity of two sorts of wool is different. The SSA–loaded wool has a greater sorption capacity than the bleached wool activated with HCl.

Removal of iron (III) from SSA - loaded wool using HCl solutions

In order to establish the conditions for removal of iron retained by the SSA-loaded wool, solutions of HCl of different concentrations were used. Results obtained by the bath method showed that 1 mol.L^{-1} HCl solution was efficient for iron recuperation without a substantial desorbtion of the sulphosalicilic acid from the wool.

Determination of iron from synthetics samples

The results obtained during the whole experiment ensure the use of the SSA-loaded wool for the separation and concentration of some iron traces from diluted solutions. The recoveries are between 99.48% and 100.87% and the RSD are below 2%. Using synthetic samples containing trace amounts of iron (III) the method has been validated [10] by regard to the accuracy and the precision. The accuracy and the precision (repeatability and intermediate precision) have been determined for sorption of iron (III) in SSA-loaded wool. The values obtained (expressed as % ± standard deviation) are: 99.05 ± 0.76 for accuracy, 98.82 ± 0.42 for repeatability and 99.63 ± 1.51 for day I and 98.58 ± 1.18 for day II.

Determination of iron from real samples

The new chelate forming material has been used for concentration and determination of iron (III) from real samples of running water. Samples of running water have been taken from North of Bucharest. The results obtained are summarised in Table 4. The quantity of iron (III) has been determined by the proposed procedure and by ICP-AES. It was noticed a good agreement between the results obtained. All the results are below the imposed value for iron (III) in running water [11]. Each value in Table 4 represents the mean of five determinations ± standard deviation.

Table 6 Determination of iron (III) in running water samples

Water	Quantity of iron (III) found		Quantity of iron (III) admitted [11] (ppm)
	proposed method (ppm)	ICP – AES[12] (ppm)	
Sample 1	0.182 ± 0.0012	0.1790 ± 0.0005	< 0.200
Sample 2	0.198 ± 0.0009	0.0195 ± 0.0014	< 0.200
Sample 3	0.141 ± 0.0017	0.0143 ± 0.0006	< 0.200

Conclusion

The blenched wool activated by bath method using 4 and 6 mol.L^{-1} of HCl solutions and loaded with sulphosalicilic acid has been studied as a new chelating material for separation and concentration of iron (III) found at trace level. The sulphosalicilic acid can be loaded on the wool fibre at the N protonated atoms by means of its sulphonic group. Its structural pattern of salicylic acid stays free and can reacts with iron (III). This SSA-wool has been

used for separation and concentration of trace amounts of iron (III) from synthetic samples. The recoveries were between 99.48% and 100.87% with the RSD below 2%. The new chelate-forming sorbent based on the sulphosalicilic acid-loaded wool may be used for the separation and concentration of the traces of iron (III) from different samples with goods accuracy and precision.

REFERENCES

1. Marinsky, J.A. (1966) *Ion Exchange*, vol. 1, Marcel Dekker, New York.
2. McGarvey, F.X. and Tamaki, D. (1991) *52nd Off. Proc. Int. Water Conf.* 228.
3. Kantipuly, C., Katragadda, S., Chow, A. and Gesser, H.D. (1990) *Talanta* **37**, 491.
4. Torre, A. and Marina, M.L. (1994) *Crit. Rev. Anal. Chem.* **24**, 327.
5. Vlădescu, L. and Moldovan, Z. (2000) *Roum. Chem. Quart. Rev.* **8**, 221.
6. Knott, J. (1985) *Proc. Int. Wool Text. Res. Conference I*, vol III, Tokyo.
7. Telegin, F. Yu., Vashurina, I. Yu., Shormanov, A. V., Ivanova, E. N., Kalinnikov, Yu. A. and Melnikov, B. N. (1993) *J. Phys. Chem*. **752**.
8. Vlădescu, L., Costache, M. and Badea, I. (2004) Acta Chromatog. **14**, 187.
9. Vareille L., (1955) *Bull. Soc. Chim. Franc*. 872.
10. *** ICH Topics Q2B, Validation of Analytical procesures: Methodology, Step. 4, (1995) CPMP/ICH/281.
11. ***Romanian STAS 1342-71.
12. Capotă, P. and Constantin, M. (1996) *Metallurgy and New Materials, vol III*, **57.**

EXPERIMENTAL METHODS FOR STUDY HIGH-PRESSURE PHASE BEHAVIOUR. PART I. STATIC METHODS.

Cristina Bogatu[*], Rodica Vîlcu[**], Anca Duță

abstract: The paper presents a review of the experimental methods used in the investigation of high-pressure phase equilibria. The main categories of methods and installations are described. For each case, the aspects concerning the type of experimental data, experimental conditions and experimental procedures are discussed.

Introduction

Information about high-pressure phase equilibrium is of importance for many separation processes, which are conducted at high-pressure especially supercritical fluid extraction. Applications of this technology cover the food, pharmaceuticals, chemical, coal and oil processing and production industry.

There are many experimental routs to obtain data about the phase behaviour of the fluid mixtures. Among these, the direct measurements remain an important source, though it is difficult and expensive to take accurate experimental data. But, it is also expensive for a company to use average data or to estimate data with a thermodynamic model if the literature does not offer (enough) experimental data. Thus, the understanding of the complex phenomena, which occur at high pressure in the critical region, is mainly conditioned by the quality of the experimental information, [1].

Classification of the experimental methods

In order to classify the experimental methods and installation it is necessary to specify the two criteria that must be taken into account. Thus:

A*) Depending on how the composition of the two coexisting phases is determined* the methods are divided in:

[*] Department of Chemistry, Faculty of Materials Science, Transylvania University of Brasov, 2200 Brasov, Romania

[**] Department of Physical Chemistry, Faculty of Chemistry, University of Bucharest, 4-12 Bd. Elisabeta, 030018, Bucharest, Romania

Analele Universității din Bucureşti – Chimie, Anul XIV (serie nouă), vol. I-II, pg. 193-203

- *analytical methods* (direct sampling methods) – involve the determination of the compositions of the coexisting phase by sampling each of them and then by analysing these samples inside (spectroscopy) or outside (refractometry, chromatography or pressure drop) of equilibrium cell, [1,2].
- *synthetic methods* (indirect methods) – no sampling is necessary. The overall composition of the mixture is known and the temperature or the pressure is adjusted until a homogeneous phase is obtained. The observation can be done visual or non-visual. Each experiment yields one point on the P-T-x phase envelope (where x represents the composition of the liquid phase). These methods are applied when the analytical path fail, i.e when the phase separation is difficult due to the similar densities of the two phases or in barotropic systems, where at certain conditions the densities of the two coexisting phase have the same value, [3].

B) Considering the working regime (criterion used in this paper) the experimental methods can be divided in:

- static methods – during the experiment, the phases does not leave the equilibrium cell;
- dynamic methods – continuous separation of the coexisting phases in a stationary regime, [3].

Based on the last criterion, this paper is a review of the static installations and techniques and gives a brief overview of different methods for the study of high-pressure phase behaviour.

Static methods

The static methods allow the obtaining of complete equilibrium data - P-T-x-y (**y** - the vapor composition) and the methods are called static analytical methods, or partial data P-T-x, when y is calculated – the case of the static synthetic (indirect) methods.

There are two reasons why it recommended calculating y:

- the density of the vapour phase is much lower than the density of the liquid phase, thus it is very difficult to extract samples from this phase without any perturbation of the equilibrium state;
- can be easily calculate by using with equations of state (EoS).

The composition of the liquid phase can be determined at atmospheric pressure, outside of the equlibrium cell (i.e. titration, refractometry) or directly inside of the cell (by spectroscopy), in the modern installations.

The main parts of a static installation are presented in Fig.1. Basically, the apparatus consist of a degassing system (2) – to eliminate the air dissolved in the pure compounds or mixtures, an equilibrium cell immersed in a liquid thermostated bath (7), a system for measuring the pressure (5).

In order to avoid the condensation, the pressure gauge and the tubings are placed in an air thermostated bath, at higher temperature than the temperature of the equilibrium cell.

The sample is introduced in the equilibrium cell (preliminary vacuumated) at fixed temperature and stirred until the equilibrium is reached. At this moment the pressure and composition are determined. The accuracy of the experimental data is limited by the measurement devices.

The equilibrium cell can be visual (with high pressure resistant windows e.g. saphire), allowing the visual observation of phase behaviour or nonvisual, usually built up from stainless steel.

Moreover if the volume of the cell is constant or can be modified, static installations are divided *in constant volume cell apparatus* (methods)-CVC methods or *variable volume cell apparatus* -VVC methods.

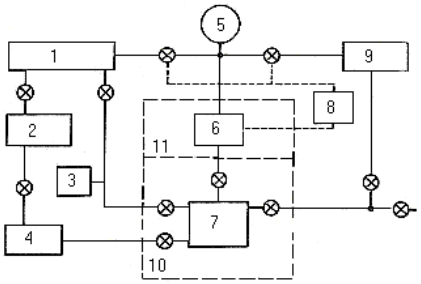

Fig 1. *Schematic representation of a static apparatus: (1, 3) –vacuum devices; (2) – degassing system; (4) - transfer chamber; (5) – pressure gauge; (6) –differential null for pressure; (7) –equilibrium cell; (8) – compressor; (9) – feed for inert gas; (10, 11) – thermostated baths.*

The general description of the static installation is valid for both synthetic and analytical measurements and some particular cases are presented in this paper.

There are two main aspects to take into account for the measurements with a static apparatus:

- the problem of degassing the sample
- the problem of taking sample from the coexisting phases and their accurate analysis.

A) ***Static installations with constant volume cell – CVC methods.***

The ***degassing problem*** is discussed especially for volatile compounds or mixture with significant volatility. Researches were developed and different solutions and apparatus were proposed:

a) In the apparatus of Van Ness and Abott [4] the degassing process is insured by the continuous flow of the liquid under vacuum condition. The authors consider 24 hours sufficient for the degassing procedure.

b) Using an installation based on the procedure of alternating freezing – melting cycles under vacuum conditions, Vilcu *at. all* [5] obtain VLE data for different pure compounds and mixtures. The measurements follow the general procedure of static installations: when

the equilibrium is reached, the pressure and temperature are measured with a mercury manometer (±20 Pa), respectively with Beckmann thermometers (±0.02 K). The composition of liquid phase is determined by refractometry, with previously calibration (±0.0002). If the total pressure [4, 5] is measured the method is also called *total pressure method.*

This procedure of freezing – melting cycles is a successful alternative for the degassing problem in the VLE static installations. Literature [5-10] presents many static types of equipment based on the degassing method previously described.

If the pressure of the sample is measured using the pressure of reference fluid, the method is called *differential pressure method.* The equipment consists of two equilibrium cells, one charged with sample, the other with reference fluid, with known vapor pressure. Some examples are the instalations presented by Morgan and Kobayashi [6], Giuliani, Polonara and Di Nicola [7,8], Stryjek [9] or Mokbel *et all*. [10].

The equipment of Morgan and Kobayashi [6] is presented in Fig. 2:

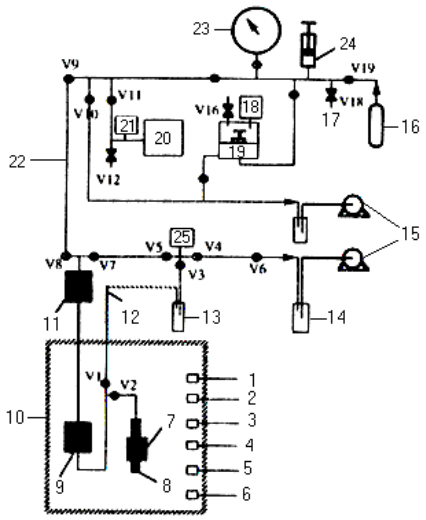

Fig. 2. *Schematic representation of the differential pressure apparatus [5] (1) – stirrer; (2, 3) – heating elements; (4) – platinum resistance thermometer; (5) –nitrogen purge; (6) –thermocouple for Over-Temperature Limit Control; (7) –magnetic slusher; (8) –equilibrium cell; (9,11) – null-type differential pressure indicator; (10) – thermostat; (12) –heated line; (13, 14) – cold traps; (15) – vacuum pumps; (16) – nitrogen supply; (17) – vent; (18, 21, 25) – thermovac vacuum gauge; (19) –air Dead Weight Gauge (1- 4136 kPa); (20) – Digital quartz Pressure Gauge (0-138 kPa); (22) - Pressure Supply and Measurements System; (23) –Heise Gauge (0-3446 kPa); (24) – Hand Pump; V1…V19 – valves.*

The equilibrium stainless steel cell (8), previously vacuumated is directly connected with the diaphragm of a differential pressure transducer and differential pressure indicators (9,11). The position of the metal diaphragm in the DPI, which separated the sample from the reference pressure, is measured when an equal reference pressure is applied on both side of the diaphragm. The pressure of the reference gas can be automatically controlled, [6]. Then, with the sample exerting its pressure on one side of the diaphragm and the reference

gas on the other side, the reference pressure is adjusted until the initial zero position of the diaphragm is reproduced. This pressure is measured with the air dead weight gauge (19). The apparatus allow measurements for pressure less than 1.3 MPa (±0.01KPa), temperatures less than 588 K (±0.02–0.09 K). The mostly used method for analysis of sample composition in the case of mixture is chromatography [11,12], but also gravimetry [5] and densimetry (*eg*. with a vibrating tube densitometer) [11, 12] are used.

The uncertainty in composition evaluation is situated in the range (± 0.002….± 0.008). The use of a chromagraph allows more accurate data and makes the analysis easier and more rapid than in the other cases.

It is also important to discuss the problem ***of sampling*** the coexisting phases because withdrawing a large sample volume from an autoclave causes a considerable pressure drop, which disturb the phase equilibrium significantly. This pressure drop can be avoided by:

- using variable volume cells or a buffer autoclave in combination with a syringe pump;
- blocking off a large sampling volume before the pressure reduction;
- withdrawing small quantityies of sample comparing with the cell volume using capillaries, special valves (HPLC - valves or fast acting pneumatic valves) syringe pumps, [1,2].

Examples of apparatus with special devices for taking very small quantity of sample are presented in literature by many authors. Wahlström and Wamling, [12] or Wagner and Vichterle, [13] installations use mobile pneumatic capillary samplers; Luna and Rodriquez [14] describe the work with capillary samplers injectors; Tochigi *et. all,* [15] apparatus contain six direction valves that introduce the sample into the gas chromatograph while Kao and Lin, [16] presents an equipment that use a micrometer syringe to withdrawn the sample at equilibrium from the coexisting phases. By reducing the quantity of extracted sample, the perturbation of the equilibrium state is avoided and the time of the experiment is reduced. The uncertainty for the composition determination depends on the accuracy of the analysis method. Literature [12-16] gives for the above-mentioned apparatus, uncertainty less than 1%.

In Romania there exist a few installations equipped with a constant volume cell, working in a static regime. It can be mentioned an apparatus for solubility data at atmospheric pressure (Laboratory of Physical Chemistry – University of Bucharest), [17], but also two other installations for high pressure (Laboratory of Physical Chemistry, University of Bucharest and respectively Laboratory of Applied Physical Chemistry and Electrochemistry, "Politehnica", University Bucharest), [18, 19].

The schematic representation of the installations Vilcu and Gainar is given Fig. 3 [18]:

The equilibrium is reached under stirring condition within a few hours. The sampling system is evacuated and valve (7') is carefully opened. A sample of about 1 mL of solvent containing gas dissolved is collected in the ampoule (8'). The gas absorbed is then desorbed and the pressure produce in this way is read using a cathetometer (attached to the mercury manometer).

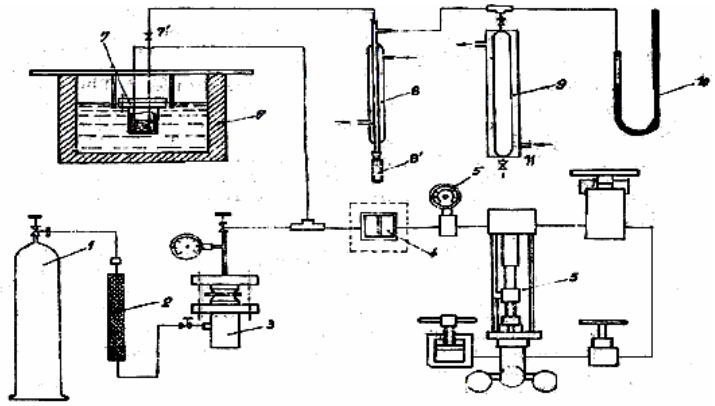

Fig. 3. *Schematic representation of apparatus for solubility data of Vilcu and Gainar [18] (1) –compressed gas bottle; (2) – steel cylinder with molecular sieves for eliminating water traces; (3) – autoclave as manostate and fine handling of gas supplying the equilibrium cell; (4) – differential monometer; (5) – pressure gauge with rotative piston and weights; (6) – thermostated bath; (7) – equilibrium cell; (7', 11) – valves; (8) – refrigerent; (8'-) ampoule for sample; (9) – thermostated reservoir; (10) – mercury manometer.*

The volume, pressure, temperature and mole number of desorbed gas can be correlated using a EoS. After the pressure is read, the valve (11) is opened atmospheric pressure air is introduced. The ampoule (8') is detached and weighed. The volume of solvent is estimated based on the solvent density and the mass of the ampoule. The apparatus work at pressure up to 5 MPa and at room temperature, [18].
Another example is the isochoric apparatus for VLE data, [19]. The elements contained are presented in Fig. 4.

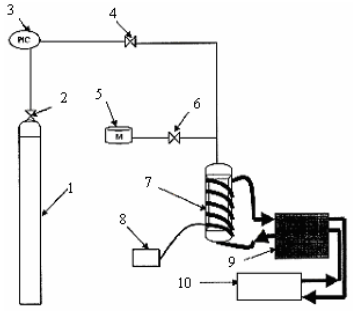

Fig. 4. *Schematic representation of the isochoric apparatus of Geană [19]. (1) – gas reservoir; (3) – pressure regulator; (2, 4, 6) – valves; (5) – manometer; (7) – constant volume cell; (8) – thermocouple; (9) – thermostat; (10) – cryostat.*

The apparatus can work at pressure up to 25 MPa (±0.5 %) and temperature in the range of 283… 350 K (±0.1 K).

B) Variable volume cell installations - VVC installations.

The use of a variable volume cell for studying high-pressure phase behaviour offers higher flexibility of the measurements. There are different possibilities to change the volume of the cell, moving up and down a piston [20] or injecting small quantity of an immiscible

fluid into the system [21]. Simultaneously, the pressure drop due to the sampling is compensated.

If the P-T-x-y complete data are obtained with VVC apparatus, the method is called *analytical VVC methods* and if the phase transition is observed at constant pressure and temperature than the method belongs to the *synthetic (indirect) VVC methods.*

Similar to the CVC methods, majority of cells are visual (with high pressure resistant windows or entire cell is built from glass) but also non-visual cell from stainless steel are used.

According to analytical VVC methods the experiments follow the same procedure described in the previous section.

In the static regime the phases are separated inside the equilibrium cell. For a given temperature and pressure, an adequate volume of each phase is collected and analysed using physico-chemical analysis method.

The perturbation of the equilibrium state caused by the sampling procedure is avoided by one of the method discussed above. Often, one [23, 24] or two pistons [20] achieve the change in volume cell.

The volume of the cell can be evaluated by measuring the position of the piston by means of a cathetometer [1, 2] or directly if a scale is attached to the cell [23].

A constructive type of this category of installations is given in Fig. 5, [21]

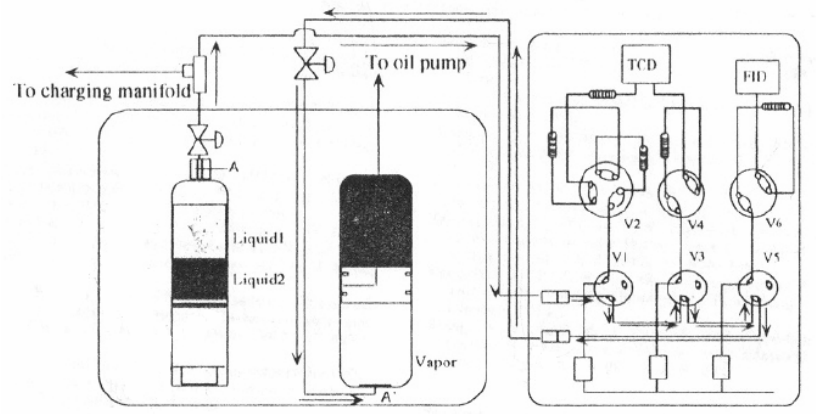

Fig.5. *Schematic representation of a VVC apparatus*

Barrufet and Rahman [20] use two PVT variable volume cells each of them equipped with a movable piston. A computer controlling stepping motor can separately change the volume of the cells and the mobility of the sample within the system can be achieved at constant temperature and pressure. The cell is connected with a gas chromatograph using specially on-line sampling system with digitally operated valves. These valves are connected to a switching valve for back – flushing to eliminate column contamination and separate columns for various phase analyses, (Fig. 5). Thus the mass of the withdrawn sample is reduced and the equilibrium is not disturbed. The uncertainty in composition determination

is less than 1% in the experimental conditions - pressures up to 27 MPa (±0.005 MPa) and temperatures up to 500 K (±0.2 K).

In Romania a similar apparatus with variable volume cell working at pressure up to 30MPa is reported by Geana *et all.* The main part of the equipment is the visual cell with two sapphire windows, one of the window acting as piston. A hand pump actions the piston, so the volume can be change between 25 and 60 cm^3. When the equilibrium is obtained samples are collected by depressurisation and expansion into glass trap (with calibrated volume) using manually operated valves. The uncertainty in mole fraction is less than 0.003.

It can be conclude that both static analytical techniques (CVC and VVC) are simple and allow obtaining complete P-T-x-y for large pressure and temperature limits, but these methods cannot be applied in the regions where the phase separation in not sharp. The quality of data is conditioned only by the accuracy of the measuring devices.

Synthetic VVC methods.

These methods are used when the experimental condition (high pressure, system characteristic) yields a lot of difficulties withdrawing and in the composition analysis of the coexisting phases (barotropic inversion points, critical region). Basically, an experiment consists of the visual observation of the Dew and/or Bubble Point pressure at various temperatures, for pure components or mixture of known composition. No sampling is necessary.

The main parts of a synthetic installation are presented in Fig. 6 [25]:

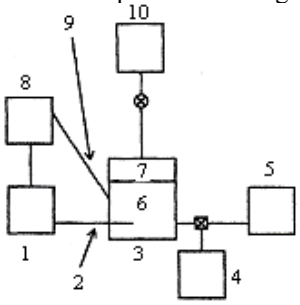

Fig. 6. *The main parts of a synthetic VVC device [34] (1)– temperature controller; (2) – thermocouple; (3) – equilibrium cell; (4) –sample inlet; (5)-pressure transducer; (6) –sample; (7) – pneumatics; (8) – powerstat; (9) – band heaters, (10) - syringe pump.*

Using one or more pistons or a pressure transmitting fluid, the pressure is modified until a homogeneous phase results. So, two and three phase equilibrium can be visual observed, but better results are obtained by using different devices - magnifiers, microscopes or video cameras, [26]**.**

In order to improve the accuracy for the volume cell evaluation different modifications in the piston geometry have been proposed. Thus, the movement of the piston can be insured using of a fluid pumped behind the piston, [27]. If a rod is attached to the movable piston, the position will be fixed by reading the displacement of the rod, with a Vernier microscope. The volume of the cell and the rod position should be first calibrated with pure liquid [28]. In the equipment presented by Kihran and Pohler [29] the piston is attached to a steel rod with feromagnetic metal pieces, acting as sensing element. The position of the

piston is registered using a piston locator screw, correlated with volume of the cell. The accuracy in volume determination is ±0.0025 cm^3. In Fig.7 is schematically presented Cailletet apparatus that respect the procedure of the synthetic variable volume cell installations.

The main part of the apparatus is a thick-walled Pyrex glass tube (Cailletet tube), about 50 cm long and with an inner diameter of 4 mm and an outer diameter of 12 mm. This tube acting as equilibrium cell and is equipped with a window, a movable piston, a pressure generator and video monitors can be also attached.

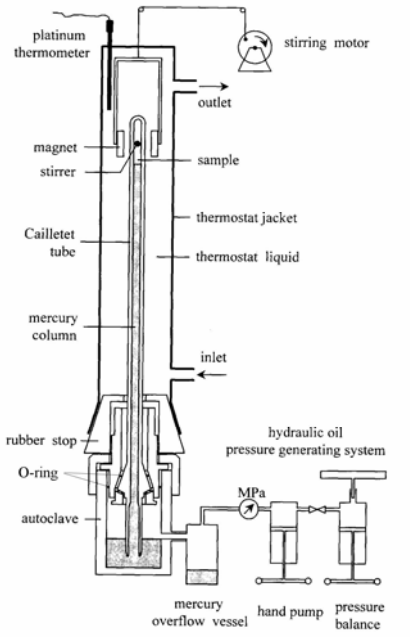

Fig.7. *Schematic representation of Cailletet apparatus*

An amount of liquid is dosed in the in the top end of the high-pressure tube by a micrometer syringe. The exact mass is determined by weighting. The liquid is degassed by alternating freezing and melting under vacuum condition (using liquid nitrogen as cooling agent). A high vacuum oil diffusion pump or a high vacuum turbo pump creates the vacuum, and the quality is controlled with an ionisation vacuum gauge.

The tube is evacuated and the other component (gaseous at room temperature) is added by displacement with mercury in a gas rack construction. Knowing the volume, pressure and temperature of the gaseous component the exact quantity of it is determine by calculation from an equation of state.

The sample is frozen in the sealed end of the Cailletet tube and the rest of the tube is filled with mercury. Under this condition the tube is transferred from the gas rack to the Cailletet apparatus. Then, the system is pressurized and after that warmed up to the room temperature using the same liquid as the thermostat liquid.

The mixture can be agitated by a stirrer (a stainless steel ball with a diameter slightly less than the bore of the glass tube), which is moved up and down by two button magnets driven by a rotating disk of a stirring motor.
The open end of the tube is placed in an autoclave filled with mercury. The autoclave is connected to a hydraulic oil system, generating the pressure by means of screw type hand pump.
The pressure is measured by means of a dead-weight pressure gauge with an accuracy of 0.005 MPa. The mercury serves as a pressure transmitting fluid between the hydraulic oil pressurizing system and the sample and provides the sealing for the sample. A Viton O-ring, placed at about 2/3 of the tube length, achieves the sealing of the connection between the tube and the autoclave.
The temperature is adjusted by a thermostat bath with circulating ethanol, water or silicon oil depending on the temperature range of interest. The temperature of the thermostat liquid is kept at the desired value with accuracy better than 0.02 K at temperatures up to 370 K.
A platinum resistance thermometer (Pt 100) records the temperature of thermostat liquid near the sample with accuracy within 0.01 K.
The Cailletet apparatus above described is suitable to perform measurement at pressure up to 15 MPa and temperature ranging from 250 K to 450 K.
According to the synthetic methods, the experiment consists on varying the pressure and temperature in order to observe the phase boundaries.
In conclusion, the synthetic methods have the advantages that allow obtaining equilibrium data near the critical region and even in the critical point or in the points of barotropic inversion, because no sampling is necessary.
Similar with the first categories of methods, the accuracy of the obtained data is conditioned by the quality of the degassing procedure and the precision of the measuring instrument.
Consequently the development of new gauge instruments designed for high-pressure conditions will insure a high quality of the equilibrium data.

Conclusions

Experimental methods and installations for investigation of high-pressure phase behaviour are presented, analysed and each category is briefly characterized.
The experimental procedure, the description of the equipment and the improvements are presented for each type of installation. For increasing the accuracy of the experimental data obtained with static techniques different solutions presented in literature are discussed and compared.

REFERENCES

1. Dohrn, R., Brunner, G., (1995) *Fluid Phase Equilibria* **106**, 213 – 282.
2. Christov, M., Dohrn, R., (2002) *Fluid Phase Equilibria* **202,** 153 – 218.
3. Nanu, D., (1999) *Bulletin of Transilvania University* **6 (14)**, 89-96.
4. Duţă, A., (1997) **Proprietăţi PVT şi ELV în sisteme binare cu n-alcani,** Teză doctorat, Bucureşti, Romania.

5. Morgan, D.I., Kobayashi, R., (1994) *Fluid Phase Equilibria* **97,** 211 – 242
6. Di Nicola, G., Giuliani, G., Passerini, G., Polonara, F., Stryjek, R., (1998) *Fluid Phase Equilibria* **153** 143-165.
7. Di Nicola, G., Passerini, Srtyjek, R., (2001) *Journal Chem.Eng. Data* 46**,** 359 - 366.
8. Di Nicola, G., Polonara, F., Stryjek, R., (2002) *Journal Chem.Eng. Data* **47,** 876 – 881.
9. Mokbel, I., Blondel-Telouk, A., Vellut, D., Jose, J., (1998) Fluid *Phase Equilibria* **149**, 287 - 308.
10. Wahlström, A., Wamling, L., (1999) *Journal Chem. Eng. Data* **44,** 823 – 828.
11. Wahlström, A., Wamling, L., (2000) *Journal Chem. Eng. Data* **45**, 97 – 103.
12. Wagner, Z., Wichterle, I., (1987) *Fluid Phase Equilibri,* **33,** 109 – 123.
13. Galicia-Luna, L. A., Ortega-Rodriguez, A., (2000) *Journal Chem. Eng. Data* **45,** 265 – 271.
14. Tochigi, K., Hasegawa, K., Asana, N., Kojima, K., (1998) *Journal Chem. Eng. Data **43***, 954 – 956.
15. Kao, C.F., Lin, W.C., (1999) *Journal Chem. Eng. Data* **4**, 338 – 342.
16. Vîlcu, R., Perişanu, Şt., Cucuiat, M., (1980) *Polish Journal of Chemistry* **54** 2043-2050.
17. Vîlcu, R., Găinar, I., Anitescu, Gh., Perişanu, Şt., (1991) *Revue Roumaine de Chemie* **36**, 421 – 427.
18. Iliş, M. L. G., (2004) **Teză doctorat**, Bucureşti.
19. Stamoulis D., (1994) **Patterns of Fluid Phase Behaviour in Binary and Quasi-binary Mixtures**,
20. Ph-D thesis Delft University of Technology, Netherlands.
21. Barrufet M. A., Rahman, S., (1997) *Journal Chem. Eng. Data* **42,** 120 – 123.
22. Gasem, K. A. M., Robinson Jr., R. L., (1985) *Journal Chem. Eng. Data* **30,** 53 – 56.
23. Scurto, A. M., Lubbers, C., M., (2001) *Fluid Phase Equilibria,* **190,** 135 – 147.
24. Secuianu, C., Feroiu, V., Geană, D., (2003) *Journal Chem. Eng. Data* **48**, 1348 – 1386.
25. Du Rand, H., Nieuwodt, I., (2002) *Journal of Supercritical Fluids* **22**, 185 – 199.
26. Alto, M., şi colaboratorii, (1996) *Journal Chem. Eng. Data* **41,** 79 – 83.
27. Reighard, T. S., Lee, S.T., Olesik, S., V., (1996) *Fluid Phase Equilibria* **123,** 215 – 230
28. Costa, M., şi colaboratorii, (1996) *Journal Chem. Eng. Data* **41**, 1104 – 1110.
29. Kiran, E., Pohler, H., Xiong, Y., (1996) *Journal Chem. Eng. Data* **41**, 158 – 165.

LA STRUCTURE ET LA RÉACTIVITÉ DES NITRILES

I. Ciocăzanu[*], D. Zăvoianu[**]

résumé : Pour pouvoir établir des relations entre la structure et la réactivité des nitriles on détermine les chaleurs de combustion et de formation de quelques nitriles non saturés aromatiques. On constate que les valeurs des chaleurs de combustion et de formation sont influencées par les effets électroniques qui se manifestent dans les molécules des nitriles étudiés.

mots clés: chaleur de formation, chaleur de combustion, piperonilidène-phénylacétonitriles, nitriles alpha-, bêta- non saturés

Introduction

Le comportement dans la réaction d'hydrolyse alcaline de quelques nitriles α, β non saturés aromatiques a été étudié dans une série de notes [1-7]. On a constaté que la présence des électrons π détermine la croissance de la vitesse de réaction et l'abaissement des valeurs des énergies d'activation. De même on a observé que la présence des substituants qui repoussent ou qui attirent les électrons dans la molécule des nitriles α, β non saturés déterminent la modification des valeurs des paramètres d'activation ($\Delta H^{\#}$) l'enthalpie d'activation et ($\Delta S^{\#}$) l'entropie d'activation.

Dans une autre série de notes [8-16], on a constaté l'influence exercée par les effets électroniques sur les valeurs des chaleurs de combustion et de formation de certains amides, acides organiques, azodérivés α, β-non saturés. Les résultats obtenus ont servi à l'étude de l'hydrolyse des aminonitriles secondaires dans la formation prébiotique des aminoacides [17].

Afin d'apporter une contribution à la connaissance des relations entre la structure et la réactivité des nitriles nous présentons les résultats obtenus en ce qui concerne les chaleurs de combustion ($\Delta_c H^o$).

[*] Université de Bucarest, Faculté de Chimie, Chaire de Chimie Physique, Bd. Regina Elisabeta, Nº 4-12, Bucarest 3, 030018, Roumanie

[**] Université de Bucarest, Faculté de Chimie, Chaire de Chimie Organique, Bd. Regina Elisabeta, Nº 4-12, Bucarest 3, 030018, Roumanie

Analele Universităţii din Bucureşti – Chimie, Anul XIV (serie nouă), vol. I-II, pg. 205-208

La chaleur de combustion ($\Delta_c H^o$) constitue un paramètre thermodynamique important qui peut caractériser une certaine substance. La chaleur de combustion ($\Delta_c H^o$) se trouve en étroite liaison avec la force de liaison chimique, l'enthalpie standard de formation ($\Delta_f H^o$), l'énergie de conjugaison et avec l'énergie de résonance.

Les nitriles étudiés sont les suivants:

- piperonylidène-phénylacétonitrile ;
- N-méthylpiperonylidène-phénylacétonitrile ;
- N-éthylpiperonylidène-phénylacétonitrile ;
- N-n-propylpiperonylidène-phénylacétonitrile ;
- N-n-buthylpiperonylidène-phénylacétonitrile ;
- N-phényl-piperonylidène-phénylacétonitrile ;
- N-benzylpiperonylidène-phénylacétonitrile.

Partie expérimentale

Pour la détermination des chaleurs de combustion on a utilisé une bombe calorimétrique adiabatique du type Gallenkamp [8].

Cette bombe est munie d'un système électronique qui permet à maintenir toujours une différence nulle de température entre l'enceinte intérieure et l'enceinte extérieure du calorimètre. La bombe calorimétrique est prévue d'un thermomètre spécial dont la précision est de 0,01º. Avec un système optique attaché on peut déterminer la température à 0,001º.

Pour les déterminations effectuées on a utilisé des fils de Cr-Ni avec la chaleur de combustion de 335 cal/g et de coton dont l'énergie de combustion préalablement déterminée a pour valeur $\Delta_c H^o$ (s, 298,15K) = - 4180 cal/g.

L'équivalent énergétique du calorimètre a été obtenu à partir d'une série de combustions à l'acide benzoïque (Riedel Haen AG Seelze Hannover, étalon thermochimique 9 E 70681) auquel on connaît la chaleur de combustion de 6311,5 cal/g. L'équivalent énergétique du calorimètre obtenu à la suite d'un grand nombre de déterminations a une valeur moyenne de 441,7 cal/degré.

Pour obtenir des valeurs plus précises des chaleurs de combustion pour les composés contenant dans la molécule de l'azote on fait les corrections pour la formation de l'acide azotique [18]. L'acide azotique est titré pour pouvoir faire les corrections respectives.

La combustion a été effectuée dans une atmosphère d'oxygène dont la pression retenue dans la bombe après un prélavage, est de 25 atm.

Résultats et discussion

À partir des équations de combustion pour les composés qui contiennent que de l'azote:

$$C_{15}H_{10}O_2N_2\,(s) + 16{,}5\ O_2\,(g) \rightarrow 15\ CO_2\,(g) + 5\ H_2O\,(l) + N_2\,(g) \qquad (1)$$

les enthalpies standard de formation des composés, d'après la loi de Hess, sont:

$$\Delta_f H^o_{C_{15}H_{10}O_2N_2(s)} = -\Delta_c H^o_{C_{15}H_{10}O_2N_2(s)} + 15\Delta_f H^o_{CO_2(g)} + 5\Delta_f H^o_{H_2O(l)} \qquad (2)$$

où: $\Delta_f H^o_{CO_2(g)}$ et $\Delta_f H^o_{H_2O(l)}$ sont les enthalpies de formation connues [11] du dioxyde de carbone et eau.

Les résultats expérimentaux des déterminations pour les chaleurs de combustion des substances étudiées sont consignés dans le tableau 1.

Des données consignées dans le tableau 1, on constate que la structure moléculaire des nitriles étudiés exerce une influence sur les valeurs d'enthalpie de combustion et de formation; ainsi une enthalpie de formation petite correspond au fait que la substance donnée présente des liaisons plus fortes, c'est à dire une plus grande stabilité.

Ainsi, des dattes du tableau 1, on observe la croissance de la stabilité moléculaire à partir du piperonylidène-phénylacétonitrile au N-n-buthyl-piperonylidène-phénylacétonitrile, conséquence due à l'effet du substituant répulsif (+I).

Tableau 1. Les chaleurs de combustion et de formation pour les piperonylidènes-phénylacétonitriles

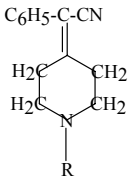

Substance	Nature du radical (R)	Formule moléculaire	$-\Delta_c H^o$ (s, 298,15 K) [kcal/mol]	$\Delta_f H^o$ (s, 298,15 K) [kcal/mol]
I	-H	$C_{13}H_{14}N_2$	1712,69	11,80
II	$-CH_3$	$C_{14}H_{20}N_2$	1870,13	6,87
III	$-C_2H_5$	$C_{15}H_{18}N_2$	2027,23	1,60
IV	$-C_3H_7$ (n)	$C_{16}H_{20}N_2$	2184,15	-3,85
V	$-C_4H_9$ (n)	$C_{17}H_{22}N_2$	2341,35	-9,02
VI	$-C_6H_5$	$C_{19}H_{18}N_2$	2425,34	23,81
VII	$-CH_2-C_6H_5$	$C_{20}H_{20}N_2$	2580,66	16,46

De même on peut interpreter l'influence de l'effet stérique du au poids moléculaire du radical alcoyle sur la croissance de la stabilité moléculaire du nitrile.

Cette influence stérique se manifeste aussi dans le cas des dérivés contenant les groupements phényl et benzyl.

Conclusion

En conclusion, la stabilité moléculaire est déterminée par les effets stériques et électroniques des divers substituants présents dans la molécule organique.

RÉFÉRENCES

1. Angelescu, E., Vasiliu, G., Zăvoianu, D., Nan, F., (1961), *Studii şi cercetări de chimie, Acad. R..P.R.* **9**, 459-464
2. Angelescu, E., Vasiliu, G., Zăvoianu, D., Greff, C., (1961), *Studii şi cercetări de chimie, Acad. R..P.R.* **9**, 477-483
3. Angelescu, E., Vasiliu, G., Zăvoianu, D., Ivan, L., (1962), *Studii şi cercetări de chimie, Acad. R..P.R.* **10**, 311-317
4. Angelescu, E., Vasiliu, G., Zăvoianu, D., (1962), *Revue de Chimie, Acad. R.P.R.,***2,** 655-660
5. Zăvoianu, D., (1960), *Chem. Oil and Gas in Romania,* **4,** 16-20
6. Zăvoianu, D., (1971), *Anal. Ser. St. Naturii, Univ. Buc.,* **2**, 183-190
7. Ciocăzanu, I., Dogaru, V., Bornaz, C., Moga-Gheorghe, S., Zăvoianu, D., (1978), *Rev. Chimie (Bucureşti),* **29,** 114-120
8. Zăvoianu, D., Perişanu, S., Moga-Gheorghe, S., Bornaz, C., (1983), *Rev. Chimie (Bucureşti),* **34/10**, 987-995
9. Zăvoianu, D., Ciocăzanu, I., Moga-Gheorghe, S., Cuza, O., Bornaz, C., (1985), *Rev. Chimie (Bucureşti),* **36/6**, 210-215
10. Zăvoianu, D., Ciocăzanu, I., Moga-Gheorghe, S., Bornaz, C., (1986), *Rev. Chimie (Bucureşti),* **37/11**, 960-967
11. Zăvoianu, D., Ciocăzanu, I., Moga-Gheorghe, S., Bornaz, C., (1988), *Rev. Chimie (Bucureşti),* **39/6**, 487-492
12. Zăvoianu, D., Ciocăzanu, I., Moga-Gheorghe, S., Bornaz, C., (1990), *Rev. Chimie (Bucureşti),* **41/3**, 234-240
13. Zăvoianu, D., Ciocăzanu, I., Moga-Gheorghe, S., (1993), *Rev. Chimie (Bucureşti),* **44/5**, 421-429
14. Ciocăzanu, I., Zăvoianu, D., (1994), *Rev. Chimie (Bucureşti),* **45/10**, 876-880
15. Ciocăzanu, I., Zăvoianu, D., (1997), *Rev. Chimie (Bucureşti),* **48/2**, 121-125
16. Zăvoianu, D., Ciocăzanu, I., (2003) *Anal.Univ. Buc.-Ser. Chimie,* **Anul XII/(I-II)**, 137-142
17. Bejaud, N., Mion-Taillades, J., (1975), *Tetrahedron*, **31/5**, 401-409
18. Rossini, F., D., (1956), **Experimental Thermochemistry,** Interscience Publishers Inc., New York, 124-150

OVERALL ACTIVATION PARAMETERS OF PROPYLENE OXIDATION IN PREMIXED FLAMES

Domnina Razus*, Codina Movileanu*, Venera Branzea*, D. Oancea **

abstract: The addition of diluents (Ar, CO_2 or air) to a stoichiometric propylene-air mixture determines an important decrease of average flame front temperature and consequently, a decrease of the average reaction rate within the flame front, as seen from burning velocity of these mixtures. The analysis of burning velocity variation against the total initial pressure and the average flame front temperature enabled the determination of the overall reaction order and overall activation energy, respectively. Such overall activation parameters are important for modelling the flame propagation in various conditions (stagnant or flowing mixtures, laminar or turbulent flow etc)

Introduction

The overall activation parameters of fuel oxidation in flames are important in many engineering applications such as CFD (Computational Fluid Dynamics) modelling of flame propagation in confined and unconfined conditions or in vented explosions [1]. The overall activation parameters (reaction order and activation energy) are readily obtained from the analysis of burning velocity dependency on the total initial pressure of fuel-oxidant mixture and on the average flame front temperature, using the relationships developed within the theory of laminar flame propagation [2,3]. In the present paper, the variation of flame front temperature was obtained by dilution of a stoichiometric fuel-air mixture with several diluents: Ar, CO_2 or air. Propylene was examined since few data on its burning velocity, especially in the presence of inert gases, are available. Burning velocities of propylene-air and propylene-air-inert mixtures (inert concentrations within 5 ÷ 20 vol. %) were determined using pressure-time records from a spherical bomb with central ignition, at ambient initial temperature and total initial pressures within 0.3 - 1.2 bar.

* "I.G.Murgulescu" Institute of Physical Chemistry, 202A Spl. Independentei, 060021Bucharest, ROMANIA
** Department of Physical Chemistry, University of Bucharest, 4-12 Regina Elisabeta Blvd., 030018 Bucharest, ROMANIA

Analele Universităţii din Bucureşti – Chimie, Anul XIV (serie nouă), vol. I-II, pg. 209-214

Experimental procedure and computing program

The explosion vessel was a stainless steel spherical bomb able to withstand pressures of 30 bar. The bomb was fitted with stainless steel electrodes and the spark gap was located in the bomb centre. Electric sparks produced by a standard motorcar induction coil were used for explosion initiation. The pressure variation during flame propagation was continuously monitored by means of a pressure transducer (Kistler 601A, coupled with a Charge Amplifier Kistler 5001 SN) and the flame front position was determined by means of an ionisation gauge. Both signals were recorded and stored by a digital acquisition system Tektronix TestLab 2505, usually at 10^4 signals per s. Other characteristics of the experimental set-up were previously given [4].

The explosive mixtures were obtained by partial pressure method, in 10 L steel cylinders, at 4 bar total pressure. The experiments were performed at ambient temperature and various total initial pressures within 0.3 and 1.2 bar.

Propylene (99.5%) was purchased from Arpechim Petrochemical Plant-Pitesti.

Compressed air, argon (99.99%) and carbon dioxide (99.5%) were purchased from SIAD-Italy. They were used without further purification

The normal burning velocity, S_u, was calculated from pressure-time records of explosion development in a spherical vessel, during the early stage of the process, according to the recently developed procedure [5] based on determination of cubic law coefficients of pressure rise.

The adiabatic flame temperatures of fuel-air and fuel-air-diluent mixtures were computed with the program ECHIMAD [6], assuming that chemical equilibrium is reached within the flame. Fifteen compounds ($C_{graphite}$, CH_4, CO, CO_2, H_2O, H_2, O_2, N_2, NO, C_2H_2, C_2H_4, C_3H_8, H, OH and O) were considered as combustion products. Their heat capacities (expressed as function of temperature with the form: $C_p = a + b \cdot T + c \cdot T^2 + d \cdot T^{-2}$), the standard enthalpies of formation at 298 K and the standard entropies at 298 K were taken from the collections of Stull [7], Barin [8] and Kubaschewki [9].

Results and Discussion

A set of data referring to propylene-air-argon mixtures with various argon concentrations is given in Figure 1. For each mixture, the burning velocity decreases as the total initial pressure, p, increases. Indeed, according to the theory of laminar flame propagation, the dependency of burning velocity of fuel-oxidant mixtures on mixture pressure p has the form:

$$S_u = S_u^{ref} \left(\frac{p}{p_{ref}} \right)^{\beta} \qquad (1)$$

where β is the baric coefficient (pressure exponent) of the burning velocity, p_{ref} is the reference pressure (usually, the ambient pressure) and S_u^{ref} is the burning velocity evaluated in reference conditions. For all hydrocarbon-air mixtures, negative values of baric coefficients are reported [3].

The overall reaction orders, n, are calculated from the baric coefficients according to the equation [10]:

$$n = 2(\beta + 1) \qquad (2)$$

Data referring to propylene-air-diluent mixtures are given in Table 1. The baric coefficients were calculated as slopes of the linear correlations $\ln S_u$ versus $\ln p$.

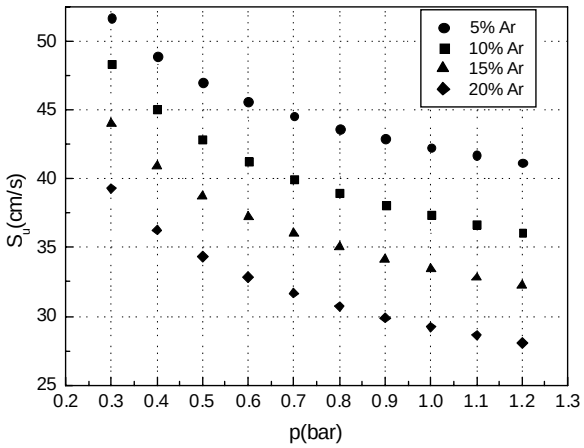

Fig. 1: *The influence of Ar dilution on burning velocity, for a stoichiometric propylene-air mixture*

Table 1. Pressure exponents of burning velocities in propylene-air-argon and propylene-air-carbon dioxide mixtures, β, and overall reaction orders n of propylene oxidation.

No.	$[C_3H_6]$ (vol%)	[diluent] (vol%)	*Argon*		*Carbon dioxide*	
			-β	n	-β	n
1	4.46	0	0.160	1.68	0.160	1.68
2	4.28	5.0	0.161	1.68	0.191	1.62
3	4.05	10.0	0.208	1.58	0.231	1.54
4	3.83	15.0	0.222	1.56	0.257	1.49
5	3.60	20.0	0.240	1.52	0.193	1.62

Similar data referring to propylene-air mixtures are given in Table 2.

Table 2. Pressure exponents of burning velocities in propylene-air mixtures, β, and overall reaction orders of propylene oxidation, n.

$[C_3H_6]$ (vol%)	3.22	3.47	3.76	4.11	4.46	4.78	5.03
-β	0.28	0.19	0.19	0.21	0.16	0.20	0.18
n	1.44	1.62	1.62	1.57	1.67	1.60	1.65

Excepting the leanest mixture ($[C_3H_6]$ = 3.22%), all propylene-air mixtures have the same overall reaction order n = 1.60, within experimental errors. Close values of the overall reaction orders, n = 1.80 - 2.0, were calculated from the pressure dependence of quenching distances [11]. For propylene-air-diluent mixtures, the overall reaction orders have also values between 1.80 and 1.50, decreasing with the increase of diluent concentration.

The overall activation energy of fuel-oxygen reaction within the flame front was calculated with the equation [12]:

$$\ln S_u + \frac{1}{2}\ln T_{fl,av} - \frac{n}{2}\ln Y = const - \frac{E_a}{2RT_{fl,av}} \qquad (3)$$

where $T_{fl,av}$ is the average adiabatic flame temperature within the flame front and Y is the mole fraction of reactive components (fuel + oxidant) in the examined mixture. The average temperature is calculated with the relationship [12]:

$$T_{fl,av} = T_0 + 0.74(T_{fl} - T_0) \qquad (4)$$

A typical set of data is given in Table 3; an average value of reaction order (n = 1.60) was used. For propylene-air-carbon dioxide mixtures, we used n = 1.74.

Fig. 2 shows the plots of the left member of eqn. (3) against the reciprocal value of average flame temperature, for a stoichiometric propylene-air mixture diluted with Ar and with CO_2. In Fig. 2, data referring to lean propylene-air mixtures (using n = 1.60) were also plotted. One may consider that such mixtures were obtained by adding excess air to the stoichiometric propylene-air system. The slopes of linear correlations give the overall activation energies.

Table 3. Burning velocities and flame temperatures of propylene-air-argon mixtures, at p_0 = 1 bar and T_0 = 298 K

$[C_3H_6]$ (vol%)	[Ar] (vol%)	T_{fl} (K)	$T_{fl,av}$ (K)	Y	S_u (cm/s)	$\ln(\frac{S_u}{cm \cdot s^{-1}}) + \frac{1}{2}\ln(\frac{T_{fl,av}}{K}) - \frac{n}{2}\ln Y$	$\frac{1000 \cdot K}{T_{fl,av}}$
4.46	0.0	2335.2	1804.7	1.00	46.04	7.57859	0.55411
4.28	5.0	2308.2	1784.8	0.95	42.22	7.52746	0.56029
4.05	10.0	2271.8	1757.8	0.90	37.32	7.43973	0.56889
3.82	15.0	2230.7	1727.4	0.85	33.42	7.36635	0.57891
3.60	20.0	2191.1	1698.1	0.80	29.22	7.27200	0.58889

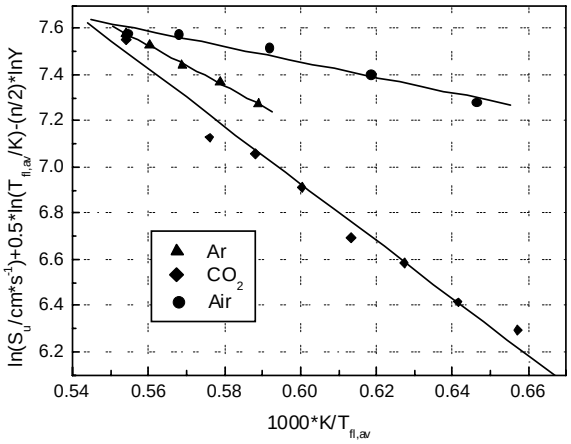

Fig. 2: *The dilution effect of Ar, CO_2 and air on burning velocity, for stoichiometric propylene-air-diluent mixtures; data evaluated at* p_0= 1 bar and T_0 = 298 K

The results are given in Table 4.

Table 4 – Overall activation energies of propylene oxidation in flames, E_a (kJ/mol)

	Ar	CO_2	Excess air
Propylene-air-diluent	146	207	56

Such values can be obtained also for any initial pressure within the studied range (0.3 – 1.2 bar), using adequate values of average flame temperature. Earlier values of the overall activation energy, determined by means of preheating method, for propylene-air mixtures with various propylene concentrations are higher: 165 kJ/mol for a lean mixture($[C_3H_6]$ = 3.51%) and 177 kJ/mol for the stoichiometric mixture ($[C_3H_6]$ = 4.52%)

A similar analysis of earlier reported burning velocities of stoichiometric propylene-oxygen-nitrogen mixtures ($[N_2]$ = 45 – 75 %)[13] gave E_a = 161 kJ/mol. The result is in good agreement with E_a = 176 kJ/mol determined from burning velocity measurements of

C_3H_6- O_2- N_2 flames stabilised on a burner, at ambient pressure [12] and with E_a = 160 - 176 kJ/mol determined from induction delays of propylene-oxygen self-ignition [14].

The dilution by Ar or CO_2 of the stoichiometric propylene-air mixture has little influence on the overall reaction order, which varies within 1.50 and 1.70. The dilution effect is observed in values of the overall activation energy: 146 kJ/mol (C_3H_6-air-Ar) and 207 kJ/mol (C_3H_6-air-CO_2) as compared to 56 kJ/mol at dilution by air. These values are relevant for the significant inerting effect of carbon dioxide on flame propagation in fuel-air mixtures.

4. Conclusions

The rate of fuel-oxidant reaction within the flame front can be described by means of overall activation parameters: overall reaction order and overall activation energy. These parameters were determined for a test fuel-oxidant system: propylene-air, in the presence of excess air or Ar and CO_2 as diluents, from burning velocities in systems at various initial pressures and various diluent concentration.

The overall reaction order has values between 1.50 and 1.80, for all investigated systems, as reported for many other hydrocarbon-air mixtures. The overall activation energies have also typical values for oxidation of hydrocarbons in flames.

REFERENCES

1. Razus, D., Krause, U., Scheid, M. and M. Berge, M. (2001) *PTB Bericht ThEx-20*, Proc. BAM-PTB Colloquium zur Sicherheitstechnik, Braunschweig, pp.79-88.
2. van Tiggelen, A., Balaceanu, J., Burger, J., De Soete, G., Sajus, L., Salé, B. and van Tiggelen, P. (1968) **Oxidations et Combustions**, **vol I**, Ed. Technip, Paris.
3. Lewis, B., and von Elbe, G. (1987) **Combustion, Flames and Explosion of Gases**, Acad.Press, 3-rd ed., New York and London.
4. Razus, D., Oancea, D. and Ionescu, N.I. (2000) *Revue Roumaine Chim* **45**, 319.
5. Razus, D., Oancea, D. and Movileanu, C. (2005) paper submitted to *J.Loss Prev.Process Ind* .
6. Geana, D., Popescu, D., Mihai, M., and Adomnica, L. (1985) *Rev. Chimie* **36**, 708.
7. Barin, I., and Knacke, O. (1973) **Thermochemical properties of Inorganic Substances**, Springer Verlag, Berlin.
8. Stull, D., Westrum, E., and Sinke, G. (1969) **The Chemical Thermodynamics of Organic Compounds**, Wiley, New York.
9. Knacke, O., Kubaschewski, O. and Hesselman, K. (1991) **Thermochemical Properties of Inorganic Substances**, Springer, Berlin, Heidelberg and New York, 2-nd Ed., 1991.
10. Potter, A., and Berlad, A. (1957) **VI-th Symp.(Intern.) on Combustion,** Reinhold, New York, p.83.
11. Oancea, D., Razus, D., Ionescu, N.I. (1992) *Rev.Roumaine Chim* **37**, 95.
12. Burke, R., Dewael, F., and van Tiggelen, A (1963) *Comb. Flame*, **7**, 83.
13. Popescu, D., Oancea, D., Gosa, V., Ionescu N.I., and Albu B. (1984) *Rev.Roumaine Chim*., **29**, 253.
14. Kusuhara, S. (1960) *Rev.Phys.Chem.Japan* **30**, 34.

A MIXED ELECTRIC DOUBLE LAYER MODEL AT THE SOLID (LIQUID) / ELECTROLYTE INTERFACE

Gh. Semenescu*, C. Cioacă **, Gh. Potcovaru ***

abstract. The tension surface defined by Gibbs in treating the interface area is structurally specified by a transition layer made up by the inner Helmholtz plane and the one containing the surface of active centres. In the double mixed electrode model, considered to be one step taken towards the microscopic-level understanding of the electrolyte interface phenomena, the electrochemical sensors operations, as well as the electric phenomena at the membrane level are explained in a simple manner, and the cyclic polarization diagrams can be more simply interpreted.

Introduction

More than four ten-year period, the working mechanism of the electrochemical sensors (SE), based on the ionic exchange equilibrium, between *membrane* containing the ion *i* and the ions *i* from the studied solution, was unanimously acknowledged and accepted by the specialists in field [1-6].

Beginning with 1974, as alternative, it was advanced a general model (based on charge transfer phenomena-CT), which admitted that the working mechanism of SE, rely on equilibria CT between the superficial active centres of the surface and the ions from the analysed solution [7-10].

From this point of view, by means of the new concept of the *mixed-selectivity*, a new classification of SE, in anion-, cation- and mixed selective-electrodes, was made.

By way of consequence, arised the idea, suggesting a microscopic treatment of the solide-, liquide- electrolyte interface processes and the structure's specification of Gibbs' tension surface [11-12], considered until then a *black box* from microscopic point of view (Fig. 1 a). Therefore, we advanced, for the solid (liquid) / electrolyte interface, *a mixed electrode double layer model,* which accounted for much better the interfacial phenomena from the interface metal-oxide / electrolyte.

---

* Faculty of Science, University of Piteşti, Romania;
** Department of Physics, Faculty of Chemistry, University of Bucharest, Regina Elisabeta Avenue, No. 4 – 12, Bucharest – 70346, Romania;
*** Department of Mathematics, Faculty of Chemistry, University of Bucharest, Regina Elisabeta Avenue, No. 4-12, Bucharest-70346, Romania

Analele Universităţii din Bucureşti – Chimie, Anul XIV (serie nouă), vol. I-II, pg. 215-221

The main features of the new model are [13]:

-The interface with the electrolyte is *heterogeneous* (it contains, associated to the oxide MO, both *active centres* with *donor character* ($O^{\delta-}$) and *active centres* with *acceptor character* ($M^{\delta+}$));

-The direct adsorption (chemosorption) leads to a total alteration of the structure's surface and, simultaneous, to a modification of its selectivity (in fact, another interface), no matter how it is produced: spontaneously (chemical), or artificially (electrochemical);

-The inner Helmholtz plane (IHP) (the plane of the contact-adsorbed ions from the electric double layer classical models) is, in this way, shifted with a molecule of solvent towards the inner of the electrolyte.

Consequently, the Gibbs' tension surface is structurally specified (Fig. 1 b) and corresponds to the *transition layer*, composed from the new IHP and the active centres of the surface [6-13].

The equilibria CT between the ions from the solution (on a level with the new IHP) and surface's active centres are, therefore, mediated by a molecule of solvent, strongly polarized.

Analysing *the fund noise* from current-time registerings on condition that the over potentials applied to be small [14], experimental arguments, in this respect, have been produced.

Such a picture on the interface solid / electrolyte, has been the basis of the new concepts, such as the mobile interface and the organization of the interelectrodic space (the structural interelectrodic arrangement), as well as the basis of the several reconsiderations in the electro-chemistry, bioelectrochemistry, corrosion of metals, polarography, etc.

It was possible, in this way, the promotion of the new concepts, such as *mixed chemical bound*, *hard intermolecular forces*, *electronic conductivity through the electrolyte solutions* (under the electrolysis threshold), as well as an *electronic model* for bioreception, transmission, processing and depositing of the information on a brain level, in which *the ionic pumps* are a simple effect and not the cause of the transmission of the nervous impulse [14].

In a shocking work [15], E. Pungor called attention about a remarkable fact that the ionic exchange mechanism, used till now to account for the working of SE, must be thoroughly reanalysed. He suggests that the adsorption phenomenon is, most likely, the first step in the mechanism of the electrode response.

It was thus considered opportune, from the theoretical and practical point of view, an attempt to systematize a large quantity of experimental data obtained in the last 30 years [14]. At first, one brings arguments in favour of the CT mechanism of SE. That presumes the structural specification of the Gibbs' tension surface (Fig. 1a and 1b) and, implicitly, the building of *the mixed electrode double layer model*, with a partial presentation of the implications following from this.

Experimental results

The classical approach of the electrode-electrolyte interface supposes a thermodynamically description of this, through observations (measurements of current, electric charge and potential) concerning the effect of the disturbances of the equilibrium state.

In the theoretical thermodynamics tackled by Gibbs, for the study of the interface, it supposes, mainly, that all the properties of the transition layer are determined by the area and the curvature of an ideal geometric surface, so-called *tension surface* (Fig 1a).

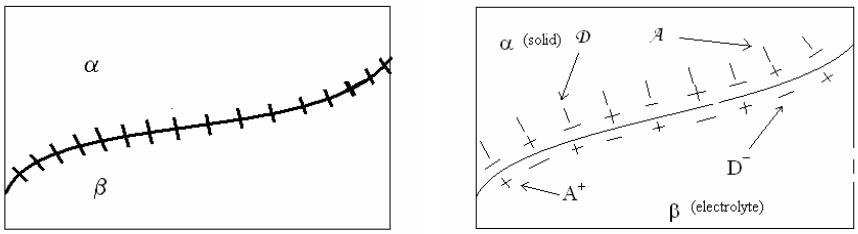

a) b)

Fig. 1 *Interface aria: a) Gibbs tension surface, b) Structure's specification of Gibbs tension surface*

The Gibbs' model has the advantage to lead at results with a wide domain of practice, without being necessary to take into account the detailed structure of the transition layer. However, such treatment does not permit the understanding in detail of the interfacial phenomena like those from the electrode / electrolyte interface. Deciphering of the working mechanism of SE, impose a structural specification of Gibbs' tension surface and a microscopic approach of the phenomena.

The working mechanism of the electrochemical sensors that is based on the ionic exchange equilibrium between membrane and the studied solution is, sometimes, in contradiction with the experimental data [6-10]. An interesting reason, which is in the detriment of this mechanism, can be expressed by a simple and reproducible experiment. One produces three liquid electrochemical sensors: the first is of the type R^+X^- and contains alchil dimetil benzil ammonium iodide as active substance, the second is of the type R^-Y^+ and contains potassium dodecyl-sulphonate and the third is of the type R^+R^- with alchil dimetil benzil ammonium dodecyl-sulphonate.

All three sensors were previously tested in corresponding aqueous solutions containing the ions of the active substances with which they were filled.

Using a milli-voltmeter with very high impedance, we obtained the results shown in Figures 2a, 2b, 2c, 2d, 2e, which represent the response of the electrodes according to Nernst's relation:

$$E = E^0 \pm \frac{RT}{zF} \ln a_i \,, \quad \text{where } a_i \text{ is the activity of the } i\text{-ion in solution.}$$

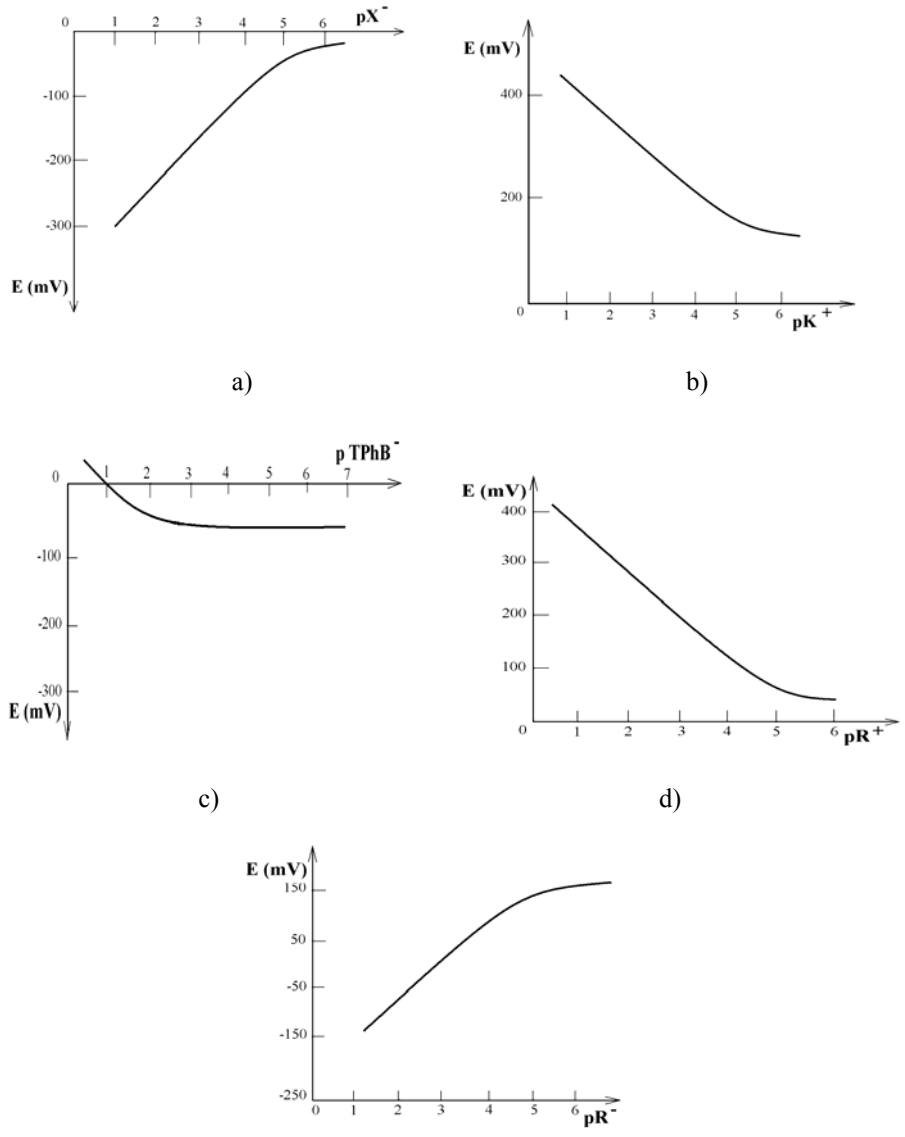

Fig. 2. *Calibration diagrams of the electrochemical sensors: a) electrode R^+X^- for the anion ClO_4^-; b) electrode R^-Y^+ for the cation K^+; c) electrode R^-Y^+ for the anion dodecyl sulphonate; d) electrode R^+R^- for the cation alchil dimetil benzil ammonium; e) electrode R^+R^- for the anion dodecyl sulphonate*

The dependence from Figure 2a presents a response of Nernst type that shows the decreasing of the potential once with the increasing of the anion ClO_4^- activity in the analyzed solution.

In Figure 2b, we have a linear dependence of the potential as a function of the variation of the cation activity K^+ from the tested solution. The potential decreases once with the decreasing of the cation K^+ activity in the analysed solution.

Until now, one can consider that the principle of the ionic exchange equilibrium is valid. Thus, these two electrochemical sensors present reversibility for the macro-cations R^+ (alchil dimethil-benzil ammonium), in the first case, and for the macro-anions R^- (dodecyl-sulphonate), in the second case.

The Figure 2c shows the response of the electrode for the dodecyl-sulphonate macro-anion for the second electrochemical sensor. It is observed that, instead of an anionic response, increasing towards values of the negative potential concomitantly with the increase of the activity of the dodecyl-sulphonate macro-anion, the response is slowly cationic, especially for the high concentrations of the potassium dodecyl-sulphonate (in accordance with the selectivity constant of the selective electrode for K^+ in the presence of sodium ions).

We obtained the similar results in the case of a sensor with alchil dimetil benzil ammonium perchlorate, tested in alchil dimetil benzil ammonium chloride solutions.

The behaviour of such ion-selective electrodes would be justified either by the too small mobility of these macro-ions, or by the fact that such macro-ions suffer a process of fast extraction from the aqueous solution to the extracting solvent of the membrane.

These speculative reasons can be easily removed by using the third electrochemical sensor, with alchil dimetil benzil ammonium dodecyl-sulphonate (R^+R^-). This sensor has reversibility relative to the dodecyl-sulphonate (R^-) and alchil dimethil benzil ammonium macro-cation (R^+) too. The cationic and anionic nernstian responses of this sensor are shown in Figure 2d and Figure 2e, respectively. These are linear functions and are not disturbed neither by the very slow mobility of the macro-ions in the studied solution, nor their extraction in the organic phase. Finally, we ask ourselves, why the supposed macro-ionic exchange equilibria are possible only in the case of the membranes made up of R^+R^- and they are not possible in the case of those made up of R^+X^- or R^-Y^+ ?

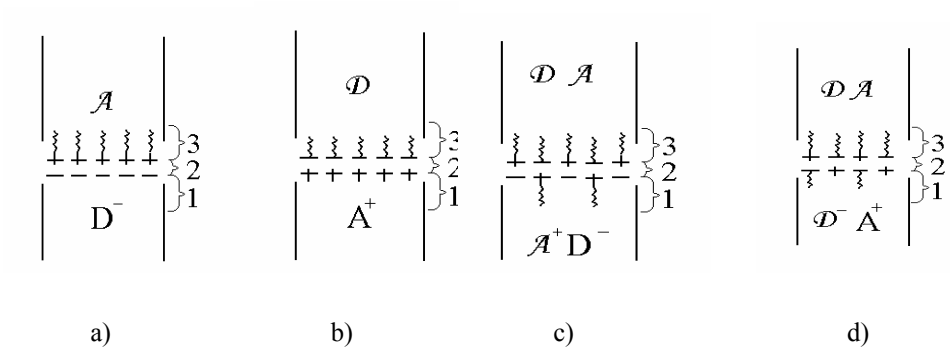

Fig. 3 *Structure of the interface in four cases: a) ideal anion-selective electrode, b) ideal cation-selective electrode, c) mixed-selective electrode for macro-cation R^+, d) mixed-selective electrode for macro-anion R^-.*

The answer can be only one, namely that the processes which determine the variation of the electrode potential versus the activity of the ion in solution are not based on the ionic exchange equilibria, but on the electronic transfer equilibria. The letter occurs between the ions in solution and the active superficial centres (counter-ions) of the selective membrane, which have a donor or acceptor character. Thus, the ion-selective interfaces, whose response are shown in Figures 2a, 2b, 2d and 2e can be simply represented in the Figures 3a, 3b, 3c and respectively 3d. As a support of this idea, we also obtained other experimental results.

Discussions

For the understanding of the phenomena, which take place at solid / electrolyte or liquid / electrolyte interface, it is necessary to take into account a double mixed electrode layer model [16, 17]. In the *mixed electrode double layer* model, the origin of the potential of electrode is sought at the level of some interfacial charge transfer equilibria, but one cannot exclude the existence of the equilibrium of ions change with their implications. The two phenomena can superpose more or less. In case of the electrochemical sensors, the ionic change between membrane and the studied solution can lead to instability of the electrode potential. With this model, one can be made some remarks about some electrochemical domains of general interest.

Conclusions

On the base of the donor-acceptor character of the active superficial centres ($\mathcal{A}$ and $\mathcal{D}$), one can give the following scheme and a general electrochemical system for the electrochemical sensors.

The aqueous solution of ions for analysis	The interphasic transition layer formed in the superficial actived positions donor ($\mathcal{D}$) and/or acceptor ($\mathcal{A}$) with a fixed concentration and the ions from solution.	The conductive inert support
PHASE I	PHASE II	PHASE III

The reply time of the electrochemical sensors is determined by the transport stage of the ions from the electrolyte to the zone IHP of the electrode. This stage is caused by the diffusion and not by the migration of the ions through membrane. The selectivity of the electrochemical sensors is associated with the chemical affinity of the ions in electrolyte for the counter-ionic active positions at the level of transition layer (A^+ and D^-), and not with their chemical affinity for the *membranar phase* in its ensemble [7-10].

Depending on the structure of the interface at the level of mixed electrode double layer, one can make a general classification of the electrochemical sensors in anion- (Figure 3a), cation- (Figure 3b), and mixed-selectives (Figures 3c and 3d).

On the basis of this model, the construction of the *i*-selective electrochemical sensors does not imply the presence of the ion *i* in the two phases lain in contact, which is necessary for the achievement of the equilibrium of ionic change, but that implies the presence of the superficial active donor positions $\mathcal{D}$ and/or acceptor $\mathcal{A}$, with a counter sign that of the ion *i*, implied in equilibrium of electrons change [7-10].

The extent of the detection limit of the mixed-selective electrochemical sensors, in the characteristic area of the potential jump from the anionic reply to that cationic or inverse is an error. It consists of the trend of over-appreciation of the electrodes performance (10^{-14} ion g I^{-1} H^+ for glass electrode or less than 10^{-20} ion g I^{-1} S^{2-}-for those ones of Ag_2S). In fact, the pH-selective glass electrode is a mixed-selective electrode with sensitivities approximately equal for H^+ and OH^-.

REFERENCES

1. Koryta, J. (1972) *Anal. Chem. Acta* **61**.

2. Buck, R. P. (1974) *Anal. Chemistry* **46** (5).

3. Gavach, G. (1973) *Electrochimica Acta* **18**.

4. Baiulescu, G. E., Coşofreţ, V. and Cristescu, C. (1975) *Rev. Chim.* **5**.

5. Pungor, E. and Toth, K. (1973) *Anal. Chem.* **4** .

6. Rechnitz, G. A. (1974) *Mechanistic aspect of ion-selective membrane electrodes. A subjective view*, International Symposion on Selective Ion-Sensitive Electrodes, Cardiff, p. 457.

7. Luca, C., Semenescu, G. and Nedea, C. (1974) *Chem. Rev*., Bucharest **25**, no. 12, p. 1015.

8. Luca, C. and Semenescu, G., (1975) *Chem. Rev*., Bucharest, **26**, no. 11, p. 946.

9. Luca, C., Semenescu, G.and Andrei, A. (1984) *Chem. Rev*., Bucharest, **29**, no. 1, p. 67.

10. Luca, C., Andrei, A.and Semenescu, G. (1989) *Chem. Rev*., Bucharest, **34**, no. 1, p. 197.

11. Semenescu, G. (1981) *Rev. Chim.* (Bucureşti) **32** (2) p. 170.

12. Semenescu, G. (1995) *Rev. Chim.* (Bucureşti) **46** (5) p. 436.

13. Semenescu, G. and Ioniţă, Gh. (1998) *Rev. Chim.* (Bucureşti) **49** (7) p. 474.

14. Semenescu, G. (2000) **Aspecte moderne în chimia interfeţelor**, Ed. Univ. Piteşti.

15. Pungor, E. (1998) *Analitical Sciences* vol. 14, *The Japan Society for Analytical Chemistry*, p.249.

16. Semenescu, G., Cioacă, C. and Iorga, B. (2000) *Acta Chim. Slov.* **47**, p. 133-141.

17. Semenescu, G., Cioacă, C., Iorga, B.and Gughea, G (2002) *Acta Chim. Slov*., **49**, p 121-138.